BRNO UNIVERSITY OF TECHNOLOGY

Faculty of Electrical
Engineering and
Communication

DOCTORAL THESIS

Brno, 2024 Anhelina Tanchak

BRNO UNIVERSITY OF TECHNOLOGY

VYSOKÉ UČENÍ TECHNICKÉ V BRNĚ

FACULTY OF ELECTRICAL ENGINEERING AND COMMUNICATION

FAKULTA ELEKTROTECHNIKY
A KOMUNIKAČNÍCH TECHNOLOGIÍ

DEPARTMENT OF ELECTRICAL POWER ENGINEERING

ÚSTAV ELEKTROENERGETIKY

INVESTIGATION OF PU-239 TRANSMUTATION FOR ACCELERATOR DRIVEN SUBCRITICAL REACTORS

VÝZKUM TRANSMUTACE PU-239 PRO PODKRITICKÉ URYCHLOVAČEM ŘÍZENÉ JADERNÉ REAKTORY

DOCTORAL THESIS

DIZERTAČNÍ PRÁCE

AUTHOR — Anhelina Tanchak

AUTOR PRÁCE

SUPERVISOR — doc. Ing. Karel Katovský, Ph.D.

ŠKOLITEL

BRNO 2024

ABSTRACT

This dissertation thesis is focused on determination of cross sections of radionuclides generated in result of spallation reaction in plutonium ($^{239}PuO_2$) target irradiated by 660 MeV energy proton beam. Moreover, the produced nuclides were also investigated using different tools to ascertain their properties. The Phasotron accelerator of the Joint Institute for Nuclear Research (Dubna) was used for irradiation of target as a generator of proton beam. The experiment was focused on the quest for short-lived radionuclides. The HPGe detectors were used for measurement of gamma spectra. The γ-spectra obtained during this experiment were processed using the DEIMOS32 software. The AD4HEL code was used for identification of the nuclei formed in the $^{239}PuO_2$ target. The comprehensive analysis of these residual products and their characteristics, serve as an important contribution to the understanding of the spallation and fission reactions between protons and ^{239}Pu in high-energy range. Additionally, the experimental data of the nuclear reaction cross sections may be valuable as reference data for theoretical simulations to study reactions, and they can be used for supplementation to the nuclear databases. As for comprehensive analysis, the experimental results were compared with simulations conducted using Monte Carlo particle transport codes, such as MCNP v.6.1. and FLUKA. As a result, received data overall correspond to the expectation having similar regions of nuclides concentrations, similar graphs, and a slight variation in the range of values (probably because of the different normalization factors of different software tools).

KEYWORDS

Transmutation; spallation reaction; Phasotron accelerator; gamma spectra; radionuclides; plutonium-239; proton beam; γ-spectroscopy; cross section; reaction yields; accelerator driven systems.

ABSTRAKT

Tato disertační práce je zaměřena na stanovení průřezů radionuklidů vznikajících v důsledku spalační reakce v terči z plutonia ($^{239}PuO_2$) ozářeného protonovým svazkem o energii 660 MeV. Kromě toho byly vzniklé nuklidy zkoumány pomocí různých nástrojů za účelem zjištění jejich vlastností. K ozáření terče byl použit fázotronový urychlovač Spojeného ústavu jaderných výzkumů v Dubně jako generátor protonového svazku. Experiment byl zaměřen na hledání krátce žijících radionuklidů. Pro měření spekter gama byly použity detektory HPGe. Spektra γ, získaná během tohoto experimentu, byla zpracována pomocí softwaru DEIMOS32. Pro identifikaci jader vzniklých v terči $^{239}PuO_2$ byl použit kód AD4HEL. Komplexní analýza těchto zbytkových produktů a jejich charakteristik významně přispívá k pochopení spalace a štěpných reakcí mezi protony a ^{239}Pu v oblasti vysokých energií. Experimentální údaje o průřezech jaderných reakcí mohou sloužit jako referenční údaje pro teoretické simulace ke studiu reakcí a mohou být použity k doplnění jaderných databází. V komplexní analýze byly experimentální výsledky porovnány se simulacemi provedenými pomocí kódů Monte Carlo pro přenos částic, jako jsou MCNP v.6.1. a FLUKA. Výstupem z experimentálních dat je, že získaná data celkově odpovídají očekávání, přičemž mají podobné oblasti koncentrací nuklidů, analogické grafy a mírné odchylky v rozsahu hodnot. Odchylka je pravděpodobně způsobena normalizačním faktorem z důvodu omezení různých softwarových nástrojů.

KLÍČOVÁ SLOVA

Transmutace; spalační reakce; fázotronový urychlovač; gama spektra; radionuklidy; plutonium-239; protonový svazek; γ-spektroskopie; účinný průřez; reakční výtěžky; systémy řízené urychlovačem.

Bibliographic citation

TANCHAK, Anhelina. *INVESTIGATION OF PU-239 TRANSMUTATION FOR ACCELERATOR DRIVEN SUBCRITICAL REACTORS*. Brno, 2024. Available also at: https://www.vut.cz/studenti/zav-prace/detail/160758. Doctoral Thesis. Vysoké učení technické v Brně, Fakulta elektrotechniky a komunikačních technologií, Department of Electrical Power Engineering. Advised by doc. Ing. Karel Katovský, Ph.D.

PROHLÁŠENÍ

I hereby declare that I have prepared my PhD thesis on the topic "Investigation of Pu-239 transmutation for accelerator driven subcritical reactors" independently under the supervision of my thesis supervisor and with the use of scientific literature, lectures, and other information sources, all of which are cited in the thesis and listed in the reference list at the end of the thesis. As the author of the said doctoral thesis, I further declare that in connection with the creation of this doctoral thesis, I have not infringed the copyrights of third parties, in particular, I have not infringed in an unauthorized manner on the personal and/or property rights of others, and I am fully aware of the consequences of violating the provisions of S 11 et seq. of the Copyright Act No. 121/2000 Coll, on copyright, on rights related to copyright and on amendments to certain acts (Copyright Act), as amended, including the possible criminal consequences arising from the provisions of Part Two, Title VI, Part 4 of the Criminal Code No. 40/2009 Coll.

……. ……...

Brno signature of the author

ACKNOWLEDGEMENTS

I would like to thank my dissertation advisor, doc. Ing. Karel Katovský, Ph.D., for his professional guidance, patience, consultation, and valuable suggestions to help me complete my research in the best possible way.

I would also like to thank to all collaborators of the JASNAPP gamma-spectrometry group participating in preparation and preformation the physical experiment involving irradiating ^{239}Pu with high energy protons at JINR, Dubna.

Many thanks to my colleague Zhurabek Khuskov from JINR for providing guidance regarding simulation in FLUKA code and further discussions on input experimental data.

Additionally, I am also thankful to my colleague and friend Robert Golomb for helping me in Monte Carlo simulations in MCNP v.6.1. code.

I would also like to thank Ing. Petr Toman, Ph.D., Head of the Department of Electrical Power Engineering at the Brno University of Technology, to provide conducive environment and support for the students and researchers to successfully furnish their goals.

I would like to express my sincere gratitude to my friend Sadam for helping with my English language, provision of unconditional moral support and motivating me to finish my dissertation.

Finally, I would like to thank my parents and grandparents for everything, my friends, my colleagues for their unwavering support and sharing of joys, worries, and time with me.

Thank you all so much for being available for me, and for believing in me! I appreciate you all!

……. ……...

Brno signature of the author

"The future depends on what you do today.
Prioritize your actions, and every moment becomes an opportunity for progress."
- Mahatma Gandhi

CONTENTS

LIST OF FIGURES

LIST OF TABLES

LIST OF ACRONYMS

IAEA	International Atomic Energy Agency
ADS	Accelerator Driven Systems
USSR	Union of Soviet Socialist Republics
MTA	The Material Test Accelerator
MINERVA	MYRRHA Infrastructure for Research and Innovation
KURRI	Kyoto University Reactor Research Institute
MEXT	Japan's Ministry of Education, Culture, Sports, Science and Technology
ESS	The European Spallation Source
FWHM	Full width at half maximum
JINR	Joint Institute for Nuclear Research
J-PARC	Japan Proton Accelerator Research Complex
JAEA	Japan Atomic Energy Agency
LEHIPA	Low Energy High Intensity Proton Accelerator
LEHIPA-RFQ	Radio Frequency Quadrupole
BARC	Bhabha Atomic Research Centre
LHEP	Laboratory of High Energy Physics
LNP	Laboratory of Nuclear Problems
CERN	the European Organization for Nuclear Research
IHEP	Institute of High Energy Physics
LINAC	Linear Accelerator
C-ADS	The China Accelerator Driven Subcritical System
MYRRHA	Multi-Purpose Hybrid Research Reactor for High-tech Applications
SCK CEN	The Belgian Nuclear Research Centre
NPP	Nuclear Power Plant
TEF-T	ADS Target Test Facility
TEF-P	Transmutation Physics Experimental Facility
NSC KIPT	National Science Center Kharkiv Institute of Physics and Technology
THOR	Thermal Hydraulics of innovative nuclear Reactors for safety
RFQ	Radio Frequency Quadruple
RR	Reaction Rate

PR	Product Rate
FM	Fissionable material
FF	Fission fragments
SA	Subcritical Assembly
MA	Minor Actinides
ISOLDE	Experimental facility at CERN
CERN	The European Organization for Nuclear Research
INCL	(Liège intranuclear cascade) a code to model light particle-nucleus interaction
INC	Intra-Nuclear Cascade
SEP	Single Escape Photons
DEP	Double Escape Photons
SNS	The Spallation Neutron Source
HPGe	High Purity Germanium
ORTEC	A company which makes designs and manufactures radiation detectors
CANBERRA	Manufactures a wide range of Silicon and Germanium Photon Detectors
SNF	Spent Nuclear Fuel
CAFe	A superconducting proton linac
TEF	Transmutation Experimental Facility
CIAE	The China Institute of Atomic Energy
RAW	Radioactive Waste
CW	Continuous-Wave
LBE	Lead-bismuth Eutectic
LWR	Light-Water Reactor
RW	Radioactive Waste
LLFP	Long-lived fission products
LLW	Low-level waste
HLW	High-level waste
ST	Spallation Target
SF	Spallation Fragments
INCN	Intra-Nuclear Cascade
DEIMOS32	A program for gamma-ray spectra analysis
RA	Reactor Assembly
APR	The appreciation for nature

SHE-factory	Superheavy Element Factory
YASNAPP-2	Experimental complex developed for spectroscopic investigations
TJ02000321-V3	Software analyzing laser-generated neutron spectrum the whole energy scope
PHITS	The Particle and Heavy-Ion Transport code System
FLUKA	Monte Carlo code for the interaction and transport of particles
MCNP	Monte Carlo N-Particle code
JEFF	Joint Evaluated Fission and Fusion Nuclear Data Library
ENDF	Evaluated Nuclear Data File Database
JENDL	Japanese standard library
INFN	The Italian Institute for Nuclear Physics
TCS	Total cross section
FLAIR	An advanced user-friendly interface for FLUKA code
PHIG-3D	PHITS Interactive Geometry viewer in 3D
MAESTRO	A multichannel analyzer (MCA) “emulation” software package

INTRODUCTION

Keeping in view the conducive environment available for nuclear energy deployment currently, it is also essential to take some measures regarding handling of spent nuclear fuels which comprise of long-lived radionuclides. By employing transmutation in ADS, those long-lived radionuclides can be converted into relatively short-lived nuclides with potentially low level of radioactivity. The handling of processed nuclear spent fuel becomes relatively easier and cost effective.

Given a large number of nuclear power plants around the world, as well as plans to build new ones, it is safe to assume that nuclear energy will continue to play an important role as part of the industry. As of November 2023, there are 436 operable reactors in 30 countries and 220 research reactors in operation over 50 countries [1]. At the same time, highly radioactive material produced during energy production poses one of the biggest challenges faced by nuclear energy.

According to the IAEA, the total cumulative amount of spent nuclear fuel in the world so far is estimated at 445 000 tHM (as of 2020). Similarly, according to [2], the spent fuel projections are described as below:

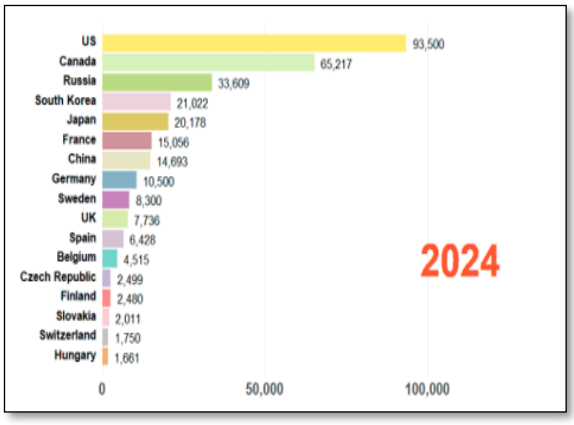

Fig.1. Global spent nuclear fuel tracker for the year-2024. SNF in Tons of Heavy Metal (tHM).

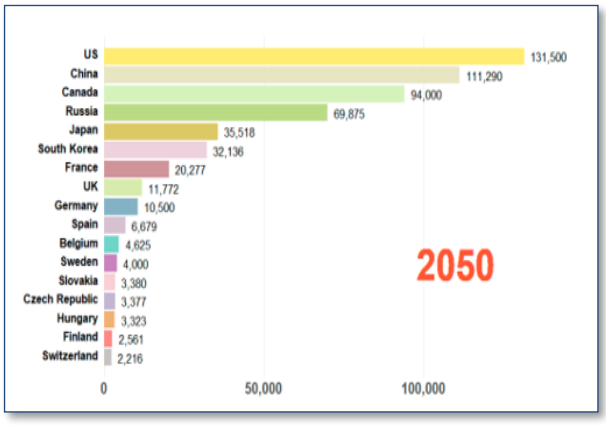

Fig.2. Global spent nuclear fuel tracker for the year-2050. SNF in Tons of Heavy Metal (tHM).

Reprocessing (extracting uranium and plutonium from SNF) is particularly practiced in countries such as Russia, France, and Japan. While deep disposal method is employed by countries such as Canada, Finland, and Sweden. Map below shows the current status of SNF inventories in 17 countries around the world in context of finding the best solution for spent nuclear fuel management strategies.

The priority of all developed countries in terms of environmental protection measures is the successful disposal and management of waste from nuclear power plants. In addition, countries with nuclear weapons are concerned about the disposal or peaceful use (conversion) of surplus weapons of plutonium and highly enriched uranium. Appropriate approaches are being developed for that in Europe, North America, Japan, and Russia [3-6].

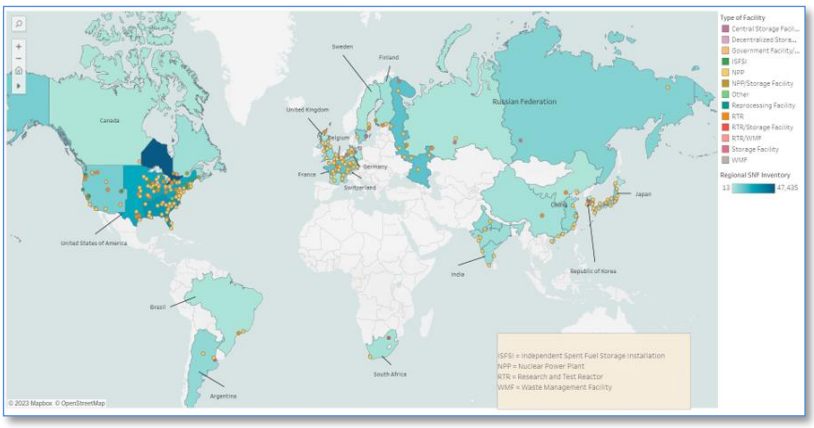

Fig.3. A review of the current nuclear power plants, research reactors, and SNF inventories across 17 countries around the globe [2].

Spent fuel contains uranium (≈ 96%), plutonium (≈ 1%) and products of fission (≈ 3%). Uranium and plutonium can be reused. Additionally, the amount of SNF is influenced by the type of nuclear reactor. Modern recycling plants dissolve spent fuel and chemically separate it into these three components: uranium, plutonium, and high-level waste.

In practice, several approaches to the final management of spent nuclear fuel are considered [7], such as:

- Reprocessing.
- Deep geological repositories.
- Nuclear transmutation.

Moreover, storage of nuclear waste also poses regulatory challenges in the form of proliferation. As spent fuel contains fissile material so it can be utilized for the development of nuclear weapons. The most promising approach from the IAEA's point of view is to process the spent fuel, which involves the back-end nuclear fuel cycle using fast neutron reactors. SNF reprocessing is the extraction of uranium and plutonium elements for reuse in the nuclear fuel cycle.

The transmutation of spent nuclear fuel involves converting long-lived radioactive elements in nuclear waste into shorter-lived or stable isotopes through nuclear reactions. This process serves two key purposes: reducing radioactive waste and mitigating nuclear proliferation risks. By decreasing the amount of plutonium in spent nuclear fuel, transmutation contributes to non-proliferation efforts, as plutonium can be extracted and potentially used in nuclear weapons. This not only enhances global security but also addresses environmental concerns associated with long-lived nuclear waste. Additionally, transmutation processes may increase the efficiency of the nuclear fuel cycle by extracting more energy from the remaining fissile material in spent fuel. This multifaceted approach aims to positively impact resource utilization and public perception of nuclear energy.

It is obvious that some isotopes of plutonium and other transuranic radioisotopes (neptunium, americium, curium) in spent fuel have half-lives of thousands to millions of years. Therefore, it can be assumed that no storage facility can guarantee complete safety against radionuclide leakage and environmental contamination for such a long time [8]. Thus, the main rationale for the processing and construction of new fast neutron reactors is to reduce the content of minor actinides and the content of fission products, which would significantly reduce the environmental impact and the associated long-term danger. Plutonium is the only

transuranic element that is released and used on a large scale. Plutonium is better as a fuel for energy production because the fission reaction of one nucleus usually forms 3 new neutrons. Plutonium can be used in nuclear reactors from two sources: as a capture product in reactors of ^{238}U isotope; or excess plutonium created for atomic bombs [9].

The reprocessing of spent fuel from thermal neutron power reactors is also required to implement a closed fuel cycle and reuse regeneration products as nuclear fuel which is a viable alternative to nuclear waste disposal. The current state of scientific and technical developments in the reprocessing of spent nuclear fuel confirms the real possibility and feasibility of closing the nuclear fuel cycle. Active new research in the field of nuclear energy allows not only to improve past projects (for more efficient use of fuel in the reactor, etc.), but also to develop new projects and technologies that would provide a constant amount of available energy in the future.

Accelerator driven systems (ADS) represent promising offer, innovative perspectives, and benefits for high-level nuclear waste (HLW) transmutation. The ADS comprised of typical nuclear reactor with particle accelerator, may open new potential benefits for disposing long-lived radioactive waste. In addition, these systems have a higher margin of safety due to their ability to stop the chain reaction by stopping the supply of protons.

Accelerator Driven Systems offer numerous advantages in nuclear energy applications. Operating in the subcritical region ensures that the process cannot uncontrollably spread, and stopping the chain reaction is as simple as turning off the accelerator, minimizing the risk of uncontrolled nuclear reactions and core meltdown. The utilization of thorium in ADS is feasible, and it efficiently burns plutonium, contributing positively to nuclear non-proliferation efforts. By eliminating the need for expensive uranium enrichment procedures, ADS provides flexibility in fuel choices and transmutation targets.

Additionally, ADS produces materials that are challenging to extract for nuclear weapons production, further enhancing non-proliferation measures. The system's ability to transmute long-lived radioactive isotopes in nuclear waste into shorter-lived or stable forms contributes to safer waste management, reducing radioactivity, radiotoxicity, and decay heat in geological repositories. Moreover, ADS extends the usability of nuclear fuel resources by extracting additional energy from existing nuclear waste, promoting a more sustainable and efficient nuclear energy cycle. Integration with renewable energy sources enhances ADS's environmental friendliness, making it a promising technology for addressing nuclear waste challenges. It also generates less radioactive waste and after 500 years, the activity level is equivalent of coal ash [10].

However, there exist a lot of technical and economic challenges to put ADS technology in practice. Continued research and development initiatives are focusing on enhancing the design, increasing efficiency, and lowering the overall expenses associated with these systems. That is why, it is necessary to investigate more experiments related to transmutation process, which will allow better understanding of physical and technical method of advanced nuclear waste transmutation technologies. It will also be beneficial for safe management of spent nuclear fuel, especially to reduce hazardous effect of HLW on environment and humans.

The detailed analysis of ADS technology, the spallation reaction, cross section of plutonium etc., has been performed in later chapters.

THE AIM OF THE DISSERTATION

The main area of this dissertation is focused on transmutation of spent nuclear fuel, specifically on the study of spallation reaction on plutonium target irradiated by the proton beam. That is related to the use of accelerator driven systems for the transmutation of long-lived radionuclides to short-lived radionuclides. This study comprises analyzing the measured data to obtain parameters for residual nuclides created in spallation reactions. Such parameters are yields of reaction products inside the target, their reaction rates, and cross sections. In addition, to compare the experimental results are compared with theoretical simulations.

The objectives of this dissertation study can be defined in several points:

- To investigate experimental methods for the characterization of spent nuclear fuel, ADS systems, deepening knowledge of nuclear physics.
- To find suitable program for modeling the reaction of protons with plutonium target using the Monte Carlo method (such as MCNP, FLUKA and PHITS).
- To improve the methodology of data processing used in the experiment to determine the yield of nuclear reactions of radioactive nuclei.
- To process the spectra of the plutonium target, which was irradiated on a proton beam with energy of 660 MeV.
- To determine all the gamma lines from each measurement positions and the efficiency of the detectors for them.
- To determine the effective cross sections of the measured radionuclides.
- To compare the experimental data with theoretical calculations.
- To execute comprehensive study of the results obtained from spectra, especially, each isomer, isotope, and their decay products.
- To demonstrate the effectiveness of transmutation in converting long-lived radioactive isotopes into less hazardous, short-lived isotopes.
- To evaluate the accuracy and efficacy of simulation codes for ^{239}Pu transmutation reactions.
- To publish and to present the results in physical journals and at conferences, to supplement existing data or to contribute new data for plutonium and research for advanced nuclear technologies such as ADS.

The main aim of the study is to investigate fission and spallation reactions of the $^{239}PuO_2$ target bombarded with 660 MeV protons. To demonstrate the feasibility and effectiveness of transmutation process.

The research method such as a γ-spectroscopy of the irradiated target was used. Aluminium foils were used for monitoring of the incident proton beam (Al monitors). As a result, the cross sections of the ^{239}Pu nucleus depending on the charge and the mass number of reaction fragments were obtained.

The dissertation consists of the following chapters:

Chapter 1 – Accelerator driven systems: brief history of ADS, the basic concepts of ADS, advantages and disadvantages of ADS, and examples of ADS research and development in different parts of the world. Additionally, it describes radioactive waste, nuclear

transmutation, fission products, spallation reaction, spallation targets, and spallation products.

Chapter 2 - Methods for determining spallation products and their cross sections: This chapter describes several main methods for determining spallation products. It also includes a description of high-purity germanium (HPGe) detectors, their advantages and main disadvantages, energy resolution, energy calibration, and determining the efficiency of the detector. In addition, it explains how to determine the reaction rate and cross section of the residual radionuclides. Various corrections used for accuracy in the measured data are also described.

Chapter 3 – Application of software for processing γ-spectra: This chapter covers the analysis and interpretation of data from gamma-ray detectors using various software packages. For instance, DEIMOS32 is used for processing gamma-ray spectra, the Efekt8.exe is used for the calculation of efficiency of HPGe-detector, and the AD4HEL code is used to calculate production and reaction rates of the radionuclides produced in the study sample.

Chapter 4 – Simulation of spallation reaction in plutonium target with 660 MeV protons: This chapter presents a description of simulation codes for spallation reactions based on the Monte Carlo method. A brief description of the MCNP code, FLUKA code, and PHITS code is given.

Chapter 5 – The experiment on a thin plutonium target: This chapter discusses the sequence of executing the short experiment on a plutonium target, such as the preparation of the sample for irradiation, details about irradiation, transport of the sample to the γ - spectroscopy laboratory, series measurement of gamma spectra, and processing of the received data.

Chapter 6 – The experimental results and analysis: Divided into three main parts, this chapter presents experimental data results showing the values of the reaction rates and cross sections of radionuclides produced in the plutonium target. Simulation results include theoretical calculations of spallation reactions using the MCNP v.6.1 code, FLUKA code, and PHITS code. The last subsection presents the results of comparing experimental data with the simulations that were performed using the Monte Carlo methodology.

CHAPTER 1
ACCELERATOR DRIVEN SYSTEM

1.1 Brief history of accelerator driven systems

Accelerator driven systems (ADS) are a relatively new development in nuclear technology, the first experimental ADS were developed in the 1990s. In the following paragraphs, the short history of the development of ADS technology will be presented.

Nuclear transmutation is the one of basic processes of accelerator driven systems. Briefly, nuclear transmutation is the process of changing one chemical element into another with the bombardment of charged particle (e.g. high-energy proton). The nuclear transmutation process was first demonstrated by Rutherford in 1919, in which charged α particles were used to transmute ^{14}N to ^{17}O. The first artificial radioactivity was enveloped by I. Curie and F. Joliot in 1933. In the discovery this phenomenon they used α particles from naturally radioactive isotopes to transmute boron and aluminum. The significant progress in this field occurred after the invention of the cyclotron by E.O. Lawrence [11], which contributed to removing problems with Coulomb barriers in heavy nuclei. The perspective of the spallation process combined with high-power accelerators can open exciting new opportunities for generating intense neutron fluxes for a variety of purposes.

The first effort to generate neutrons through accelerators was made in 1940s by Ernest Lawrence and W. N. Semenov situated in United States and USSR respectively. Later, to produce fissile material from accelerators, MTA [12] project was launched at Lawrence Livermore Radiation Laboratory. Above mentioned ideas were employed in the development of subcritical reactor through ADS, which is controlled by external neutron source (see Fig.1.2). In terms of nuclear reaction, the ADS are quite similar to nuclear reactors. Like nuclear reactors, the ADS also employ fast and thermal neutron spectra.

Nuclear energy was presented as favorable solution for the generation of power during 1950s and 1960s. However, due to the dual use of nuclear material for proliferation as well as for nuclear generation alerted the researchers to explore alternate means. One of the means to generate energy was the establishment of subcritical reactor energized by particle accelerator. The fundamental idea behind this concept is to use powerful beam of protons or other particles to initiate nuclear reaction in the target material. Through this, the energy can be generated without the possibility of critical chain reaction.

During 1990s, an Italian physicist Carlo Rubbia, introduced the concept of ADS to address the radiological waste and safety concerns associated with conventional nuclear reactors. The idea involves acceleration proton on target material for the further production of neutrons and keep the reactor in subcritical state to avoid self-sustaining nuclear reaction.

During the early 2000s, various experimental projects focused on ADS (Accelerator Driven Systems) were launched in Europe and Japan. Among these initiatives, The MYRRHA (Multi-purpose Hybrid Research Reactor for High-tech Applications) project in Belgium is one of the iconic projects to build a prototype ADS reactor to demonstrate the feasibility of ADS technology in various significant domains ranging from medical applications and industrial applications to nuclear waste transmutation. Moreover, it will also demonstrate the practical usability of ADS technology for research purposes and to build first ADS based sub-critical reactor. It uses lead-bismuth eutectic (LBE) as coolant and spallation target material [13].

The first phase of the project is called "MINERVA" (MYRRHA Infrastructure for Research and Innovation) in which the construction and operation of 100 MeV proton accelerator will be completed. This phase of the project is primarily concerned with successful establishment of proton beam with operation reliable enough for purposes of ADS.

After successful deployment of the MINERA Phase, the subsequent phases involving construction and operation of reactor will be pursued. The timeline for the complete construction of ADS based reactors is by the end of this decade (2020s).

Recently, many work has been carried out to establish the operational performance as well as sustainability of ADS. Furthermore, emphasis has also been put to explore new applications of ADS based systems. One such very important application can be transmutation of radioactive nuclear waste. This area of research seems promising and very beneficial because through this, the longstanding problem of getting rid of nuclear waste can be solved.

At the present time, globally many ADS research projects are in progress, but this technology is still in the experimental stage. Many technical, political, and economic challenges need to be handled before ADS can be practically applied in the fields of medicine, radioactive waste disposal and generation of relatively energy. Due to huge potential benefits of Accelerator Driven Systems, a lot of active research and subsequent development strategies are in progress in the world today.

1.2 The basic concepts of ADS

Accelerator driven systems are complex systems which contain several physical phenomena. Basic concepts of ADS [14] are as follows:

- **Particle accelerator:** The particle accelerator is the most significant part of the ADS. It generates high energy proton or deuteron beam directed at sub-critical core. The particle accelerator initiates the nuclear reaction and subsequently can turn it off. The particles are accelerated at very high velocities very much close to the speed of light by employing electromagnetic fields in the accelerator. The most commonly used are Linear accelerators (linacs) and circular accelerators (cyclotrons and synchrotrons) [15].
- **Target material:** Target material plays a key role in generation of neutron to establish nuclear reaction. Normally, heavy metal like lead or tungsten is used as spallation target material. Besides production of neutrons, the target material can also be used as material to generate isotopes or transmute radioactive nuclear waste. Moreover, target material also serves as coolant material for spallation reaction. Lead-bismuth eutectic (LBE) is one of the commonly used targets as well as coolant material for the ADS designs.
- **Spallation:** The process in which high-energy protons and deuterons, accelerated by particle accelerator, interact with target nuclei is called spallation reaction. Through this reaction, neutron as well as daughter elements can be created. These neutrons can be used to initiate nuclear reactions in fuel materials or to produce medical isotopes.
- **Subcriticality:** Unlike traditional reactors which establish sustainable chain reaction and as well as achieve criticality, the ADS employs subcriticality and is not self-sustainable because ADS employs external source of neutrons and maintains neutron multiplication factor below 1, which prevents a chain reaction from occurring. Due to this inherent design feature, the reactor can be shut down by shutting down the neutron source.

- **Safety systems:** The are many safety systems designed to be used in the ADS to protect the environment, humans and avoid potential hazards. The safety systems of ADS include Shutdown Systems, Neutron Beam Monitoring System, Radiation Monitoring and Shielding, Cooling Systems, Containment Systems, Emergency Response and Evacuation Plans. Besides these, many physical barriers are also employed.

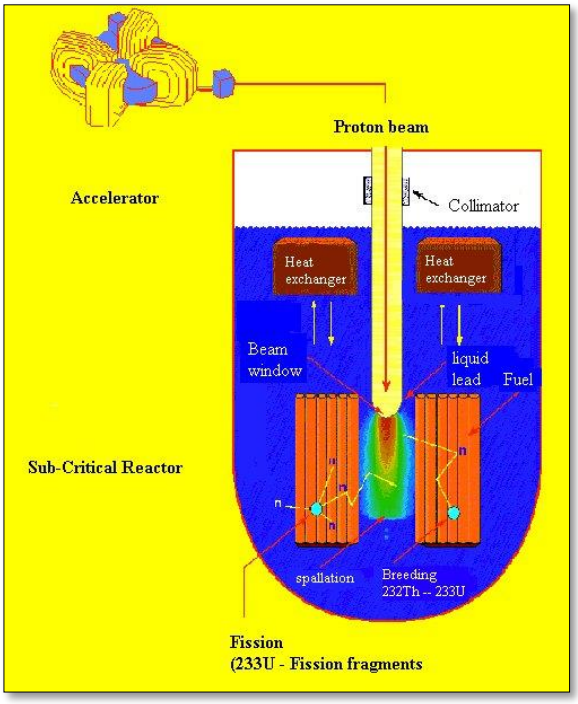

Fig.1.1. The basic concept of ADS [16].

To summarise, accelerator driven systems (ADS) are advanced nuclear systems which consist of a high-power proton accelerator, a spallation target, and a subcritical core (coupled to the spallation target). These subcritical systems use a heavy metal target that produces neutrons when bombarded by a high-power beam that releases enough energy to power the accelerator.

The ADSs can be used for several purposes, including:

- **Nuclear energy production**: One of the main applications of ADS is produce nuclear energy while keeping the reactor in subcritical state. The subcritical core uses uranium or plutonium to produce heat. The is subsequently transferred to the coolant. The coolant absorbs the heat and transfer it to heat exchanger. The liquid in the secondary loop converts into steam and finally used to rotate the turbine as prime mover for electricity generation from electric generator.
- **Nuclear waste transmutation:** The ADS offers a promising solution for the successful transmutation of radioactive waste. In this process long-lived radioactive isotopes are converted into short lived or stable radioactive isotopes.
- **Medical isotope production:** The ADS has huge potential for the production of medical isotopes for diagnostic and therapeutic purposes. Through ADS, a continuous and reliable supply of medical isotopes can be maintained. Moreover, due to customization of neutron flux, more specific isotopes can be produced for specific applications.

- **Basic research:** The ADS has significant potential in carrying out research in the fields of Nuclear Physics, Material Science, Neutrino Physics, Fundamental Particle Interactions, Astrophysics and Cosmology, and Radiobiology. Moreover, the high-energy proton beam can be used to create and study exotic nuclear states or test materials under extreme conditions.
- **Nonproliferation:** The ADS can significantly reduce the proliferation risk by transmutation of nuclear used fuel and plutonium disposals. Moreover, the ADS technology also employs secure fuel cycle, which means fuel is created to achieve subcriticality and by keeping in view non-proliferation concerns. It also reduces the amount of nuclear fuel to be used in reactor. Less fuel generates less radioactive waste, which reduces the risk of misuse.

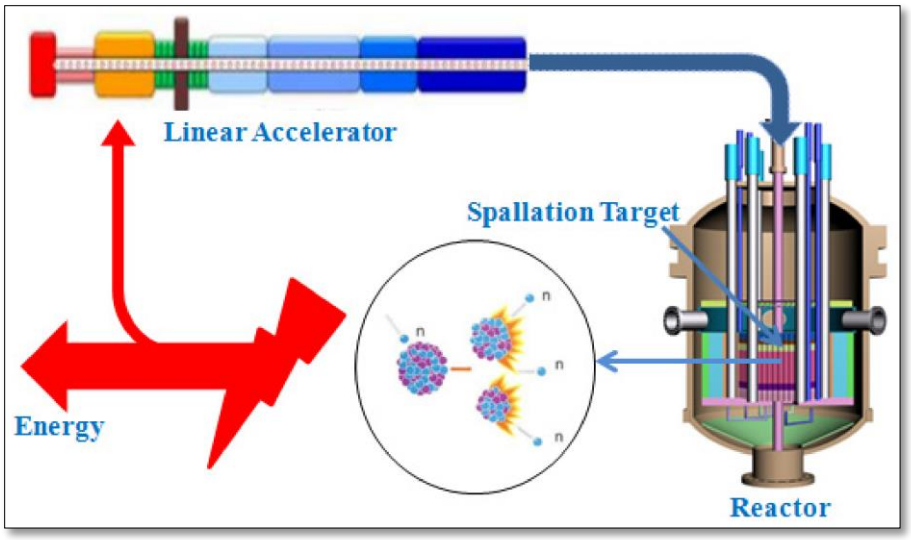

Fig.1.2. Scheme of accelerator driven systems [17].

As ADS burns material that does not have a high enough fission factor to neutron capture to support a fission chain reaction, such a system can only work when neutrons are fed to it. In the ADS system, neutrons produced by combustion cause the fuel to be distributed by subsequent neutrons resulting from this fission**.** Therefore, the ADS can be turned off simply by stopping the proton beam, eliminating the need to insert control rods to absorb neutrons and make the fuel assembly subcritical. The ADS are considered safer than conventional fission reactors because they stop when the input current is turned off [18].

Neutrons with varying energies can be used in subcritical reactors, especially the low energy neutrons have less capability to carry out sustainable fission on their own. So, in ADS, main focus is on the establishment of high energy particle beam as a source of neutrons. Low energy neutrons can also initiate a nuclear reaction on fuels with low fissile content, such as minor actinides produced as radioactive waste from conventional reactors. Moreover, Accelerator Driven System can accommodate fuel comprising up to 50% waste and convert it into shorter-lived and less radiotoxic fission products.

The establishment of neutron population divergence in a core of the reactor depends on characteristics of nuclear materials being employed. Which comprise of effective fraction of delayed neutrons, the Doppler Effect, and the possibility of absorption of neutron by fuel, fertile material, coolant, and moderators. However, if reactor materials contain unfavourable properties, such as high concentration of minor actinides like Np, Am, and Cm, it becomes challenging to control reactor power and minimize the possibility of power excursions to

acceptable levels. In order to transmute nuclear waste successfully from spent reactor fuels, the use of ADS employing subcritical reactors driven by external high energy particles is quite promising. These reactors are regarded as deterministic in terms of safety.

Without the use of subcritical systems based on high-current proton accelerators, it will probably not be possible to completely dispose of minor actinides (MA). The fact is that for these isotopes there is a very small proportion of delayed neutrons, which provide stable control of a conventional critical reactor. In addition, other parameters that ensure the safe operation of the critical reactor, such as the margin of reactivity of the zone with MA, the reactivity effect of heat loss, Doppler fuel ratio, impose significant limitations on the creation of a critical reactor with MA. Thus, it turns out that it is impossible to build a stable critical reactor with fuel, consisting of more than 15 - 20% of MA [19].

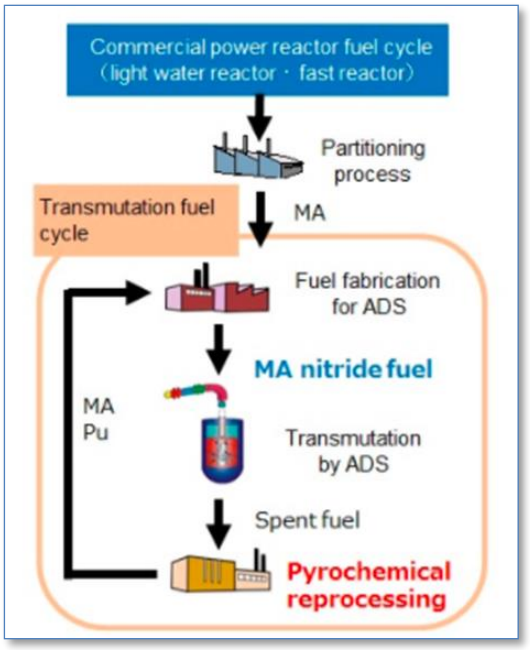

Fig.1.3. Schematic diagram of the fuel cycle of MA transmutation using ADS [20].

In essence, ADS, with its subcritical fuel, will increase safety because it is protected from a few types of critical accidents. However, the same amount of heat is produced by radioactive decay, regardless of whether traditional methods are used, or ADS is used, which means that the same safety risks exist in case of cooling failure after shutdown of the reactor [21]. Nowadays, scientists actively working that solve this issue by implementing passive cooling system in cases of accidents.

The ADS is well adapted to burn fuel, which produces a small number of delayed neutrons, which in critical reactors leads to bad criticality control. Increased safety of ADS is provided by regulation of beam current. In ADS, you can burn repeatedly pure minor actinides until they are completely burned. This reduces their content in waste by hundreds of times compared to waste in one cycle.

1.3 Advantages and disadvantages of ADS

As mentioned previously, accelerator driven systems can be used for several purposes, like waste transmutation, medical isotope production, etc., they have unique safety systems and are employable for nonproliferation. In the following section, the advantages and disadvantages of ADS will be evaluated.

Some of the key advantages of ADS are:

- **Enhanced Safety:** In terms of safety, ADS offers enhanced safety feature as compared to conventional nuclear reactors. In case of loss of power or coolant, ADS automatically shutdowns the reactor and the need to employ active coolant systems can be eliminated. Moreover, the ADS operates in subcritical region and cannot sustain the nuclear reaction on its own without external particle accelerator. Operating with subcriticality makes the ADS safer and potentially reduce the risk of developing high temperatures in the core enough to melt the fuel.
- **Reduced Nuclear Waste**: With the help of nuclear fuel transmutation process, the long-lived radioactive isotopes can be converted into short-lived rather stable isotopes. These short-lives rather stable isotopes relatively decrease the cooling requirements of spent fuel pool as well as other stringent conditions necessary to be maintained in the storage facility. This could potentially lead to the reduction of the required storage time for nuclear waste from thousands of years to a few centuries.
- **Fuel Flexibility:** The ADS has the potential to use many types of nuclear fuels. For-example, the conventional nuclear reactor fuels such as uranium and thorium can also be used in ADS. As conventional fuels are readily available so they can be employed without disturbing the supply chain. Additionally, the ADS can also use certain types of nuclear waste, to generate energy. This flexibility in fuel selection facilitates even better resource utilization and the potential conversion of existing nuclear waste into useful fuel. It may also be noted that use of different fuels may require new fuel fabrication techniques as well as technology. The ADS also uses less fuel than conventional reactors making is relatively safer when it comes to accidents like loss of coolant.
- **Improved Proliferation Resistance:** Proliferation resistance refers to the ability to restrict diversion of nuclear fuel or technologies for the purpose of nuclear weapons proliferation. As ADS operates with subcritical reactor, consumes less fuel, and generates relatively less radioactive waste, so it significantly contributes to proliferation resistance. The ADS can be successfully operated with thorium fuel, which makes it less desirable for production of weapon grade fissile material. However, it is important to uphold comprehensive safeguards, international cooperation, and stringent non-proliferation measures including ADS.
- **Load Following and Grid Stabilization:** Load following refers to the ability of the reactor to adjust its power output in regard with grid demand. In this domain ADS offers better control because power output can be adjusted by modulating the accelerator's neutron beam. This feature makes ADS suitable power generation with improved and fine stability. Through fast response and provision of ancillary services like frequency and voltage regulation, ADS has the potential to significantly contribute to grid stability and effective control. ADS can also be coupled with renewable energy resources. Renewable energy resources provide intermittent power. During the period of high-power generation, extra power can be used in particle accelerator. It may also be noted that deployment of ADS in energy generation systems needs further research, technological advancement, and operational strategies.

- **Higher Thermal Efficiency:** Thermal efficiency refers to percentage of heat from a nuclear reaction that is converted into electricity. The ADS can operate at relatively high temperatures as compared to conventional nuclear power plants. Moreover, improved heat transfer, use of advanced coolants such as supercritical carbon dioxide (sCO_2) or liquid metals like lead or lead-bismuth, and potential use of waste heat recovery system makes ADS design suitable to generate higher thermal efficiency.
- **Research and Development Opportunities:** The ADS technology offers diverse range of applications. It can offer further research and development in nuclear science and engineering. With the help of particle accelerators, the characteristics of advanced materials as well as nuclear fuels can be explored extensively. Moreover, the process of transmutation and waste management techniques can contribute to advancements in the field of nuclear energy. The collaboration among academia, funding & research institution, government is necessary is overcome the challenges associated with successful deployment of ADS.

The ADS designs present relatively increased flexibility as well as diversity in fuel composition without compromising safety. The advantage of using ADS is their ability to use non-fissile and non-conventional fuels such as Thorium. The dependance on conventional fuels such as Uranium and Plutonium can be limited because conventional fuels also pose threat of proliferation. Furthermore, the safety of ADS stems from the system's inherent property of shutting down upon deactivation of particle accelerator. The ADS also maintains sufficient criticality margin, thus not inducing reactivity related transients. The severe accidents caused by super criticality in conventional reactors can be effectively avoided. It also offers adjustable fuel burn-up by modulating the accelerator's particle beam and achieves fine power control.

The subcritical nature of the reactor employed by the ADS mitigate the concerns of power excursions. The accelerators offer better solution to manipulate power and flux as compared to conventional nuclear reactors where control rods are used as neutron absorption material. In accelerator driven sub-critical reactors the source neutrons (spallation neutrons) and the fissile fuel (fission neutrons) are not directly linked with each other. Due to this phenomenon, ADS operation is relatively safer and reliable [22, 23].

Recently, a lot of research as well as developmental work is in progress on ADS subsystems such as charged particle accelerators and finding the suitable target materials. However, there is still needed to expand the scope of this research to the development of particle accelerators which can handle very high energy beams. The further details on important projects as well as research will be shared later in this chapter.

Despite having numerous advantages, there are also some disadvantages as well limitations involved in the deployment of ADS based systems. Some of the disadvantages are given below.

Some of the disadvantages [23, 24] are:

- **Complexity and cost:** The ADS designs employ many technologically advanced systems like particle accelerators and spallation reactions on target materials. The most challenging part is development of high energy particle beams with precise control and energy. It involves advanced engineering and precise calculations. Moreover, selection of target material with appropriate properties to withstand high energy beams, manage excessive heating and provide cooling is quite challenging task. Moreover, to house all these main components, there is also requirement of infrastructure. To establishment of a fine control in each components adds a layer of complexity and cost in ADS design.

- **Energy efficiency:** Despite having high thermal efficiency, ADS design can have lower energy efficiency compared to traditional nuclear reactors. The particle accelerator requires a huge amount of energy as well as cost in ADS design. While in conventional reactors, a separate neutron source is not required to maintain the self-sustaining reaction. Therefore, ADS design itself consumes a huge amount of energy. This energy demand can offset some of the energy produced by the reactor, reducing the overall net efficiency.
- **Limited fuel options:** The ADS primarily requires specialized processing of the fuel to make it suitable for spallation reaction. It may restrict the flexibility of ADS in terms of readily available fuel supply.
- **Neutron flux:** The ADS produces high energy particles flux which can cause radiation damage to the reactor components. Furthermore, the gradual damage to reactor components may require costly maintenance.
- **Accelerator Reliability**: The continuous functioning of ADS depends solely on the efficient and reliable working of particle accelerator. Any deficiency in the operation of particle accelerator will also shut down the whole system. To ensure long-term reliability and availability of the accelerator system, it is a critical to establish the continuous working of particle accelerator which is quite challenging.
- **Neutron Source Complexity:** The neutron source or spallation is one of the main components of ADS design. The target material may not perform the intended functions due to long exposure to the high energy particles and partial degradation over time. It may also require replacing the target material periodically. The complexity stems from the establishment of precise and controlled specific neutron spectrum suitable for target material.
- **Limited Operational Experience:** In the case of conventional nuclear self-sustaining reactor, a lot of research has been concluded. Hundreds of reactors are in operation in the world. While in case of ADS, there is no full-scale ADS based system in operation in the world today. Lack of operational history and uncertainty discourages the investors to venture in this new world.
- **Radioactive Waste Management:** The sub-critical reactor based on ADS may be relatively safer for the environment and human health as compared to conventional nuclear reactors. It may also offer a substitutional benefit, but it still generates the radioactive waste. The safe handling and successful final disposal of radioactive waste will surely be a point of concern for many.
- **Development and Deployment Challenges:** Limited commercial deployment and lack of experience feedback pose a big challenge in order to ensure the reliable operation of the ADS. The ADS technology is relatively not as mature as technology associated with conventional reactor is. Therefore, it may require a significant amount of time to build confidence in this technology and to shift it from the research stage to commercial viability.

1.4 ADS research and development

- **KURRI Research Project:** This ADS experiment began in March 2009 at the Kyoto University Reactor Research Institute (KURRI). The research project was commissioned by Japan's Ministry of Education, Culture, Sports, Science and Technology (MEXT) six years earlier. The experiment involved irradiation of a heavy metal target installed inside the critical node with a 100 MeV proton beam from the accelerator, which generated neutrons because of spallation of the nucleus of subcritical fuel [25].

- **LEHIPA and The Purnima Subcritical Facility:** LEHIPA (Low Energy High-Intensity Proton Accelerator) is a research initiative by the Bhabha Atomic Research Centre (BARC) in Mumbai, India. The accelerator program is focused on the development of a powerful (high-energy) proton accelerator for various scientific and industrial applications. The target energy and current will be 1 GeV and 30 mA, respectively. The first stage, presently under development is a 20 MeV (30 mA) Linac injector, the Low Energy High-Intensity Proton Accelerator (LEHIPA). LEHIPA consists of a 50 keV proton ion source. The first two segments of the LEHIPA-RFQ (Radio Frequency Quadrupole) have been commissioned with a proton beam accelerated to 1.24 MeV. This project also includes building experimental facilities to study the properties of these particles [26].

  The Purnima Subcritical Facility is a research facility in BARC, that was designed to study nuclear materials under extreme conditions. It operates at subcritical levels. The main target of the facility is research on nuclear materials' behavior under high pressure, temperature, and interactions with high-energy particles. The Purnima Subcritical Facility is equipped with experimental apparatus, safety systems, and detectors, that can provide safety and controlled specific experimentation.

- **C-ADS:** The China Accelerator Driven Subcritical System (C-ADS) is an ADS project, led by the Institute of High Energy Physics (IHEP) of the Chinese Academy of Sciences. The primary objective of this research is to develop a subcritical reactor system driven by a high-energy proton accelerator. The C-ADS project involves constructing a 1.5 GeV proton accelerator with a beam power of up to 10 MW. In February 2021, the successful commissioning of a 10 mA, 205 kW continuous-wave (CW) proton beam at an energy of 20 MeV, marked a significant step in the project's progress.

  The idea is to sustain fission reactions in a subcritical reactor core (comprising of lead-bismuth-cooled core surrounded by a fertile material blanket) with generated neutrons (that are absorbed by the fertile material in the blanket). This whole process is achieved with the help of controlled high energy particle beam (electron or proton) pointed at a spallation target (heavy metal). This process can produce energy and transmutes nuclear waste, as a result, reducing its volume and radiotoxicity. This system can also employ highly abundant non-fissile fuels such as thorium, which generates less radioactive waste. "CAFe is the world's first CW superconducting proton linac stepping into the hundred-kilowatt level". With further investment and development, it has the big potential to drive substantial advancements in science, industry, and medicine [27].

- **MYRRHA Project:** Multifunctional Hybrid Research Reactor for High-tech Applications is currently the largest and the only planned ADS project in Europe [13]. This is an advanced research initiative led by the Belgian Nuclear Research Centre

(SCK CEN) and its international partners. The MYRRHA project is unique in a way that it is the first innovative reactor in the world to use a lead-bismuth eutectic as its primary coolant and a thermal capacity of 50-100 MW. It is designed as a system that uses an accelerator to operate in subcritical and critical modes. The MYRRHA will promote the development of technologies in the field of energy, nuclear medicine, industry, renewable energy resources infrastructure for diverse applications, nuclear materials, waste management, medical isotope production, neutron imaging, and non-destructive testing. In addition, what makes MYRRHA unique, compared with other reactor prototypes is its hybrid nature, utilizing the advantages of conventional fission-based and fission reactors. This kind of approach significantly enhances safety, sustainability, energy output, and fuel efficiency [28].

- **The European Spallation Source (ESS) Research Facility:** The European Spallation Source is a research facility for conducting experiments using neutron scattering technology located in Lund, Sweden. It will be a state-of-the-art neutron source using spallation. The experiments are planned to be performed on a 600-meter linear accelerator accelerating protons to high energies and colliding them with a heavy metal (tungsten target) to generate intense neutron beams. As a result of the interaction of the nuclei of the target material with the accelerated particles, the fission of these nuclei and the emission of neutrons will occur. These neutrons will be captured by highly sensitive sensors that will measure their characteristics. These beams will enable studies of atomic and molecular structures in various scientific disciplines. The ESS, a collaboration between 13 European countries, has a budget of over €1.8 billion and aims to be completed in 2025 [29].
- **JINR (Joint Institute for Nuclear Research):** The JINR is a research institute located in Dubna, Russia. Several studies have been conducted on the irradiation of small targets on direct proton beams in order to study the physical aspect of nuclear power generation and transmutation of radioactive waste from reactors using high-energy beams which is generated by Phasotron. The fundamental experimental facilities of JINR are primarily the Nuclotron (accelerator of light and heavy ions), cyclotrons U-400 and U-400M. They are used for the synthesis of super heavy elements and light exotic nuclei DC280 for superheavy element synthesis, IBR-2 pulsed neutron reactor, and Phasotron proton accelerator. A new experimental facility – Baikal neutrino telescope (Baikal-GVD) and collider NICA are under construction [30]. The JINR has executed significant contributions to nuclear physics, including the discovery of elements like dubnium, seaborgium, and hassium. It collaborates with global organizations such as CERN and Fermilab. This collaboration fosters international scientific cooperation and is essential for advancing knowledge of matter and the universe.
- **NSC KIPT Accelerators:** Subcritical Assembly Neutron Source, which was constructed in NSC KIPT, Kharkiv, Ukraine, specializes in particle accelerator design, construction, and operation. Research in this institution has been focusing on advancing accelerator technology for scientific research, including technology applications, and medical purposes. The electron linear accelerator, the driver of the SA, was designed and manufactured at the Institute of High Energy Physics (IHEP), Beijing, China. In 2022, the accelerator was assembled in NSC KIPT and was under beam commissioning and tests. Future of this project in unclear now [31].
- **Electron Linear Accelerator:** The Institute of High Energy Physics (IHEP) is a prominent research institution located in Beijing, China. One of its notable accomplishments is the design and manufacturing of the electron linear accelerator,

which serves as the driver of the Synchrotron Radiation (SA) facility. Linac is used in a wide variety of applications including the study of particle physics, radiation therapy, non-destructive testing, material research, and fundamental research. The expertise and technological advancements achieved by IHEP in accelerator physics have played a significant role for the development of advanced research facilities and the promotion of scientific collaborations nationally and internationally [32].

- **J-PARC Transmutation Experimental Facility (Japan):** The Japanese project called the Transmutation Experimental Center (TEF) [33] is part of the Japanese Proton Accelerator Research Complex (J-PARC) project. The TEF consists of two individual facilities: ADS Target Test Facility (TEF-T) and Transmutation Physics Experimental Facility (TEF-P). The TEF-T is equipped with a liquid lead-bismuth spallation target bombarded by a 400 MeV - 250 kW proton beam in which candidate proton beam window materials of the ADS are to be irradiated. The main goal of the J - PARC TEF is to carry out research on transmutation technology, which involves the conversion of long-lived radioactive isotopes into shorter-lived or non-radioactive isotopes. The system focuses on three areas of research: 1) Physics of reactors of subcritical systems and fragmentation targets. 2) Control of subcritical system and power by means of the external accelerator. 3) Transmutation of the power of the subcritical nucleus using a given number of minor actinides and long-term fission products. Overall, the J-PARC (TEF) is one of the most advanced transmutation research facilities in the world. The research has the big potential to significantly reduce the environmental impact of nuclear waste.

- **Venus I, II, III Projects:** The projects emphasize the development of liquid metal-cooled fast reactors (ADS technology) at the Institute of Nuclear Energy Safety Technology (INEST), Chinese Academy of Sciences. In July 2005, China started building at China Institute of Atomic Energy (CIAE), the first fast thermal-coupled accelerator-driven system (ADS) sub-critical reactor - Venus I, which was completed in 2010. It consists of a 4 MWt subcritical lead-bismuth cooled core coupled to a 7 MeV, 10 mA proton accelerator. Venus II, launched in 2011, aimed to develop a larger-scale facility capable of producing 10 MWt for multiple purposes. The project completed in December 2016. Another part of the project, Venus III started in 2016, which focuses on designing a commercial scale 1000 MWt ADS system for electricity generation and waste transmutation. The institute carry out a series of tests to obtain data on the core parameters that can be used in the development of high-power proton accelerators, subcritical lead-bismuth-cooled cores, and safety/control systems [34].

- **THOR:** THOR (Thermal Hydraulics of innovative nuclear Reactors for safety) is a research project, funded by the European Commission. It focuses on studying the thermal-hydraulic behavior and safety of innovative nuclear reactor designs, including ADS. It especially aims to enhance the understanding of heat transfer, fluid flow, and associated phenomena in ADS. The THOR project may vary depending on the participating organizations, funding sources, and the specific objectives of each research phase. Moreover, the main goal remains the advancement of thermal-hydraulics knowledge for the safety and efficiency of innovative nuclear reactors [35].

1.5 Nuclear transmutation

“The basic process of accelerator driven systems is nuclear transmutation”.

Transmutation - is the transformation of one element (or isotope) into another during radioactive decay or after bombardment with high-energy particles. The purpose of using nuclear transmutations is, above all, a reduction in the number of long-lived radionuclides remaining in spent nuclear fuel (SNF) after irradiation of fresh nuclear fuel in nuclear reactors. Almost any nuclear radiation can be used for transmutation, but neutrons give the greatest efficiency due to the absence of a Coulomb barrier and large interaction cross sections.

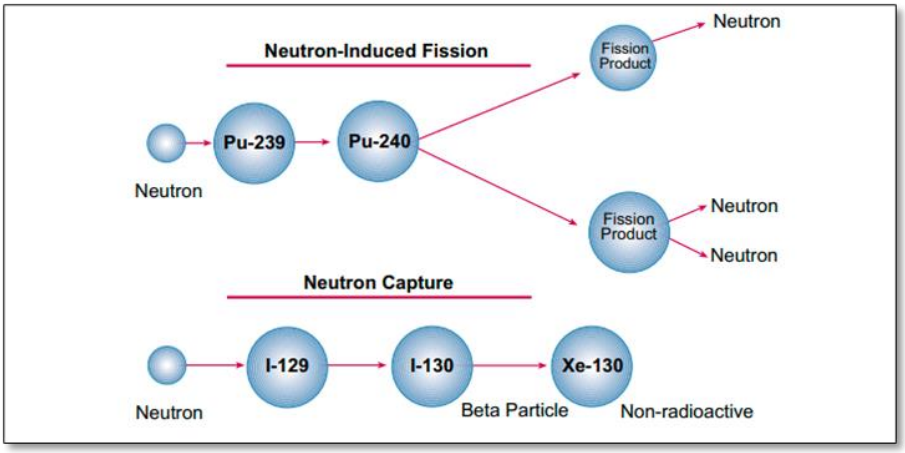

Fig.1.4. Two examples of transmutation [12].

Nuclear transmutation finds diverse applications in nuclear science and technology, encompassing areas such as nuclear waste management, production of medical isotopes, and nuclear fuel generation. One of the key advantages of nuclear transmutation is its capacity to transform radioactive waste into less harmful or potentially non-radioactive substances, thus aiding in the safe disposal and long-term management of radioactive materials.

Within the realm of nuclear waste management, transmutation offers a means to decrease both the volume and radiotoxicity of nuclear waste. This process involves subjecting the waste to irradiation using high-energy particles, such as neutrons. As a result, the radioactive isotopes present in the waste undergo transmutation, transforming into more stable or less hazardous isotopes.

Transmutation can also serve as a valuable technique for the production of medical isotopes utilized in the diagnosis and treatment of various diseases, including cancer. By subjecting specific target materials like uranium or thorium to irradiation with high-energy particles such as neutrons, it becomes possible to generate specific isotopes that hold significance in medical applications.

In addition to its role in nuclear waste management and medical isotope production, transmutation has the potential to be utilized for the production of nuclear fuels. By employing transmutation techniques, such as converting thorium into uranium, it becomes feasible to generate nuclear fuel sources that are not only more abundant but also hold the promise of enhanced safety compared to conventional uranium-based fuels [23].

Nuclear transmutation stands as a significant domain of research and development within the field of nuclear science and technology, holding the promise to foster significant progress in energy production, waste management, and medical applications. Its potential

impact across these domains underscores its importance and the ongoing efforts dedicated to advancing this field.

In the context of radioactive waste management, transmutation plays a significant role, particularly in subcritical systems controlled by accelerators. These systems utilize long-lived components of radioactive waste (RAW), primarily minor actinides (MA) such as isotopes of Np, Am, and Cm. These isotopes are crucial for transmutation processes. Subcritical systems effectively capture and utilize a portion of the neutrons present in the neutron energy spectrum for transmutation purposes. Minor actinides are considered the most dangerous because of their toxicity.

In addition to minor actinides, subcritical systems can destroy fission products. The main problem is long-lived fission products, such as ^{99}Tc and ^{129}I, which pose the greatest danger in terms of long-term (several thousand years) safe storage of radwaste.

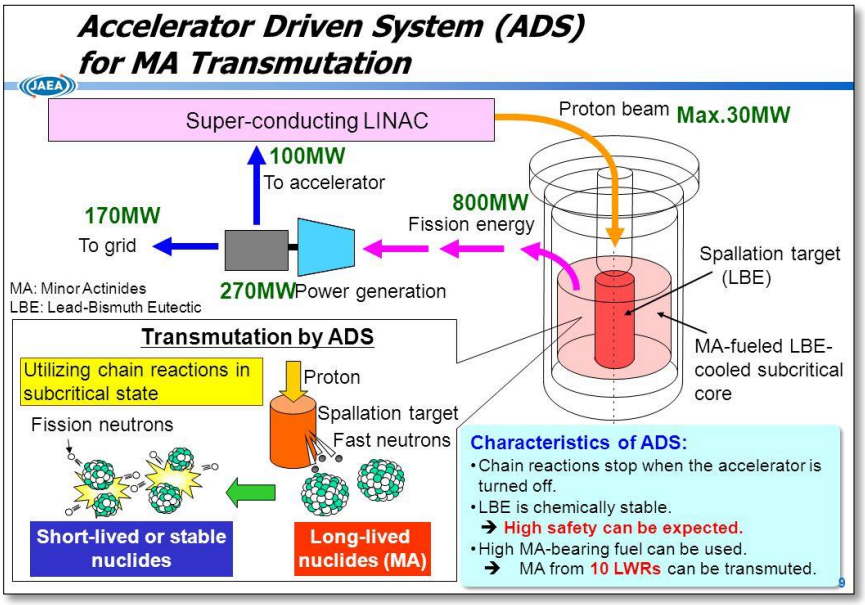

Fig.1.5. Using ADS for MA transmutation [36].

Transmutation is a promising strategy for reducing the long-term risks associated with nuclear waste, however, several problems of this strategy must be considered:

- **Technical feasibility:** Scaling transmutation technologies up to commercial-scale systems may be challenging because they have been developed and tested in laboratory and prototype settings, only. These systems will need to operate reliably and efficiently for long periods of time, another hand, it must be potential to process large amounts of nuclear waste. In additional, some LLFPs due to their small neutron capture cross sections are not able to capture enough neutrons for efficient transmutation.
- **Cost:** Transmutation technologies are limited by the expensive and cumbersome need to separate LLFP isotopes before they can undergo transmutation. In addition, it is likely to be expensive to develop, construct and operate new facilities, as well as the transportation and handling of nuclear waste.

- **Safety:** Careful attention to the design and operation of these systems can improve the safety of the system and can minimize the risk of accidents or unintended releases of radioactive materials.
- **Regulatory and policy issues:** The development and deployment of these technologies will require regulatory approval and may be subject to public scrutiny and opposition. Moreover, there may also be legal and policy issues related to the ownership, transportation, and disposal of nuclear waste.
- **Limited applicability:** Transmutation technologies may not be appropriate for several types of radioactive waste, because some isotopes may be difficult or impossible to transmute. Additionally, these technologies may only be effective for reducing the long-term risks associated with nuclear waste, which means short-term storage or disposal solutions might still be necessary.

Transmutation holds promise as a strategy for reducing the long-term risks associated with nuclear waste. However, a careful comprehensive approach must be given to the technical, economic, safety, regulatory, and policy issues involved [37]. More research and development are needed to optimize transmutation technologies and ensure their safety and effectiveness.

1.6 Nuclear waste

Radioactive waste (RW) is generated at all technological stages of the nuclear fuel cycle i.e., in the extraction and processing of uranium ore, in the manufacture and use of nuclear fuel, regeneration of irradiated fuel, and finally decommissioning of nuclear facilities.

Radioactive waste refers to material that contains radioactive isotopes or radionuclides that can't be reused and must be safely disposed of. Nuclear power plants together with other facilities e.g., medical & industrial processes, and research institutions are the main sources of radioactive waste.

Normally, radioactive waste is divided into two main categories: low-level waste (LLW) and high-level waste (HLW). The LLW typically refers to radioactive waste which have low concentrations of radioactive isotopes and can include materials such as contaminated protective clothing, tools, secondary reactor components and laboratory equipment [38].

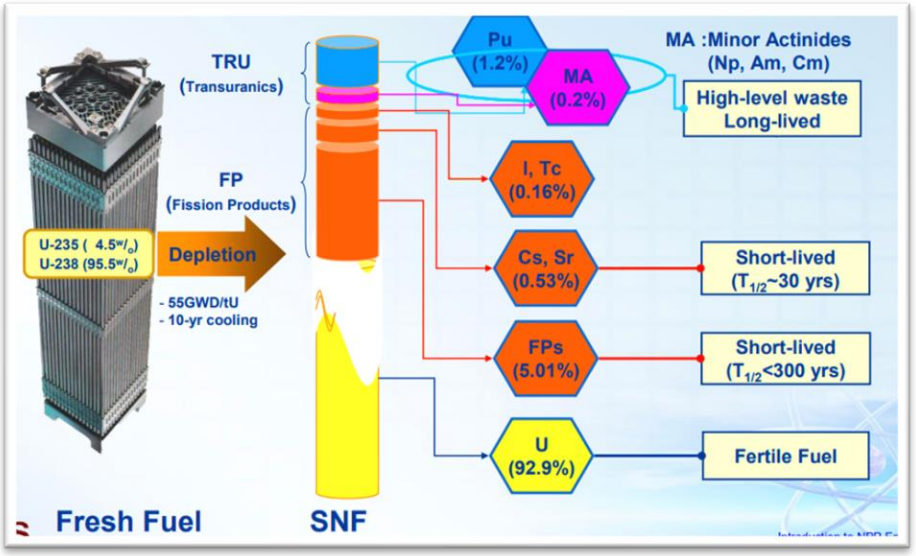

Fig.1.6. PWR Spent Nuclear Fuel [39].

High-level waste, on the other hand, contains much higher concentrations of radioactive isotopes and is typically generated during the reprocessing of spent nuclear fuel in nuclear reactors or nuclear weapons production facilities. It consists of fission products and transuranic elements such as plutonium and minor actinides.

Compared to HLW, LLW contains short-lived radionuclides which generally are less hazardous. While HLW is characterized by their high levels of radioactivity and long half-life periods.

Radioactive waste is hazardous and poses a significant risk to human health and environment. The exposure to high levels of radiation can cause damage to cells and tissues, leading to increased risk of cancer and other health problems. Radioactive waste can release into the environment (the air, water, soil, flora, and fauna etc.,) through accidents, leaks, and improper handling during storage, transportation, and reckless final disposal.

The primary objective today is to mitigate risks to human health and the environment while addressing regulatory concerns associated with radioactive waste. This involves enhancing storage, incineration, and burial methods in specialized facilities tailored to the specific type and level of radioactivity. Despite these improvements, there remains a potential for radioactive releases. To further contain this risk, ADS technology can be utilized to reprocess nuclear waste, making it suitable for various useful applications beneficial to various industries. Additionally, ADS reprocessing offers a substantial reduction in the generation of final waste that requires disposal.

1.7 Fission fragments

Fission products are generated by the fission of ^{235}U or ^{239}Pu to transmute them to stable nuclides; they should capture one or more neutrons and then undergo β-decay. Higher actinides or transuranic elements are formed due to the capture of neutrons in ^{235}U, ^{238}U, or ^{239}Pu nuclei and their resulting β-decays. To transmute higher actinides into stable nuclides, they must undergo neutron capture and sequential fission, a process that produces energy and makes transmutation attractive in terms of energy.

Fission products are the radioactive isotopes, which are typically highly radioactive and can remain so for hundreds or thousands of years. In fission process, a neutron deposits its energy into a heavy nucleus and split it into two isotopes by releasing a large amount of energy in the form of gamma rays as well as further neutrons (see Fig.1.7). The newly created nuclei are highly unstable and may undergo radioactive decay, thus releasing additional particles and energy in the form of alpha, beta, and gamma radiation. This induced fission reaction can be written as:

$$FM + n \rightarrow FF_1 + FF_2 + (2-4)n, \tag{1.1}$$

where FM represents fissionable material (such as $^{235}_{92}U$), n is the neutron, and FF_1 and FF_2 are the two fission fragments.

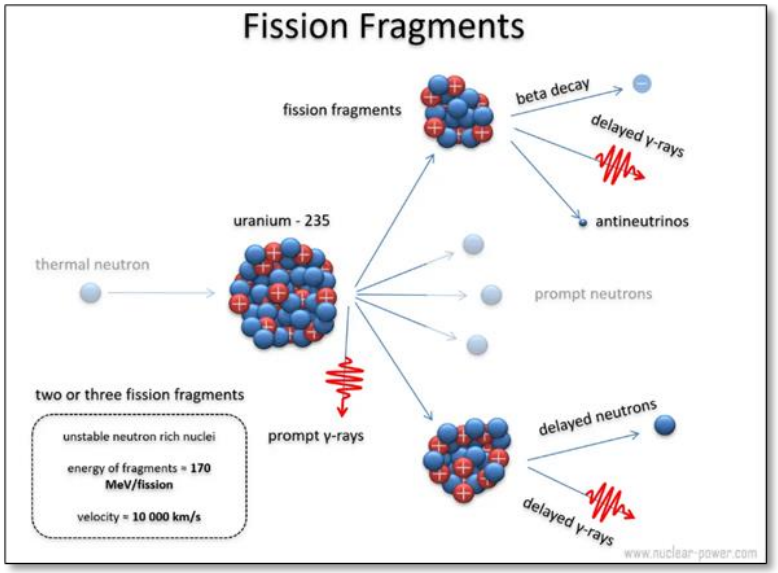

Fig.1.7. Pictorial representation of fission fragments [40].

Production of fission products by nuclear fission can vary with respect to type of fuel, the neutron energy, and other factors. The most common isotopes of fission reactions are cesium, strontium, and iodine. Fission products are treated as a significant source of radiation and pose a great risk to human health and are hazardous to the environment. Safe disposal of fission products is posing a challenge for the nuclear industry and needs additional research and technology development to ensure that highly radioactive and dangerous waste can be safely handled.

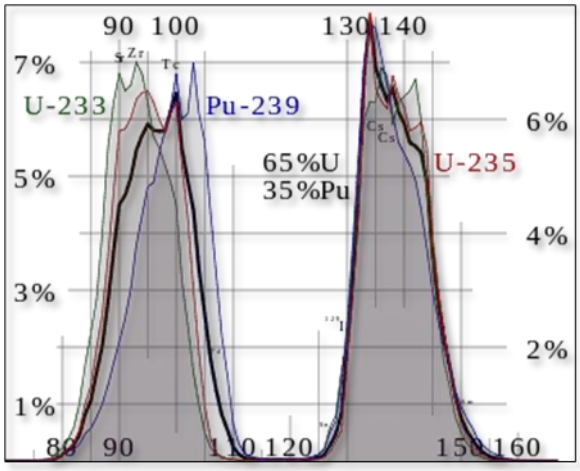

Fig.1.8. Fission fragment yield for different nuclei [40].

Products	Emitted energy (MeV)
Prompt energy:	
Fission fragments	168
Fission neutrons	5
γ emission	7
Radioactivity:	
β decay (electrons)	8
β decay (neutrinos)	12
γ emission	7
Total	207

Fig.1.9. Energy from Uranium Fission [40].

The most probable fragment masses are around mass 95 (Krypton) and 137 (Barium). Most fission products of uranium have either mass number (90 - 100) or mass number (130 - 140). Lighter FF (~100 MeV) has more energy than heavy FF (~68 MeV).

Fission products and minor actinides with half-life expected for transmutation are:

Technetium-99 has a half-life of approximately 211 000 years, which is the most significant long-lived fission product of uranium. Due to long life, it also poses challenge in the form of long-lived radioactive waste. During the thermal fission of ^{235}U, ^{99}Tc production yield is 6.0507%. Due to this, it is a potential target for transmutation using ADS.

Plutonium-239 is a one of the three main isotopes (others are ^{235}U and ^{233}U) demonstrated usable as fuel in thermal spectrum nuclear reactors. It's a strong alpha-particle source with half-life about 24 1100 years. It can be transmuted into less dangerous materials through a process named "burning". This higher actinide produced in nuclear weapons and can be used as a fuel or can be reprocessed and used for the construction of nuclear explosive devices.

Americium-241 is a synthetic radioactive actinide that is produced in nuclear reactors. Same as ^{239}Pu, it is a potent alpha-particle emitter and has a half-life of 432.2 years. It is used in different applications, such as smoke detectors, industrial gauges, and neutron sources. It could be one of the potential materials for transmutation by ADS.

Neptunium-237 is a higher actinide with a half-life of about 2.14 million years which is a strong alpha-particle emitter. It is considered a significant contributor to the long-term radioactivity of nuclear waste. It is produced as a byproduct in nuclear reactors and is usually considered a waste product itself. It can be transmuted into less dangerous isotopes by "burning".

Cesium-137 is a radioactive isotope found in nuclear waste which is produced as a byproduct of nuclear fission, primarily in nuclear reactors and nuclear weapons detonations. Its half-life is about 30.07 years and is a potent strong γ - emitter. It is also one of the many targets on which transmutation in ADS is aimed.

Transmutation is a very perspective and promising technology which can help reduce the risks posed by nuclear waste by converting dangerous isotopes of such materials into their less dangerous or even non-radioactive stable isotopes, further research, and development of this kind of technology is required to ensure its effectiveness and mostly the safety.

Table 1. Fission products and higher actinides with a half-life expected for transmutation [41].

Fission product	Half-life [years]	Higher actinide	Half-life [years]
^{79}Se	1.13×10^{6}	^{237}Np	2.144×10^{6}
^{90}Sr	28.79	^{241}Am	432.2
^{93}Zr	1.53×10^{6}	^{243}Am	7.37×10^{3}
^{99}Tc	2.11×10^{5}	^{244}Cm	18.10
^{126}Sn	$\sim1\times10^{5}$	^{238}Pu	87.7
^{129}I	1.57×10^{7}	^{239}Pu	2.411×10^{4}
^{137}Cs	30.07	^{240}Pu	6.563×10^{3}
^{107}Pd	6.5×10^{6}	^{241}Pu	14.35
		^{242}Pu	3.733×10^{5}
		^{234}U	2.455×10^{5}
		^{235}U	7.038×10^{8}
		^{236}U	2.342×10^{7}
		^{238}U	4.468×10^{9}
		^{245}Cm	8.5×10^{3}
		^{246}Cm	4.73×10^{3}
		^{247}Cm	1.56×10^{7}
		^{248}Cm	3.4×10^{5}

Dose rate is one of the main characteristics of spent fuel. Approximately 95% of the dose rate is due to gamma radiation of fission products, the rest is accounted for by the share of accumulated actinides. The greatest contribution to the dose is made by short-lived isotopes of Zr, Nb, Mo, Tc, Ru, Rh, I, Cs, Xe, Ba, La, Ce, and Pr.

Short-lived isotopes are radioactive substances with relatively short half-lives, typically lasting seconds, minutes, or days. These isotopes emit a substantial amount of radiation within a brief period, posing risks to both human health and the environment.

However, when considering the overall contribution of short-lived isotopes to the total radiation dose received by individuals or populations, their impact is often relatively minor.

Due to their short half-lives, these isotopes decay rapidly and tend to remain localized, limiting their potential consequences. On the other hand, long-lived isotopes like ^{137}Cs and ^{90}Sr, with half-lives of 30 years and 29 years respectively, continue to release radiation for extended periods, posing significant hazards to human health over time.

The initial radioactivity of spent fuel primarily arises from short-lived by products of nuclear fission, while actinides become the dominant contributors after several hundred years of storage. Over the course of several hundred thousand years, the radioactivity of spent fuel gradually diminishes to the equilibrium level observed in natural uranium used for fuel production. However, the processing of spent fuel, involving the extraction of uranium and plutonium, significantly reduces this timeframe to several tens of thousands of years [41].

1.8 Spallation reaction

A spallation reaction is a type of nuclear reaction in which a particle with very high energy (a proton, a neutron, etc.) bombards a heavy nucleus – target, for instance, uranium, lead, or mercury. This particle transfers some energy to the target nucleus, causing it to become excited and split (Fig.1.10) due to inelastic nuclear reactions. Resultantly, it releases a large amount of energy and produce a variety of several fragments including neutrons, protons, α-particles, and other nuclear fragments. Additionally, it also produces isotopes that can be used for a variety of applications, such as medical imaging, cancer therapy, and other industrial processes. Due to the high neutron yield and ease of their production, the use of protons minimizes the energy cost of generating neutrons.

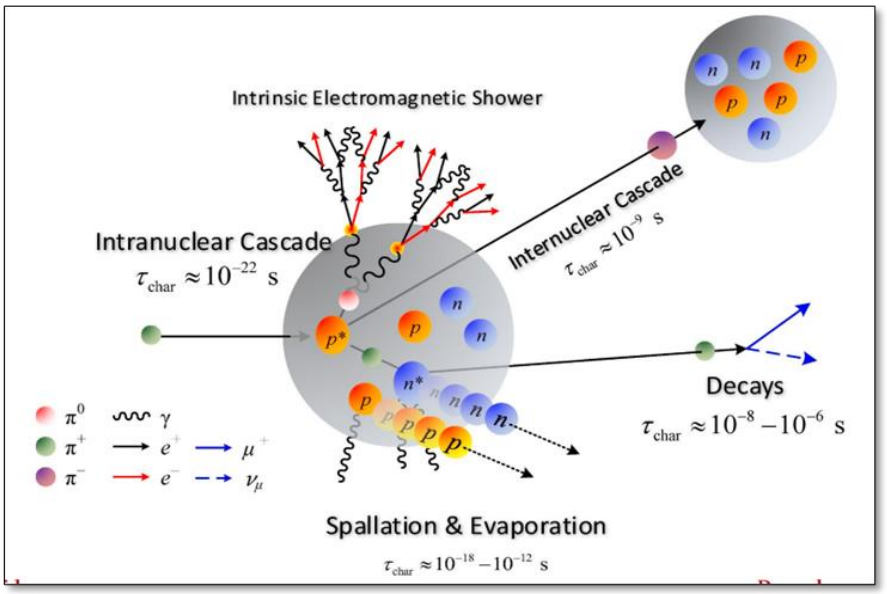

Fig.1.10. Processes during Spallation & Evaporation [42].

Spallation reactions are used in a variety of applications. Primarily, they are used for study the properties of nuclei and the behaviours of nuclear reactions in nuclear research facilities and to produce isotopes in medical centres and industrial facilities.

One example of a spallation reaction facility is the Spallation Neutron Source (SNS) located at Oak Ridge National Laboratory in the United States. The SNS uses a linear accelerator to accelerate protons with an energy of 1 GeV to produce neutrons for a variety of scientific experiments and applications [43].

The interaction of the spallation reaction with the proton can be presented in the form:

$$p + ST \rightarrow SF1 + SF2 + \cdots + SF_m + (k_1)\, n + (k_2)\, p, \qquad (1.2)$$

where ST is the target of spallation, SF represents “m” fragments of spallation, and k_1 is the number of neutrons, k_2 is the number of protons. The number of neutrons generated depends on the type of target and the energy of the incident particles [44].

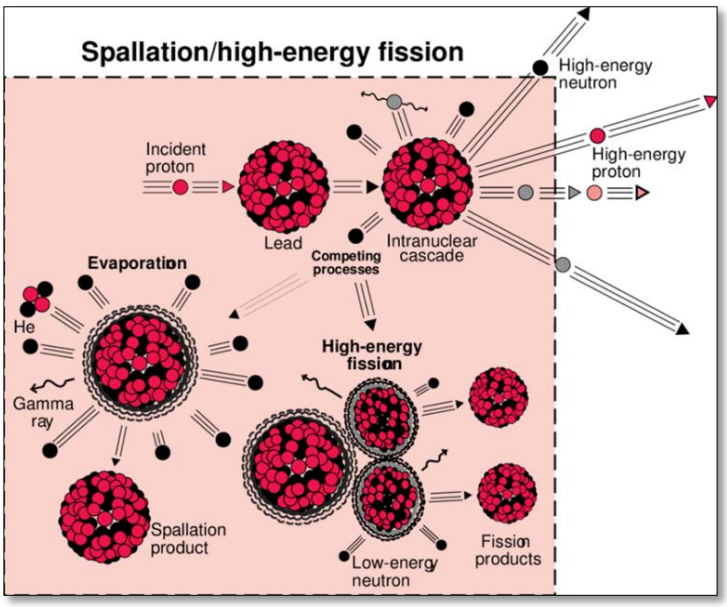

Fig.1.11. The scheme of a spallation reaction [45].

The spallation reaction can be divided into several phases, each with its own characteristics and mechanisms.

Phases of the spallation reaction:

- **Intra-Nuclear Cascade (INC) (pre-equilibrium phase)** [46]: This phase is characterized by a rapid energy transfer and can occur in around 10^{-22} seconds. In the first stage, the high-energy particle reacts with nucleons-neutrons and protons, inside the nucleus and transfers some of its energy to the nucleus. The nucleus becomes excited and may emit one or more nucleons (neutrons or protons) before it reaches equilibrium. The emission of nucleons during this phase is called pre-equilibrium emission.

  These reactions set off a chain of events deep within the nucleus, like a series of energetic fireworks, with protons, neutrons, and pions all having energy greater than 20 MeV. In this "nuclear dance", some of these speedy particles manage to break free as secondary particles, while others slow down and share their energy with the nucleus, leaving it in an excited state.

  As a matter of fact, the de Broglie wavelength interacts with individual nucleons in the target nucleus the projectile shares its kinetic energy with the target nucleons by elastic collisions, and the cascade of nucleon-nucleon collisions continues. The size and shape of the INC usually depend linearly on the energy of the incident particle and the number of target nucleons.

- **The de-excitations modes (equilibrium phase, duration: ~10^{-20} - 10^{-16} s):** After the end of the intra-nuclear cascade, when the last nucleon is ejected (once the target nucleus reaches equilibrium), the nucleus remains in the excited state. The de-excitations of the residual nucleus can occur in two main ways: evaporation and fission. The choice between these reactions (fission and evaporation) depends on the size and shape of the nucleus, as well as the amount of excitation energy it has absorbed.

- The evaporation - a special mode of excitation for non-fissile or fissile nuclei, which are excited over the energy required to separate one neutron. In this case, the excited nucleus emits nucleons or light nuclei (D, T, ^{3}He, α, Li, etc.).
- During the fission process (into two fragments similar in proton number), the nucleus changes its shape, first reaching the 'saddle' point where the fission takes place, then the split point, where the nucleus splits into two fragments with different masses.

In addition, de-excitation of the residual nucleus can also occur after-equilibrium phase. In this phase, the residual nucleus undergoes additional reactions, such as gamma-ray emission or further fission or evaporation, until it reaches a stable state. Typically, this phase can take several microseconds or longer, but it depends on the specific reaction and the properties of the residual nucleus.

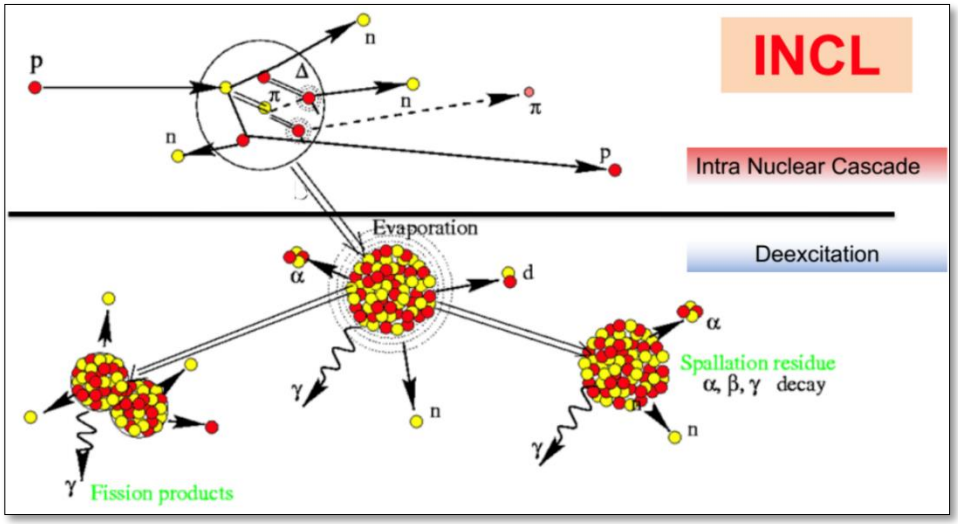

Fig.1.12. Upper part, 1st stage, the intra-nuclear cascade. a proton collides with a nucleus composed of both protons and neutrons, it triggers a reaction that leads to the release of various particles, such as pion (π) and Delta (Δ). The lower part, 2nd step, deals with the de-excitation of the hot remnant nucleus from the cascade. (Example of a reaction processed by INCL [47]).

Photon radiation is also possible during de-excitation. Until the excitation energy of the nucleus falls below the binding energy of the last nucleon, the nucleus will emit particles. At this stage, about 8 MeV energy will be evacuated from the nucleus in the form of gamma radiation. The nucleus formed after gamma decay is often a radioisotope. This radioisotope will decay until a suitable stable nucleus is formed. Therefore, if the gamma radiation ends, it does not mean that the process of de-excitation has taken place [48].

In spallation reactions, the residual nuclei (or spallation products) and the emitted neutrons (or spallation neutrons) play a crucial role.

Overall, the spallation reaction is a complex process that involves several distinct phases, understanding the dynamics of these phases is essential for predicting and controlling the behaviour of spallation reactions. In addition, using spallation reactions is an important tool in nuclear science and engineering, and they have a variety of applications in nuclear energy production, medical isotope production, research, medicine, and industry.

1.9 Spallation targets

A spallation target is a component of a spallation neutron source or accelerator-driven system that is designed to absorb high-energy particles (such as protons) and can generate a big number of neutrons due to spallation reactions. The target material is typically made of heavy metals, such as tungsten or lead, which can withstand the high heat and radiation levels generated by the spallation process.

In general, all heavy materials with high density (for example materials with a high content of Z, such as U, Th, Pb, Ta, W, Hg, etc.), can be used as the targets of spallation source. The greater the atomic number of the element, the greater the number of released neutrons.

The design of a spallation target is crucial for the performance and efficiency of a spallation neutron source or ADS. The target must be able to absorb the high-energy particles without melting or being damaged. Moreover, it must be able to dissipate the heat generated by the spallation process. The target material must be chosen to optimize the production of the desired isotopes or neutron flux, depending on the purpose.

Solid targets for spallation reactions must meet several requirements to ensure their proper functioning and to avoid damage from the high-energy particles involved in the spallation process. Requirements and characteristic for solids targets of spallation reaction are:

- **High melting point:** The spallation targets in particle accelerators undergo severe conditions which they need to endure in order to perform the intended function. One of the most severe conditions is high temperature. Therefore, it is essential for spallation target to endure that high temperature. Having high melting point is one of main characteristics of spallation target. Tungsten, molybdenum, and graphite are the commonly used materials having melting points of 3422°C, 2623°C and 3600°C respectively. (Lead is also considered as a heavy metal, and have a melting point of 327.5°C.)
- **High thermal conductivity:** High thermal conductivity is one of the important characteristics of spallation targets. Materials with high conductivity can effectively transfer heat to the coolant and prevent overheating. Thermal conductivities of Tungsten, Molybdenum and Graphite are 173 W/m·K, 138 W/m·K and 2000 W/m·K respectively.
- **High radiation resistance:** High radiation resistance is another crucial characteristic of spallation target. In order to ensure longevity and performance, spallation target should endure high radiation resistance. The materials should exhibit resistance to displacement damage, retention of mechanical properties, minimal swelling and especially radiation tolerance of crystal structure.
- **High mechanical strength:** Spallation targets are exposed to extreme conditions, therefore should maintain structural integrity and long-lasting performance. They should withstand thermal cycling, mechanical loading, and vibration. Moreover, they also possess high yield strength, ultimate tensile strength, ductility, and structural stability. By having these characteristics, the material can effectively resist deformation or damage caused by the intense conditions during the spallation process.
- **High purity:** For the optimal operation of the spallation neutron source or accelerator-driven system, the target material should exhibit a high level of purity and maximal corrosion resistance. This is necessary to prevent any contamination of the system. Even

minor impurities can have a detrimental impact on the system's performance and efficiency. Additionally, the target material should be easily manufacturable and compatible with joining other materials through processes like welding or upholstery [49].

Additionally, spallation targets should produce neutrons with a wide range of energies, from several eV to several GeV and should be able to generate neutrons continuously or in pulses (nanoseconds). The choice of materials with above mentioned characteristics also depends on factors such as the specific application, operating conditions, and compatibility with other components of the system [50].

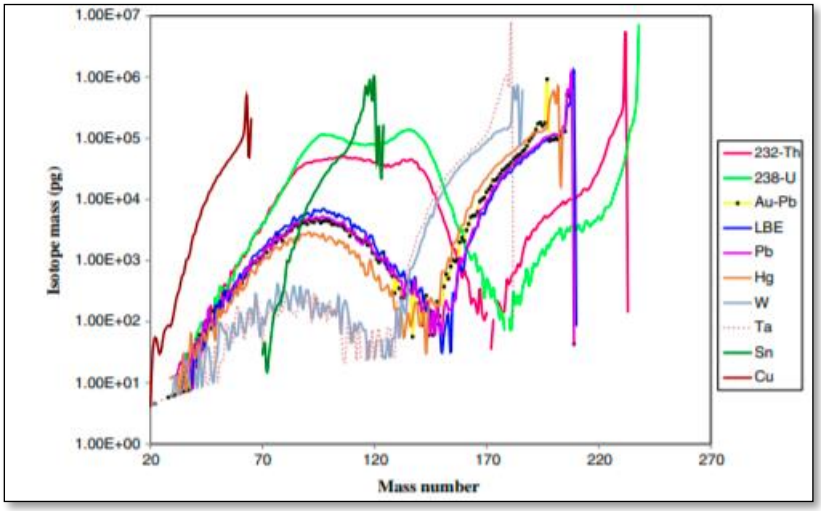

Fig.1.13. Comparison of radionuclide production in different spallation targets. Particles are the protons of energy 1 GeV. Target diameter = 15 cm, length = 60 cm (MCNPX 2.6.0 code) [51].

1.9.1 Characteristics of neutron sources

Spallation neutron sources present several advantages compared to other neutron sources like research reactors or nuclear reactors. These advantages include:

- **High neutron flux:** The high neutron fluxes is desirable property of the neutron source. Due to high flux, more neutrons will be produced for their utilization in diverse applications such as industrial and medical applications. Moreover, high flux is also useful for high resolution neutron imaging, faster data acquisition, increased sensitivity, and short time measurement.
- **Continuous operation:** It refers to the ability to generate and sustain an uninterrupted generation of high energy particles and subsequent release of neutrons. Conventional nuclear reactors require shut down for maintenance of refuelling while ADS offers uninterrupted operation because it can facilitate online refuelling. The continuous operation makes them suitable for experiments requiring constant neutron exposure for extended period of time. Spallation sources reliably produce stable and uninterrupted neutron beam, allowing for prolonged experiments without the limitations imposed by reactor schedules or maintenance requirements.
- **Flexibility:** Spallation sources exhibit a high degree of flexibility, as they produce wide range of neutron energies and intensities which can be customized to suit the

specific requirements of diverse experiments. This flexibility is achieved with the help of introducing adjustment in the intensity of proton beam, as well as bringing the different target materials into use. Such customization options enable a wide range of experiments and applications to be conducted effectively by accommodating diverse research needs and facilitating scientific exploration across multiple disciplines.

- **Safety:** spallation sources offer a higher level of safety due to several factors. Firstly, spallation sources generate relatively smaller quantities of radioactive waste, reducing long-term environmental impact. Secondly, the absence of a self-sustaining chain reaction in spallation sources minimizes the risk of nuclear accidents. Additionally, the utilization of non-radioactive target materials, such as tungsten or lead, further mitigates the potential risks associated with spallation sources. Overall, these safety considerations make spallation sources a favourable choice in terms of radiation safety and accident prevention.
- **Cost-effective:** Spallation sources are potentially advantageous over conventional reactors in term of cost involved due to reduced infrastructure and maintenance requirements. Comparatively simpler design of spallation sources reduces the associated costs for construction and operation. Additionally, spallation sources offer lower operating costs, as they do not employ expensive fuel or intricate cooling systems. These cost-effective characteristics make spallation sources desirable option for neutron research, offering efficient and economical alternatives to conventional nuclear reactor-based facilities.

Additionally, spallation sources offer fine control and synchronization with experiments by the production of pulsed neutron beams. This enables researchers to study dynamic processes and time-dependent phenomena [24]. Moreover, spallation sources generally produce lower levels of background noise, resulting in improved signal-to-noise ratios and enhanced sensitivity for experiments.

1.9.2 Examples of spallation targets

There are several elements which possess the desirable characteristics to be used as spallation targets depending on the specific application and performance requirements. Some common elements used as spallation targets include:

- **Tungsten:** In various industrial and research applications, Tungsten is used as spallation target due to its desirable physical and metallurgical properties (e.g., low corrosion, resistance to radiation damage, good availability, and low cost, etc.). Tungsten also has very high melting point (approx. 3400 °C) as well as better thermal conductivity. Tungsten also has high density (approx. 19.3 g/cm^3) which facilitates efficient energy transfer and more neutron reactions within given volume. However, it was found that tungsten is corroded by water when irradiated, that is why tantalum (Ta) is used as lining material.
- **Tantalum:** Tantalum is another material commonly used as spallation target in industry and research. It has high melting point of around 3.017 °C, easy to process and weld, retains ductility after irradiation, resistant to corrosion and has good neutron yield. It also has high density of approximately 16.6 g/cm^3 which makes it suitable for high neutron productivity within given volume. The disadvantage of such a target is the relatively high neutron absorption cross section, also in the range of

epithermal energy. This leads to high radioactivity and overheating of the targets used.

- **Lead:** Lead also has certain favourable properties to be used as spallation target. It is inexpensive and abundant. It is often used in low- to medium-power spallation neutron sources. However, lead is not considered the best choice because of its low melting point of approximately 327.5 °C. Moreover, low density ($\approx 11.34\ g/cm^3$), less neutron production, susceptible to radiation damage and chemical reactivity makes Lead less favourable option to be used in ADS.
- **Bismuth:** Bismuth has certain advantages to be used as spallation target. It has The properties of good moderator, high neutron production, low activation properties, and availability. However, it also has certain limitation in terms of having low melting point (approximately 271.4 °C), low density compared with tungsten and tantalum, soft and brittle in terms of mechanical properties. Bismuth can be utilized for some specific applications.
- **Mercury:** Though mercury does not possess the best characteristics to be used as spallation target due to its lower density, target stability, radiation damage and corrosion characteristics. However, it is useful for certain specific applications because of its liquid state. This material possesses excellent thermal conductivity, which enables it to transfer heat efficiently, while also exhibiting a low neutron absorption cross section. However, its use is restricted because of being toxic in nature. It requires specialized handling and containment systems.
- **Carbon:** Carbon-based materials such as graphite and diamond are not commonly used as primary spallation target, but they do have certain secondary applications in ADS based systems. They can used as moderator material in ADS designs, secondary target or reflector, and beam windows. Moreover, they also possess good radiation resistance.
- **Uranium:** Natural or depleted uranium also can be used as a spallation target material. Uranium is considered as an element with high atomic number, that makes it effective for producing neutrons through spallation reactions. However, uranium and thorium are less commonly used for spallation compared to materials such as tungsten or lead.
- **Thorium:** Thorium is material that can be used in spallation targets, too. Same as uranium, thorium has a high atomic number and can be applicable for effectively neutrons producing by way of spallation reactions. Now a day, thorium has been considered as a potential nuclear fuel due to its abundance and can be potentially used in advanced reactor designs.

The elements such as iron, copper, and gold, can also be used as spallation target to carry out specific research. The choice of spallation target needs to be evaluated carefully and tailored with respect to the kind of intended function they need to perform. The choice of material depends on several factors such as desired neutron flux, mechanical and chemical properties and especially performance requirements.

1.10 Spallation products

Spallation products refer to radioactive isotopes generated through spallation, a process triggered by the collision of high-energy particles, such as protons, with a target material like tungsten or lead. Upon collision, the nuclei of the target atoms undergo fragmentation, resulting in the release of neutrons, protons, and other particles. These particles, in turn, can collide with other nuclei within the target material, initiating subsequent nuclear reactions and generating additional particles.

The composition of spallation products encompasses a diverse array of radioactive isotopes, contingent upon factors like the target material and the energy level of the incident particles. Among the frequently encountered spallation products are isotopes of elements like cesium, strontium, iodine, and xenon, as well as heavier isotopes of elements like lead and bismuth. These isotopes can exhibit high levels of radioactivity, characterized by short half-lives ranging from fractions of a second to several days or weeks.

The distribution of residual nuclei generated collision of 1.4 GeV proton beam with Lead - Bismuth target as shown in Fig.1.14.

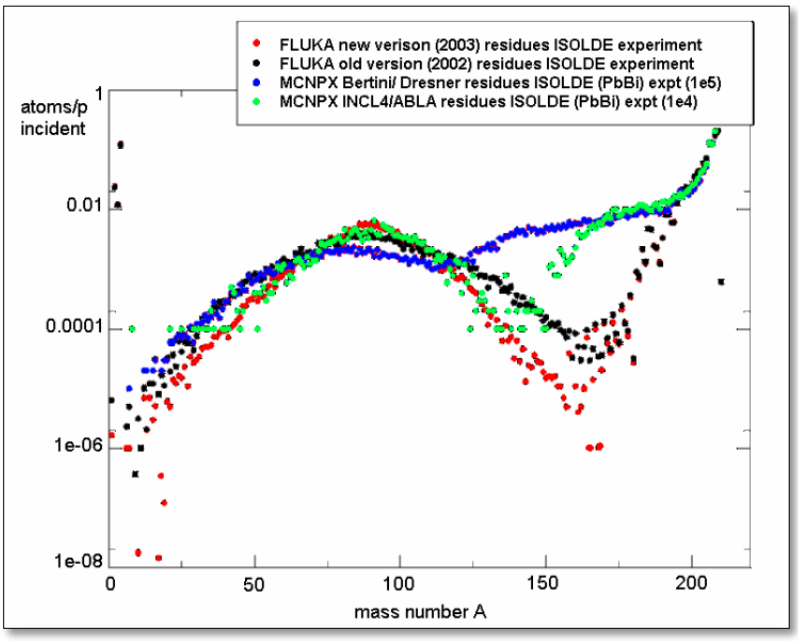

Fig.1.14. Distribution of the spallation products in a thick target in ISOLDE experiment, calculated with FLUKA and MCNPX code [52].

When subjected to a high-energy proton beam, the propensity for spallation and fragmentation increases, resulting in the production of neutron-deficient products located on the left side of the stability line in the chart of nuclides. During the intranuclear cascade and evaporation process, lighter nuclides with lower mass numbers are ejected as fragments from the target nucleus. Nuclides with mass numbers around 100 primarily arise from fission reactions. Stable lead isotopes range from mass numbers A=204 to A=208. The remnant nuclei close to the target mass are the residual products of the spallation evaporation process.

The predicted distributions of these spallation products vary among different Monte Carlo codes, as illustrated in Fig.1.14, due to slight discrepancies in the physical models employed to simulate the spallation process.

The products of spallation reaction are divided into two areas of the nuclide diagram, (see Fig.1.15). Right upper part - heavy proton residues formed as a result of evaporation; in the central part are the fission products [53].

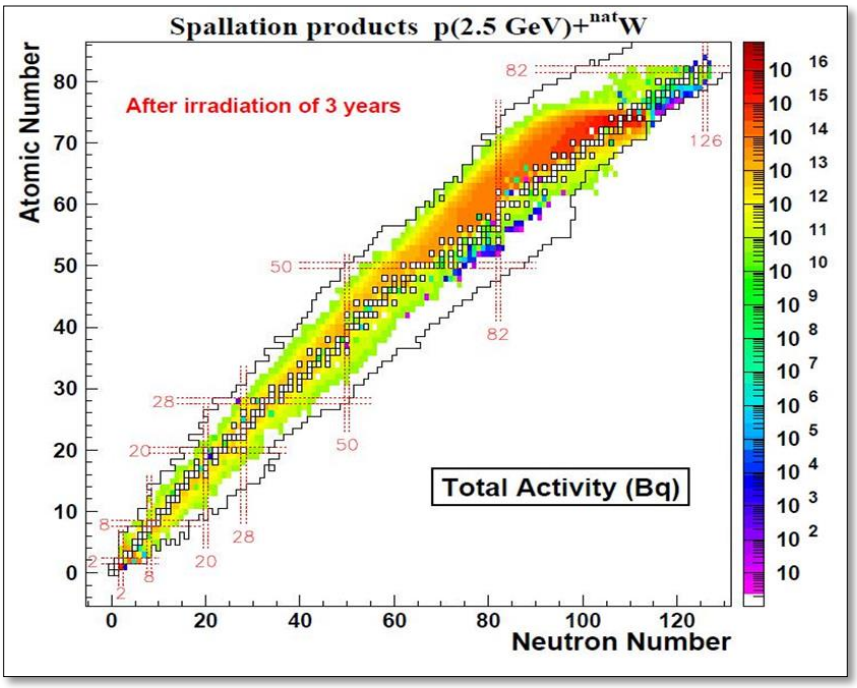

Fig.1.15. Activity of the different isotopes produced by the spallation reactions in the ESS tungsten target as a function of the charge and mass of these isotopes at the end of a 3-year irradiation period [54].

Products that lack sufficient neutrons can be located on the left side of the stability line in the chart of nuclides (Fig.1.15), as they are generated when a high-energy proton beam induces spallation and fragmentation.

Spallation products are significant to scientists and engineers working in various fields such as materials science, nuclear physics, and nuclear engineering. They find utility in diverse applications including the production of medical isotopes for imaging and therapy, exploration of material behavior in extreme conditions, and the development of new nuclear fuels and waste management strategies. However, it is essential to handle and dispose of these products safely, as they can pose risks to human health and the environment.

The method for determining spallation products e.g., Gamma spectroscopy, Mass spectrometry, Activation analysis, Radiochemical analysis, Neutron capture spectroscopy will be described in Chapter 2.

CHAPTER 2

METHODS FOR DETERMINING SPALLATION PRODUCTS AND THEIR CROSS SECTIONS

2.1 Methods for determining spallation products

Direct kinematics [55, 56] is used when a relativistic light projectile hits a heavy target. Combustion products determined by this method, which stop at the target, are detected by γ-spectroscopy and mass spectrometry. The goal of this measurement is to measure the properties of the reaction products obtained as a result from that reaction. In the initial state, the target material is bombarded with particles and photons. As a result, the products produced by this reaction are detected and measured in the laboratory frame. To estimate information about the structure and properties of the target nucleus, the properties of the beam and the target material during the initial phase are compared with the properties observed during the final phase of the reaction.

Inverse kinematics [57] - When a heavy nucleus moving at high speeds collides with a target, certain intermediate products are ejected from the target in the forward direction. These intermediate products can be promptly detected and analyzed while they are in flight using the suitable methods. This method allows to measure the number of states of meta-stability of residual nuclei, and the use of radioactive targets while consuming less beam time.

In inverse kinematics, the role of projectile and target material is reversed. The target nucleus is accelerated to high energies and takes the role of projectile and projectile itself e.g. heavy ion takes the role of being a target. In this mode of reaction, the particle beam is stationery and target material are in motion state. The spallation products are detected and measured in the center-of-mass frame.

This method is employed to study rather unstable and short-lived nuclei which are hard to produce because the accelerated nuclei can be carefully selected and precisely controlled. The study of unstable nuclei is of particular interest of academics and researchers in the field of nuclear and astrophysics.

One challenge which requires careful attention during this method is shift from laboratory frame to center of mass frame because angle and energies change from one reference frame to the another. Therefore, there is need to correctly analyze the inverse kinematics data in order to obtain significant information regarding the properties of exotic nuclei and the dynamics of spallation reactions.

Several methods are employed to determine spallation products depending on the applicability and the kind of target being studied. The important methods are given below:

A. Gamma spectroscopy

Gamma spectroscopy [58] is a relatively simple, yet powerful technique used to identify and estimate gamma-ray emissions from radioactive isotopes, especially, to identify spallation products, which often emit gamma rays, as they decay. This quality makes gamma spectroscopy not only a cost-effective but versatile tool for analyzing radioactive materials, that can be used in various fields. For instance, nuclear power plants, environmental monitoring, radioactive waste management, health physics, investigation of nuclear materials, medical applications, industrial process monitoring, etc.

Overview of work steps for determination of radionuclides using gamma spectroscopy:

- **Source Preparation:** First, obtained a research target that contains radioactive isotopes of interest. Depending on the purpose of the application, the sample can be in different states: solid, liquid, or gas. The sample preparation typically involves several procedures such as collecting, concentrating, and sometimes chemically processing the material to extract the radioactive isotopes.

- **Gamma-Ray Detection:** Gamma rays are a penetrating form of electromagnetic radiation emitted by radioactive isotopes during their decay process. To detect these gamma rays, typically specialized detectors are used. High-purity germanium (HPGe) detectors or scintillation detectors are used for this purpose. These types of detectors are capable of converting gamma rays into electrical signals.

- **Spectrum Acquisition:** The research radioactive sample is placed near the detector, also it can be placed at different distances to the detector, then the detector records the incoming gamma radiation. After this, over time, a spectrum is obtained that represents the energy and intensity of the identified gamma rays. Depending on the desired accuracy, the half-time of the radionuclides (in the research sample) and the activity of the sample reduces or increases the time of the recording of the spectrum.

- **Energy Calibration [59]:** A calibration of the detector procedure is carried out to precisely determine the energy of the detected gamma rays. This procedure includes interaction of the detector with gamma-ray sources (isotopes) of known energies and forming a relationship between the measured signals and the corresponding energy intensities. Usually, calibration is done using standard radioactive sources with well-known gamma-ray emission lines.

- **Spectrum Analysis**: After successful energy calibration, the next step will be the spectrum analysis to identify and quantify the radioactive isotopes present in the study sample. The main aim of this analysis is to compare the energies and intensities of the gamma-ray peaks in the received spectrum with known γ - ray energies from respective isotopes. In identification and quantification process of gamma-ray peaks (isotopes), special software tools such as DEIMOS, Genie, Gemini etc. are typically used.

- **Isotope Identification:** Identification of the specific isotopes which are present in the study sample involves comparing the energies of the gamma rays detected in this sample with γ - ray energies from the calibration source. Considering that each isotope

has a unique γ - ray energy spectrum, it allows identification based on these characteristic γ - ray peaks.

- **Quantification:** The concentration or activity of the specified isotopes is provided by the intensity of the γ - ray peaks in the obtained spectrum. By comparing the gamma peak intensities to calibration factors received from standard sources of well-known activity, the activity or concentration characteristics of the isotopes in the original sample can be ascertained.

- **Interpretation and Reporting:** The final step in the gamma spectroscopy is to interpret and report the results of identifies isotopes for further analysis and research. The obtained information is essential and can be used for a wide range of applications, such as radiation safety assessments, research studies, nuclear materials studies, and/ or environmental monitoring, etc.

Overall, gamma spectroscopy is considered a complex and universal technique for determining the spallation products. However, there exist additional factors to account for, such as background radiation, detector efficiency, distance to detectors, half-time decay isotopes, and sample geometry.

B. Mass spectrometry

Mass spectrometry [60] is the analytical instrument for identifying and quantifying the products of nuclear reactions. In the realm of analytical laboratory procedures, this method involves sorting a sample's elements according to their mass, and it can proudly claim a legacy of more than a century. Prominent physicists like W. Wien and J.J. Thomson, along with their peers, laid the groundwork for the determination of mass-to-charge ratios through this approach [61].

Usually, the technique is used to determine the mass and composition of individual atoms or molecules. It employs search for spallation products by analyzing the isotopic composition by measuring their mass-to-charge ratio. As the products of spallation are highly radioactive and have short half-lives, so it can be difficult to study them using traditional methods.

Recently, various kinds of research are focused on nuclear materials that involve the detection and measurement of amounts of isotopes in ^{238}U, ^{239}Pu, ^{232}Th, fission products and spallation products. To ascertain the characteristics of reactor fuel assembly, burn-up [62] of nuclear fuels [63-71] and the determination of fission products is a key concern of NPP efficiency. The low detection limits and the chance to obtain an isotopic ratio make mass spectrometry well-suitable for such applications. The characterization of fission products, considering elemental concentration and isotopic configuration should be implemented not only using alpha spectrometry but also by the means of mass spectrometry.

Overall, mass spectrometry can be particularly useful in spallation studies conducted in nuclear physics research, nuclear engineering, and accelerator-driven systems. It helps a lot in understanding the spallation process, evaluating the effectiveness of target materials, and optimizing spallation-based applications such as neutron production, isotope production, and nuclear waste transmutation.

C. Activation analysis

Activation analysis [72, 73] is a nuclear analytical technique that can be used to identify spallation products by measuring the gamma-ray emissions from the activated sample which is the radioactive emission of nuclei excited in the process of induced nuclear transformations. It involves irradiating a sample with neutrons or other particles to produce radioactive isotopes. These radioactive isotopes then decay, emitting gamma rays that can be detected by a detector.

The radioisotopes produced from nuclear interactions of various nature and complexity can be stable or radioactive. Reaction on a certain isotope of an element results in a radioactive product with a characteristic decay pattern. The intensity of the gamma rays emitted from products is proportional to the unique concentration of the radioactive element in the sample. Once the individual concentration of each isotope is known, the amount of total sample can be quantified by summing up the individual concentrations.

In activation analysis, the change in activity over time can be estimated with the help of following equation:

$$A_t = \frac{6{,}02\cdot 10^{23} m\cdot \Phi\cdot \sigma\cdot c}{M}\left(1 - e^{-\lambda\cdot t_a}\right)\cdot e^{-\lambda\cdot t_b} \qquad \textbf{(2.1)}$$

A_t: activity of the radioactive isotope over time (Bq).
m: mass of the element sample containing radioactive isotope (g).
c: concentration activated isotope in the sample (e.g., atoms per cubic centimeter).
Φ: neutron flux density, (neutron/(cm^2·s)).
λ: radioactive decay constant (function of half-life), (s^{-1}).
σ: reaction cross section (the probability of nuclear reaction), (cm^2).
M: molar mass of isotope (g/mol).
t_a: activation time (s).
t_b: time elapsed since the end of irradiation (s).

The number of particles or quanta registered during the measurement time t will be as follows:

$$N_t = \frac{6{,}02\cdot 10^{23} m\cdot \Phi\cdot \sigma\cdot c\cdot p}{M\cdot \lambda}\left(1 - e^{-\lambda\cdot t_a}\right)\cdot e^{-\lambda\cdot t_b}\cdot\left(1 - e^{-\lambda\cdot t_u}\right)\cdot a \qquad \textbf{(2.2)}$$

N_t: number of radioactive nuclei of the isotope at specified time (number of nuclei).
p: probability that a nuclear decay event will result in the emission of characteristic radiation.
m: Mass of the element sample containing radioactive isotope (g).
t_u: "Dead" time of the recording equipment (s).
$a = (\varsigma\cdot\varepsilon\cdot\chi\cdot\xi)$ is the coefficient which considers the experimental conditions.
ς: coefficient taking into account the absorption and scattering of activating particles or radiation in the sample.
ε: radiation detection efficiency induced activity emitted from a point corresponding to the center of the sample.
χ: coefficient taking into account the "dead" time of the recording equipment τ.
ξ: factor that takes into account the self-absorption of the characteristic radiation of induced activity in the sample.

This equation is called the activation equation.

Derived from the activation equation, utilizing the measured absolute activity value (A_t), along with established irradiation and measurement conditions, along with reference to tabulated nuclear characteristics, enables the computation of the target element's quantity. This approach, known as the absolute method in activation analysis, can be facilitated with greater ease by concurrently subjecting a precisely known quantity of the element-to-be-measured and a standard sample to irradiation. Post-irradiation, results can be obtained through instrumental or radiochemical means. In both scenarios, the activities of the standard and test specimen are gauged under identical conditions, with provisions for adjustments due to chemical yield, radioactive decay, and other factors. The element's concentration is determined through a straightforward ratio calculation:

$$\frac{m_x}{m_{cm}} = \frac{A_x}{A_{cm}} \quad \textbf{(2.3)}$$

where:
$m_{x:}$ amount or mass of target element being determined (g).
$m_{cm:}$ amount or mass of the standard sample (g).
$Ax:$ activity of target element being determined (s^{-1}).
$A_{cm:}$ activity of standard sample (Bq or s^{-1}).

Referred to as the relative method, this variation is so named due to its inherent characteristic: the requirement for an exact knowledge of the nuclear particle flux is eliminated, as long as it remains consistent across the entire volume during its application.

Activation analysis is a precious tool for studying highly radioactive spallation products or radionuclides with short half-lives, which are difficult to measure using other methods.

Categorized by the specific nuclear particles employed to collide with atomic nuclei, activation analysis methods are classified into three types: neutron activation analysis, photoactivation analysis, and charged-particle activation analysis. Each of these techniques possesses distinctive characteristics, benefits, preferred domains of application, and, naturally, limitations.

Broadly speaking, the utility of each approach is defined by how a particular type of nuclear particles interacts with matter and the accessibility of suitable sources for the purpose of irradiation.

D. Radiochemical analysis

The radiochemical analysis [73, 74] is a powerful method for the determination of spallation products, which are obtained as a result of a high-energy particle striking a target nucleus. This method of chemical analysis is using radioactive isotopes to identify and quantify existing other chemical elements or compounds of the research target. This technique involves isolating and purifying the specific isotopes (of interest) from a study sample and then identifying their decay properties and determining their identity or/and concentration.

Radiochemical analysis draws on two widely recognized features of radioactivity: the capacity for highly sensitive and straightforward measurement of radioactive emissions, and the ability to tag chemical compounds with radioactive tracers.

This radionuclide technique often has higher sensitivity than other analytical method. This ability makes this method very useful for determining radionuclides with half-lives ranging from several minutes to several years. Since these radionuclides have extremely low masses, mostly short periods of half-lives, these characteristics make their identification extremely challenging.

Because of the high sensitivity, the activity of as low as 0.2 Bq (^{3}H, ^{125}I, ^{132}I) and even 0.01 Bq (several γ-emitters, e.g., ^{24}Na, ^{38}Cl, ^{42}K, ^{46}Sc, ^{59}Fe, ^{60}Co, ^{65}Zn, ^{182}Ta, ^{198}Au and etc.) can be easily detected. Radionuclides with total activities of about 0.1–20 kBq can be used in analytical applications.

In general cases, with deviations below 1%, the radiochemical analysis assumes that various isotopes of the same chemical element show the same properties in any macroscopic physical or chemical process.

Laboratory equipment should demonstrate certain properties to generate accurate and reliable results. It should be highly sensitive to measure the low level of radiation, able to detect radiation from target efficiently, decrease the influence of background radiations on the results, maintain its same performance throughout the measurement. Counting rates, measured using Geiger–Müller, scintillation, or semiconductor detectors, are commonly compared with appropriate standards to derive quantitative data. Pulse analyzers can provide both qualitative and quantitative insights into specific constituents of a sample when connected to a compatible radiation detector.

E. Neutron capture spectroscopy

Neutron capture spectroscopy (NCS) [75] is a method for determining the existence of isotopes in a sample after irradiating with neutrons and measuring the gamma-ray emissions which obtain as a result of the capture of the neutrons by particular isotopes. The amount of energy released by the unstable isotope after capturing neutron provide broad information about the isotope present in sample. Main advantages of the NCS method include high sensitivity and non-destructive nature. This technique is a powerful method to identify and measure spallation products, especially radionuclides with high neutron capture cross sections.

The choice of selection of suitable method depends upon nature of isotopes, level of sensitivity required, availability of equipment and financial constraints. Moreover, every method has its pros and cons. For example, radiochemical analysis is a sensitive but destructive method, so the sample that is being analyzed is destroyed in the process. While NCS is comparably less sensitive but non-destructive. Furthermore, mass spectrometry has good sensitivity for detection of concentration but not as specific radiochemical analysis or NCS.

The choice of method for determining spallation products will depend on the specific needs of the experiment. The radiochemical analysis or NCS can be the best choice if purpose is to identify small concentration of isotopes with high sensitivity. If the goal is to determine the concentration of a wide range of isotopes and generate comprehensive analysis, then mass spectrometry may be the best choice.

Experimental techniques like gamma spectroscopy and mass spectrometry provide real-world data about the isotopes produced through spallation reactions. This data is then compared to simulation model predictions to verify the accuracy of the models, leading to

improvements in both our understanding of spallation processes and the design of related equipment for various practical applications.

2.2 High-purity germanium (HPGe) detectors

The introduction of using semiconductors for gamma-ray detection has opened a new accurate measurement possibility, the reason is that semiconductors detectors have very good resolution, compared with other types of detectors. For example, using NaL detector for getting the γ - ray peaks whose resolution is very wide because the two peaks are so close to each other that it is impossible to exactly split up, in addition, low-energy peaks can be not visible.

High-purity germanium (HPGe) detectors are semiconductor diodes with a p-i-n structure in which the intrinsic (i) region is sensitive to ionizing radiation, especially X-rays and γ - rays. The p-i-n structure means that it consists of three regions in the semiconductor material: 1) a p-type region (positive charge carriers); 2) an intrinsic or i-type region (intrinsic or undoped); 3) an n-type region (negative charge carriers) [76].

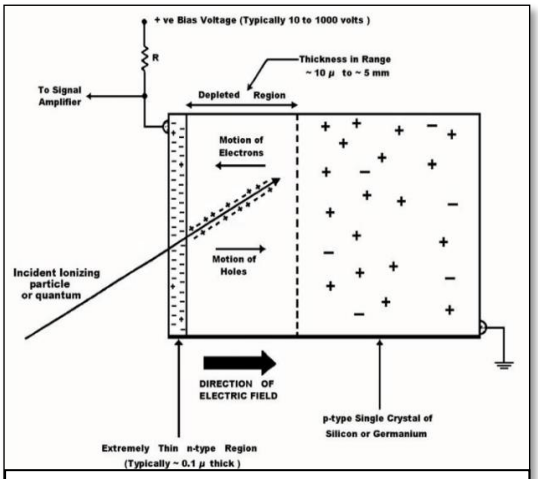

Fig.2.1. Principle of semiconductor detector [77].

The p-i-n structure of HPGe detectors can be elaborated as below:

i. **P-Type Region:** In this region, a detector is doped with a small number of impurities. This process creates extra positively charge carriers which are called "holes". It represents the main charge carriers that exist (occur) in this p-type region.

ii. **Intrinsic (I-Type) Region:** this intrinsic region is electrical neutral because it is not doped and has an equal quantity of electrons and holes. In this region, ionizing radiations (gamma rays or X-rays) interact and generate electron-hole pairs**.**

iii. **N-Type Region:** consider the n-type region, same as in the p-type region, is doped with a small number of impurities that create additional charge carriers but, in this case, negatively charged instead of positive. The majority charge carriers in this n-type region are electrons**.**

In insulators, there exists a substantial energy gap between the valence band and the conduction band, making it challenging to overcome this gap even with elevated temperatures and increased energy. However, in semi-conductors, this band gap is small, and it is very easy for the electrons to cross this gap and reach from valence band to conduction band upon application of small amount of energy. This transfer creates a hole in valence band which resultantly create positive charge for conduction.

When the reverse offset is applied, an electrical field extends across the intrinsic or depleted region of the detector. When high energy photons from ionizing radiations interact with intrinsic or depleted region of the detector, they generate electron-hole pairs. These pairs move towards their respective electrodes after applying the electrical field. The charge transmitted to electrodes is proportional to energy deposited in the doped region by the

ionizing radiations. This charge is converted into a voltage pulse by an integral charge sensitive preamplifier.

The thickness of the depletion region (depletion depth) d for this type of detector, is described by the equation:

$$d = \left(\frac{2\epsilon V}{eN}\right)^{1/2}, \tag{2.4}$$

where, ε is the dielectric constant, V is the reverse bias voltage, N is the net impurity concentration in the semiconductor material, e is the electron charge.

HPGe detectors use a high-purity germanium crystal, which ensures that there should be less impurities to interact with the whole process of measurement. It because of high purity and less interference by unwanted charges, that makes HPGe detectors highly reliable with exceptional energy resolution and precise γ - ray spectroscopy.

Nowadays, the high-purity germanium detectors can have as less as 0.8 x 10^{10}cm^{-3} net impurity concentration.

2.2.1 Energy resolution

The energy resolution of the HPGe detector is shown by the following equation:

$$FWHM = \sqrt{(w_d^2 + w_e^2)}\,, \tag{2.5}$$

where, w_d is the peak width that is created by detector effects, and it depends on energy; w_e are peak width in consequence of electronic effects.

The calculation of w_d parameters can be obtained by formula:

$$w_d = 2\sqrt{(2\ln(2))F \cdot E(keV) \cdot w}\,, \tag{2.6}$$

where, F is the fano factor; w is the energy needed to create an electron-hole pair.

The energy required to produce an electron-hole pair for germanium is low ($w \approx 3$ eV), this provides the creation of a large number of electron-hole pairs, and it makes good resolution as a result. The width depends on the detector's capacitance and the bias voltage. In addition, the capacity of the detector depends on the size of the detector [78].

Fig.2.2 illustrates a comparison of naturally occurring background radiation, detected using four distinct types of radiation detectors. Plastic scintillator detectors lack the capability to distinguish gamma peaks. Sodium iodide (NaI) and cadmium zinc telluride (CZT) detectors offer a limited capacity to differentiate gamma lines. Conversely, High Purity Germanium (HPGe) exhibits a high level of resolution capability.

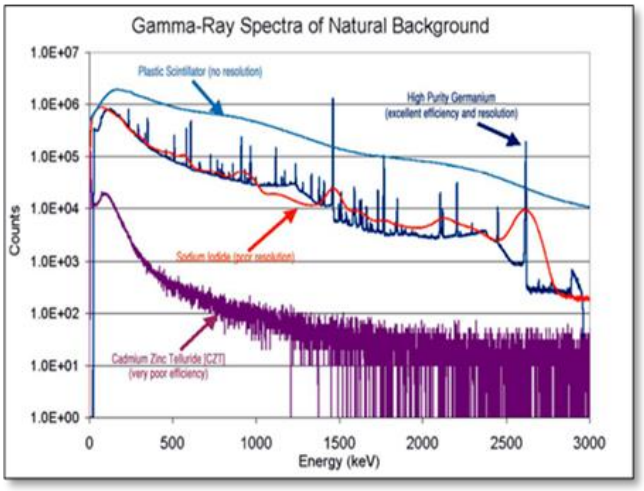

Fig.2.2. Comparison of four different types of radiation detectors for natural background radiation [79].

Each radionuclide naturally emits a distinct set of γ - ray energies, akin to how a fingerprint uniquely characterizes an individual. These energy levels are quantified in units of electron volts (eV) or kiloelectron volts (keV), predominantly falling within the 30 keV to 3000 keV range. However, they are not uniformly distributed across this span; numerous energies are closely situated with only minimal keV intervals. For precise identification, the capability to measure these energies with an accuracy of roughly $1/10^{th}$ of 1 % is imperative. High purity germanium detectors offer this level of precision, whereas sodium iodide detectors yield approximately 6 parts in 100 accuracies. This discrepancy becomes evident upon comparing spectra generated by NaI and HPGe detectors [79].

2.2.2 Advantages of HPGe detectors

- **High energy resolutions.** The detector accurately registered the energies of incoming gamma rays or X-rays, and it provides precise identification and analysis of isotopes or other sources of ionizing radiation. Typically, resolution for 1332 keV: 1.7 keV (or 0.13%) with F.

- **Sensitivity:** Even at low energy levels, the detector is sensitive to ionizing radiation, it provides effective detection of low intensity ionizing radiation.

- **Wide energy range:** Germanium detectors can be used in wide different fields, from environmental monitoring to nuclear physics research, because they can detect from a few keV to several MeV γ - ray energies.

- **Minimal noise:** The detectors have low electronic noise, which helps to provide accurate and reliable measurements (especially with weak radiation signals).

- **Long-term stability:** In the cases handled and operated correctly way, HPGe detectors demonstrate maintaining long-term stability over extended periods of operation.

2.2.3 The main disadvantages of the germanium detector

- **Cost:** HPGe detectors are expensive in comparison with other types of detectors which are used for measure ionizing radiation. It's because of high cost of production and deficit of germanium as a material.

- **Fragility:** Germanium detectors within operation range are delicate and sensitive to mechanical shock and vibrations.

- **Cooling requirements:** Due to its small band gap (0.7 eV), the germanium detectors should operate at low temperatures, such as cryogenic temperatures, approximately -196°C or 77 K, to prevent leakage current from thermally generating electrons holes pairs in the depletion zone. It will substantially reduce the energy resolution of the detector. To fulfil the cooling requirements, liquid nitrogen (77 K) is used for the detector mounted in a vacuum chamber. This safeguards the sensitive detector surfaces against moisture and substances that can condense on them.

- **Power consumption:** Cooling systems required continuous power consumption only if no liquid nitrogen is used.

- **Background radiation:** germanium detectors are sensitive to background radiation, for this reason in environments with increased background radiation levels, usually shielding and background subtraction techniques are used.

Overall, this type of detector is widely used not only in nuclear physics such as measurements of ionizing radiation, but also in astrophysics, medical purpose, and environmental monitoring. HPGe detector is considered one of the most highly sensitive detectors that provide accurate measurement of γ - rays and X-rays that are generated (emitted) by radioactive sources or cosmic events [80].

2.3 Calibration of a germanium detector

Calibration of a germanium detector is one of the essential processes for the correct analysis of receiving data, it establishes consistent relationships between the detected signals and the corresponding energy levels of incoming radiation. As mentioned before, germanium detectors are widely used for γ - ray spectroscopy as they have high resolution and sensitivity for easy collecting and obtaining results. The process of calibration is necessary to ensure true identification and representation of the energies deposited from ionizing radiations of various radioactive sources.

Indication of the individual energy lines acquired in spectrum detector and performing subsequent qualitative analysis for assigning specific radionuclides existing in the sample entail energy calibration of the detector.

Basic Calibration Steps

The calibration process of the germanium detector involves following steps [81]:

- Initial Setup: Setting up of detector electronics as well as connectivity with data acquisition system and the necessary electronics.

- Source Selection: Selection of known radioactive source with desired energy range. Common calibration sources include ^{60}Co, ^{137}Cs, and ^{241}Am.

- Acquisition (record) of Spectra: Placing the calibration sources in desirable vicinity to the detector to acquire gamma-ray spectra in data acquisition system.

- Peak Identification: Map the peaks of known gamma ray sources and analyze with the help of software tools like Genie2000, DEIMOS or similar spectroscopy software.

- Energy Calibration: This involves the conversion of channel numbers to energy by fitting the known gamma ray peaks with linear or polynomial equations and formation of calibration curve by relating channel numbers and corresponding gamma-ray energies.

- Verification: Validation of calibration by calculation of energies of various other sources and subsequently comparing them with known energies. It is necessary that both values should match within a reasonable tolerance.

- Energy Resolution: Mapping the resolution of the detector at different energy levels as per procedure and equation already discussed above. It is very important step in assessing detector's performance at different energy levels.

- Uncertainty Assessment: During the process of measurement certain factors like background radiations and electronics limitation may affect the whole calibration process. There is need to identify the causes and quantify the uncertainty in the calibration process.

Full Width and Half Maximum (FWHM) Resolution

The Full Width and Half Maximum (FWHM) [82] resolution is quantification of the resolution of the detector. It is described by the relation:

$$FWHM = \frac{F_0 + F_1\sqrt{E}}{C_1}, \tag{2.7}$$

where, F_0, F_1 and C_1 depend upon the characteristics of specific detector used in the experiment and are measured experimentally. While 'E' represents the energy of the γ - rays (in keV).

Above equation depicts that resolution of the detector is not constant term rather improves as the energy of the gamma rays increases as the peak becomes narrower and which facilitates the detection of several different peaks.

Well known gamma-ray sources with precise energy information are used to calibrate the germanium detectors. The calibration set contained ^{137}Cs, ^{57}Co, ^{152}Eu, ^{60}Co, ^{109}Cd and ^{133}Ba. Energy calibration and dependence half-widths are shown successively in Fig.2.3 and Fig.2.4 with the set parameters, the following was achieved FWHM=1.37 keV resolution for the ^{137}Cs peak (661.66 keV) and FWHM=1.78 keV resolution for the ^{60}Co peak (1332.5 keV).

For example, energy calibration and dependence of the FWHM half-width on the energy for the HPGe detector are shown in Fig.2.3 and Fig.2.4

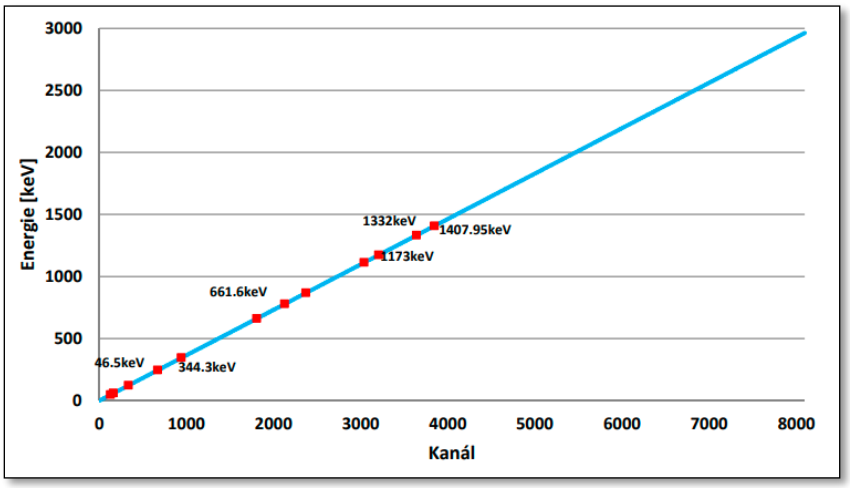

Fig.2.3. Energy calibration of the HPGe detector.

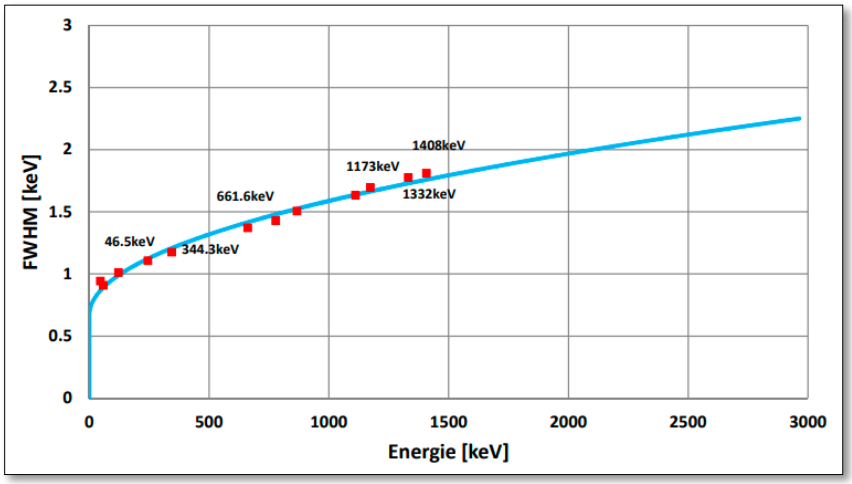

Fig.2.4. Dependence of the FWHM half-width on the energy for the HPGe detector.

Energy Calibration [83]

The measurement of γ - ray energy with respect to channel numbers or ADS counts is generally represented by following linear equation:

$$E = a + b \cdot C \tag{2.8}$$

where, E represents γ - ray energy (keV); C stands for channel number (or ADC counts) corresponding to the γ - ray peak; "a" and "b" corresponds to calibration parameters and quantified during calibration process. Parameter "a" represents the intercept or the energy offset, and "b" represents the energy calibration coefficient or the channel-to-energy conversion factor. The values of both constants are estimated by known gamma-ray energy peaks fitted into linear equation.

The point sources given in Table 2 below can be used during the calibration process of the detector. The shape of the spectrum and photopeak efficiency ratio curve are determined by the single line emitters like ^{54}Mn, ^{203}Hg, ^{113}Sn, ^{137}Cs and ^{60}Co. To cover the whole range of

energy for determining the photopeak efficiency curve, ^{210}Pb, ^{241}Am, ^{109}Cd, ^{152}Eu, ^{137}Cs, ^{54}Mn and ^{88}Y are utilized. The ^{152}Eu is used for calculation of angular efficiency dependence.

Table 2. Gamma point sources employed to calibrate the detector.

Isotope	Energy (keV)	Intensity Iγ (%)
^{210}Pb	46.539	4.25
^{241}Am	59.5412	35.9
^{109}Cd	88.04	3.61
^{139}Ce	165.864	80
^{203}Hg	279.1967	81
^{113}Sn	391.690	64
^{152}Eu	121.7817 244.6975 344.2785 778.9040 1112.074 1408.006	28.58 7.583 26.5 12.942 13.644 21.005
^{137}Cs	661.657	85.1
^{54}Mn	834.848	99.976
^{60}Co	1173.237 1332.501	99.9736 99.9856
^{88}Y	898.042 1836.063	93.7 99.2

Computer based calibration

In addition, different computer software can also be used to energy calibration of germanium detectors, for instance, the DEIMOS32 [84] software uses several point radiations sources that cover a large energy range. The shape of the energy calibration in the program DEIMOS32 is given by the relation:

$$E = C_0 + C_1 x + C_2 x^2 + C_3 x^3 \quad (2.9)$$

where E is the gamma-ray energy in keV; x is the channel number corresponding to the gamma-ray peak. C_n are calibration coefficients determined during the calibration process.

However, the actual function implemented in "DEIMOS", or any other software program can be more complex and may need additional correction factors and non-linear calibration functions to improve accuracy. There is also needed to periodically repeat the calibration process as germanium detectors may drift over time.

Half Life Factor

The radioactive materials also undergo transformations depending upon the half-life of that radioisotope. There is need to accommodate the half-life factor in the emission rate. For example, when ^{60}Co undergo nuclear transformation, it emits 1332 keV photon. The National

Institute of Standards and Technology (NIST) calibrate radioactive sources on the basis of nuclear transformations per second (NT/s). In order to accommodate this decay in the calibration process, monthly correction is needed. For ^{60}Co (half-life 5.27 years), a decrease in emission rate of 1.1% per month can be observed. Following formula is used to correct for source decay:

$$N_p = N_0 \cdot e^{-(\ln(2))^{t/T}}, \tag{2.10}$$

where N_p - present rate of emission; N_0 - original rate of emission; t - elapsed time; T - half-life (5.27 years for ^{60}Co).

Above formula calculates present emission rate while keeping into account original emission rate and other above-mentioned variables.

Absence of Calibration Standards

When there is no access to NIST or other properly calibrated source, one can employ a 3 in. x 3 in. sodium iodide with thallium (NaI(TI)) scintillation detector for a direct side-by-side comparison of the efficiency of a germanium (Ge) detector. Both detectors are exposed to γ - rays of the same intensity from the same source.

To address potential interference issues, it is recommended to perform integration on the upper half of the 1332 keV peak and then double the result. This approach effectively mitigates the impact of 1173 keV γ - rays on the accurate determination of the intensity of the 1332 keV peak in the NaI(TI) detector's response.

Finally, to achieve most accurate and representative reading from germanium detectors, it is essentials to follow laboratory and instruments procedures and guidelines.

2.4 Determining efficiency of HPGe detector

The efficiency of germanium detector refers to the ability to correctly capture and record a γ - ray photon emitted from a radioactive source. It is probability of the phenomenon that how efficiently a detector can detect and quantify gamma-ray emissions.

The measurement of Full Energy Peak (FEP) efficiency is one of the very important features of γ - ray detectors. To determine the accurate value of efficiency for quantitative spectroscopy comes with many challenges because of the unavailability of calibration standards at high energy i.e., above 3 MeV energy. Moreover, estimating correct source strength and geometry regarding source to detector distance also affect the measurement process. If enough data points are not available, then it becomes very challenging to determine the shape of the efficiency curve in the regions where efficiency behaves as a complex function of energy.

Certain factors affect the efficiency of the detector e.g., γ - ray energy levels, distance between source and detector and successful calibration at higher energy levels. In order to calculate the absolute efficiency of a γ - ray detector, there is need to perform some pre-measurement steps which include following the calibration process as discussed previously during discussion regarding basic steps in the calibration process. Briefly, these steps include efficiency calibration by calibrating the detector using standard γ - ray sources of known energies and activities, measurement of source activity, determination of geometry (solid

angle) depending upon the laboratory arrangement of all equipment and finally correct for any absorption parameters and attenuation in the detector or source. All these factors, directly or indirectly affect the process of efficiency calculation [86].

Types of efficiencies, commonly used in γ-spectroscopy:

In γ - ray spectroscopy, several types of efficiencies are used to explain the work performance of γ - ray detector system. Through these efficiencies, it is easy to establish the detection and measurement performance of the detector. The commonly used types of efficiencies are given below.

- **Geometric Efficiency ($\varepsilon_{geometric}$)**

Geometric efficiency of the detector measures how effectively a detector collects and measures gamma-rays emitted by the source. It takes into account the spatial collection of rays depending upon the solid angle and distance between source and detector. The solid angle also quantifies the amount of radiation directed at the detector by the source. Accordingly, the values of efficiency also change with respect to the spatial distribution of the source. If self-attenuation (attenuation of radiation by the radiation source itself) is ignored, then it can be safely assumed that radiation emissions from a radioactive source are often considered to occur isotopically.

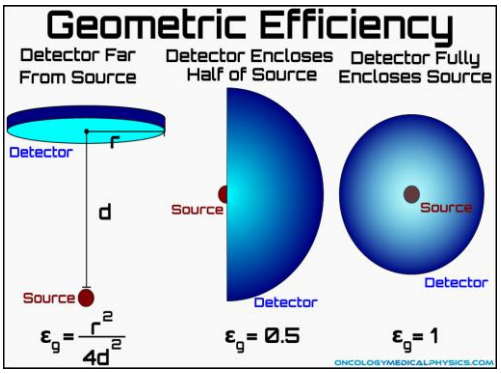

The geometric efficiency can be approximated by comparing the detector's entrance area to the surface area of a sphere with a radius equal to the distance between the source and the detector.

$$\varepsilon_{geometric} \approx \frac{r^2}{4d^2} \qquad (2.11)$$

where, r is the detector radius, *d* is the source-to-detector distance.

The provided equation holds true when certain conditions are met when the radiation source can be treated as a point source, when the detector's surface approximates a circular shape oriented toward the source, and when the distance between the source and detector significantly exceeds the detector's radius. If these conditions are not satisfied, one can determine the geometric efficiency by calculating the solid angle (in steradians) subtended by the detector using the equation below:

$$\varepsilon_{geometric} = \frac{\Omega_{detector}}{4\pi} \qquad (2.12)$$

where, $\Omega_{detector}$ represents the solid angle covered by the detector, measured in steradians.

In case, if the detector covers half of the area of the source, the efficiency will be 50% and to maximize the efficiency, it is imperative that detector should cover the as maximum area of the source as possible. The maximum efficiency of 100% can be achieved if detector covers the whole area of the source as given in the above figure [87].

- **Intrinsic Efficiency**

Intrinsic efficiency [88] is the measure of the ability of the detector to successfully convert gamma-rays into electrical pulses. It also takes into account detector's composition, thickness and interaction probability with the source. The intrinsic efficiency can be calculated by the following equation:

$$\varepsilon_{in}(E) = \frac{\text{the number of counts produced by the detector}}{\text{the number of } \gamma\text{−rays striking the source}} \tag{2.13}$$

$$\varepsilon_{in}(E) = \frac{N_c(E_\gamma)}{A_0 \int_t (E_\gamma, t)} \tag{2.14}$$

Where $\varepsilon_{in}(E)$ represents the likelihood that a photon interacting with the detector will produce a pulse that falls within the full energy peak of the spectrum. It quantifies the detector's ability to accurately detect and record such events; $N_c(E_\gamma)$ represents corrected net peak area in counts/s; A_0 represents activity of the source at the time of standardization in (Bq) and it is important for standardization. Additionally, $\int_t$ represents the probability density function (PDF) of detecting a γ - ray within a certain time interval after calibration, this parameter can be given by the formula below:

$$\int_t = \frac{I_\gamma}{\lambda} \exp(-\lambda t_D)(1 - \exp(-\lambda t_c)), \tag{2.15}$$

where, I_γ - absolute γ - ray emission probability; λ - decay constant; t_D - the time interval between when the detector was calibrated and the current measurement; t_c - duration of the count (s); $\exp(-\lambda t_D)$- represents the probability that no decay event has occurred in the time interval t_D; $(1 - \exp(-\lambda t_c)$ - represents the probability that at least one decay event occurs within the counting duration t_c.

The equation (2.15) describes the probability of detecting a γ - ray within a given time interval after calibration.

- **Detector Efficiency ($\varepsilon_{detector}$)**

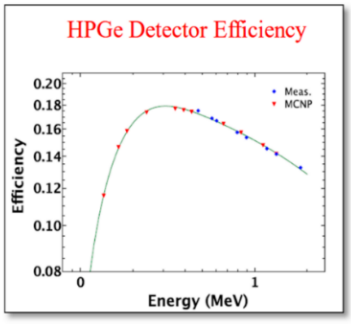

Detector efficiency [89] is a combination of intrinsic efficiency and geometric efficiency. It overall measures the probability of incident gamma rays on the detector as well as subsequent successful detection of the rays by the detector.

The efficiency of a detector (denoted as ε) is calculated as the proportion of detections or counts registered by the detector compared to the overall quantity of particles emitted from a radiation source. This efficiency metric is affected by multiple factors, including geometric efficiency, intrinsic efficiency, and detector dead-time.

$$\varepsilon = \frac{counts\ recorded}{Total\ number\ of\ radiation\ perticles\ emitted} \tag{2.16}$$

- **Total (absolute) efficiency**

Absolute efficiency is determined by dividing the number of counts recorded by the detector by the number of gamma-rays emitted by the source. It is quantification of the γ -rays emitted by the source and gamma rays detected by the detector. It takes into account the source activity, detector efficiency and the distance between both of them. The determination of the absolute efficiency (A_t) for the tested detector involves assessing its performance in relation to the reference crystal's efficiency at a designated energy level (e.g., 1332 keV) while also factoring in the distance between the detector and the radiation source. Next, this absolute efficiency is divided by $1.2 \cdot 10^{-3}$, representing the absolute efficiency of a standard 3-inch by 3-inch NaI(Tl) crystal at 1332 keV and located 25 cm from the radiation source. The comparison of these two values forms the foundation for establishing the relative efficiency specifications of the germanium detector.

$$\varepsilon_t(E) = \frac{the\ number\ of\ counts\ (of\ any\ size) produced\ by\ the\ detector}{the\ number\ of\ \gamma-rays\ emitted\ by\ the\ source} \tag{2.17}$$

The γ - rays emitted by the source and their subsequent detection by the detector depends upon solid angle as well as γ - rays emitted by the source compensated with self-absorption.

Finally, the absolute efficiency (η) can be computed using the following formula:

$$\eta = \frac{N}{(A \cdot \Omega)} \cdot \frac{1}{(1 - C)} \tag{2.18}$$

where:
N: Number of counts.
A: Activity of the radioactive source in decays per second (Bq).
Ω*:* The solid angle subtended by the detector, usually expressed (sr).
C (*Self-absorption correction):* Correction factors related to self-absorption effects within the radioactive source and the detector material.

It's crucial to recognize that efficiency calculations are intricate and require careful consideration of certain factors. Additionally, the efficiency of a germanium detector can vary with respect to the energy of γ - rays. Therefore, it is advisable to present efficiency data in the form of curves or tables at different energy levels to facilitate practical applications [90].

- **Relative Efficiency**

As the name depicts, relative efficiency is relative comparison between the two detectors (one being the standard reference with high efficiency). It serves the purpose of comparing the performance of different detectors and correct any inconsistencies in detector size, design, and materials.

Efficiency of one detector relative to another, commonly described by following formula:

$$\varepsilon_{rel}(E) = \frac{efficiency\ the\ detector}{efficiency\ of\ a\ NaI\ crystal\ (diametr\ and\ lenghth\ of\ 7.62\ cm)} \tag{2.19}$$

each at 25 cm from a point source with 1332 keV (line of ^{60}Co).

Conventionally, the relative efficiency of coaxial germanium detectors is compared with standard 3-in.-diameter, 3-in.-long NaI(Tl) scintillator at 1332 keV. The measurement is guided by the IEEE Standard Test Procedures for germanium detectors for ionizing radiation (ANSI/IEEE 325–1996) and in the equivalent IEC standard. The ^{60}Co source, under the purview of the National Institute of Standards, is situated at a distance of 25 cm from the endcap surface, and a count is conducted for a set duration to measure the intensity of the 1332 keV peak [91].

- **Peak Efficiency (ε_{peak})**

Peak efficiency is subset of absolute efficiency and pertains to the effectiveness of detecting γ - ray peaks within the energy spectrum. This measurement is often provided for specific gamma-ray energies or points of interest. Peak efficiency is the measure of effectiveness of detector to record the energy levels of interest at the time when source emits that energy peaks. It takes into account various factors, such as the absorption of gamma-rays in the detector material and the performance of the electronics employed in the spectroscopy system.

$$\varepsilon_{peak} = \frac{N_{peak}}{N_{source}} \tag{2.20}$$

where:
ε_{peak} is the peak efficiency.
N_{peak} is the number of counts in the peak of interest in the γ - ray spectrum.
N_{source} is the number of gamma-ray emissions from the source at the energy of interest.

Peak Efficiency measures the effectiveness of detecting any peak within the γ - ray spectrum. However, also exist another parameter which called Full-Energy Peak Efficiency that specifically quantifies the efficiency of detecting the full-energy peak, which is important for precise γ-ray spectroscopy measurements.

- **Full energy peak (photopeak) efficiency**

Full-Energy Peak Efficiency ($\varepsilon_p(E)$) is a vital factor in γ - ray spectroscopy using germanium detectors, especially for precise intensity measurements of γ - ray sources. It specifically represents the efficiency of detecting the full-energy peak, which corresponds to the energy of the emitted γ - ray photon. The $\varepsilon_p(E)$ accounts for the likelihood of γ - rays avoiding multiple interactions within the detector material and ultimately contributing to the formation of the full-energy peak in the spectrum. Its significance lies in its central role in quantifying source intensities, enhancing spectroscopic precision, reducing the occurrence of false peaks, and facilitating the calibration process.

$$\varepsilon_p(E) = \frac{the\ number\ of\ full\ energy\ peak\ counts\ produced\ by\ the\ detector}{the\ number\ of\ \gamma-rays\ emitted\ by\ the\ source} \tag{2.21}$$

The efficiency curve is a graphical depiction of how a detector's efficiency varies with the energy of incident γ - rays. It serves as a valuable tool for comprehending how the detector's effectiveness changes across the spectrum of γ - ray energies. Essentially, the efficiency curve provides insights into the likelihood of the detector successfully detecting γ - rays over a range of energies. For example, in Fig.2.5, the curve illustrates the absolute

detection efficiency of the HPGe detector for full-energy peaks when point sources are positioned at various distances from the detector.

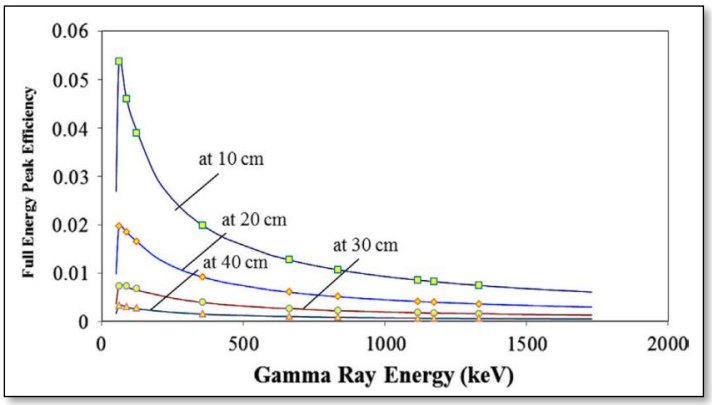

Fig.2.5. The full energy peak of the HPGe detector is assessed with respect to γ - ray energy and the distance between point sources positioned on the axis. These functions are derived by fitting experimental data points [92].

Efficiency parameters are pivotal in γ - ray spectroscopy, exerting a profound impact on the precision and dependability of measurements made using γ - ray detectors. In the realm of scientific research, experts frequently find it imperative to consider these efficiencies when dissecting and making sense of gamma-ray spectra. This practice enables them to derive valuable insights about the radioactive sources under investigation, ensuring the validity and accuracy of their findings.

Efficiency vs. Calibration of detector

The equation given below defines the efficiency (ε) [93] of a γ - ray detector for a specific energy (E). This equation is essential in calibrating the detector to accurately determine radionuclide activities through qualitative analysis. According to [94], the detector efficiency for a given peak is defined by the relation:

$$\varepsilon(E) = \frac{S}{A \cdot t \cdot Y \cdot K_w \cdot U_f} \tag{2.22}$$

Where:
ε(E) is the efficiency for energy E.
S is the net peak area (after background subtraction), (counts).
A is the activity of the calibration source, (Bq).
t is the measurement time (Live Time), (s).
Y is the yield (representation of E energy per decay), (keV/decay).
U_f is the conversion constant for the case of specifying the activity in units other than Bq.
K_w is the correction factor for the time elapsed between the reference date and the measurement date. It accounts for the decay of the radionuclide in the calibration source over time.

The correction factor K_w is determined using the below formula:

$$K_w = e^{-\frac{ln\,(2)t_w}{T_{1/2}}} \tag{2.23}$$

In equation (2.22), t_w is the decay time (s) (the time interval during which the system waits before making a measurement). To create an effective calibration, it is necessary to use several radionuclide standards of known composition and activity. According to formula (2.23) above, for each energy line radionuclides used, the efficiency is calculated, including any density corrections or corrections for coincidence. The values thus obtained are entered into the DEIMOS32 application, which calculates the coefficients of equation (2.23) determining the efficiency curve for the whole energy interval:

$$ln(\varepsilon) = \sum_{i=0}^{n} b_i \, (ln(E))^i \tag{2.24}$$

Where:
b_i are the coefficients determined by calculation.
E is the energy of the photopeak (keV).
ε is the efficiency in the photopeak energy E.

The efficiency calibration of the detector was performed for a point source at the front of the detector and at 25 cm above the detector face.

2.5 Determination of the reaction rate and cross section of the residual radionuclides

Gamma-ray spectrometry is employed for the identification of radionuclides and the quantification of their activity levels. The γ-ray spectra were generated from experimental findings and processed using the DEIMOS32 program. The characteristic gamma radiation spectra of the emitted residual nuclei in the target are measured by a high-purity germanium semiconductor detector (HPGe). The spectrum plays crucial role for determining the experimental rates of the reaction products.

The method of induced activity can be used to study radioactive isotopes formed in the target. In a laboratory experiment conducted without real-time monitoring, we begin by subjecting the target nucleus to a charged particle beam, such as protons, to induce its initial excitation. After this irradiation, we generate a combination of nuclides, some of which remain stable while others become radioactive. These distinct nuclides can be identified based on their different half-lives and the energy they release during the decay process.

When studying a nuclear reaction, the main parameters of the probability of its occurrence at different energies of incident particles are the "output" of this reaction, the angular and energy distribution of the reaction products.

The creation of residual product nuclei during proton interactions with a target nucleus results from intranuclear processes like spallation, fission, fragmentation, and the evaporation of light nuclei and nucleons. The overall pattern of proton interactions with a target nucleus is as follows:

$$^{A_T}_{Z_T}T(p,x)^{A}_{Z}N \tag{2.25}$$

In this context, the notation (p,x) denotes a specific type of nuclear reaction. Letters T and N represent the chemical symbols for the target and resulting product nucleus. The AT and ZT stand for the mass number and charge of the target nuclide, while A and Z denote the mass number and charge of the nuclide generated as a result of the nuclear reaction. The yields of radioactive products in nuclear reaction are determined by the following formula:

$$Y = \sigma(E) \cdot \Phi(E), \qquad (2.26)$$

where σ(E) is cross sections of a nuclide production and Φ(E) is the proton flux density.

The result of the nuclear reaction, at a specific energy of incoming particles, represents the fraction of reactions that occurred relative to the total number of particles that struck the target, assuming all target nuclei were exposed to the same stream of incoming particles. This yield can be computed when we have knowledge of the effective cross-sectional area of the process, denoted as σ.

$$Y_B = \frac{I_0 - I}{I_0} = \frac{I_0(1-e^{-\sigma n})}{I_0} = 1 - e^{-\sigma n} \approx \sigma n, \qquad (2.27)$$

where, I_0 is initial intensity or flux of incoming particles (e.g., particles cm^{-2} s^{-1}), and I - the intensity or flux of particles after they have interacted with the target material.

For a thick target, in which there is both a change in energy and a decrease in the flow of particles, the expression for the output of nuclear reactions has a more complex form [83].

Above mentioned both formulas are complementary. Both formulas can be used depending upon the known variables. For example, if the cross section and proton flux density are known then equation (2.26) can generate the results and if effective cross section (σ) and number of target nuclei (n) are known then equation (2.27) can be used to compute the actual yield of the reaction.

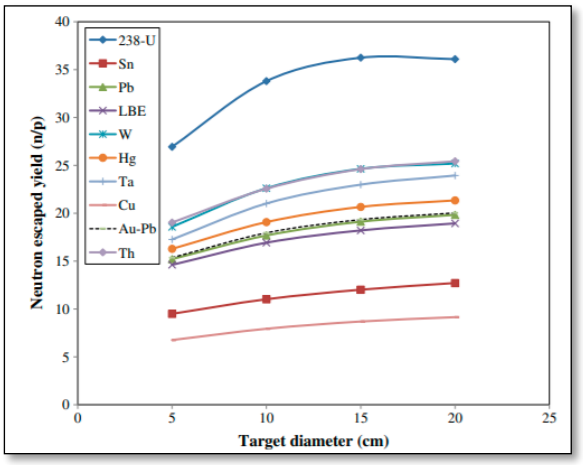

Fig.2.6. Comparison of neutron yield variations in the effect of target diameter enhancement. Particles are protons of energy 1 GeV (thickness (target) = 30 cm) [96].

To elucidate the build-up of reaction products during proton beam irradiation, a series of kinetic equations is employed. The solution to these equations, in terms of the reaction rate, hinges on factors including the decay constants of the radioactive nuclei in question and the conditions of irradiation. Analytical formulations for the reaction rate are derived, particularly for scenarios involving two- and three-branch decay chains.

In this research study, we focused on measuring the production of nuclides that exclusively occur in two-link decay chains. We also took into account the reaction rate equations outlined in reference [97].

The reaction rate is a measure of the frequency of interactions or collisions happening within a volume of one cubic centimeter during a period of one second. This parameter is

essential for comprehending the effectiveness and dynamics of the spallation process. In a standard PWR reactor, the reaction rate is approximately 10^{20} fissions occurring per second.

Simply describing, Reaction rate represents the number of produced residual nuclei Q (A_r, Z_r) per one atom in the sample N_A and one incident particle per second N_p according to the following equation:

$$Q_a(A_r, Z_r) = \frac{S(E_\gamma)\cdot\lambda\cdot\frac{t_{live}}{t_{real}}\cdot\eta}{(1-e^{-\lambda t_{irr}})\cdot e^{-\lambda\cdot t_{cool}}\cdot(1-e^{-\lambda t_{real}})\cdot\varepsilon_{eff}(E_\gamma)\cdot I_\gamma(E_\gamma)} \tag{2.28}$$

This equation integrates various factors, including the reaction's cross section, the decay of generated nuclei, the time intervals within the experiment, and the detection efficiency. It's a sophisticated formula employed in nuclear physics to ascertain the rate at which nuclear reactions happen under specific experimental circumstances. Below formula also takes into account correction factors, already explained in section 2.6.

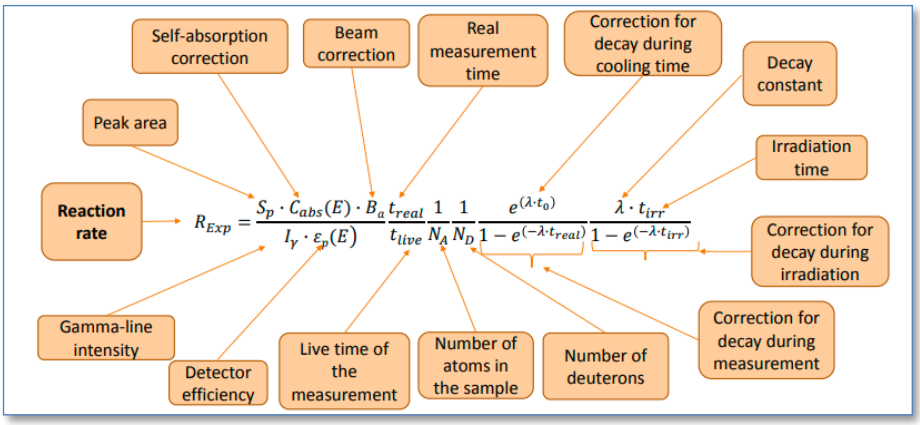

Fig.2.7. Equation for reaction rate calculation [98].

To determine the number of residual nuclei (B) and the reaction rate of each detected isotope (RR) [99]:

$$B = \frac{S(E_\gamma)}{m_s}\frac{1}{I_\gamma}\frac{t_{real}}{t_{live}}\frac{\exp(\lambda t_{delay})}{1-\exp(-\lambda t_{real})}\frac{\lambda t_{irr}}{1-\exp(-\lambda t_{irr})} \tag{2.29}$$

$$R_R = B\frac{A}{N_A}, \tag{2.30}$$

where, $S(E_\gamma)$ - gamma line range, m_s – target mass, t_{real}, t_{live} - real measurement time and live time, which accounts for the time during the measurement when the detector was actively acquiring data (excluding dead times) respectively, λ – the rate of decay, t_{irr} - irradiation time, A - mass number of target atoms, N_A – Avogadro number ($6.022145 \cdot 10^{23}$ [mol^{-1}]).

The accuracy of predicting the yield of product nuclei is estimated at ≈ 30%. The greatest difficulty in determining the yields of reaction products is that experiments with heavy target nuclei can detect only 80 to 100 product nuclei, while the actual yield of nuclides is an order of higher magnitude.

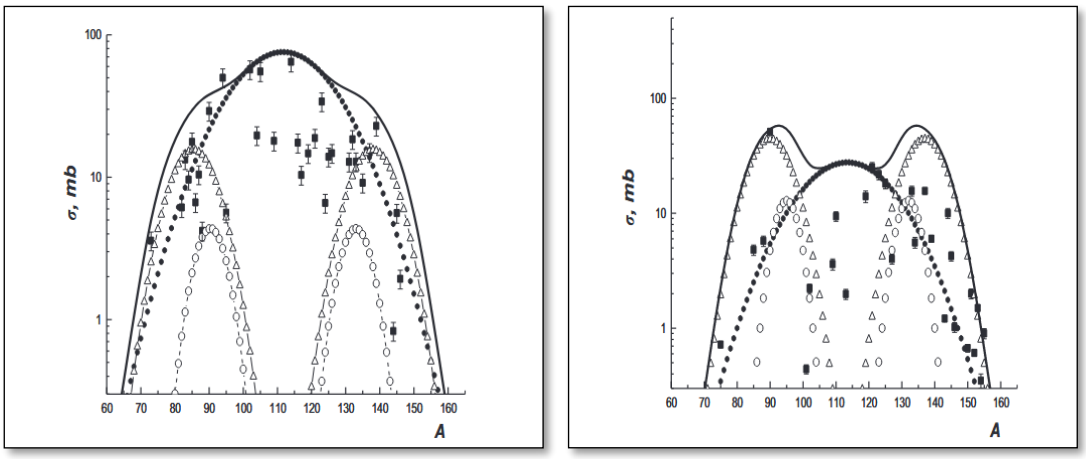

Fig.2.8. Mass-yield distribution of proton-induced fission of ^{237}Np and ^{238}U at the energy 660 MeV [100, 101]. The total fission yield is represented by the solid curve and experimental data by solid circles.

The 660 MeV proton induced mass yield distribution for ^{237}Np, ^{238}U, ^{241}Am, and ^{239}Pu share certain similarities i.e., all afore-mentioned heavy isotopes are fissile and undergo fission upon incidence of high energy proton beam. Moreover, with such a high energy, it is relatively easy to overcome fission barrier in these nuclei, that's why all these isotopes successfully undergo fission. The fission with high energy also plays critical role in creating similar type of fission process.

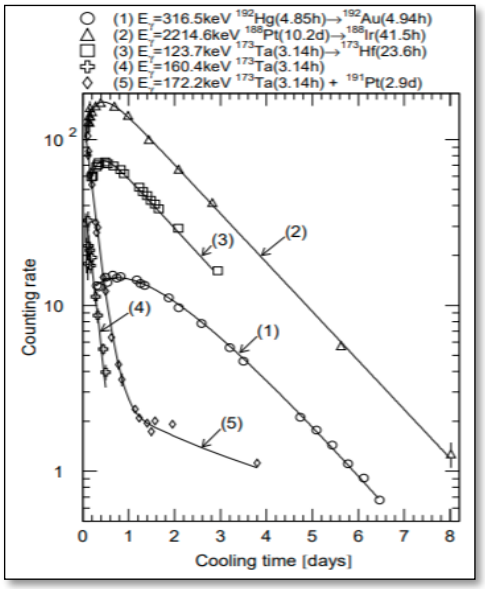

Fig.2.9. The typical examples of the decay curves. A curve (1) is for the chain ^{192}Hg→^{192}Au. Curves (2) is for ^{188}Pt→^{188}Ir. Curves (3) is for ^{173}Ta→^{173}Hf. Curves (4) is for the independent ^{173}Ta decay. Curve (5) is for the independent ^{173}Ta+^{191}Pt decay [102].

Even though these nuclei all share the ability to undergo fission and are exposed to high-energy protons, there are still differences in how their fission processes play out. These differences are primarily due to the unique makeup of each nucleus, the types of fragments produced and additional reactions that might happen during fission. All these factors work together to create variations in the types and amounts of fission products we observe when protons induce fission in these nuclei.

In simple terms, cross section (σ) measures the likelihood of a reaction happening at a certain energy level (E), and its standard unit of measurement is square meters (m^2). However, it generally more convenient to express cross section in a much smaller unit called a "barn" (b), where 1 barn is equivalent to 10^{-28} m^2 or 10^{-24} cm^2.

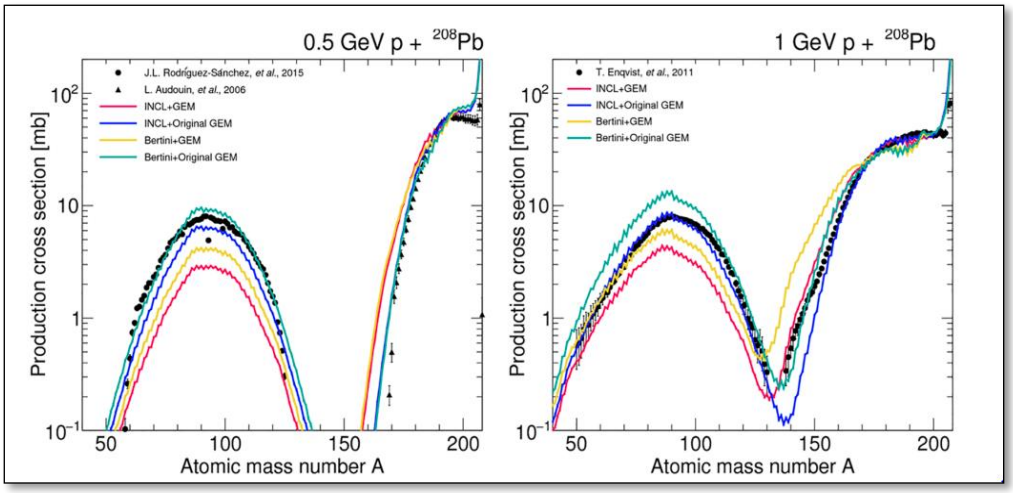

Fig.2.10. Comparison of production cross section measured (Audouin et al., 2006; Enqvist et al., 2001; Rodríguez-Sánchez et al., 2015) and calculated with four combinations of the physics models for the 0.5-GeV and 1-GeV ^{208}Pb (p,x) reaction [103].

The count of registered γ-ray photons with energy E_γ, $S_\gamma(E_\gamma)$ can be written as:

$$S_\gamma(\mathrm{E}_\gamma) = \left[\mathrm{N_a}(\mathrm{t_2}) - \mathrm{N_a}(\mathrm{t_3(real)})\right] \varepsilon_\gamma(\mathrm{E}_\gamma)\mathrm{I}_\gamma(\mathrm{E}_\gamma)\frac{\mathrm{t_{3,l}}}{\mathrm{t_{3,r}}} \tag{2.31}$$

Where:

$S_\gamma(\mathrm{E}_\gamma)$ is the number of registered γ - ray with energy E_γ (count).
$\mathrm{N_a}(\mathrm{t_2})$ is the number of radioactive nuclei registered at time $\mathrm{t_2}$ (count per s).
$\mathrm{N_a}(\mathrm{t_3(real)})$ is the number of radioactive nuclei registered at the real time $\mathrm{t_3}$ (count).
$\varepsilon_\gamma(\mathrm{E}_\gamma)$ is the absolute efficiency of registration γ – quanta with energy E_γ.
$\mathrm{I}_\gamma(\mathrm{E}_\gamma)$ describes the intensity of γ-ray photons with energy E_γ (photons per second per unit area).
$\mathrm{t_{3,l}}$ is the live time of the detector of the time interval (s).
$\mathrm{t_{3,r}}$ is the real time of the detector of the time interval (s).

This equation takes into account the difference between the number of γ - ray counts recorded at the initial time, t_2, and the actual time of measurement, t_3 (real). This difference is then adjusted by considering how effectively the detector captures γ - ray photons (the absolute γ - ray detection efficiency), the rate at which γ - ray photons are emitted (the intensity of γ - ray photons), and the relative duration of measurement times for the left and right parts of the setup (the ratio of live times). Essentially, it helps us calculate the final count of γ - ray photons recorded by accounting for various factors that affect the measurement.

The cross section of the reaction σ_a is determined by the expression:

$$Q_a = \sigma_a N_p N_{targ} \tag{2.32}$$

Where:

Q_a denotes the rate of reaction expressed in reactions per second (s^{-1}).

N_p is flux of particle (s^{-1}) that is passing through the target.

N_{targ} is the number of nuclei per cm^2 of the target surface.

σ_a represents the reaction (a) cross section (b).

$$N_{targ} = N_A \cdot \frac{m}{A} \cdot S, \tag{2.33}$$

where, N_A is the Avogadro number ($6.022 \cdot 10^{23}\,\mathrm{mol}^{-1}$), A represents the amount of this value in 1 mol (g) and S (cm^2) denotes target area.

Proton flux density N_p can be given as:

$$N_p = \frac{N_{N_a}\lambda_{N_a}}{N_{Al}\sigma_{st}F_{N_a}} \tag{2.34}$$

Where:

N_p is proton flux density measuring (particles per cm^2 per s).

N_{N_a} is the number of target nuclei (N_a) per unit area (typically 1 cm^2) of the target surface (nuclei per cm^2).

λ_{N_a}: This is the mean free path of the protons within the target material. This is the average distance a proton travels before it interacts with the target material.

N_{Al}: This is the number of target nuclei (typically aluminum nuclei) per unit volume (cm^3) of the target material.

σ_{st} This represents the probability of scattering events, specifically the total scattering cross section for protons interacting with aluminum nuclei. It quantifies the likelihood of protons scattering during their interaction with aluminum nuclei.

F_{N_a}: This factor considers how much of the proton beam effectively interacts with the target nuclei (N_a) by taking into account factors such as the beam's shape and the geometry of the experimental setup.

The N_a stands for the number of radioactive nuclei after irradiation over time and can be calculated by formula given below:

$$N_a(\tau) = \frac{Q_a}{\lambda_a}\left(1 - e^{-\lambda_a \tau}\right), \tag{2.35}$$

To compute the cross section for targets with intricate isotopic compositions or when the studied isotope is integrated into a chemical compound, the following formula is employed:

$$\sigma_a\left(E_\gamma(j)\right) = \frac{S_\gamma\left(E_\gamma(j)\right)\lambda_a \frac{t_{r,i}}{t_{l,i}}}{N_p N_{targ}\varepsilon_\gamma I_\gamma\left(E_\gamma(j)\right)\left(1-e^{-\lambda_a \tau_1}\right)e^{-\lambda_p t_{2,i}}\left(1-e^{-\lambda_a t_{r,i}}\right)}, \tag{2.36}$$

where, λ_a (s^{-1}) is the decay constant for the nucleus a, $\varepsilon_\gamma(E_\gamma(j))$ is absolute efficiency of registration of γ-quanta with energy $E_\gamma(j)$, $I_\gamma\left(E_\gamma(j)\right)$ is the intensity of γ - ray decay with energy $E_\gamma(j)$ and $\tau_1, t_2, t_{r,i}, t_{l,i}$ represent irradiation time, delay, real (measurement time) and life measurement time, respectively [103].

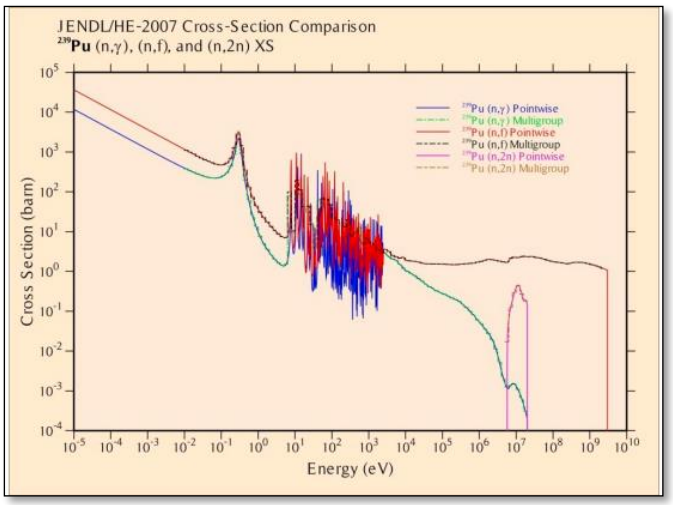

Fig.2.11. Cross sections of (n, γ), (n, f), and (n,2n) reactions in ^{239}Pu radionuclide [104].

As the likelihood of neutrons being in close proximity to the nucleus increases when their velocity decreases, the cross section for neutron capture reactions (σ) will follow an inverse relationship with neutron velocity (v). In simpler terms, as neutron velocity goes down, the probability of neutron capture goes up, and this relationship follows what is known as the "1/v law."

$$\sigma \approx \frac{1}{v} \approx \frac{1}{\sqrt{E}} \tag{2.37}$$

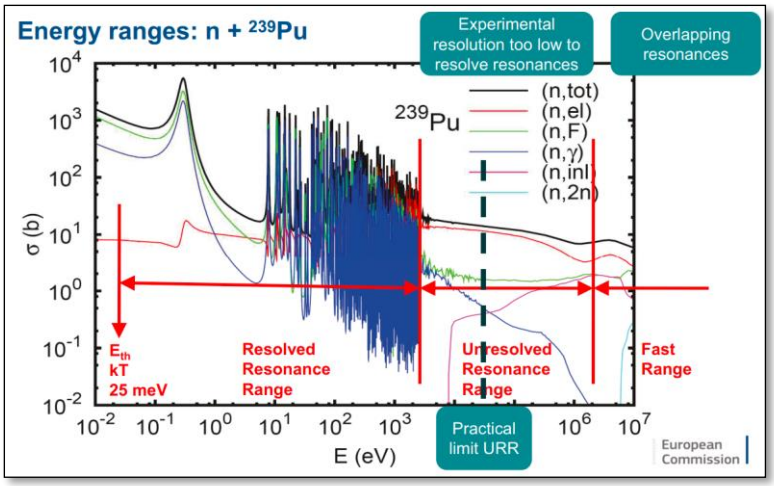

Fig.2.12. Cross sections of n+^{239}Pu reaction (energy rate is from 0.01 eV to 10 MeV) [105].

Calculating experimental uncertainty

Understanding the potential errors in physical measurements is crucial. Certain values, like γ - ray energy, γ - line intensity, the area under a Full Energy Peak (FEP), or the half-life of a measured radionuclide, cannot be determined with absolute precision. Instead, they fall within a range of measured values. To quantify individual deviations, we employ either direct or indirect measurement methods. Direct deviations are directly measured, while indirect deviations are derived from related variables. In the case of calculating the reaction rate, an

indirect method is used. This method utilizes a relationship obtained from the literature [96] to assess and determine the extent of these deviations.

$$\bar{x} = \frac{\sum_{i=1}^{n} \omega_i x_i}{\sum_{i=1}^{n} \omega_i}, \tag{2.38}$$

where, 'x' represents the weighted average, which serves as a statistical measure of central tendency for a set of measured values denoted as 'x_i' (with 'i' ranging from 1 to 'n'). The 'ω_i' values are weighting factors that account for experimental bias, defined as $\omega_i = 1/\sigma^2$, where 'σ^2' represents the experimental variance associated with each measurement. The determination of the weighted average 'x' relies on Gaussian distribution and can be approached in two ways: one that considers the internal variance of measurements, denoted as $\sigma^2(x,int)$, and another that takes into account external variance, indicated as $\sigma^2(x,ext)$. Internal and external variance equations are given below [106]:

$$\sigma^2(\bar{x}, int) = \frac{1}{\sum_{i=1}^{n} \omega_i}, \tag{2.39}$$

$$\sigma^2(\bar{x}, ext) = \frac{\sum_{i=1}^{n} \omega_i (x_i - \bar{x})^2}{(n-1)\sum_{i=1}^{n} \omega_i}. \tag{2.40}$$

The distinction between internal and external deviation lies in their independence and dependence on individual measured data. The deviation value ultimately depends on the magnitude of either the internal or external deviation. It's important to note that, apart from these deviations, the measurement's systematic error, which isn't accounted for in either internal or external deviation, should be considered for a comprehensive assessment of measurement accuracy. For illustration purposes, a relationship considering external deviation is provided, but if the calculation were performed using internal deviation, the values of external and internal deviation would differ. The calculation of the overall or total deviation, denoted as ΔX_{tot}, is determined by the following equation:

$$\Delta\bar{x}_{tot} = \sqrt{(\Delta\bar{x}_{ext})^2 + (\sigma_{st})^2} \tag{2.41}$$

When determining the total deviation, the deviations mentioned above are combined with variations in sample mass, particle beam integral, effective cross section, and the efficiency curve of the HPGe detector. Additionally, corrections as outlined in subsection 2.5 are taken into account.

Additionally, for all energy spectrum is calculated weighted average, internal error, and external error [111].

Weight of x_i:

$$w_i = \left(\frac{1}{\Delta x_i}\right)^2 \tag{2.42}$$

Weighted average:

$$\bar{X} = \left(\frac{\sum_{i=1}^{n} w_i x_i}{\sum_{i=1}^{n} w_i}\right) \tag{2.43}$$

Internal error:

$$\Delta\overline{X_{int}} = \left(\sqrt{\sum_{i=1}^{n} w_i}\right)^{-1} \tag{2.44}$$

External error:

$$\Delta\overline{X_{ext}} = \left(\sqrt{\frac{\sum_{i=1}^{n} w_i (x_i - \bar{X})^2}{(n-1)\sum_{i=1}^{n} w_i}}\right)^{-1} \tag{2.45}$$

Final error is estimated as maximum of internal and external errors.

2.6 Correction factors

In order to determine the reaction rate, it is imperative to apply certain corrective factors in order to ascertain correct and reliable values. These corrective factors compensate various errors or biases faced during the process of measurement. Some of the important corrective factors are given below:

Dead Time Correction for Reaction Rate

It refers to the correction during which detector is still processing the previous radiation events and act as insensitive towards the new radiation events for very small during of time. There is need to account for all the radiation events in order to determine the accurate reaction rate. So, this correction factor plays crucial role in ascertaining the actual reaction rate. Following formula can be used for dead time correction:

$$R = \frac{R_{obs}}{1 - R_{obs}} = \frac{t_{real}}{t_{live}}, \tag{2.46}$$

where, R stands for corrected true event rate (reactions per second (s^{-1})), R_{obs} is the observed event rate without dead time correction (reactions per second (s^{-1})), τ is the dead time of the detector (s), t_{real} and t_{live} stands for real time and live time respectively.

The R_{obs} is normally higher than R due to missed events during detector dead time. When $R_{obs}\tau$ is relatively small, indicating that the dead time is short compared to the time intervals between events, the correction factor approaches unity (2.39). In such cases, the observed event rate provides a reasonably accurate estimate of the true event rate. However, when $R_{obs}\tau$ becomes significant, signifying that the dead time is comparable to or longer than the time between events, the correction factor diminishes below.

Efficiency Correction

Efficiency correction accounts for two factors. First, not all radiations emitted by the source are not detected by the detector due to geometry constraints. Second, detector efficiency is dependent upon energy levels. In order to ensure the correct measurements, both factors need to be accounted for.

$$\frac{1}{\varepsilon_{FEP}(E_\gamma)} \tag{2.47}$$

The formula given above accounts for the efficiency correction. The term in the denominator denotes Full-Energy Peak Efficiency.

Attenuation Correction

When radiation passes through certain materials, they attenuate due to scattering and self-absorption. In order to account for these factors in the intensity of radiations, there is need to measure the attenuation factor. The attenuation factor should be multiplied with measured intensity in order to find the correction intensity.

$$I = I_0 \cdot e^{(-\mu x)}, \tag{2.48}$$

where, I is intensity of the radiation after it has traveled through a material x; I_0 is the incident intensity of the radiation before it enters the material. It indicates how strong the radiation was at its source; μ is linear attenuation coefficient (cm^{-1}) characterizes how effectively the material interacts with and weakens the radiation as it passes through. It depends on both the material's properties and the radiation's energy; x signifies the distance or thickness of the material that the radiation traverses. It's essentially the path length through which the radiation travels within the material. Overall, term $e^{(-\mu x)}$ represents attenuation for as previously used for determining corrected reaction rate.

Background Subtraction

During measurement of activity, background radiation from naturally occurring radioisotopes or cosmic rays can influence the quantification process. Therefore, in order to get the true representation of the source activity, it is essential to subtract the background fee.

$$S'_{bcg}(E_\gamma) = K_{norm} \cdot S_{bcg}(E_\gamma) = \frac{t_{l,spec}}{t_{l,bcg}} S_{bcg}(E_\gamma) \tag{2.49}$$

where $S'_{bcg}(E_\gamma)$ represents the adjusted background area for the FEP at energy E_γ. This adjustment is necessary to remove the influence of background radiation; $K_{norm} = \frac{t_{l,spec}}{t_{l,bcg}}$; is a normalization factor, computed as the ratio of the effective measurement time for the spectrum of interest ($t_{l,spec}$) to the net measurement time for the natural background spectrum ($t_{l,bcg}$). This factor accounts for differences in measurement durations between your spectrum of interest and the background spectrum.

The $S_{bcg}(E_\gamma)$ stands for the total area of the background peak at gamma-ray energy E_γ, as observed during the actual measurement time. This equation describes the subtraction of the background from the measured spectrum at the net measurement time.

The equation of sample activity is given in the following form:

$$A(t_{decay}) = A(t_{irr})\, e^{-\lambda t_{delay}} \tag{2.50}$$

where λ is decay constant; A is activity of sample; t_{irr} - total irradiation time (s); t_{delay} is the time between the end of irradiation and the start of each measurement.

Self-Absorption Correction

When measuring the activity of the radioactive sample, the emitted rays can be absorbed by the sample material itself. Self-absorption needs to be accounted for in order to measure the accurate values. The correction factor to be applied after the measurement are denoted in terms of self-absorption coefficient.

Self-absorption corrected count rate can be determined by equation given below:

$$N = \int_0^t N_0 e^{(-\mu x)} \frac{dx}{t} = N_0 \frac{1-e^{(-\mu x)}}{\mu t} \tag{2.51}$$

The N stands for measured count rate, N_0 is ideal count rate without self-absorption effect, μ is the linear attenuation coefficient, x is the thickness of the sample material through which the radiation travels and t is the measurement time [109].

Self-absorption coefficient $\eta_A(E_\gamma)$ can be determined by equation given below:

$$\eta_A(E_\gamma) = 1 - \frac{1-e^{(-\mu(E_\gamma)t)}}{\mu(E_\gamma)t} \tag{2.52}$$

To determine the number of residual nuclei (B) and the reaction rate of each detected isotope (RR) formula (2.29) and (2.30) were used corrections [110]:

Correction for the intensity of gamma transition:

$$\frac{1}{I_\gamma(E_\gamma)} \tag{2.53}$$

Correction for the decay from the end of irradiation to the end of measurement:

$$\frac{1}{e^{-\lambda t_{delay}}} \tag{2.54}$$

Correction for the decay during irradiation:

$$\frac{1}{1-e^{-\lambda t_{irr}}} \tag{2.55}$$

Corrections showing the decay during the measurement:

$$\frac{1}{1-e^{-\lambda t_{real}}} \tag{2.56}$$

Correction of detector energy nonlinearity

The calculation of non-linearity [112] for the germanium detectors plays a crucial role for the acquisition of accurate results. Non-linearity may lead to inaccuracies and resultantly make the whole measurement process doubtful. When we've already matched a peak, we can confidently attribute it to the corresponding isotope listed in the nuclear database, but this confidence only holds if there's a strong agreement in terms of energy. Integral nonlinearity,

in this context, serves as an indicator of how much the energy to-channel relationship deviates from being perfectly linear.

$$E_\gamma(x) = a_1 + a_1 \cdot x \tag{2.57}$$

where E_γ is the γ-line energy, x is the channel number, and a_0 and a_1 are the roots of this function.

We employ calibration data to rectify the effects of nonlinearity in our system, a process carried out using the specialized spectroscopic software DEIMOS32 [113]. Through this calibration, we derive specific parameters that describe how the relationship between energy and channel varies in our individual semiconductor HPGe detectors. Remarkably, we can ascertain these essential parameters using data from just two carefully selected peaks in our spectrum. The nonlinearity of the system is mathematically characterized by the following relation:

$$corF(E_\gamma) = a_0 + a_1 E_\gamma + a_2 E_\gamma^2, \tag{2.58}$$

where a_i are measured nonlinear function roots for HPGe detector. The nonlinearity deviations are determined using the γ-energies of the measured calibration emitters.

The use of correction factors for germanium detectors is absolutely vital in making sure that our gamma-ray spectroscopy measurements are accurate and dependable. These correction factors take into account a range of factors, both related to the equipment itself and the surroundings, that can impact the collected data. They serve as invaluable tools for researchers and technicians across a range of fields, including nuclear physics, environmental monitoring, radiological assessment, and materials analysis.

CHAPTER 3

APPLICATION OF SOFTWARE FOR PROCESSING γ-SPECTRA

Analyzing and interpreting data from gamma - ray detectors is a standard procedure in γ - ray spectroscopy. Various software packages are available for this task, each offering distinct features and functionalities.

The DEIMOS32 [113] software, a collaborative effort between the Institute of Nuclear Physics in the Czech Republic (Řež) and the Joint Institute for Nuclear Research in Dubna, Russia, was specifically developed for the processing of γ - ray spectra. This program helps in identifying the positions of peaks, calculating their areas, and analyzing various other parameters within the spectra.

Determining the efficiency of an HPGe detector and fitting a mathematical function to experimental efficiency data concerning γ - ray energy using the Effekt8.exe program involves a series of key steps. This process begins with collecting efficiency data at different gamma-ray energy levels, launching the Effekt8.exe program, choosing a suitable mathematical function, often a polynomial, to describe the relationship between efficiency and γ - ray energy. It also needs fitting this function to experimental data and evaluating the fit's quality using statistical metrics, visualizing the results through graphs, documenting and reporting the fitted function's parameters, validating the fit with other data or simulations. The specific choice of function and its order hinges on the detector's characteristics and the shape of the efficiency-energy curve, necessitating careful consideration and, at times, fine-tuning for accuracy. Remember that the choice of the fitting function and order may depend on the specific characteristics of your HPGe detector and the behaviour of the efficiency-energy curve.

The identification of nuclei formed in ^{239}Pu samples as a result of nuclear reactions with protons was carried out using the AD4HEL code [117]. This software serves as a tool for analyzing and interpreting data from experiments involving the irradiation of ^{239}Pu samples with protons.

To verify and validate the obtained results, a simulation of the experiment was conducted using tools such as MCNP v.6.1 [121], PHITS [134], and FLUKA [125]. Comparing the experimental findings with the outcomes produced by these software applications serves to affirm the accuracy of the results and provides valuable insights into the spallation reaction process. It's important to note that there are only a limited number of computer codes available for simulating the interaction of high-energy particles with matter, particularly in the context of nuclear reactions.

3.1 DEIMOS32

The DEIMOS32 [113] is a software program designed to manage and analyze multichannel pulse-height spectra generated by various HPGe instruments commonly found in the market. It offers both interactive manual and automatic evaluation modes, allowing users to process data efficiently. The outcomes of the analysis can be saved in multiple output files for further use.

The software's performance is influenced by the careful selection of specific peak regions, adhering to prescribed criteria. Additionally, DEIMOS32 includes functionality for calibrating detector efficiency. It supports the identification of isotopes and facilitates the calculation of their absolute activity levels. Furthermore, users can conveniently edit data within the program using its built-in text editor.

The DEIMOS32 is specifically crafted to manage data generated by HPGe detectors, which capture the energy from γ - ray interactions and represent it in terms of channel numbers. In the realm of γ - ray spectroscopy, one crucial procedure is the calibration of the detector's efficiency. The DEIMOS32 offers the capability to carry out this calibration, a fundamental step in ensuring the precise quantification of radioactive substances. Moreover, the program boasts the ability to recognize isotopes by scrutinizing the distinctive features of γ - ray peaks within the spectra. This feature plays a pivotal role in discerning the radioactive sources contained within the samples under examination.

The energy and peak areas of gamma rays are determined using the DEIMOS32 program, which allows you to find peaks in the gamma spectrum and determine their position, area, and width (operates in automatic or interactive modes). The program has 6 main windows: configuration, spectrum window, peak estimation, detector efficiency calibration, activity calculation and text editor (they all open in the main window).

The background is calculated as the sum of linear and step functions. When all γ-spectra are processed by the DEIMOS32 program, the spectra are “cleaned” from background lines.

In addition, the maximum possible upper limit of the line area is determined $S_\gamma^{lim}(K_i)$:

$$S_\gamma^{lim}(K_i) = \frac{3}{2}\sqrt{N(K_i)} \cdot (FWHM), \tag{3.1}$$

where $N(K_i)$ is the number of samples in the channel, FWHM – the width of the line at its half height.

In addition, the peaks of double and single (SEP and DEP) departures are taken into account in the spectra. The curves of the intensities of the peaks of a single (or double) outburst to the peaks of total absorption are set in separate calibration measurements. These relations are practically independent of the distance between the RA source and the detector. The areas of the SEP and DEP peaks are calculated based on the areas of the total absorption peaks.

The necessary information about the spectrum, as well as the analysis mode are in the input configuration file. You can set all this information in the configuration window. Basic settings include calibration, peak search parameters, analysis mode, and input and output files for analysis. DEIMOS32 uses several formats like DAT, MCA, SPE, CNF, CHN, SPC, etc. Channel numbers are limited to 16 thousand. Spectra can be stored in ASCII, SAMPO, SPE, ORTEC S100, MCA, ORTEC, CHN formats. The spectra can be processed one by one or processed in batch mode without any restrictions.

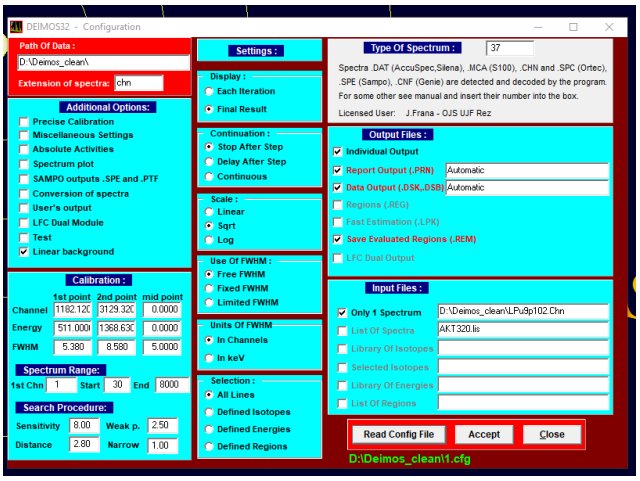

Fig.3.1. Configuration window.

There are several ways to calibrate energy and peak width versus channel number. The simplest way is to enter several channel-energy-FWHM values that act as an approximate two-point linear calibration ($= a_0 + a_i \cdot c$; $FWHM = b_0 + b_1 \cdot sqrt(c)$, c - channel number). This method is usually used if the error is less than 0.5 keV across the spectrum. Higher accuracy can be achieved by fitting and calibrating peaks in the spectrum.

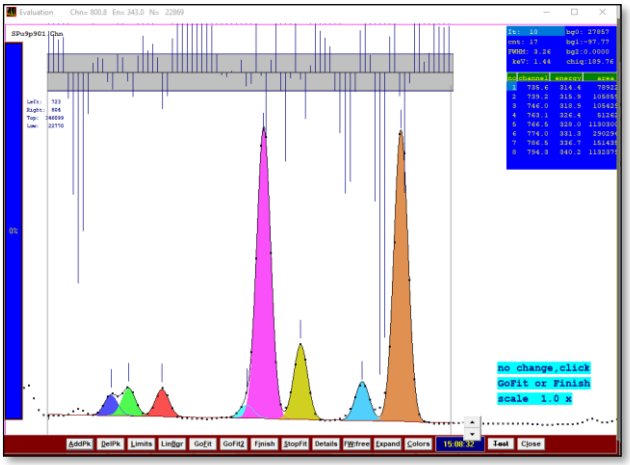

Fig.3.2. Multiplet analysis window.

Peak search is performed manually or automatically. Selected in the spectrum of the peak or region for analysis and then displays the corresponding multiplet. It also supports the possibility to change the borders and add or remove peaks in the analysis. In automatic mode, the program itself looks for peaks and sets the boundaries of the multiplet. Manual and automatic modes can be used at any time during spectrum processing. Determining the peak parameters is a major part of the analysis. The simplest is to define the boundaries of the selected peak by integrating the channel content program with background removal. A quick but only approximate analysis of the peak position is performed at the beginning of the fit. This is done in order to have an approximate idea of the position of the selected peaks.

Overall, DEIMOS32 emerges as a versatile software solution tailored for the thorough examination of gamma-ray spectra collected using HPGe detectors. Its versatility renders it a valuable asset for researchers engaged in nuclear physics and other domains where the precise analysis and quantification of radioactive materials are paramount.

3.2 Calculation of efficiency of HPGe-detector

When high-energy gamma radiation interacts with matter, it can lead to the formation of electron-positron pairs. Subsequently, these positrons can annihilate with electrons, giving rise to two photons with energies of 511 keV each. In the context of germanium detectors, there is a significant likelihood that these 511 keV photons will impinge on the detector, leading to distinctive features in the recorded spectrum. These features manifest as peaks, and their boundaries or limits are determined by specific mathematical expressions. These expressions quantify the probabilities of events resulting in single escape peaks (SEP) and double escape peaks (DEP). The limits of these peaks are determined by the following expressions:

At elevated levels of gamma radiation energy, there is a potential for annihilation radiation to escape. When a positron-electron pair is formed, the positron's subsequent annihilation generates two photons, each with an energy of 511 keV. In the case of germanium detectors, there is a notable likelihood that one of these annihilation photons may exit the detection system. If only one photon manages to escape, it will manifest as a single output peak (SEP) in the recorded spectrum. When both photons escape, a double output peak (DEP) is observed.

The area of the SEP or DEP peaks can be determined relative to the area of peak E, which represents the full energy peak:

$$S(E_{SEP}) = S(E_\gamma) \cdot \epsilon_{SEP}(E_\gamma) \tag{3.2}$$

$$S(E_{DEP}) = S(E_\gamma) \cdot \epsilon_{DEP}(E_\gamma) \tag{3.3}$$

$\epsilon_{SEP}, \epsilon_{DEP}$ - coefficients of single and double peaks determined experimentally. The coefficients remain constant and are not influenced by the distance between the target and the detector. Fig.3.3 illustrates the relationship between $\varepsilon_{EP}(E_\gamma)$ and the peak energy, showcasing how it varies with changing peak energy values.

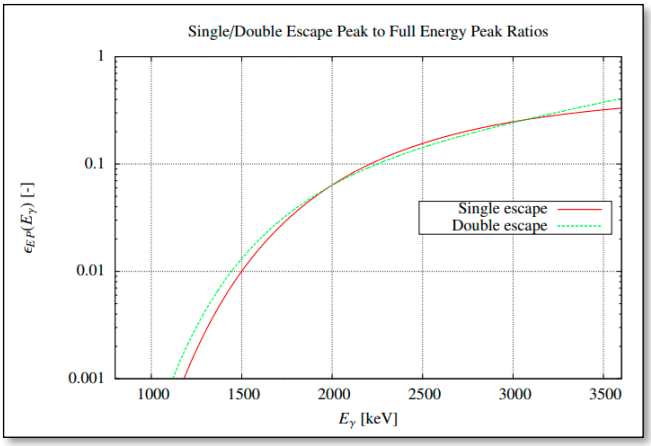

Fig.3.3. Determination of dependency of SEP/DEP and full-peak area ratios on full-peak energy E_γ through experiment [114].

$$\left|E_\gamma - E'_\gamma\right| < n \cdot \sqrt{a^2 + (\Delta E_\gamma)^2 + \left(\Delta E_y^{bcg}\right)^2} \tag{3.4}$$

E_γ - energy of the gamma spectrum. E'_γ - energy of a single (double) peak, ΔE_γ, ΔE_y^{bcg} - are their errors, n is a variable determined by the statistic (~1), a is a correction that considers the nonlinear effect for the experiment a = 0.15 keV.

$$\left|E_\gamma - E'_\gamma\right| < m \cdot FWHM\left(E_\gamma\right) \cdot E_\gamma / N_{ch}\left(E_\gamma\right) \tag{3.5}$$

m - a correction that considers the non-Gaussian nature of the gamma peaks (usually m=1). N_{ch} - channel number E_γ.

The experimentally measured points were determined by function:

$$\epsilon_{EP}\left(E_\gamma\right) = \exp\left(s_0 + s_1 \ln\left(E_\gamma\right) + s_2 \ln\left(E_\gamma\right)^2 + s_3 \ln\left(E_\gamma\right)^3 + s_n \ln\left(E_\gamma\right)^n\right) \tag{3.6}$$

where, s_0, s_1, s_2, s_3, s_n – coefficients are found using Efekt8.exe and confirmed by Python script. Below, Fig.3.4 shown view of the relative efficiency of the full energy peak on the graph.

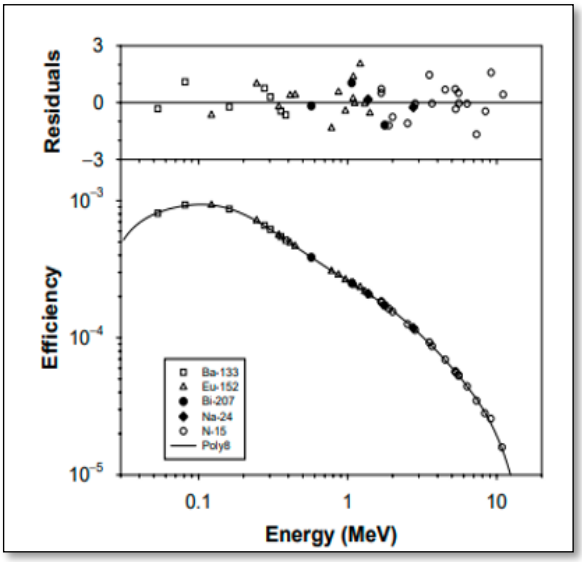

Fig.3.4. The lower curve represents the relative efficiency of the full energy peak, which has been calculated by fitting an 8th - order polynomial to the complete dataset. The upper curve illustrates the normalized residuals associated with this data [114].

The value s_i is set by the program Effekt8.exe are given in the Table 3. Details about this experiment is given in [115]. Below is an example how looks calculated parameters s_i.

Table 3. Experimentally determined parameters $\epsilon_{EP}(E_\gamma)$ of the function [115].

	SEP		DEP	
	s_i [-]	Δs_i [-]	s_i [-]	Δs_i [-]
0	-2.0866027851	0.2860230746	-1.3273140355	0.1814312750
1	13.8832738535	1.1099975243	12.8053750577	0.8383854495
2	-8.2291578426	1.3992857931	-8.9129115117	1.1473203273
3	1.7178618884	0.5675750337	2.6470549618	0.4847393276

The full energy peak efficiency correction factor ($\eta_e(E_\gamma)$) is calculated according to formula:

$$\eta_e(E_\gamma) = \exp\left(a_0 + \sum_{i=1}^{np} a_i ln^i(E_\gamma)\right), \tag{3.7}$$

The parameters "a_i" correspond to the coefficients of the efficiency curve. These coefficients are determined through a series of measurements and calibration standards using the Effekt8.exe program. These measurements involve gamma peak energies represented by "E_γ". The program Effekt8.exe calculates these coefficients to create an efficiency curve that characterizes how the detection system responds to γ - ray energy at various energy levels. This curve is essential for adjusting and ensuring the accuracy of measurements in nuclear and radiation applications.

The same kind of function of polynomials of the 8th degree was used to describe the dependence of the absolute efficiency of registration on the energy of γ - quanta (see Fig.3.5).

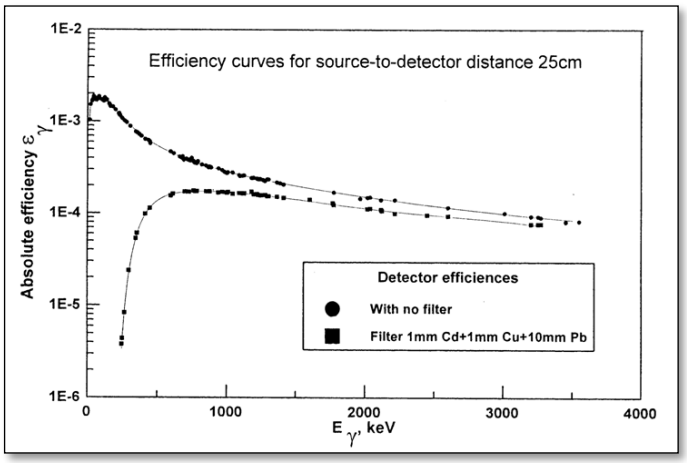

Fig.3.5. Dependence of absolute efficiency of γ-radiation of HPGe-detector on γ-quanta [116].

3.3 Description of AD4HEL code

The AD4HEL code [117] is a specialized program designed for analyzing neutron spectra produced by lasers. It exclusively supports the .prn file format and is capable of processing gamma spectra.

Moreover, this software provides the capability to compute production and reaction rates, where the production rate is expressed as the number of reactions occurring in a sample

per second. The reaction rate is quantified as the number of reactions normalized for each incident particle and each atom of foil, requiring integration of the flux.

Additionally, various values and results are stored in an ".xlsx" file located within the "out" folder.

Program description

Table 4. The information which is displayed for each spectrum in AD4HEL code.

Name	file name
Start of measurement	date and time of start of measurement
Live time	net measurement time t_{live} (s)
Real time	total measurement time t_{real} (s)
Detector	detector designation
Position	indication of the position in which the sample was during the measurement
Sample name	name of the measured sample
Measurement number	measurement number
Weight	sample weight (g)
Molar mass	molar mass (mol)
Cal en_1	calibration energy (keV) - lower value
Cal en_2	calibration energy (keV) - higher value
Delayed time	time between the end of irradiation and the beginning of measurement (s)
Element	an element (or list of elements) forming the material of the sample
Fraction by weight	weight fraction (-),
Density	material density (g / cm^3)
Thickness	sample thickness (mm)
Non-point	correction for sample non-point

Main section offer

The main section Main in the menu is used for basic work with spectra. By selecting the Work Directory user loads the folder with the *.prn* spectrum files from DEIMOS32.

The names of the individual files must be in one of the following forms:

- a5NaCl3p_2, where a is the designation of the detector; 5NaCl is the name of the sample; 3 is the measurement number and p_2 is the position during measurement.
- aNaCl5_3_p_2, where the sample name, measurement number and position are separated during the measurement underscores.

The spectrum information is then loaded into the main window in the form of a list. Double by clicking on the selected spectrum (or by marking the spectrum and selecting the Open Selection) it is possible to display information about the given spectrum.

Irradiation Info (Fig.3.6) is used to enter the basic parameters of irradiation (end time irradiation, duration of irradiation and integral of incident particles).

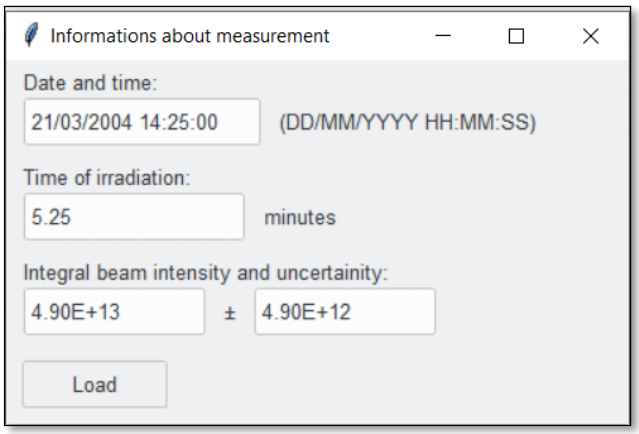

Fig.3.6. Window for setting irradiation parameters.

Sample Weights (Fig.3.7) allows the user to enter information about the weights of each sample together with the calibration energies that were used to evaluate the spectra. When measuring, and evaluation a linear calibration of the channel-energy dependence was used as standard. Here it is possible correct for the actual course of nonlinearity if it was determined and inserted into the library of nonlinearity.

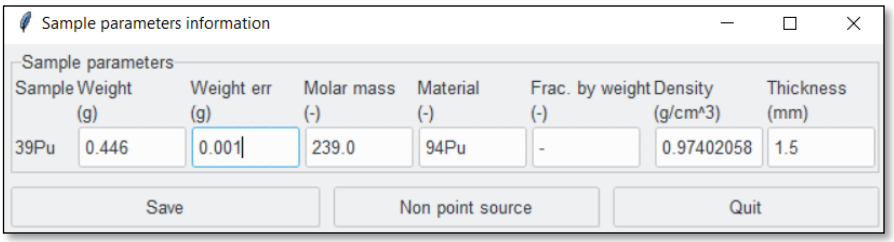

Fig.3.7. Window for entering information on sample parameters information.

Sample Thickness is used to retrieve information to calculate the self-absorption correction. If the sample consists of only one element, the user enters the chemical designation of the element, which consists of the sample material and the sample thickness. If the sample material is a compound, it is necessary to In the Material field, enter the designation of the elements forming the compound separated by a slash, then the mass a fraction in which the ratios will be in the same order as their respective elements, the density of the material and sample thickness.

The inputs described above are automatically saved in the parameters.txt file in this folder spectrum, which allows the relevant values to be read automatically when the folder is reopened.

The Correction option is used to select the calculated corrections. Efficiency correction detector (Efficiency) is necessary for further calculations, correction for detector nonlinearity (Nonlinearity) is strongly recommended especially for more complex spectra with a large number of peaks. The calculation of the correction for nonlinearity is conditioned by entering the calibration energies the calculation of the correction for self-absorption (Attenuation) is possible after entering the sample information in the Sample Thickness section.

It is also possible to read the peaks of single and double trips (Escape peaks) and read by the background (Background). The relevant calculations are performed by clicking on the Calculate button corrections.

Selection of libraries

The data necessary to calculate the individual corrections are read from the libraries stored in the folder libraries, which is created next to the main file. The libraries menu allows the user to load their own library. The format of each library is described below. For all libraries, comments are marked with a double cross symbol.

a. Self-absorption. The AttLib.lib library is used to calculate the self-absorption correction and its change is possible with the help of Attenuation selection.

b. The library includes data for individual elements that make up the material of the sample used. The first line of data for each element contains the name of the element, composed of its proton number and chemical symbols, followed by the letter C. The following is information on whether the coefficients are functional interspersed with one curve (0) or two curves (1). Next, the material density is entered in g / cm^3 and the value of the separation energy in MeV (in the case of a single curve interpolation, the value of the separation energy) energy 0). The next lines contain the individual points of the function μ / ρ, describing the decrease in radiation intensity as it passes through the material. Each line contains the element name, the energy in MeV, and the value of the function for this energy in cm^2 / g. The data for each element is separated by a line of crosses.

c. Background reading. The Background.fon library contains data for reading the background. Use the item to change the file Background.

The data for a given detector is indicated by the name of the detector in the first position of each line. The first line shows the effective measurement time t_{live}. The next lines after the detector designation contain the energy of a given peak, the absolute magnitude of the energy uncertainty, the area of the peak and the absolute magnitude of the uncertainty areas.

d. Detector efficiency. The data for calculating the detector efficiency corrections are contained in the Efficiency.lib library by can be changed when selecting Efficiency. The format of the library can be seen in Table 5.

Table 5.Format of the library for correction for detector efficiency.

```
a   p4  0 keV       # Dubna detA
8.7068775580    -0.8540568058   0.0155963966    -0.1849935725   -0.0769994015   0.0253357634    0.0140929659    0.0015693362    0

a   p5  0 keV       # Dubna detA
8.3958715085    -0.8476246288   0.0187964018    -0.1929499796   -0.0766444061   0.0325082148    0.0170920522    0.0019079381    0

a   p6  0 keV       # Dubna detA
8.1016090970    -0.8543624351   0.0238895199    -0.1895002838   -0.1084188070   0.0069761375    0.0102687460    0.0012952164    0

a   p7  0 keV       # Dubna detA
7.7286871472    -0.8640281061   0.0815055722    -0.1220334923   -0.0997574436   -0.0049543266   0.0056088431    0.0008113684    0
```

The library contains data for each detector and each position in which the measurement was performed. The first line consists of the detector designation, the measuring position, the separation energy in keV and the unit information energy used to determine the coefficients of the function (keV, MeV or APR). Depending on whether the interpolation of the function consists of one or two curves, followed by one or two lines containing the coefficients of the polynomial in the exponent of the corresponding function.

e. Detector nonlinearity. The data for calculating the detector nonlinearity correction are contained in the NonLin.lib library, which can be changed when selecting Nonlinearity.

The formatting is similar to the library for calculating detector efficiency. For each the detector is the first line formed by the designation of the detector, followed by information on the separation energy in keV. Depending on whether the data was interleaved with one or two curves, one or two rows of function coefficients.

f. Beam nonlinearity. The information for calculating the correction for nonlinearity of the particle beam with which the samples have been irradiated is located in the deck_carb.txt file and can be changed when Beam Fluctuation is selected. The file consists of three columns of data - date, time, and number of particles in the beam.

g. Energy of γ - lines. The gamma.lib library is used to calculate the reaction rate and its change is possible during selection Gamma Intensity (all). The individual lines always contain the energy of the γ line, the absolute magnitude of the energy uncertainty, the intensity, and the absolute magnitude of the uncertainty of the intensity, the isotope designation, the half-life and the absolute magnitude half-life uncertainties, followed by one.

*Isotope names may contain various additional letters; in the case of the letter "**m**" or "**M2**" etc. is the so-called isomer (metastable level) of a given isotope. The second case is the letter "**D**" following the standard isotope designation, e.g., "^{130}LaD". This symbol is used when ^{130}La is part of a decay series and the parent isotope ^{130}Ce is converted to ^{130}La, has a significantly longer half - life than ^{130}La. In that case, it is the decay curve for ^{130}La is determined primarily by the longer half-life of the parent radionuclide. The gamma_lib_ref.lib library has the same format, which contains data for reference only radiators. It can be changed when selecting Gamma Intensity.*

h. Activity of reference emitters. The Activity.lib library contains information about reference emitters. The library change is possibly by selecting Activity. The individual lines always contain information about one reference emitter, in the format that is shown in Table 8. The first is the chemical designation of the isotope, then the identification number, reference date, reference activity in Bq and reference activity uncertainty.

Calculation of reaction rate

After uploading the files with the spectra, adding the necessary information in the Spectra section, and calculating required corrections, it is possible to proceed to the main calculations. The user has a choice between by calculating the production rate (PR) and the reaction rate (RR). The PR or RR item is used for this in the menu.

The windows for both types of calculations are practically the same, only the RR option allows you to perform them in addition correction for beam nonlinearity. The window is divided into two parts. In the Fig.3.8 there is a window for displaying the graph. The user selects the sample for which the calculation is to be performed, together with the isotope and energy of the γ line. It is also possible to set whether a correction should be made for coincidences and in the case of RR calculation beam nonlinearity correction.

Upon clicking the "Calculate" button, the program checks whether the selected energy is present in the recorded spectra. If it is, the spectrum will be displayed in the results list. Following that, the program will present the calculated values for RR (Reaction Rate) or PR (Production Rate), along with their associated uncertainties, coincidence or beam fluctuation corrections, the number of transformations, and the time interval between the end of irradiation and the measurement.

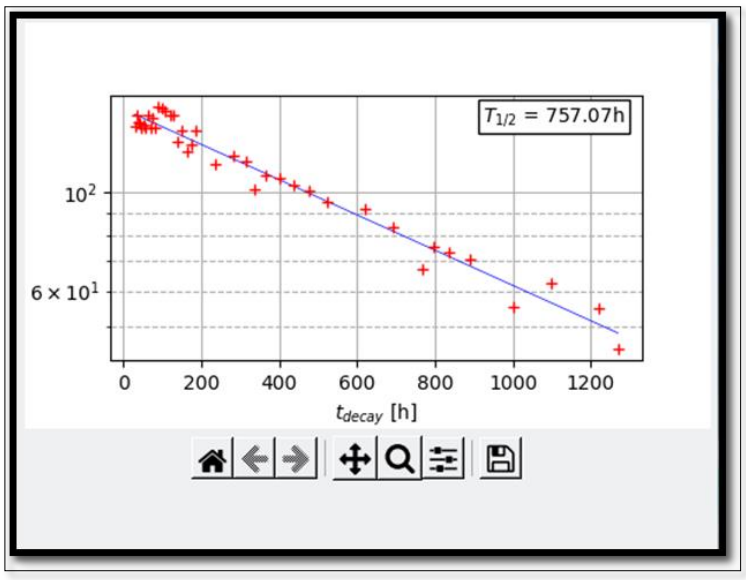

Fig.3.8. Part of the window for calculating the reaction rate.

The user can choose specific values for further processing using checkboxes. The "Plot" button enables the plotting of selected data, and the "Save to XLSX" option saves the data to a file named "RR (PR) results.xlsx" in the Output folder. Furthermore, the "Add to export file" function adds the selected values to memory for the final calculation.

At the same time, the decay curve is plotted, i.e., the dependence of the number of transformations of a given isotope on time. From this curve the half-life $T_{1/2}$, f is calculated, which together with the reference half-life decay from the library $T_{1/2}$, tab shown in the graph. Buttons below chart allow the user to change the layout of the chart and export it as an image.

CHAPTER 4

SIMULATION TOOLS AND THEIR ROLE IN ADVANCING EXPERIMENTAL UNDERSTANDING

4.1 The Monte Carlo method

In this study, the Monte Carlo method was applied for calculating reaction rate and cross section of radionuclides which were obtained in plutonium target after irradiating it with high-energy proton beam. The Monte Carlo method [118, 119] is a numerical technique employed for simulating the behavior of diverse scientific and engineering fields, such as radiation transport, nuclear physics, nuclear reactor design, radiological protection, determining cross sections of radionuclides and other particle interactions, etc. Unlike deterministic algorithms, this method is inherently stochastic. It revolves around conducting numerous random experiments using a system model. The key aspect is the use of a high-quality pseudo-random number generator (actual random numbers are not necessarily required). The outcome is a probability associated with a specific effect.

In a typical Monte Carlo approach, the process unfolds as follows:

1. Characterize the statistical properties of potential inputs.
2. Generate multiple sets of potential inputs that conform to the identified statistical features.
3. Employ deterministic calculations with these input sets.
4. Conduct a statistical analysis of the results. Generally, the error linked to the outcomes decreases in relation to the square root of the number of experiments, expressed as $1/\sqrt{N}$.

The precision of the results in the simulation is contingent on the quantity of trials carried out. The square root of the simulated events' number exhibits an inverse relationship with the statistical error. In practical terms, to halve the error, the number of simulated events must increase fourfold. Achieving sufficiently accurate results for intricate accelerator driven systems is made feasible within a reasonable timeframe thanks to the utilization of high-speed parallel computers. These computers can concurrently generate a multitude of events [119].

In this study, the Monte Carlo method was applied for calculating reaction rate and cross section of radionuclides which were obtained in plutonium target after irradiating it with high-energy proton beam. As a basic concept, this method is based on random sampling which helps to estimate numerical results. The output depends on how much number of events are used in simulation, increasing number make probability of events higher. It means that using high number of events makes our result less uncertain and provides more reliable output. In this context, the study of the cross section of radionuclides involves modelling the behaviors of particles (e.g., protons and secondary particles produced in the p + $^{239}PuO_2$ reaction) during interaction with the target material.

Main characteristics of experiment which need to be defined for the simulation through Monto Carlo based simulation codes are geometry, composition of target, and initial conditions such as energy distribution of particles. The use of random numbers may determine the direction and energy of particles, fragments after interaction or collision. This

interaction can cover several processes such as scattering, absorption, etc. Appropriate physical models and special cross section data are employed in order to simulate interaction between particles (proton) and target (plutonium). In the case of FLUKA, this cross section data is based on evaluated nuclear data libraries such as JEFF, ENDF, JENDL, etc.

When each particle interacts with the material under study, program determines how much interaction occurred and calculates cross section probabilities. To ascertain correct statistical information, the simulation should be repeated for many particles. To ascertain the cross section, one divides the count of particular interactions by the overall number of simulated particles. This calculation yields an estimation of the cross-sectional area for the given radionuclide and target material while taking into account the specified conditions of the simulation. The Monte Carlo simulations estimate the error in the result. In this study, the Monte Carlo method is used for verification and validation of results by comparing simulation data with experimental results.

Comparison of experimental data with simulation results can significantly improve Monte Carlo method-based simulation programs. It also improves the economy of difficult and rather expensive experiments in the future.

4.2 MCNP code

The accelerator driven system is a modern type of reactor which can be effectively utilized for disposing of high-level nuclear waste. In this system, the spallation target plays a crucial role by converting a high-energy particle beam into low-energy neutrons. One key factor for practical purposes is to determine how many neutrons are produced for each proton in the spallation target. This crucial value, however, is impacted not solely by the material employed but also by the target's size, attributed to the internuclear cascade. To calculate and study this, the MCNP code is one of the main useful tools [120].

The MCNP (Monte Carlo N-Particle) [121, 122] computer code is based on Monte Carlo method. It is specifically designed for simulating the transport and interaction of 34 types of particles, and 2000+ heavy ions, such as photons, neutrons, electrons, etc, in various materials and complex geometries. The MCNP code was developed by Los Alamos National Laboratory. The MCNP has many application in various field, such as detector design, radiation protection & dosimetry, radiation shielding, medical physics, radiation therapy planning, accelerator target design, decontamination & decommissioning, fission and fusion reactor design, etc. Additionally, this code can simulate criticality of system (nuclear criticality safety).

Data for light ions like protons is easily available for a variety of target materials. However, for other light ions with atomic numbers between 1 and 3 ($1 \leq Z < 3$), the data is often limited to interactions with light targets (atomic number less than 4). When dealing with higher energy levels or interactions with heavier targets with no tabulated data, we use model physics in simulations. The shift from low to high energy depends on the type of particle and the data library in use.

Several stages are involved in nuclear physics simulations depending on factors such as the type and energy of the projectile particle, the target isotope, and the chosen physics model. These stages include intranuclear cascade, pre-equilibrium, evaporation, coalescence, and residual decay [123].

In a spallation reaction simulation using MCNP, the procedure is segmented into three distinct stages, with each stage utilizing a dedicated model. The initial stage is the Intra-Nuclear Cascade (INC), which occurs concurrently with a pre-equilibrium phase. Subsequently, there is an equilibrium evaporation phase, which competes with a fission channel (in which fission fragments go through an evaporation process dependent on their excitation energy). Following evaporation stage, after is a de-excitation process for the remaining nucleus, leading to the generation of gamma rays. The MCNP allows users to select different models for describing each of these stages in the spallation reaction.

Figure given below, demonstrates the calculations of different INC physical models for residual nuclei simulated in MCNP code.

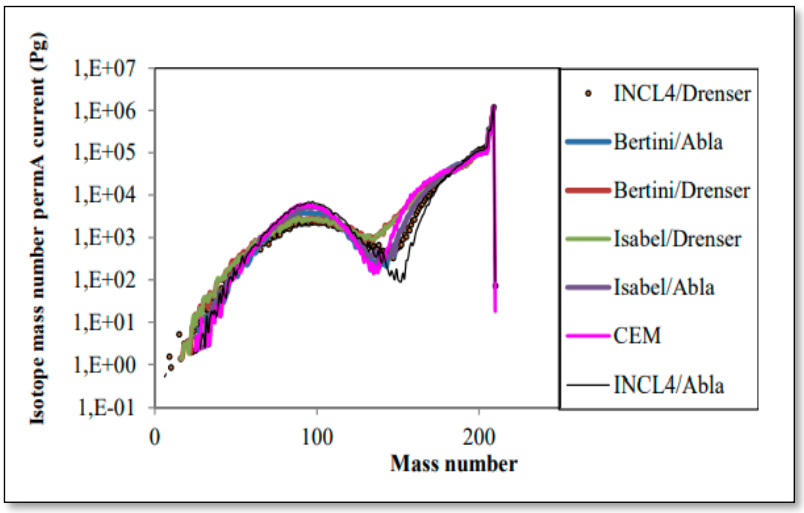

Fig.4.1. Comparison of different INC physical models for calculations of residual nuclei production in LBE target, diameter: 15 cm, height: 60 cm [124].

When simulating the movement of particles through a specified shape and considering collisions and ways to reduce uncertainty, the simulation relies on random numbers. These numbers help represent the likelihood of different events happening. Each simulation run has its own set of random numbers, making it independent from others. As the particle goes through the simulation, various events are recorded. The MCNP code has different ways to keep track of these events, like measuring the current and flow on surfaces, the length of the path taken, detecting particles at specific points, tracking particle heating, fission heating, counting particles' energy or charge deposited, using mesh for measurements, creating radiographic images, considering perturbations/sensitivity, and employing specific methods for certain measurements. The results and their certainties are calculated by looking at the whole set of independent event records [123].

4.3 FLUKA code

In the present day, the FLUKA code [125] is considered as one of the most powerful particle transport codes, which usually used for simulating the interactions of particles with matter in the wide energy range (MeV to TeV) [126]. This code includes in itself a lot of application such as high-energy physics, radiation protection, shielding research and even cosmic events. The FLUKA code [127, 128] is a general-purpose Monte Carlo code. This code was collaboratively developed by the European Organization for Nuclear Research (CERN) and the Italian Institute for Nuclear Physics (INFN).

The FLUKA code utilizes the famous Monte Carlo method to evaluate the particle path and subsequent interactions. It has numerous advantages in terms of calculating total cross section area by utilizing particle of several types and wide energy ranges. Moreover, with the wide base of iterations, it achieves high accuracy and ensures user friendly interface to visualize and analyse the results. The FLUKA Code employs wide range of particle interaction libraries to calculate total cross section (TCS). It ascertains probability of both absorption and scattering by using the material interactions along with composition available through its libraries [129].

In order to define various parameters and settings for the simulation in FLUKA, it employs various “cards”. The "cards" are essential input lines in the simulation's configuration file, detailing parameters, and settings. Key cards such as START, BEAM, PHYSICS, MATERIAL, REGION, DEFINE, SOURCE, and STOP play distinct roles in shaping the simulation. The START card initializes the simulation and specifies the number of particle histories, while the BEAM card defines properties of the particle beam. The PHYSICS card specifies interaction models, MATERIAL describes material properties, and REGION assigns materials to geometry regions. The DEFINE establishes parameters, SOURCE specifies particle source characteristics, and the STOP card marks the simulation's conclusion. These cards collectively compose the input file, influencing particle behaviour, interactions, and scoring throughout the simulation.

For editing FLUKA input files and visualization of output files [130], FLUKA uses FLAIR software. The FLAIR is entirely based on python and Tkinter. Moreover, FLAIR utilizes gnu-plot for visual representation of particle simulations. The FLAIR also provides the visual representation of geometry based on the input file (see Fig.4.2).

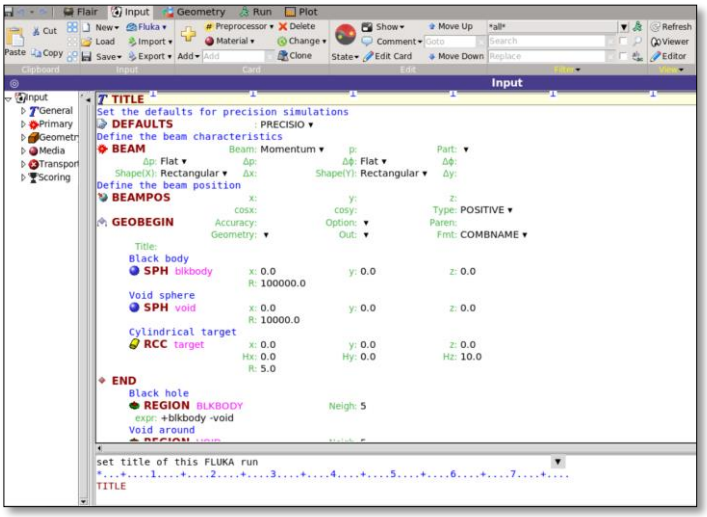

Fig.4.2. View of FLUKA visualization interface (FLAIR).

Explanation reaction rate and cross section in FLUKA code context [131]. The mean free path (λ) denotes the average distance a particle travels within a material before undergoing an interaction. The macroscopic cross section (Σ) in units of [cm^{-1}] represents the probability of interaction per unit distance and exhibits an inverse relationship with the mean free path. The mean free path and macroscopic cross section depend on the structure of material, particle energy and type of particle.

The count of reactions (R) occurring within a specific time range for N identical particles is equal to N times the total distance traveled by a particle (l) multiplied by the probability per unit distance (Σ):

$$R = Nl\Sigma \tag{4.1}$$

Therefore, the reaction rate:

$$\dot{R} = \frac{Ndl}{dt\,\Sigma} = Nv\Sigma, \tag{4.2}$$

where v – the average particle velocity.

The reaction rate inside the volume element dV is:

$$\frac{d\dot{R}}{dV} = n(r,v)v\Sigma, \tag{4.3}$$

Assuming that $n(r,v) = \frac{dN}{dv}\ (cm^{-3})$, and $v = \frac{dl}{dt}\ (cm\ per\ s)$.

Fluence rate or flux density is given by formula:

$$\dot{\Phi}\ (r,v) = n(r,v)v, \tag{4.4}$$

and has units $(cm^{-3} \cdot cm \cdot\ s^{-1}) = (cm^{-2} \cdot s^{-1})$. For describing the density of particle beam is used fluence which is measured $(particles\ per\ cm^{-2})$:

$$\Phi\ (r,v) = n(r,v)dl \tag{4.5}$$

In this case, the number of reactions which occur inside a volume V is describe by formula:

$$R = \Sigma\Phi V \tag{4.6}$$

For obtaining microscopic cross section σ , it is necessary to divide the macroscopic cross section by the number of atoms per unit volume N_0. ($\sigma(barn = 10^{-24}cm^2)$):

$$\frac{probability/cm}{atom/cm^3} = \frac{probability \cdot cm^2}{atom} = atom\ effective\ area \tag{4.7}$$

Both the microscopic cross section (σ) and the macroscopic cross section (Σ) share a similar physical interpretation, representing the "probability of interaction per unit length." However, the length is measured in different units for each.

The FLUKA is very good tool for simulating spallation reactions. In order to simulate spallation reaction of high energy protons with study target, following steps are followed (detail of experiment see in Chapter 6):

1. **Defining Geometry:** It includes description of position, deviation, and parameters of main components. Also, it is obligatory to specify the position and orientation of the project beam and target within the geometry.

2. **Defining Materials:** The FLUKA Code has special material cards to define each material and its associated properties for the simulation. The program uses special nuclear data libraries and low-energy neutron cross sections libraries for the target material definition. For simulation of correct results, it is important to calculate density of target.

3. **Defining Particle Source:** The proton beam source characteristics are specified, such as energy in MeV, the direction of the beam towards the target, irradiation time in seconds, and power of specific particle beam.

4. **Estimators (scoring) and Detectors:** The FLUKA Code employ estimators "scoring" to score particle interaction characteristics. It involves regions to collect relevant data, for instance particle fluence, energy deposition, and secondary particle production. For example, the values for different types of products which can be achieved through RESNUCLEI Card scoring in FLUKA code can be seen in Fig.4.3.

WHAT(1) : type of products to be scored
= 1.0: spallation products (all inelastic interactions except those induced by neutrons below the threshold for multigroup treatment)
= 2.0: low-energy neutron products, i.e., those produced by neutrons below the threshold for multigroup treatment (provided the information is available, see Note 1).
= 3.0: all residual nuclei are scored (if available, see above)
= 0.0: resets the default (= 1.0)
Default = 1.0 (only spallation products are scored)

Fig.4.3. RESNUCLEI Card settings in FLUKA on the basis of "stored" products [132].

5. **Defining Physics Processes:** After scoring the next task is to select the physics models and parameters relevant to reactions in study target.

6. **Setting Run Parameters:** The run parameters are defined using "START Card". It is a necessary component to commence the simulation in FLUKA. It plays a crucial role in specifying the number of particle histories, a vital parameter required for running the project and establishing the quantity of particle histories since it directly affects the statistical precision of the simulation outcomes. The snapshot depicting START Card is given below in Fig.4.4.

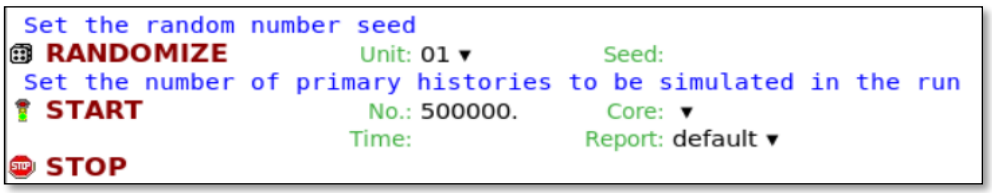

Fig.4.4. START Card in FLUKA input.

7. **Analyzing Results:** After completing simulation, Results are analyzed in the output files generated by FLUKA, it's necessary to extract relevant information, such as reaction rate or product yield data for residual radionuclides.

The FLUKA generates three distinct file types:

- Text files, denoted by the extension "_sum.lis": These files contain averaged distributions, standard deviations, and cumulative (integral) quantities.
- An unformatted file: This file is specifically crafted to substitute the N unformatted estimator files in subsequent post-processing.
- A text file labeled with the extension "_tab.lis": This easily readable file is designed for compatibility with graphics codes.

Calculation of cross section [133]: The isotope production per primary particle can be obtained using a RESNUCLEI card. The term "isotope production per primary particle"

stands for number of isotopes produced as a result of spallation reaction between high energy beam and target material. It evaluates the possibility of generation of specific isotopes through nuclear reactions.

For obtaining cross section of residual nuclides, these results should be normalized by the (p + $^{239}PuO_2$) cross section which can be calculated through the inelastic scattering length in the output material table and by the reaction probability (number of proton stars in the output too, assuming that they take place in the target only). Calculation of normalization factor is described below.

Normalization factor is composed of following further measurements:

1) The (p + $^{239}PuO_2$) cross section σ (mb) (that can be retried from the inelastic scattering length in the out-material table – "fluka.out").

$$\sigma = \frac{\mathrm{M}}{\lambda \cdot \rho \cdot N_A \cdot 10^{27}} \tag{4.8}$$

where M is a molar mass ($\mathrm{g/mol}$), ρ – target material density ($\mathrm{g/cm^3}$), λ - inelastic scattering length for protons at beam energy (cm), and N_A is the Avogadro number ($\mathrm{mol^{-1}}$).

2) The reaction probability: it means number of proton stars in the output of FLUKA, assuming that they take place in the target only.

After calculation of factors, there is need of RESNUCLEI result (isotope production per primary particle) which is located in "tab.list". Finally, this result should be divided by factor 2 (the reaction probability) and multiplied by factor 1 (p + $^{239}PuO_2$ cross section). The final result after calculation provides cross section [mb] for all residual nuclides which are produced in target after spallation reaction.

4.4 PHITS code

The PHITS (Particle and Heavy Ion Transport Code System) [134] is also one of the particle transport simulation codes based on Monte Carlo method. The Japan Atomic Energy Agency (JAEA) developed PHITS code to simulate particle transport of different types (e.g., protons, neutrons, electrons, heavy ions, photons) through matter. The use of PHITS code is broadly applicable in science and engineering, with a particular emphasis on nuclear and particle physics, spallation reactions and other nuclear physics phenomena, radiation therapy, nuclear reactor design, space radiation shielding, and other related areas.

In PHITS simulations, geometry can be displayed in virtual 3-dimensional view by using PHIG-3D. The geometry and input parameters format that is adopted in PHITS is very similar to MCNP code, it means, that geometries written in the MCNP format, can also be easily converted to the PHITS code readable format and vice versa.

Various quantities, such as energy deposition, fission information, flux distribution, and isotope production yields, etc. can be obtain in PHITS simulation by implementing "tally" estimator (output section) functions [135].

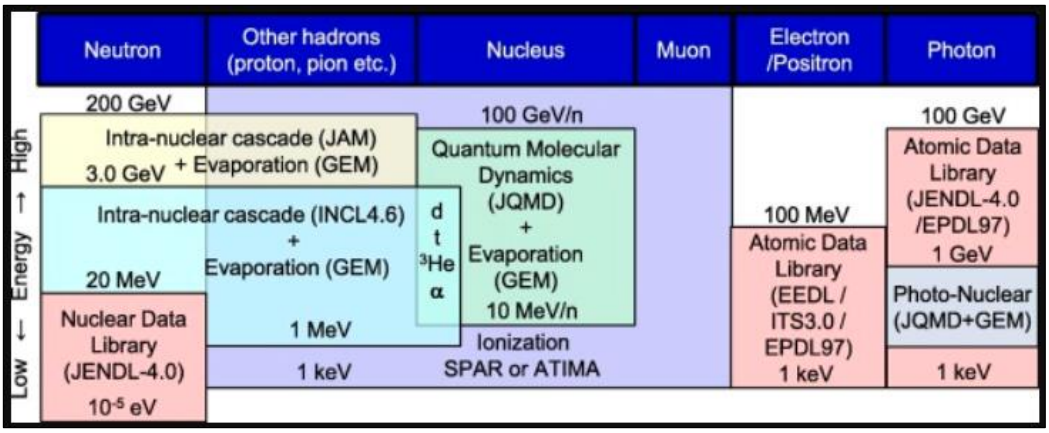

Fig.4.5. Physics models recommended for use in PHITS for simulating nuclear and atomic collisions [135].

For simulation in PHITS code, it is obligatory to write correct input.file, which consists of several main section, briefly described below:

Geometry Definition: It is related to defining the geometry of a simulation that includes information about the target material, the shape and size of its geometry, and All materials that may have an impact on particle transport.

Particle Sources: It specifies the main characteristics of the incident (projectile) particles, such as their type, energy, and direction.

Tally: consist of a description of the desired result.

The PHITS code proves to be a valuable tool for computing energy deposition in a spallation target. An illustration of its utility is found in [135], where the simulation of energy deposition in a spallation target, specifically lead (Pb), is detailed. In this scenario, a high-energy proton beam irradiated the target, employing the PHITS 2.52 code for the simulation. Furthermore, the study outlines the definition of spallation products obtained from the target following the spallation reaction.

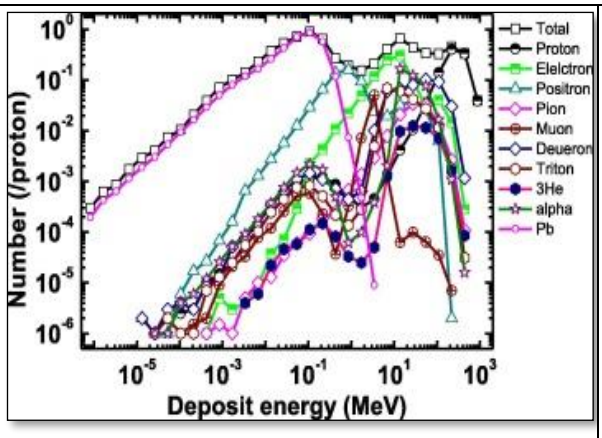

Fig.4.6. Illustrates energy deposition distributions in a lead (Pb) target, highlighting examples of different particles and lead recoil nuclei [136].

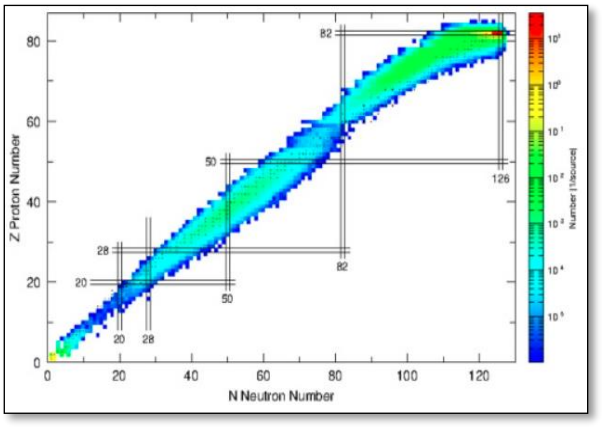

Fig.4.7. Displays the distributions of neutron number (N) and charge number (Z) for spallation products in a lead (Pb) target subjected to bombardment by 1.0 GeV protons [137].

The PHITS code, in event generator mode, helps us understand how energy is deposited in a spallation target. It calculates energy distributions from various particles and nuclei, such as protons, electrons, positrons, pions, muons, light nuclei (d, t, ^{3}He, α), and recoiling nuclei (^{204}Pb, ^{206}Pb, ^{207}Pb, ^{208}Pb), as shown in Fig.4.6.

After an intense spallation reaction in the lead (Pb) target, produced protons and neutrons are accompanied by a variety of spallation products, as seen in Fig.4.7. In the low neutron number range, there are many light nuclei liked, t, ^{3}He, and α. In the mid-range, a significant amount of fission products appears, indicating a competition between high-energy fission and evaporation. In the high neutron number range, you find recoiling nuclei like ^{204}Pb, ^{206}Pb, ^{207}Pb, and ^{208}Pb. The kinetic energies of these particles contribute to heating up the nucleus, leading to energy deposition in the spallation target.

The experiment described in this dissertation, involve a 660 MeV proton beam directed at a plutonium target, shares similarities with the above-mentioned study conducted on lead with a 1 GeV proton beam. Both experiments involve the interaction of high-energy proton beams with heavy target materials. In both cases, the intense spallation reactions produce a variety of particles, including protons, neutrons, and various spallation products. The resulting N-Z distributions in the spallation products showcase a wide range of elements and isotopes. Moreover, the kinetic energies of the produced particles and recoiling nuclei contribute to the heating of the nucleus, leading to energy deposition in the spallation target. This parallelism underscores the relevance of insights gained from the lead-target study to the understanding of the dynamics and outcomes of our experiment with a plutonium target under similar conditions. This similarity can prove to be one of the options to determine the accuracy of our study.

In summary, the Monte Carlo method and simulation codes like FLUKA, MCNP, and PHITS play a crucial role in enhancing our knowledge of particle transport and radiation interactions. This is particularly relevant to my experiment, which involves a 660 MeV proton beam targeted at plutonium.

The stochastic nature of the Monte Carlo method proves invaluable in accurately simulating complex physical processes. The FLUKA stands out as a versatile and widely used code, excelling in simulating particle transport across various applications, including medical physics and radiation shielding. The MCNP code, tailored for high-energy particles and nuclear processes, is essential in nuclear and particle physics, meeting the specific requirements of experiments involving energetic proton beams. The PHITS code, with its event generator mode, is instrumental in studying particle interactions and energy deposition in intricate environments, contributing directly to insights gained in my experiment.

However, it's crucial to recognize that these simulation tools have limitations, particularly in precision when dealing with complex materials like plutonium. They may also face challenges in accurately predicting certain uncommon nuclear reactions under specific experimental conditions. Additionally, the computational demands of these simulations require a careful balance between speed and precision. Being aware of these limitations is essential for interpreting simulation results cautiously, considering the specific conditions and materials involved in our experiment.

Subsequent chapters will present detailed results, technical insights, and comprehensive findings from using these tools in our experiment, enriching our understanding and applications of the experimental outcomes.

A GLANCE AT PREVIOUS EXPERIMENTS TO STUDY TRANSMUTATION

This part of dissertation aims at giving a general overview of the current transmutation studies for ADS, that are similar studies to this experiment that is described in this dissertation, across the world. As already known that minor actinides, including plutonium, together with LLFPs [138], represent a small fraction of spent nuclear fuel but it produces most of the long-term decay heat and radiotoxicity of HLW.

Removing plutonium and minor actinides from spent fuel would thus decrease the spent nuclear fuel radiotoxicity [139]. The transmutation process will help to convert of certain long-lived radioactive isotopes into more manageable or less hazardous isotopes, that should reduce the long-term radiotoxicity and heat load of the nuclear waste. As a result, there is still ongoing research on this topic worldwide. Below are examples of several investigations which are related to this topic.

Research on thin lead target [140] were perform at Radium institute St. Petersburg (Russia). Main purpose of this experiment was to determine production of residual products and their cross section while irradiating the target (Pb) with 660 MeV protons. The duration of irradiation was 11 minutes. From the activity of ^{24}Na obtained in aluminium foil, it was determined that the proton beam had an intensity of $1.80 \times 10^{+1}$ 1 p/(cm^2 s). The cross section result for 660 MeV in this experiment was 10.8 mb. Executing of this experiment helped obtain new data for determining cross section of short-lived nuclides.

The measurements of cross section of radionuclides in study targets at proton energies from 200 to 1000 MeV are describe in [141]. Intervals between energies was 100 MeV. The target materials were chosen such as ^{233}U, ^{235}U, ^{238}U, ^{232}Th, ^{237}Np, ^{239}Pu, ^{nat}Pb and ^{209}Bi. Experiments were performed in PNPI of Russia using PNPI synchrocyclotron. The measurement technique relies on the simultaneous detection of fission fragments using two parallel plate avalanche counters (PPACs) positioned in close proximity to a target.

This experiment [142] highlights the measurements of cross section of residual nuclides in uranium and thorium targets bombarded with 1 GeV protons supplied by the PS-Booster at CERN. The obtained data was compared to ISOLDE beam intensities produced by 600 MeV protons generated by the CERN synchrocyclotron to determine the differences. The data was collected for testing purposes, considering various conditions. As a result of experiments, it was concluded that the decay of mother radionuclides, their collection time etc., can affect the release of several isotopes.

Research at [143] is described about modelling of spallation neutron source in context of transmutation by using acceleration driven system (ADS). High energy proton accelerator is used for transmutation of ^{239}Pu, minor actinides such as ^{237}Np, ^{241}Am and long-lived fission products such as ^{99}Tc and ^{129}I. Reason for choosing these radionuclides is that they are directly created during normal operation of NPP. Secondly, these nuclides consider as the most dangerous in spent nuclear fuel due to the radiotoxicity (minor actinides) and long-lived. Curium is considered as actinide which cannot be transmuted. The fission reaction is occurring in the core after spallation reaction of high energy protons with spallation target. These reactions lead to the production of neutrons. As results of the experiment, several parameters were investigated such as spallation protons and neutrons yielding, energy distribution of them, heat deposition, fission products which were obtained after reactions,

transmutation rate to study MA. Additionally, MCNP code in combination with The Los Alamos High Energy Transport Code (LAHET) were used in the calculation.

This article [144] describes the first radiochemical studies of the ^{239}Pu transmutation process for an ADS setup driven by relativistic protons. The results of ^{239}Pu transmutation were compared with results of transmutation for ^{l29}I and ^{237}Np radionuclides. Proton beam had energy of 0.53 and 1.0 GeV. The obtained database is useful for future applications of accelerator driven systems for nuclear waste transmutation, in addition for energy amplification (subcritical reactor). The results of this study show that a subcritical system can destroy plutonium very effectively. The rate of fission of plutonium is significantly high.

Determination of residual nuclei formation and their cross section in ^{239}Pu and ^{nat}U targets (experiments) is described in [145]. This study was part of the large experiment in JINR Dubna in cooperation with several research institutions and universities. The energy of proton beam was 660 MeV. Detail of these experiment and processing methodology which was used in it is described. The study involves investigating experimental cross sections for reactions induced by protons with an energy of 660 MeV, focusing on various fission products, minor actinides, and both "major" actinides such as plutonium, uranium, and thorium.

Investigation of the transmutation of long-lived radionuclides such as ^{129}I, ^{237}Np, and ^{239}Pu on natural uranium are presented in [146]. The experiment was performed by using the Synchrophastron at the Joint Institute for Nuclear Research (JINR) in Dubna, (Russia). The study targets were sealed in aluminium holders. The reaction of relativistic protons in energies range from 0.5 GeV to 1.5 GeV with uranium or lead targets stacks was used for generating spallation neutrons. In this article, all results (summary) of transmutation investigations are shown, which were performed on the Synchrophastron until the year 2002, especially experiments of proton energy of 0.5 and 1.0 GeV.

In the study [147] the yields of obtained radionuclides in ^{209}Bi targets are described. Thin targets were irradiated with 130 MeV and 1.5 GeV proton beam. Direct c-spectrometry was used for measuring product yields. The ASPRO code was used for processing c-spectra which were obtained after measurement. The SIGMA code based on GDISP database was used for calculation of cross section of radionuclides. The ^{27}Al(p,x)^{24}Na reaction was used for monitoring of proton beam. Obtained experimental results compared with computer simulation in codes such as the HETC, LAHET, INUCL, CASCADE, GNASH and CEM95.

The following experiment [148] consist of irradiation different thin targets such as ^{182,183,184,186}W with protons energies 0.2, 0.8 and 1.6 GeV, respectively. ITEP U-10 proton accelerator was used for irradiation of targets. These targets were irradiated by proton accelerator 51 times in total. GENIE2000 program was used for processing γ – spectra. Monitoring of the proton fluence was performed by using the ^{27}Al(p,x)^{24}Na reaction. SIGMA code was used for identification product yields of residual nuclides. SIGMA code is based on PCNUDAT database. In the result of these experiments, 4315 cumulative and independent yields of radionuclides were calculated. Indicated residual nuclides have lifetime from 8 minutes to 32 years.

In work [149] results for six experiments carried on the ITEP U-10 proton accelerator with proton energies 300, 500, 750, 1000, 1500, and 2600 MeV are present. For ^{56}Fe(p,x) reactions, cross sections of residual nuclides which obtained due to this reaction were calculated. Direct γ-spectrometry was used for determination of product yields. Obtained

experimental results were compared with 15 different simulation codes, for example, such as MCNP, LAHET, and CASCADE-2004, etc. More specific details about these experiments can be found in article. As a results, 221 yields of radionuclides were found, with half-lives ranging from 6.6 minutes to 312 days.

In the study [150] nuclear formation of cross sections for 65 nuclides, which obtained as results of irradiation of thorium foils with 800 MeV protons have been documented. The data is being used as valuable benchmarks to evaluate computational predictions for theoretical code development. The measured data are compared with the outcomes predicted by MCNP6 event generators. This data is instrumental in evaluating the potential of 800 MeV proton productions for generating radioisotopes which can be used in medicine (radiotherapy).

Between 2011 and 2017, international collaboration project which was called the "Energy and Transmutation of RAW" conducted a series of experimental investigations focusing on study of subcritical accelerator-driven systems (ADS). In these experiments, a subcritical uranium target, known as QUINTA assembly, underwent irradiation using 0.66 GeV protons, deuterons, and ^{12}C nuclei. The assembly QUINTA consisted of 512 kilograms of natural uranium (natU). The irradiation by deuterons, and ^{12}C nuclei were carried out with energies ranging from 1 GeV to 4 GeV. The Phasotron and Nuclotron accelerators (JINR) were used for irradiation of targets. The Kharkov group also participated in these experimental studies. For obtaining more precise results, MCNPX 2.7 code was used for simulation irradiation of the QUINTA assembly. Also, for same reasons the INCL4-ABLA physics model and LAQGSM code were applied for calculation of results. More detail and results of these investigation are described in [151].

The investigation [152] described the results of irradiation of the ^{232}Th target and Al collector with an internal proton beam. The targets underwent bombardment with energies of 100 and 600 MeV by the JINR Synchrocyclotron accelerator. As a result of the fragmentation 45 nuclides for thorium target and 55 nuclides for aluminium collector were identified. For comparison the obtained cross sections of the reaction results, theoretical calculations by MCNP v.6.1 code were performed.

At the Laboratory for High Energies at the Joint Institute for Nuclear Research (JINR) in Dubna, several other experimental investigations were conducted on the transmutation of certain long-lived radioactive nuclei, such as ^{129}I, ^{237}Np, ^{239}Pu, ^{Nat}U and lanthanum are described in [153]. The experiments were conducted at the Synchrotron accelerator with relativistic protons in the energy range of 0.5 GeV $\leq$ Ep $\leq$ 1.5 GeV. All the findings indicate that using of subjecting a 10-mA proton beam with an energy of 1 GeV on a lead (Pb) target has the potential to transmute a significant quantity of the studied examples (^{129}I, ^{237}Np, ^{239}Pu, etc.) within one month. This provides evidence supporting the notion that accelerator driven systems can, in principle, be employed for large-scale transmutation. However, further investigation is required to enhance understanding and optimize the application of this technology.

In the study [154] of the transmutation efficiency of spent radioactive waste components, such as ^{233}U, ^{235}U, ^{236}U, ^{238}U, ^{237}Np, ^{238}Pu, and ^{239}Pu was performed. This study was focused on the natural uranium spallation target bombarded with 660 MeV protons. MCNP 6.2 code was used for comparing experimental reaction rates of residual nuclide data with theoretical simulations. MCNP 6.2 code was based on updated versions of the ENDF/B-VIII. and JENDL/HE data libraries.

CHAPTER 5
THE EXPERIMENT ON A THIN PLUTONIUM TARGET

The investigations described in this dissertation study were performed as a part of experiments at the Joint Institute for Nuclear Research (JINR) in Dubna (Russia), (within cooperation of several research institutions and universities). Several experiments were executed in the end of 1990s, which contributed to developing nuclear data for ADS technologies, especially for proposal using transmutation. Plutonium, uranium, neptunium, americium, iodine, and other isotopes' cross section measurements have been studied. Many similar investigations in this field already been performed by other groups, e.g. Sn isotopes irradiation [155] and thick target studies [156, 157].

This study is the last part of four irradiation experiments which were consisted of two irradiation experiments on natural uranium targets [158, 159] and two irradiation experiments with ^{239}Pu isotopic targets. Each two experiments were based on almost similar principles, except irradiation time and samples which were used. Uranium samples were in form of thin foils. Plutonium sample has another structure than U, it was covered into aluminum container, additionally hermetically closed by manufacturer. During U and Pu irradiations, average proton current was around 0.8 μA. Short experiments were performed to observe short-lived isotopes in the range from minutes to several hours while the longer ones were for identification long-lived isotopes.

Long irradiation of plutonium target is investigated by K. Katovsky in his doctoral study [160]. Next step of this investigations is calculating cross section of short-lived isotopes, which obtained in short irradiation of plutonium target, and this is the main objective of this dissertation thesis.

5.1 The steps of experiment on plutonium target

The experiment consists of irradiation using proton beam with an energy of 660 MeV at thin target comprising of a mixture of $^{239}PuO_2$. In general, the experiment on thin plutonium ($^{239}PuO_2$) target consist of four main parts:

- Preparation
- Irradiation and transport
- Measurement of gamma spectra
- Processing of the received data

A. Determination of the mean proton flux

Aluminium foils were used as proton beam monitors. It's well-understood interaction between protons and aluminium. Aluminium is good material which has low dependence on its properties when subjected to high-energy proton beams. Additionally, aluminium is biocompatible, cost-effective material, with excellent thermal conductivity and good radiation hardness, commonly available for fabrication in various forms. Aluminium demonstrates excellent chemical stability, that helps reduce the probability of undesirable reactions with other materials in the experimental setup.

Proton beam monitoring was performed based on activated aluminium foils using the

reactions ^{27}Al(p,3pn)^{24}Na, ^{27}Al(p,3p3n+)^{22}Na, and ^{27}Al(p,10p11n+)^{7}Be. Specifically, the main monitoring reaction involved ^{27}Al(p,3pn) ^{24}Na.

Table 6. Nuclear-physics characteristics of the nuclides produced in the ^{27}Al(p,x) monitor reactions.

Product	γ − energy (keV)	I_γ − abundance (%)	$T_{1/2}$
^{24}Na	1369.0	100	(14.9590±0.0012)h
^{22}Na	1274.5	99.944±0.014	(2.6088±0.0014) h
^{7}Be	477.6	10.5±0.6	(53.29±0.07) d

When monitoring the number of protons trapped on the Al plate, the knowledge of the effective cross section of the p + Al reaction and their small energy dependences at high energies were used.

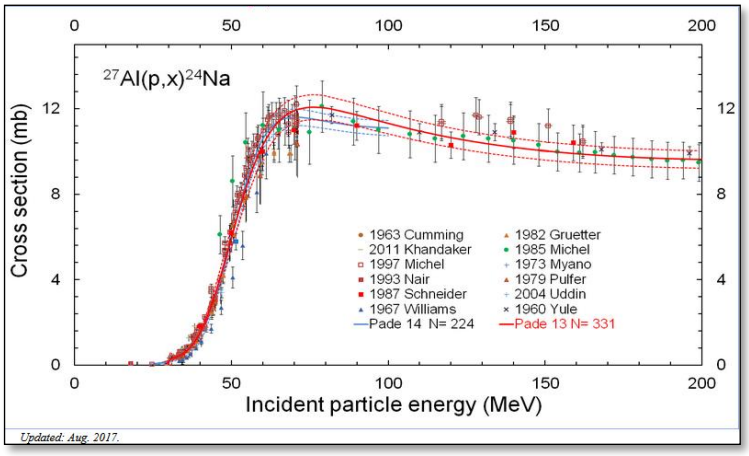

Fig.5.1. The ^{27}Al(p,x)^{24}Na reaction excitation function in the 10 - 200 MeV proton energy range [161].

However, ^{27}Al (p,3pn) ^{24}Na reaction is usually affected by the parasitic neutron reaction ^{27}Al(n,α)^{24}Na. This effect depends on the distance of the aluminium foil from the proton source, with a reasonable choice it is an effect in the order of units or tenths of a percent. Control reaction can be carried out by reactions of ^{27}Al(p,3p3n)^{22}Na and ^{27}Al(p,10p11n)^{7}Be. When placing the foil directly on the target, these reactions can provide 30% less proton integral flux.

For example, for determine the mean proton flux density Φ(E) consider the ^{27}Al(p,x)^{22}Na monitoring reaction. Fig. 5.2 compiles the experimental data of 23 works made from 1951 to 2011 in 25 MeV - 1.0 GeV energy range. In cases where experimental cross section values were not available for certain energy ranges, they were estimated through linear interpolation of the logarithms of the cross section values at the boundaries of the given range.

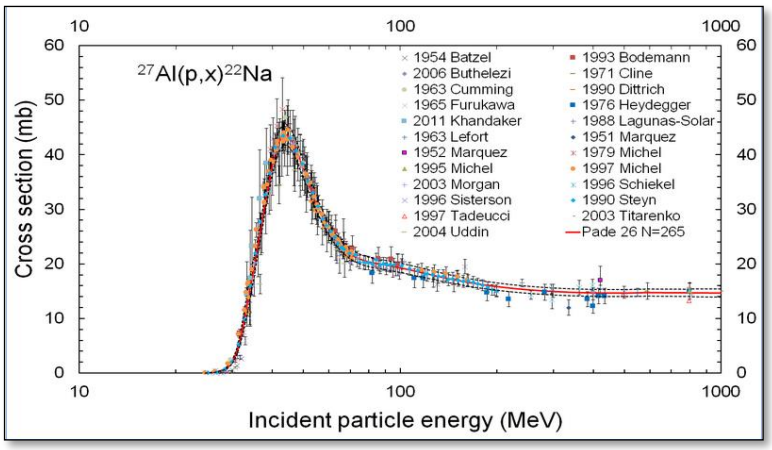

Fig.5.2. Cross sections for the $^{27}Al(p,x)^{22}Na$ reaction, including uncertainties [162].

In this case, the time and sample area-averaged density of proton flux (protons per cm^2 per s) and its error are determining as:

$$\widehat{\Phi} = \frac{R^{22Na}}{\sigma^{22Na}} \qquad \frac{\widehat{\Delta\Phi}}{\widehat{\Phi}} = \sqrt{\left(\frac{R^{22Na}}{R^{22Na}}\right)^2 + \left(\frac{\Delta\sigma^{22Na}}{\sigma^{22Na}}\right)^2}, \tag{5.1}$$

where R^{22Na} is the ^{22}Na production rate and σ^{22Na} is the monitor-reaction cross section at a given energy. The analytical expression to calculate the ^{22}Na production rate is described in more detail in [162].

Because ^{24}Na, ^{7}Be, and ^{22}Na are all generated after irradiation the same experimental sample, the ratio of their cross sections can be expressed as follows [163]:

$$\frac{\sigma^{24Na,7Be}}{\sigma^{22Na}} = \frac{A_0^{24Na,7Be}}{A_0^{24Na}} \frac{(\lambda\eta\varepsilon)^{22Na}}{(\lambda\eta\varepsilon)^{24Na,7Be}} \frac{F^{22Na}}{F^{24Na,7Be}} \times \frac{1+(\bar{\sigma}_{n,x}^{22Na}\Phi_n/\bar{\sigma}_{p,x}^{22Na}\Phi_p)}{1+(\bar{\sigma}_{n,x}^{22Na,7Be}\Phi_n/\bar{\sigma}_{p,x}^{22Na,7Be}\Phi_p)} \tag{5.2}$$

In formula (2.28), t_{irr} represents irradiation time for a single sample; given by $t_{irr} = [(K-1)T + \tau]$, where K, T, and τ are parameters. Given that the Φ_n/Φ_p ratio is approximately 0.8 – 2 % within proton beam energies ranging from 0.07 to 3.0 GeV, the calculations of the cross sections ratio can be calculated in a simplified form:

$$\frac{\sigma^{24Na,7Be}}{\sigma^{22Na}} = \frac{A_0^{24Na,7Be}}{A_0^{24Na}} \frac{(\lambda\eta\varepsilon)^{22Na}}{(\lambda\eta\varepsilon)^{24Na,7Be}} \frac{F^{22Na}}{F^{24Na,7Be}} \tag{5.3}$$

Table 7. The calculated ratios of neutron-induced to proton-induced yields of ^{24}Na, ^{22}Na and ^{7}Be formed in ^{27}Al+p [164].

Degrader	Nuclide	$\overline{\sigma_n}$ (mb)	σ_p (mb)	$\frac{N_n}{N_p}$	R (%)
Al	^{24}Na	31.1	11.4	0.0301	8.21
	^{22}Na	12.8	18.1		2.13
	^{7}Be	0.0143	0.99		0.043

Where (in Table 7), $\overline{\sigma_n}$ is effective production cross sections with the normalized neutron spectra; σ_p is the cross section for the proton-induced reaction at energy of 120 MeV;

$\frac{N_n}{N_p}$ is the ratio of neutrons to protons passing through the foils; R is neutron-induced to proton-induced yields.

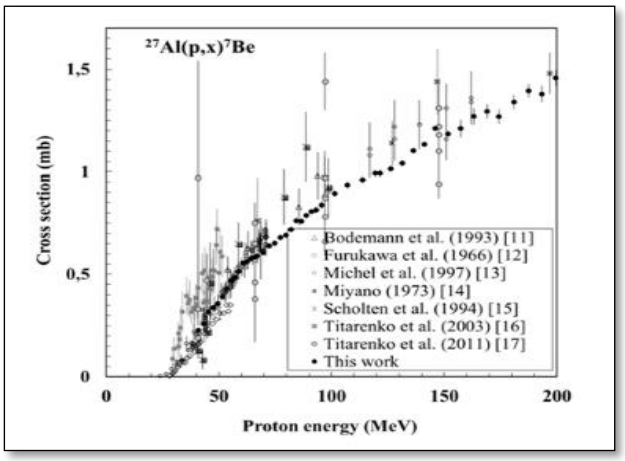

Fig.5.3. Cross sections of the production of ^{7}Be in the ^{27}Al+p reaction [164].

For proton energy monitoring above 100 MeV, ^{22}Na/^{7}Be ratio is better suited than the ^{22}Na/^{24}Na ratio as the fraction of ^{24}Na produced by secondary neutrons are substantially higher than in the cases of ^{22}Na and ^{7}Be. Also, investigated the ^{27}Al(p,x)^{7}Be process for monitoring purposes, as ^{7}Be has a convenient half-life of 53.22 d and a sufficiently strong γ - line at 477.6 keV.

B. Preparation of sample

The sample is a cylindrical disk which has a diameter (Ø) of 21 mm and a thickness of 1.5 mm. ^{239}Pu weighs 446 mg. However, plutonium sample inside aluminium container was composed of $^{239}PuO_2$, has weight of 506 mg and it was dispersed in aluminium powder, additionally covered by thin Al foil. Pure plutonium isotopic mixture which consists of 99% of ^{239}Pu, and rest consists of ^{236}Pu, ^{238}Pu, ^{240}Pu, ^{241}Pu, ^{242}Pu (appropriate decay chains isotopes) were used in this experiment. Density of $^{239}PuO_2$ target is 0.974(12058) g/cm^3. Due to covering plutonium target in the duralumin container, nuclei phenomena were suppressed, and all residual nuclei were stopped within study sample. Intrinsic activity before irradiation of plutonium was 1.0 MBq, however, total activity of the sample was 1.02 GBq.

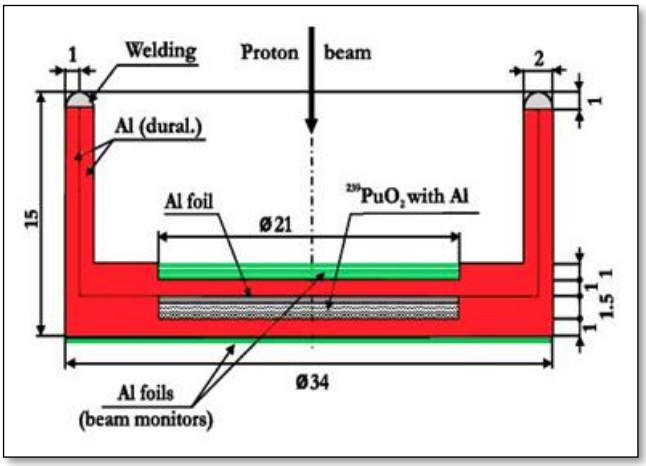

Fig.5.4. Arrangement and description of the plutonium target. Dimensions are shown in mm.

To preserve the configuration of the $^{239}PuO_2$ sample, it was enclosed in a duralumin container (Al-capsule), forming an effective "sandwich" structure (see Fig.5.4). Sample of $^{239}PuO_2$ sealed in Al-capsule, was produced by the Institute of Physics and Power Engineering in Obninsk, Russia. The container was sealed to maintain the sample's geometry, and the entire assembly was subsequently subjected to irradiation. Pre-irradiation and post-irradiation of plutonium, sample was tested for hermetical properties. This involved assessing alpha activity on the target surface as a key indicator of any changes or effects resulting from the irradiation process.

Table 8. Information about plutonium target.

	Pu sample No. 4
Weight of Pu [mg]	**446**
Weight of PuO2 [mg]	**506**
Total activity [GBq]	**1.02**
PuO_2 layer size	**ø 21 x ~ 1.5**
Al capsules - ID material	**AD-1 ГОСТ-4784-74**
- Size [mm]	**34 x 15 x 1**
- Weight [g]	**17.9**
Resistance - Humidity	**98 %**
- Temperature	**-50 – +50°C**
- Pressure	**25 Pa – 105 kPa**
- Frequency	**5 – 50 GHz**
- Accelerations	**5 – 50 $m \cdot s^{-2}$**
- The punch	**50 $m \cdot s^{-2}$ za 100 s**
The manufacturer	**ТНЦ-РФ ЭФИ Obninsk**
ID	**71-046-04**

As was mentioned before, aluminium foils were used as monitors for the incident proton beam. One Al foil was placed above the target to collect plutonium target fragmentation nuclides. Three aluminium foils were put in front of the target to suppress impacted nuclei phenomena and one additional Al foil, behind the target as a control foil, The thickness of each aluminium foil was 34 μm. Aluminium monitors were used due to sufficient information about the reaction of the proton with aluminium, as well as due to the low dependence of this material at high energies. Results of monitoring were relatively good - within 10% maximal differences. That sandwich was sealed into a package to preserve the sandwich geometry and was then directed to irradiation. Radioactive materials were enclosed in an aluminium holder (special duralumin alloy) with diameter of 34 mm.

Table 9. Several parameters of Aluminium monitors.

No	Weight [mg]	Thickness [mm]
1	54.8	**0.0586**
2	54.8	**0.0586**
3	54.4	**0.0582**
4	142.7	**0.0583**
5	54.0	**0.0578**
6	53.4	**0.0571**
7	54.3	**0.0581**
8	**142.6**	**0.0582**

Foil numbers 1,2,3 and 5,6,7 is having diameter 21 mm, and foil numbers 4,8 are of 34 mm, and thickness 0,0581 mm. The activities in the aluminium monitors are measured on the ORTEC NEW detector in the second geometry from the detector, without filter.

C. Irradiation of sample

Duralumin container with $^{239}PuO_2$ sample had specific parameters that confined the maximum proton intensity to 10^{15} protons, limiting the duration of irradiation to a maximum of six hours. Additionally, labour protection regulations prohibited irradiating plutonium at the same proton current level as uranium (in the first part of the whole experiment).

The longer irradiation lasted 90 min with integral intensity of $5.61 \cdot 10^{14}$ and 17 nA on the target, which is described in [165]. The short plutonium irradiation was performed after 12 minutes of experiment with natural uranium and was lasted 5.25 min which is described in this research. At the output beam current of 2.02 μA, the integrated proton flux was $(4.93 \pm 0.1) \cdot 10^{13}$ (integral intensity) and proton current on the study target was 25 nA. Ionization chambers were used for monitoring beam profile, stability of beam profile was very good. However, stability of beam current during irradiation was changing within 30 % range. Average beam profile parameters for plutonium target were FWHM(x) = 1.50 cm and FWHM(y) = 2.31 cm.

Date of experiment, real irradiation time, beam current, average beam profile parameters, during both experiments on plutonium target are shown below in Fig.5.5.

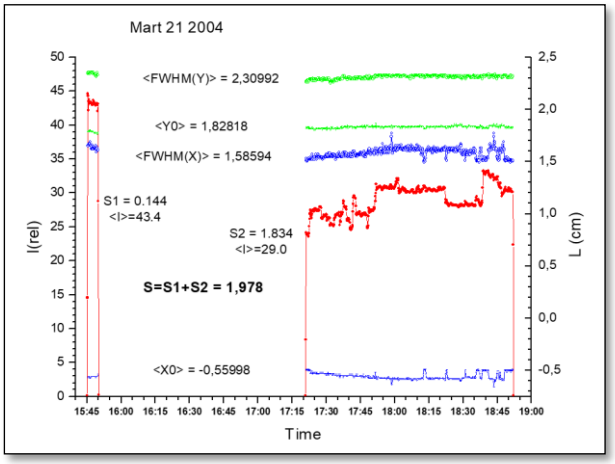

Fig.5.5. Graph of irradiation of both experiments of study targets.

The experimental sample was irradiated using the Phasotron. From an experimental perspective, the Phasotron stands out as a unique research facility, offering a high-intensity proton beam with a capacity of up to 10^{13} particles per second and reaching a maximum energy of 660 MeV. More detail information about this accelerator is described below.

Phasotron is a cyclic accelerator of heavy charged protons in which particles move in a constant and uniform magnetic field and are accelerated in a high-frequency electric field decreasing in frequency. Phasotron operates in the mode of acceleration intervals repetitive with a certain frequency. The frequency of the accelerating field in the working part of each interval falls in accordance with the energy of the particles, and then returns to its initial value. After that, the next acceleration interval begins.

Table 10. Characteristics of JINR Phasotron accelerator.

The 660 MeV JINR Phasotron is characterized by following parameters	
Maximum average bean power	1.0 kW
Maximum proton energy	660 MeV
Proton energy deviation	6 MeV
Maximum average beam intensity	$2 \cdot 10^{13}$ p/s
Number of protons per pulse	$0.8 \cdot 10^{11}$
Pulse rate	250 Hz
Pulse length (FWHM)	20 μs
Pulse microstructure: - bunch length - interval between bunches - number of bunches per pulse	 10 ns 70 ns ≈ 300

The Phasotron facility is designed to create beams of protons and to carry out scientific research and applied work on the extracted beams. The Phasotron has 10 beam channels, which are used for experiments with π-mesons, muons, neutrons, and protons.

Table 11. Several parameters of Phasotron.

Phasotron
Set during 1979-1984 by reconstruction of old Synchrophastron at the Laboratory of Nuclear Problems, JINR Dubna
Accelerates protons up to (659±6) MeV
Intensity ~10^{13} protons
Electrical current ~ 5μA
Bunches (with length of ~ 10ns) follow in ~70 ns intervals
Modulation frequency ~ 250Hz

Also, Phasotron has an efficient output system.
- Fast ejection ratio is 50-60%.
- Slow output (stretching) allows you to output from the Phasotron almost continuous beam [166].

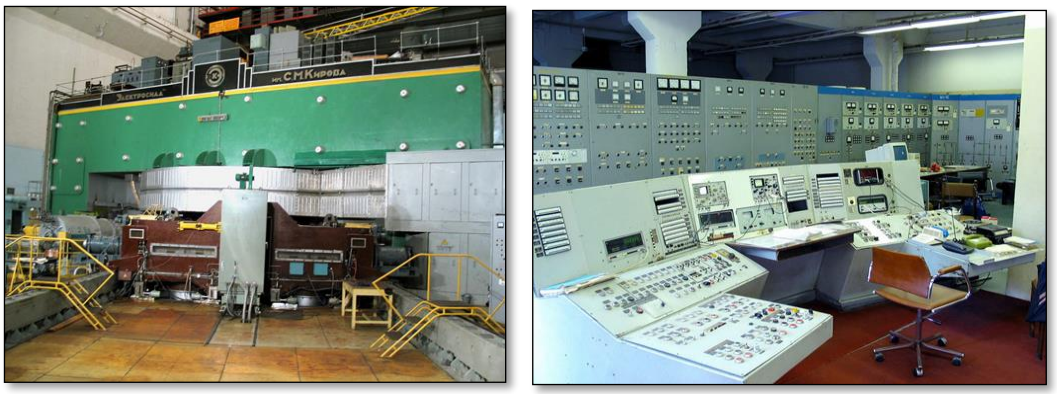

Fig.5.6. a) Appearance of the Phasotron; b) The Phasotron control panel.

Overall, a notable advantage of this facility is its long-term stable operation mode. Additionally, the strategic location ensures a relatively short distance between the Phasotron experimental hall and the γ - spectrometry laboratory, enabling the swift transport of irradiated samples within a few minutes. This capability facilitates the timely and efficient measurement of short-lived radioisotopes which is very important in this research.

Table 12. Several irradiation parameters.

Real irradiation time	Seconds from the start	Current (nA)	Seconds
14:27:43	0.00	0.00	0.00
14:27:52	9.00	49.77	9.00
14:28:01	18.00	60.92	18.00
14:28:10	27.00	60.82	27.00
14:28:18	35.00	61.46	35.00
14:28:27	44.00	61.60	44.00
14:28:36	53.00	60.31	53.00
14:28:45	62.00	60.38	62.00
14:28:53	70.00	63.17	70.00
14:29:02	79.00	62.91	79.00
14:29:11	88.00	62.95	88.00
14:29:19	96.00	62.80	96.00
14:29:28	105.00	62.65	105.00
14:29:37	114.00	62.79	114.00
14:29:46	123.00	62.59	123.00
14:29:54	131.00	62.73	131.00
14:30:03	140.00	62.76	140.00
14:30:12	149.00	62.95	149.00
14:30:21	158.00	63.25	158.00
14:30:29	166.00	63.24	166.00
14:30:38	175.00	63.33	175.00
14:30:47	184.00	63.42	184.00
14:30:56	193.00	63.55	193.00
14:31:05	202.00	63.60	202.00
14:31:13	210.00	63.52	210.00

Table 12. Several irradiation parameters, continuation.

14:31:22	219.00	63.42	219.00
14:31:31	228.00	63.59	228.00
14:31:40	237.00	63.29	237.00
14:31:48	245.00	62.53	245.00
14:31:57	254.00	62.88	254.00
14:32:06	263.00	62.28	263.00
14:32:15	272.00	62.67	272.00
14:32:23	280.00	64.46	280.00
14:32:32	289.00	62.84	289.00
14:32:41	298.00	63.37	298.00
14:32:50	307.00	30.72	307.00
14:32:58	315.00	0.00	315.00
	5.25	**64.46**	
		58.10	

Here, in Table 12 time of irradiation was 5.25 min, and 64 nA - maximum current during irradiation and average current was 58.10 during irradiation. In Fig.5.7 and Fig.5.8 are shown Intensity of the proton beam during irradiation.

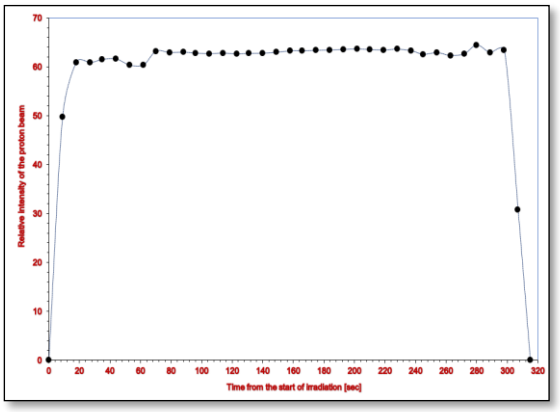

Fig.5.7. Intensity of the proton beam during irradiation.

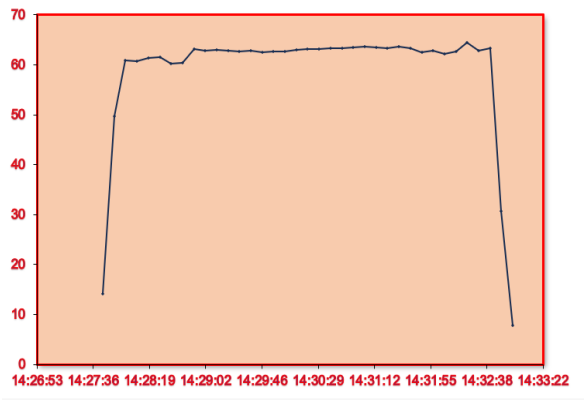

Fig.5.8. Intensity of the proton beam during irradiation in real time.

D. Detection

After irradiation, the samples were removed from the Phasotron chamber and immediately transferred from irradiation room No. IX to the YASNAPP-2 spectroscopic complex. In this γ - spectroscopy laboratory gamma spectra were measured using two HPGe detectors, one detector was ORTEC GMX-20190 with efficiencies 28.3% and another one CANBERRA GR-1819 detector with efficiency 18.9%. (With resolutions between 1.78 keV and 1.86 keV over the 1332 keV line.) The measurement of irradiated sample started approximately five minutes after the end of irradiation.

Table 13. Quantity of measured spectra during irradiation of plutonium target.

Type of spectra	Plutonium-239
Al monitors	5
Before irradiation, background	16
Short irradiation	83
Measurement of beam	9
Calibration spectra	48

Due to the high activity of the sample, the irradiation was carried out at different distances from the detector. Measuring times were increasing, distance of samples from HPGe decreasing. Intensive measurement lasted for 14 days, then samples were measured from time to time for more than two years. Total number of 83 plutonium spectra for short plutonium irradiation were acquired. About 500 other spectra (calibration, monitors, background) were measured considering whole experiment (long and short irradiation). It should be noted, that after irradiation, both stable and radioactive nuclides are produced, characterized by different half-lives and decay energies.

Fig.5.9. View of CANBERRA detector.

The transfer time of the plate to the detectors was not more than 10 minutes. The measuring position was chosen so that the dead time of the detector did not exceed 20%, and in the case of active samples did not reach more than 10%. In the case of weak active samples, we placed them as close as possible to the detector so that the detection efficiency should be as high as possible - it is important to identify even weak activation products, and measurement time is limited by the need for frequent sample rotation.

a) b)

Fig.5.10. a) HPGe is ORTEC detector. b) Dewar filled with liquid nitrogen.

Approaching the detector, the probability of coincidence effects (summation and evaluation of peaks) and the occurrence of the miss effect increases. Correction of these side effects should be made to the resulting reaction rate.

E. Filters

The filters play a crucial role by working as sift through the radiation, not allowing pass certain energy components while letting others pass through. According to the strength of the activity and especially the type of spectrum, cadmium (Cd) and copper (Cu) filters were used. In this measurement setup, these filters were placed between research target and the HPGe detectors (CANBERRA and ORTEC). Radiation passes through the filters and engages with the detector. It helps in achieving specific measurement goals, which were mentioned before.

The filter absorbs low gamma-energy quanta in the spectrum and the X-ray quantum forms the energy dependence curve of the detector efficiency. As for actinides, which often have their own low-energy gamma particle, this use of the filter is very advantageous. Cadmium (Cd) and copper (Cu) have a small number of nucleons. These materials are chosen, for this experiment, because of their ability to absorb the X-rays, which resultantly reduces background radiation, and improves the overall quality of radiographic or radiation shielding applications.

As mentioned before, cadmium filters, because of its high γ - ray absorption efficiency, usually use to attenuate or absorb gamma rays, especially at lower energies. In addition to this, cadmium filters suppress low-energy gamma rays or X-rays and improve the energy resolution of γ - ray detectors. This property is important to ensure precise energy measurements in γ - ray spectroscopy.

In order to get rid of low-energy γ - rays, copper filters were used. After interaction of gamma rays with a copper filter, it undergoes Compton scattering or photoelectric absorption, and as a results low-energy gamma rays are absorbed. It helps obtain a cleaner gamma spectrum, reducing interference from low-energy γ - rays and background radiation, additionally, it enhances the energy resolution of gamma spectrometers.

By using copper filters to weaken undesired low-energy γ - rays, the resulting spectrum becomes clearer, making it simpler to recognize and measure specific radioactive elements based on their unique gamma energies. Additionally, these filters help cut down on dead time in the detector. Dead time is the period when the detector doesn't respond after

detecting a gamma-ray event. By reducing low-energy events, the dead time is minimized, enabling more precise counting at higher gamma energies**.**

Therefore, filters play significant role in gamma spectrometry, they are useful in many ways, such as for attenuating low-energy γ - rays, improving energy discrimination, reducing background radiation, enhancing energy resolution, aiding in isotope identification, facilitating efficiency calibration, and reducing detector dead time. They also help obtaining accurate and reliable γ - ray spectra.

Measurements were typically conducted in the energy range from 50 to 3500 keV**.** During the measurement process, the activity of the sample decreased, so active sample closer to the detector were repositioned, as an option, it is possible to change the filter. It is important to note that any change in position or filter would mean a change in detector efficiency. All positions in combination with filters had to be well measured using calibration emitters. Because main objective in this study were looking for unknown activation products with different half-lives. Activated sample were measured sequentially many times, while adjusting the measurement time.

Measurement of the irradiated foil lasted 11 hours during which eighty-three spectra were obtained for plutonium target (in short experiment). The twenty-four spectra were obtained for 1 - 5 position, and 18 spectra for calibration detector. For 6 - 9 position, fifty-nine spectra were obtained along with 30 spectra for calibration. To obtain data from the spectrometers, the software MAESTRO v.4.10 from EG & G ORTEC was used, the data was extracted in binary *.chn* format.

Table 14. Description of measurement of plutonium target.

Position	Detector	Filter	Location of sample considering gaps	Number of spectra	Number of calibrations spectra
1	**CANBERRA**	2Cd+2Cu	**incorrectly inserted extension, gap 9 cm from the last gap in the house**	**6**	**2**
2	**CANBERRA**	2Cd+2Cu	**last space in the house (1st from the end)**	**6**	**5**
3	**CANBERRA**	2Cd+2Cu	**penultimate gap in the house (2nd from the end**	**6**	**2**
4	**CANBERRA**	2Cd+2Cu	**5th from the end, i.e. 6th from the detector**	**6**	**4**
5	**CANBERRA**	2Cd+2Cu	**7 from the end, 4 from the detector**	**2**	**5**
6	**ORTEC New**	2Cd+1Cu	**5th gap from detector**	**2**	**8**
7	**ORTEC New**	2Cd+1Cu	**4th gap from detector**	**6**	**7**
8	**ORTEC New**	2Cd+1Cu	**3rd gap from detector**	**8**	**7**
9	**ORTEC New**	2Cd+1Cu	**2nd gap from detector**	**43**	**8**

During efficiency calibration several criteria were met. Only well-established standards were used for calibration spectra, an energy range of 50 keV–2500 keV was

covered, systematic errors (i.e., dead time, etc.) were minimized or eliminated. single interpolation curve was created for the whole energy range. Additionally, the method could be extendable to absolute efficiencies. For more detail information about efficiency calibration method, refer to Chapter 2.1.

The calibration of detector efficiency was performed by using standard calibration point sources, such as: ^{133}Ba, ^{109}Cd, ^{57}Co, ^{60}Co, ^{152}Eu, ^{226}Ra, ^{228}Th, ^{88}Y with several γ - lines ranging from 80 keV up to 2614 keV. Nuclear decay data of the calibration standards can be seen in Table 15.

Table 15. Nuclear decay data of the calibration standards.

Radionuclide	Activity (Bq)	Half-time (year)	Energy (keV)
^{109}Cd	1317300	1.263244	88.0336
^{133}Ba	57120	10.551	80.8949 276.3989 302.8508 356.0129 383.8485
^{57}Co	120700	0.743984	122.06065 136.47356
^{60}Co	92400	5.271129	1173.228 1332.492
^{226}Ra	33000	1600	609.312 351.932 295.224 1120.287 1764.494 241.997 1238.110 768.356 1377.669 934.061 2204.210 1729.595 1407.980 1509.228 665.453 1155.190 1847.420 1280.960 806.174 1401.500 785.960 1661.280 2447.860 2118.550

Table 15. Nuclear decay data of the calibration standards, continuation.

^{228}Th	46060	1.912	84.373 238.632 240.986 277.371 300.087 510.77 583.187 727.330 785.37 860.557 1620.5 2614.511
^{88}Y	259700	0.291926	898.042 1836.063

Measured data was processed using standard γ-spectrometry method, for the – γ-peak area determination, background suppression, target isotopes own background suppression, calibration, identification ($T_{1/2}$, E_γ, I_γ) and corrections etc.

CHAPTER 6
THE EXPERIMENTAL RESULTS AND ANALYSIS

6.1 Experimental date results

A. Result of calculation efficiency of detectors

The efficiency of the detector was assessed through the program script Efekt8.exe. The fitting of efficiency was accomplished using a similar script called Efektfit.exe. The Efekt8.exe program enables the determination of parameters, such as detector efficiency, for each position, along with other related efficiency-related parameters (refer to Appendix 1 for details). The script Efektfit.exe is employed to calculate fitting coefficients for these positions, utilizing the output file generated by Efekt8.exe as its input file for the calculation. For illustration, the calculated efficiency of the ORTEC detector (9^{th} position) is presented in Table 16 below.

Table 16. Energy dependence of germanium detector efficiency for 9^{th} position.

Energy (keV)	Efficiency	Error of efficiency
88.04	0.00132	3.98E-5
121.7817	0.0161	4.83E-4
244.6975	0.03926	1.18E-3
295.98	0.03833	1.15E-3
411.1163	0.02708	8.13E-4
443.965	0.02985	8.96E-4
488.6792	0.02397	7.20E-4
563.99	0.02555	7.67E-4
688.67	0.01984	5.95E-4
778.904	0.01755	5.26E-4
810.451	0.01584	4.75E-4
867.378	0.01616	4.85E-4
964.079	0.01562	4.69E-4
1005.272	0.01428	4.29E-4
1085.869	0.01464	4.39E-4
1089.737	0.0148	4.44E-4
1112.074	0.01425	4.28E-4
1212.948	0.01288	3.87E-4
1299.14	0.0114	3.42E-4
1332.501	0.00909	2.73E-4
1408.006	0.01158	3.47E-4
1457.643	0.01212	3.64E-4
1836.063	0.00727	2.18E-4

To ascertain the reaction rate and, consequently, the cross section of the reaction, it is essential to obtain output parameters from the EfektFit.exe script. The fitting coefficients, as detailed in Table 17, must be identified, and incorporated into the library (Efficiency.lib).

These coefficients are crucial for the program responsible for calculating reaction rates of residual nuclides following the AD4HEL code.

Table 17. Coefficients of the efficiency fit of HPGe-detector for 9th position (2nd gap from detector).

a_0	9.42607862
a1	-0.58882596
a2	-2.55936675
a3	-9.59018186
a4	-12.92307482
a5	-8.30244701
a6	-2.57257978
a7	-0.30110439

Other calculated values of efficiency of the detectors (ORTEC and CANBERRA) and their fitting coefficients for their efficiency are shown in Appendix I, II, respectively. As was mentioned before, positions 2-5 were measured in CANBERRA detector, and positions 6 - 9 were measured in ORTEC detector. Table 16 indicates that for detector ORTEC, the energy with the highest efficiency value is 244.6975 keV. This γ-line belongs to the standard ^{152}Eu source.

The Fig.6.1 and Fig.6.2, shows the relationship between efficiencies and energies for both detectors in all positions. From these figures, it can be observed that ORTEC detector has better efficiency than CANBERRA detector.

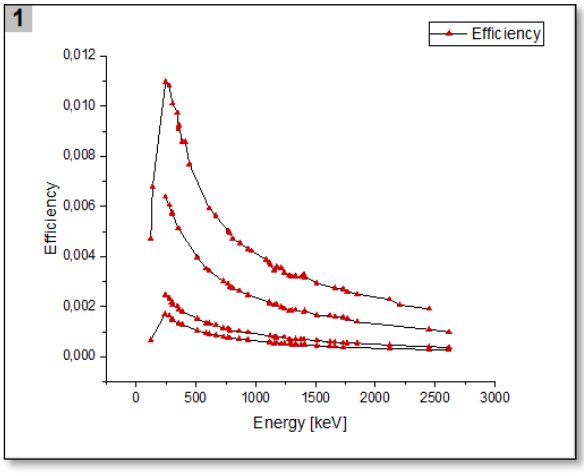

Fig.6.1. Experimental efficiency data for calibration of CANBERRA detector.

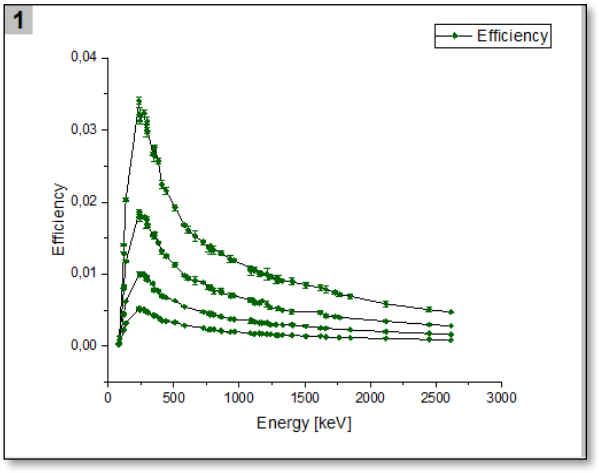

Fig.6.2. Experimental efficiency data for calibration of ORTEC detector.

As mentioned in Chapter 5, filters were used during the measurements, so for both detectors we do not have many energy points below the energy of 200 keV (for more detail see Chapter 5 D. Filters).

B. Calculation of correction of detector energy non-linearity

The results of calculation of non-linearity for the germanium detectors which were used during measurements are shown in Table 18. The calculation of this corrections is

important for getting reliable and accurate results of measurements.

Table 18. Nonlinearity coefficient for detectors.

Detector	a0	a1	a2
ORTEC	-0.76265	0.00106	1.88E-08
CANBERRA	-0.42524	-0.00026	6.30E-07

The detail information about this correction is described in Chapter 2 (part 2.6. correction of detector energy non-linearity). One example of calculation of non-linearity for the germanium detector ORTEC is shown below in Table 19.

Table 19. An example of calculation the non-linearity of an ORTEC detector.

Database energy	a0	a1	a2	Chanel	δ	Measured energy
2614	-0.76265	0.001062	1.88E-08	5958.913	2.14	2616
510.77	-0.76265	0.001062	1.88E-08		-0.22	510.442

It ensures that the data collected are representative of the true energy of the detected radiation in measurement spectra, allowing for meaningful analysis in following investigation of reaction rate and cross section of residual nuclides.

C. Results of cross section calculation of residual nuclides for measurements performed with CANBERRA detector

As mentioned in previous Chapter 5, 24 spectra were obtained during measurements for 1 - 5 positions, and 18 spectra for calibration of CANBERRA detector. During measurements with this detector, 2Cd+2Cu filters were utilized. Unfortunately, the data for the first position could not be processed due to an insufficient number of calibration spectra (only 2 calibration spectra were available). Furthermore, an error occurred in the first position where the extension was incorrectly inserted, creating a gap of 9 cm from the last gap in the house.

A similar situation occurred for position 3, where only 2 calibration spectra were obtained. To address this issue, a "special" coefficient was determined, enabling the utilization of energies from other spectra to enhance the precision of the detector efficiency for the 3rd position. The second position was measured as the 1st from the end (last space in the house). Following the 2nd position, all subsequent positions of the plutonium target were placed sequentially closer to the detector.

Results of processing spectra in positions 2 - 5 are shown below in Table 20. The Table 20 shows the name of the isotope, the energy and intensity of each γ-line, the half-life (literary and experimental data), the reaction rate of the formation of the radionuclides, the cross section of the reaction and their errors that belong to these isotopes.

All the major photo peaks of the nuclide appeared in the gamma spectra were chosen. Another requirement for selecting radionuclides is that the analyzed photo peaks exclusively belong to the nuclide of interest, with no interference from other nuclides sharing the same gamma energy. Additionally, the decay curve of each selected photo peak must align with the half-life of the nuclide of interest. Only those photo peaks whose experimental half-life agrees

within 10 % of the reference value were chosen for analysis.

Table 20. The results of effective cross sections of the fragmentation and spallation products of the plutonium target.

Isotope	E, keV	I_γ, %	RR, s^{-1}	dR, s^{-1}	$\sum\sigma$,barn	$\Sigma d\sigma$, barn	$T_{1/2fit}$, hours	$T_{1/2tab}$, hours
^{98m}Nb	722	73.8	2.63E-29	1.47E-30	1.17E-04	9.19E-06	1.56	0.85
	787	93	3.08E-29	1.64E-30			0.8	0.85
	1169	17.8	4.95E-30	3.25E-31			1.26	0.85
^{92}Sr	1383	90	5.94E-30	2.98E-31	2.05E-05	1.03E-06	2.41	2.71
^{91m}Y	555	95	1.48E-29	1.34E-30	5.12E-05	4.65E-06	1.3	0.83
^{90m}Y	479	90.7	7.27E-30	3.67E-31	2.52E-05	1.27E-06	3.49	3.19
^{89}Rb	658	10	7.01E-30	7.67E-31	3.28E-05	4.51E-06	0.89	0.25
	1031	58	1.13E-29	8.70E-31			0.26	0.25
	1248	42.6	9.99E-30	5.95E-31			0.27	0.25
^{88}RbD	1836	21.4	1.80E-30	1.69E-31	1.03E-05	6.42E-07	1.17	2.84
^{87}Kr	402	49.6	8.10E-30	4.39E-31	2.80E-05	1.52E-06	1.44	1.27
^{49}Cr	61	16.4	7.47E-30	4.53E-31	2.59E-05	1.57E-06	1.25	0.7
^{41}Ar	1293	99	2.24E-30	1.25E-31	1.31E-05	1.31E-06	0.95	1.82
^{239}U	74	48	7.29E-29	8.91E-30	2.52E-04	3.08E-05	1	0.39
^{227}Pa	64	6	1.05E-28	1.25E-29	3.62E-04	4.32E-05	1.05	0.81
^{202}Bi	657	60.6	2.19E-29	1.16E-30	7.58E-05	4.01E-06	1.83	1.72
^{201m}Bi	846	5	1.77E-28	1.21E-29	9.87E-05	4.45E-06	1.33	0.98
^{197}Tl	1383	1.25	6.53E-28	3.30E-29	2.26E-03	1.14E-04	2.47	2.84
^{149}Nd	155	5.93	4.79E-29	5.21E-30	1.66E-04	1.80E-05	1.56	1.73
^{142}La	641	47	6.22E-30	3.20E-31	2.15E-05	1.11E-06	1.39	1.52
^{138}Cs	462	30.7	5.23E-30	4.63E-31	4.62E-05	3.47E-06	0.77	0.56
	1435	73.6	1.76E-29	8.89E-31			0.57	0.56
^{137}Nd	307	10	1.61E-28	9.70E-30	3.30E-04	5.61E-05	0.38	0.64
^{135m}Cs	846	95.9	3.13E-30	1.64E-31	3.58E-05	2.68E-06	0.67	0.88
	786	100	4.58E-30	7.68E-31			0.89	0.88
^{134}I	846	95.4	4.55E-29	2.38E-30	2.78E-04	2.41E-05	0.67	0.88
	883	64.9	9.94E-29	6.52E-30			1.02	0.88
	1612	4.29	5.10E-30	5.43E-31			0.36	0.88
^{125}Cs	526	24	1.59E-29	1.28E-30	5.50E-05	4.42E-06	0.35	0.75
^{123}Xe	148	49	5.52E-29	2.88E-30	1.91E-04	9.98E-06	1.8	2.08
^{118m}Sb	1229	100	3.02E-29	1.72E-30	8.87E-05	6.05E-06	2.85	5
	1050	97	1.38E-30	3.20E-31			5.19	5
^{116m}SbD	843	11.2	1.08E-29	2.24E-30	3.05E-04	4.45E-05	0.16	1
	1293	100	1.02E-28	1.27E-29			0.94	1

Table 20. The results of effective cross sections of the fragmentation and spallation products of the plutonium target, continuation.

^{116m}In	**1293**	**84.4**	**5.30E-29**	**2.79E-30**	**1.84E-04**	**9.66E-06**	**0.93**	**0.9**
	1097	56.2	8.57E-30	4.61E-31			0.91	0.9
^{107}Rh	303	66	2.27E-29	1.24E-30	7.86E-05	4.30E-06	0.36	0.36
^{104}Tc	358	89	1.12E-29	7.51E-31	4.15E-05	1.18E-05	0.28	0.3
	530	15.6	9.75E-30	1.08E-30			0.29	0.3
	536	14.7	9.80E-30	1.15E-30			0.49	0.3
	884	10.9	1.54E-29	2.88E-30			0.56	0.3
	1612	5.8	4.86E-30	6.13E-31			0.29	0.3
^{104}Ag	555	92.6	1.19E-29	1.61E-30	5.06E-05	8.15E-06	1.29	1.15
	1528	7.1	1.72E-29	1.71E-30			2.38	1.15
^{101}Mo	590	19.2	1.49E-29	9.34E-31	4.16E-05	8.12E-06	0.17	0.24
	695	6.66	9.40E-30	1.75E-30			0.39	0.24
	1013	13	2.44E-29	1.81E-30			0.13	0.24
^{101}Tc	306	89	1.35E-27	2.41E-28	4.25E-04	6.54E-05	0.32	0.24

As a result of processing the gamma spectra obtained from the irradiated plutonium ($^{239}PuO_2$) target, 48 gamma lines were detected. Identification was successful for 30 nuclides based on their energy and half-life, ranging from 18.3 minutes to 5 hours. The identified nuclides belong to mass numbers (A) within the range of 24 - 239, with an accumulation of radionuclides in the regions of mass numbers 87 – 149 and 197 – 239. Additionally, two nuclides, namely ^{41}Ar and ^{49}Cr, were also identified. The distribution of these radionuclides is depicted in Fig.6.3.

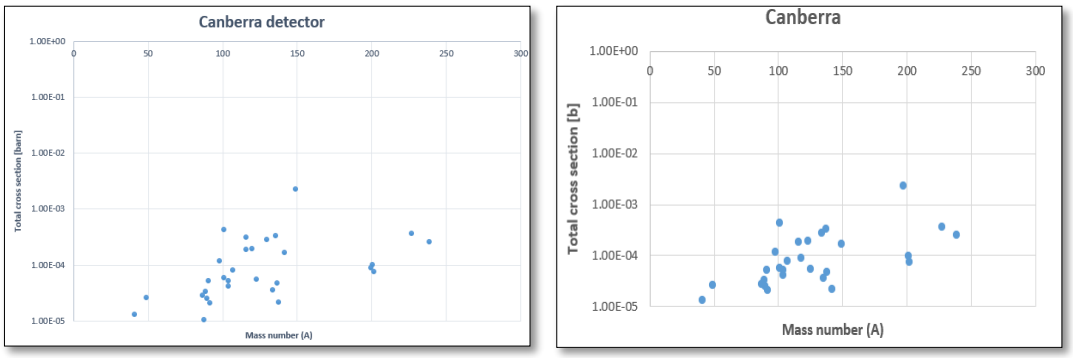

a) b)

Fig.6.3. Total cross section values as a function of mass number of all radionuclides measured by CANBERRA detector: a) together with daughter nuclides; b) without daughter nuclides.

If the name of the isotope contains additional letters such as "m" it means this is isomer (metastable level) of a given isotope, e.g., ^{90m}Y or ^{116m}In. Moreover, the second case is the letter "D" following the standard isotope designation, it means that this nuclide is part of a decay series, and that “parent” isotope is converted to another radionuclide (“daughter”). In this case, the parent nuclide possesses a significantly longer half-life than the "child" nuclide. Consequently, the decay curve for the "child" is primarily determined by the longer half-life

of the parent radionuclide.

During the processing of spectra and calculations of reaction rates and cross sections for the obtained spectra, the presence of ^{24}Na was observed. Typically, ^{24}Na exhibits two high-intensity energy peaks at 1368.633 keV and 2754.028 keV. However, in positions 2 - 5, only one peak with an energy of 1368.633 keV was determined. The results of the calculations for ^{24}Na are presented in Table 21.

Table 21. The result of calculation of cross section for ^{24}Na.

Isotope	E, keV	I_γ,%	RR, s^{-1}	dR, s^{-1}	$\sum\sigma$,barn	dσ, barn	$T_{1/2fit}$, h	$T_{1/2tab}$, h
^{24}Na	1368	100	2.36E-28	1.18E-29	8.15E-04	4.08E-05	14.7	14.96

D. The result of cross section measured with ORTEC detector

ORTEC detector was employed for measurements in positions 6 - 9. A total of 59 spectra were obtained during these measurements, with an additional 30 spectra acquired for calibration purposes. The last measurement of the plutonium target in the 9th position was performed in the second gap from the detector (closer to the detector), resulting in 43 spectra. The processed results of the spectra in positions 6 - 9 are presented in Table 22 below.

Table 22. The results of effective cross sections of the fragmentation and spallation products of the plutonium target measured by ORTEC detector.

Isotope	E, keV	I_γ, %	RR, s^{-1}	dR, s^{-1}	$\sum\sigma$,barn	dσ, barn	$T_{1/2fit}$ hours	$T_{1/2tab}$ hours
^{99}Mo	140.536	89.4	1.53E-28	1.79E-29	4.96E-04	8.05E-05	65.39	65.94
	739.352	12.6	1.32E-28	1.48E-29			55.31	65.94
^{97}NbD	658.088	98	4.86E-29	5.44E-30	1.68E-04	1.88E-05	16.35	16.91
^{96}Nb	460.161	26.6	3.12E-29	3.51E-30	1.02E-04	2.50E-05	24.4	23.35
	568.88	58	3.83E-29	4.37E-30			21.05	23.35
	777.744	96.5	2.81E-29	3.18E-30			25.89	23.35
	849.872	20.5	2.42E-29	2.75E-30			25.17	23.35
	1200.14	~20	1.41E-29	1.82E-30			23.02	23.35
^{92}YD	934.429	13.9	3.00E-29	3.86E-30	9.35E-05	1.61E-05	4.72	3.54
	1405.28	4.8	2.26E-29	2.57E-30			3.85	3.54
^{82}Br	555.473	70.8	1.63E-29	1.89E-30	3.76E-04	6.25E-05	34.18	35.3
	617.92	43.4	6.30E-29	7.33E-30			38.51	35.3
	698.144	28.5	1.45E-29	1.67E-30			37.69	35.3
	777.706	83.5	1.40E-28	1.59E-29			32.91	35.3
	827.721	24	1.72E-29	1.96E-30			36.55	35.3
	1043.98	27.2	1.61E-29	1.82E-30			39.62	35.3
	1317.50	26.5	1.49E-29	1.73E-30			48.52	35.3
	1475.15	16.3	1.11E-29	1.25E-30			26.23	35.3
^{69m}Zn	438.706	94.8	5.03E-30	5.88E-31	1.74E-05	2.03E-06	14.58	13.76

Table 22. The results of effective cross sections of the fragmentation and spallation products of the plutonium target measured by ORTEC detector, continuation.

^{48}V	1312.29	97.5	4.08E-30	3.52E-31	1.41E-05	1.22E-06	383.4	383.4
^{48}Sc	984.102	100	9.60E-30	1.08E-30	2.82E-05	3.85E-06	43.23	43.67
	1312.29	101	2.05E-30	2.58E-31			48.42	43.67
^{239}Np	228.42	10.8	2.16E-28	2.45E-29	7.46E-04	8.48E-05	53.46	56.57
^{206}Bi	496.948	15.3	3.88E-28	4.35E-29	1.07E-03	1.87E-04	104.7	149.8
	803.364	99	3.59E-30	5.13E-31			149.8	149.8
	881.386	66.2	6.63E-30	1.20E-30			1408.	149.8
	893.79	15.7	9.92E-30	1.44E-30			78.75	149.8
	1099.10	13.5	1.38E-29	5.75E-30			149.8	149.8
	1596.37	5.0	2.88E-28	3.16E-29			79.6	149.8
^{186}Ir	297.76	62.3	6.09E-29	7.26E-30	2.13E-04	3.67E-05	17.7	16.64
	772.987	8.9	6.22E-29	7.73E-30			14.55	16.64
^{183}Os	115.212	20.6	5.86E-28	7.24E-29	2.03E-03	2.50E-04	12.18	13
^{182}Os	510.975	55	3.93E-28	2.33E-29	1.36E-03	8.07E-05	29.1	22.1
^{147}Gd	228.48	63	3.44E-29	3.65E-30	1.19E-04	1.26E-05	40.24	38.06
^{136}Cs	818.403	100	1.29E-29	1.44E-30	3.96E-05	7.78E-06	311.2	315.8
	1047.92	80	1.26E-29	1.41E-30			273.8	315.8
	1235.42	20	7.69E-30	9.87E-31			209	315.8
^{135}XeD	249.86	90	2.47E-29	2.84E-30	8.54E-05	9.82E-06	12.11	9.14
^{135}I	1260.34	28.9	3.35E-30	3.75E-31	1.16E-05	1.30E-06	6.2	6.57
^{135}Ce	573.386	10.4	1.27E-28	4.15E-29	9.47E-04	3.06E-04	25.92	17.7
	606.82	18.8	7.91E-29	9.02E-30			16.36	17.7
	782.502	10.6	3.86E-28	7.73E-29			30.74	17.7
	827.721	5.14	1.44E-28	6.49E-30			18.19	17.7
^{133}I	529.422	87	3.17E-29	3.55E-30	1.10E-04	1.23E-05	20.82	20.8
^{132}Te	228.421	88	2.87E-29	3.22E-30	9.91E-05	1.11E-05	69.42	76.9
^{132}La	464.536	76	3.81E-30	4.41E-31	1.32E-05	1.53E-06	4.9	4.8
^{132}ID	522.258	16	2.50E-29	2.94E-30	2.12E-04	4.03E-05	62.3	76.9
	629.984	13.3	4.07E-29	5.43E-30			20.04	76.9
	667.87	99	4.63E-29	5.22E-30			77.94	76.9
	772.989	75.6	1.59E-29	1.80E-30			56.57	76.9
	812.354	5.5	8.76E-29	9.86E-30			67.26	76.9
	954.415	17.6	1.40E-29	1.58E-30			73.1	76.9
^{131m}Te	772.989	49.9	1.36E-28	2.05E-29	4.70E-04	7.11E-05	27.32	30
^{130}I	510	0.85	8.04E-29	8.45E-29	1.91E-03	8.09E-04	12.24	12.36
	536.08	99	1.68E-29	1.88E-30			11.8	12.36
	668.106	96	2.05E-29	2.32E-30			13.55	12.36
	739.375	82	1.68E-29	1.91E-30			15.26	12.36
	1156.78	11.3	7.51E-28	2.18E-28			15.26	12.36
^{128}Sb	629.874	31	1.18E-29	1.70E-30	4.80E-05	9.07E-06	10.01	9.01

Table 22. The results of effective cross sections of the fragmentation and spallation products of the plutonium target measured by ORTEC detector, continuation.

	743.217		**1.74E-29**	**1.97E-30**			**12.38**	**9.01**
	753.687	100	2.59E-30	2.94E-31			7.05	9.01
^{127}Sb	473.254	25.8	3.53E-29	4.06E-30	1.12E-04	1.84E-05	93.63	92.4
	684.912	37	2.91E-29	3.41E-30			119.1	92.4
^{126}Sb	694.743	100	1.36E-29	1.94E-30	9.65E-05	1.59E-05	305.7	299.0
	667.524	100	3.05E-29	8.88E-30			96.94	299.0
	721.247	53.8	3.46E-29	4.15E-30			308.2	299.0
^{124}I	602.692	63	3.52E-29	3.94E-30	1.04E-04	1.60E-05	87.9	100.2
	1691.17	10.9	2.14E-29	2.40E-30			98.76	100.0
^{122}Sb	564.017	71	2.72E-29	3.05E-30	9.42E-05	1.06E-05	65.17	65.38
^{121}Te	573.013	80.3	1.82E-29	1.73E-30	6.31E-05	6.00E-06	416.5	402.7
^{120m}Sb	1171.25	100	2.21E-29	2.47E-30	8.21E-05	1.32E-05	135.2	138.2
	1024.08	99.4	2.51E-29	2.92E-30			62.37	138.4
^{117m}Cd	1065.85	23.1	7.50E-30	9.17E-31	2.27E-05	4.65E-06	2.5	2.49
	1997.55	26	4.88E-30	6.07E-31			2.78	2.49
	1432.96	13.4	6.74E-30	7.70E-31			3.48	2.49
^{117}InD	158.515	87	7.13E-29	9.67E-30	2.11E-04	3.48E-05	4.49	3.36
	553.005	100	2.48E-29	2.78E-30			3.15	3.36
^{116}SbD	1293.53	84.8	4.37E-30	6.55E-31	1.51E-05	2.27E-06	2.64	2.49
^{112}AgD	617.686	43	1.87E-27	2.10E-28	6.30E-03	7.26E-04	22.87	21.03
	1387.68	5.4	4.50E-29	5.21E-30			21.14	21.03
^{105}Ru	724.064	47	7.42E-29	8.47E-30	2.71E-04	4.43E-05	4.72	4.44
	469.372	17.5	8.18E-29	9.60E-30			4.89	4.44

The processing of γ - spectra measured by the ORTEC detector revealed the detection of 82 γ - lines, corresponding to 36 radionuclides based on energy and with half-lives ranging from 2.49 hours to 17.68 days. The identified nuclides have mass numbers within the range of 24 - 239, with spaces distributed in the range of values 147 - 182, as illustrated in Fig.6.4.

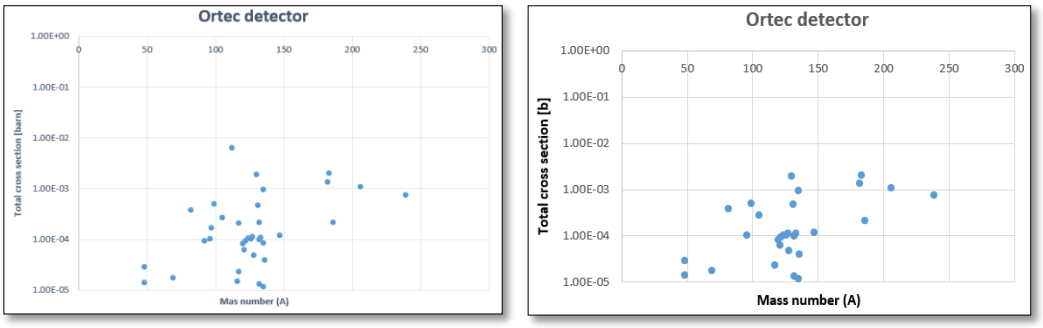

b) b)

Fig.6.4. Total cross section values verse mass number (A) of all radionuclides measured by ORTEC detector: a) together with daughter nuclides; b) without daughter nuclides.

The nuclides were selected based on the same criteria applied to the CANBERRA

detector. An example illustrating the decay curve for ^{133}I at an energy of 529.89 keV, observed in the $^{239}PuO_2$ sample after irradiation, is presented in Fig.6.5. The fitted half-life for this radionuclide is determined to be 21.59 hours.

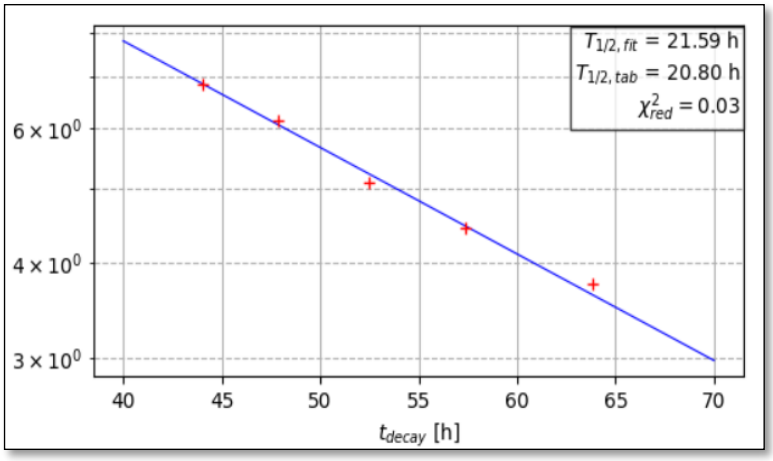

Fig.6.5. Decay curve of ^{133}I at energy 529.89 keV observed in the study sample after irradiation: 660 MeV p + $^{239}PuO_2$. (Position 9th)

In this case, the presence of ^{24}Na was also observed during the processing and evaluation of the measurement spectra, too. In measurement positions 6 - 9, two high-intensity energy peaks at 1368.633 keV and 2754.028 keV were clearly visible. The results of the calculations for cross section parameters of ^{24}Na are shown in Table 23.

Table 23. The result of calculation of cross section for ^{24}Na.

Isotope	E, keV	I_γ,%	RR, s^{-1}	dR, s^{-1}	$\sum\sigma$,barn	dσ, barn	$T_{1/2fit}$ hours	$T_{1/2tab}$ hours
24Na	1368	100	1.14E-27	1.29E-28	3.31E-03	5.02E-04	13.94	14.96
	2753.9	99.94	6.01E-28	6.72E-29			14.51	14.96

In addition, the decay curve of ^{24}Na for the gamma line of 1368.6 keV is displayed in Fig.6.6. This decay curve is directly obtained from the AD4HEL code. The fitted half-life of ^{24}Na in position 9 is determined to be 13.94 hours. Decay curve of ^{24}Na at energy 1368.6 keV is shown in the Fig.6.6. Where, χ^2_{red} measure of how well a theoretical or expected distribution (model) fits the observed data. The formula for χ^2 is given by:

$$\chi^2 = \sum \frac{(O_i - E_i)^2}{E_i}; \quad (6.1)$$

where:

O_i is the observed value (experimental data) for a given point.

E_i is the expected value (predicted by the model) for the same point.

If values of χ^2 generally are close to 1 or significantly less than 1 then they should be considered as good fit. The value of χ^2_{red} = 0.01 (from Fig.6.6) that mean that determined half-life is fitted enough well.

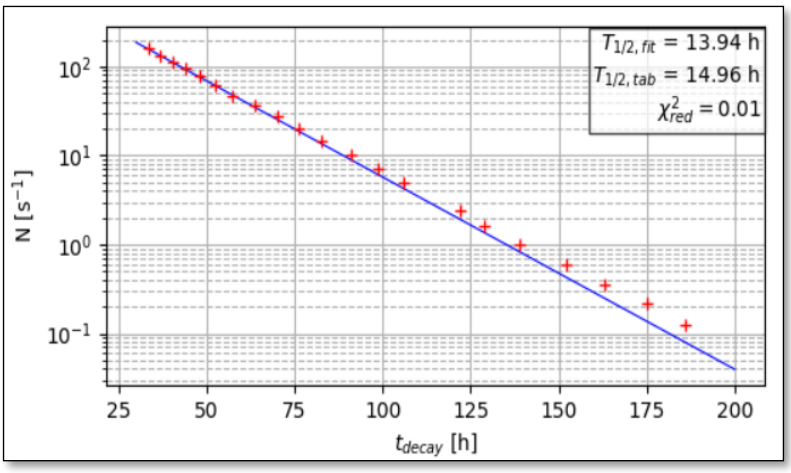

Fig.6.6. Decay curve of ^{24}Na at energy1368.6 keV observed in irradiation (Position 9th).

The obtained results suggest that the reaction products in the studied scenario are predominantly composed of nuclides with short half-lives. This observation aligns with the anticipated outcomes of transmuting long-lived nuclides found in spent nuclear fuel into shorter-lived fragments. The successful transmutation of long-lived nuclides into shorter-lived fragments has implications for the development of advanced nuclear technologies such as ADS technologies.

As mentioned in previous chapters, by converting long-lived radionuclides into isotopes with shorter half-lives, the overall radiotoxicity and decay heat of the nuclear waste can be decreased. As a result, the application of this method can simplify long-term storage and disposal considerations.

6.2 Simulation results

B. MCNP v.6.1

Below are the results of the simulation of the spallation reaction of protons with a ^{239}Pu target using the MCNP v.6.1 code. The MCNP v.6.1 use ENDF/B-VII.1 nuclear and atomic data libraries. In Fig.6.7, cross sections for the plutonium target irradiated by 660 MeV protons are shown with respect to the mass number A. Fig.6.8 displays cross sections for the plutonium target irradiated by 660 MeV protons with respect to the proton number Z of radionuclides. The black line in both figures represents the sum of cross sections for all nuclides that share the same value of atomic mass (Fig.6.7) or the same value of charge number (Fig.6.8), formed as a result of the reactions.

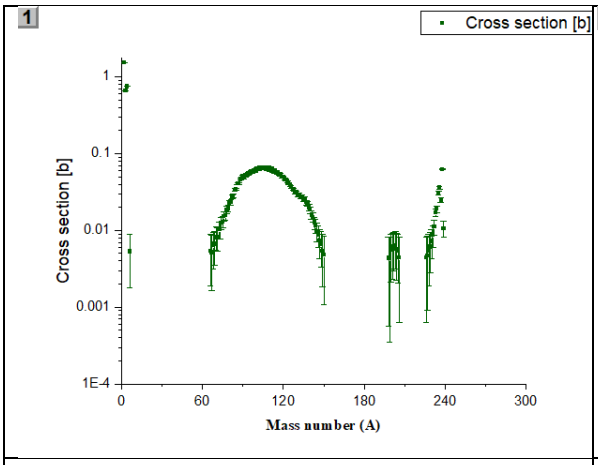

Fig.6.7. Cross sections for plutonium target irradiated by 660 MeV protons.

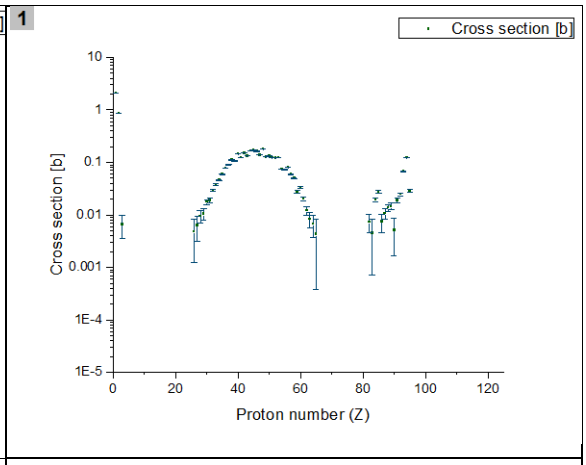

Fig.6.8. Cross sections for plutonium target irradiated by 660 MeV protons.

Fig.6.9 and Fig.6.10 represent errors for the calculated cross section data in the MCNP v.6.1 code. Upon consideration of these figures, it is evident that the errors are not substantial, indicating that the results of the simulation can be deemed sufficiently reliable.

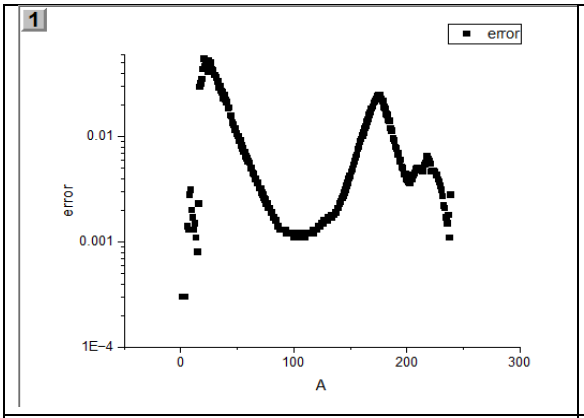

Fig.6.9. Error of cross section per mass number A.

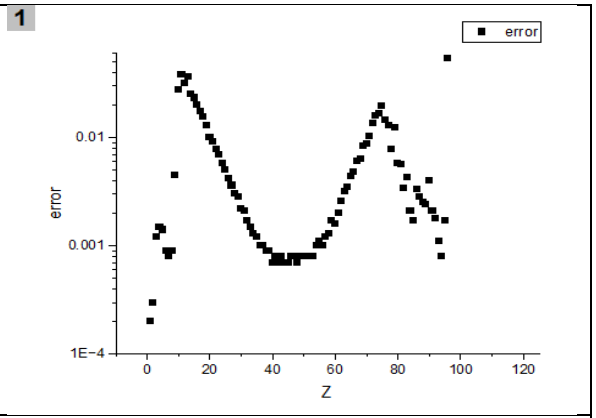

Fig.6.10. Error of cross section per proton number Z.

To validate experimental results for spallation reactions, the MCNP v.6.1 code was employed to compare and confirm these results with the outcomes obtained from the simulations (result comparison see below in Discussion part).

B. FLUKA code result of simulation 660 MeV p + ^{239}Pu reactions

Considering simulation spallation reaction of high energy protons (660 MeV) with plutonium ($^{239}PuO_2$) target in FLUKA code, following steps were defined and followed:

1. **Definition the Geometry:** Definition the geometry of this simulation, including the target material, which consist of $^{239}PuO_2$ compound, its dimensions, and parameters of the proton beam.

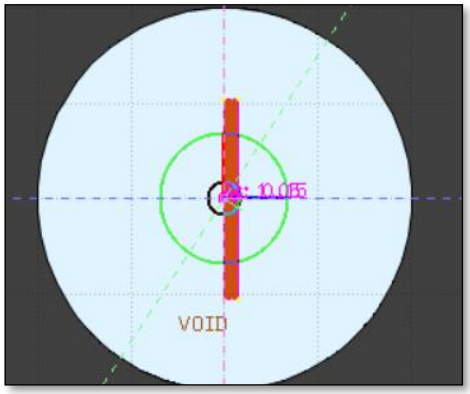

Fig.6.11. Side view of target geometry in FLAIR.

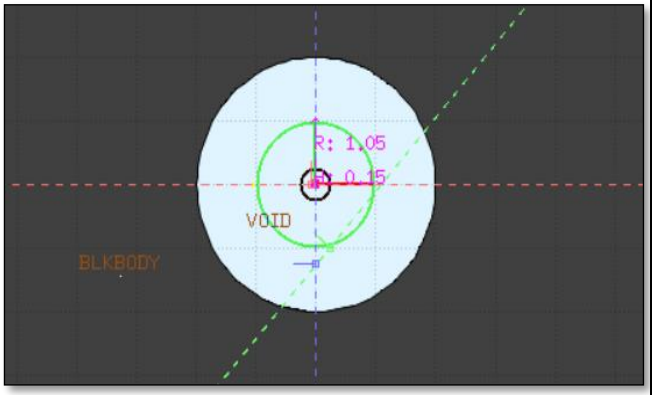

Fig.6.12. Top view of plutonium target geometry in FLAIR.

2. **Definition the Materials:** In this simulation, $^{239}PuO_2$ compound was defined by a MATERIAL card plus COMPOUND Card. In additional to MATERIAL card, the default card LOW-MAT was used. The program uses special nuclear data libraries and low-energy neutron cross sections libraries for the target material definition. For simulation of correct results, it is important to calculate density of target. Calculation of density of $^{239}PuO_2$ compound (target) is described below.

Table 24. Input data for calculation density of target.

Several parameters of target	Value with units
Radius (r)	1.05 cm
Thickness (h)	0.15 cm
Weight (m)	506 mg = 0.506 g

Density:

$$\rho = \frac{m}{V} \ (\text{g/cm}^3) \tag{6.2}$$

Volume:

$$V = \pi \cdot r^2 \cdot h = 3.14 \cdot \ 1.05^2 \ \cdot 0.15 = 0.519 \ (\text{cm}^3) \tag{6.3}$$

The value of constant π is approximately 3.14159.
Therefore, ρ ($^{239}PuO_2$)= 0.506/0.51944288 = 0.97412058 g/cm^3.

3. **Define the Particle Source:** the energy of protons was fixed at 660 MeV, directed towards the center of the target. The irradiation time was 325 seconds, and the power of the proton beam was determined. Additionally, the source of particles was defined as a monoenergetic proton beam.

4. **Estimators (scoring) and Detectors:** In this study, RESNUCLEI scoring card was used for calculation of residual nuclei production in plutonium target, it records production yield of residual nuclides. This card is the command required to define a detector to track and record all information which is related to residual nuclei produced during the simulation.

5. **Define Physics Processes:** After scoring the next task is to select the physics models and parameters relevant to reactions in plutonium target. The EVAPORATION model with "New Evaporation with Heavy Fragment" was chosen as a physics model.

6. **Setting Run Parameters:** In the measurement**,** the number of particle histories, in this study, was set up 500 000 particles for obtaining better results.

7. **Analyzing Results:** Product yield data of residual radionuclides were obtained in this study for RESNUCLEI card in "tab.lis" output file.

8. **Calculation of cross section after using RESNUCLEI scoring**: Considering formula ((4.7) in Chapter 4) were find and calculated all parameters for converting product yield of residual nuclides to cross section in (mb) units. The parameters are shown in Table 25.

Table 25. Parameters for defining of cross section in (mb).

Material of target	$^{239}PuO_2$	
Inelastic Scattering length	179.6 cm	
Density of target	0.974121 g/cm^3	
Avogadro constant	6.02E+23 mol^{-1}	
Molar mas of target	271 g/mol	
Multiplication factor (1)	2.57E+03	
Reaction probability (Dividing factor (2))	9.62E-04	Number of stars generated per beam particle for proton

Additionally, FLUKA code also provides graphs. The FLAIR uses gnu-plot to produce plots. The graphs, obtained in result of this simulation are shown in Figs.6.13, 6.14 and Figs.6.15, 6.16.

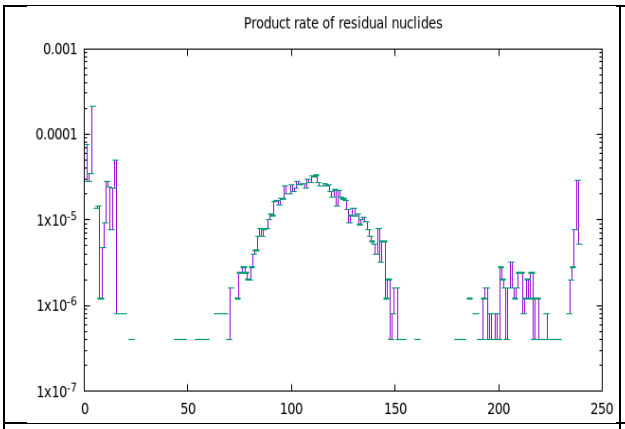

Fig.6.13. Product yield per mass number A.

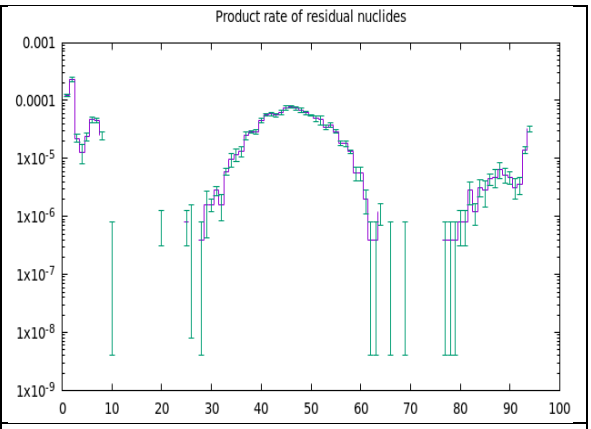

Fig.6.14. Product yield per proton number Z.

Figures 6.15 and 6.16 represent A-Z-Plots created using FLAIR gnu-plot. The Chart of the Nuclides visually organizes all the identified nuclei based on two key characteristics: A,

the atomic mass number defining the total number of nucleons, and Z, the atomic number representing the quantity of protons.

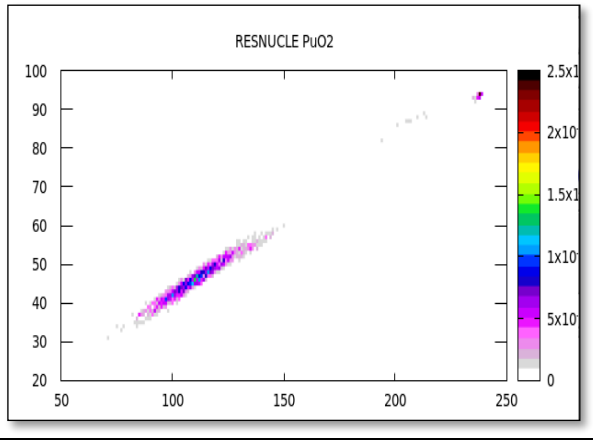

Fig.6.15. A-Z-Plot using FLAIR (and gnu-plot) In range A between 50 to 250, and Z from 20 to 100.

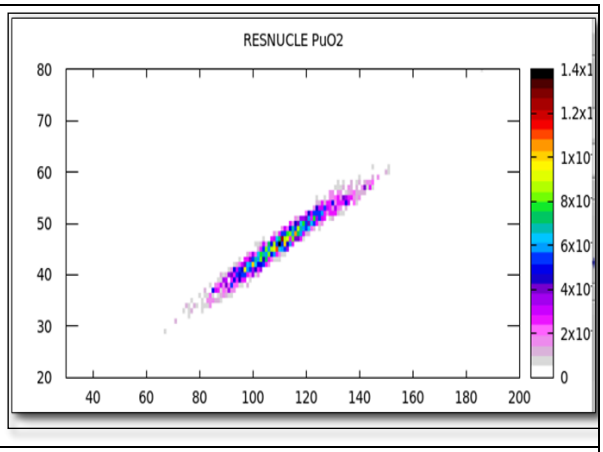

Fig.6.17. A-Z-Plot using FLAIR (and gnu-plot) In range A between 30 to 250, and Z from 20 to 80.

C. The obtained results in PHITS code simulation

In the context of spallation reaction simulation, various tools can be employed such as the T-Yields tally, dchain-sp, or inucr02 examples. The T-Yields tally provides information on produced nuclei. In PHITS, tallying is regarded as a process for collecting and recording information about specific quantities or events during the simulation.

In the figure below, the graphical interface of the PHITS code depicts the appearance of the $^{239}PuO_2$ target. Figures 6.18 and 6.19 illustrate the general geometry of the target used in all examples. In these representations, yellow colors denote the aluminum cover, blue represents aluminum foils, and pink signifies the study target.

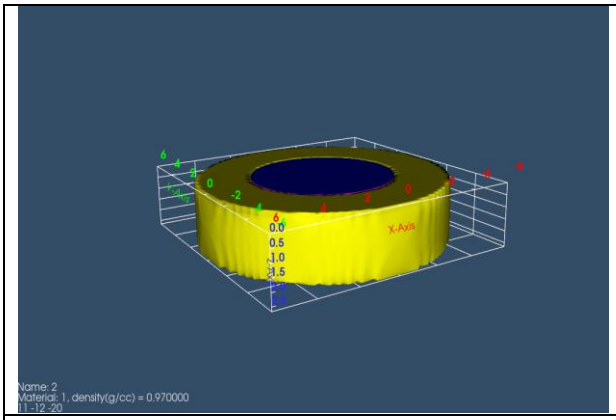

Fig.6.18. PHITS geometry of $^{239}PuO_2$ target.

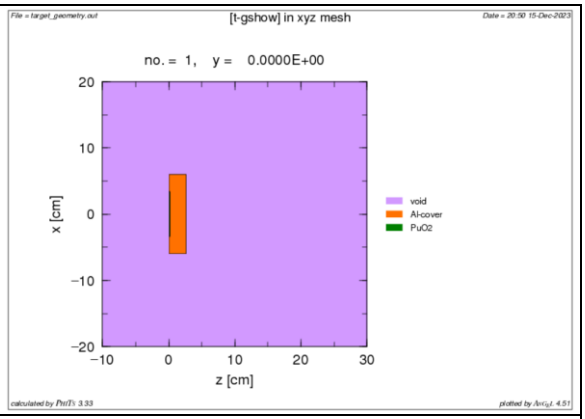

Fig.6.19. PHITS geometry of study case plotted by ANGEL v.4.51. (dchain-sp tally).

The inucr02 tally result of simulation

In case of using "inucr02" example in PHITS, it is possible to calculate cross section in (mb) depending on energy in MeV. The result of simulation of reaction

660 MeV p + $^{239}PuO_2$ considering all parameters of performed experiment is represented in Fig.6.20. For comparison of observation results of cross section of reaction were used data from EXFOR database (in graphical image) that is shown in the Fig.6.21 below.

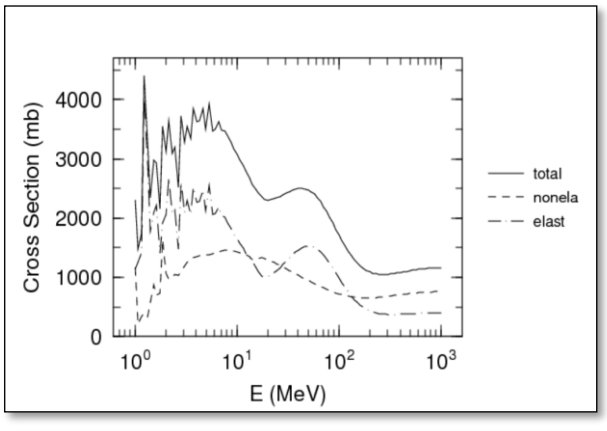

Fig.6.20. Calculated result of cross section for $^{239}PuO_2$ target in energy range from 10 to 1000 MeV.

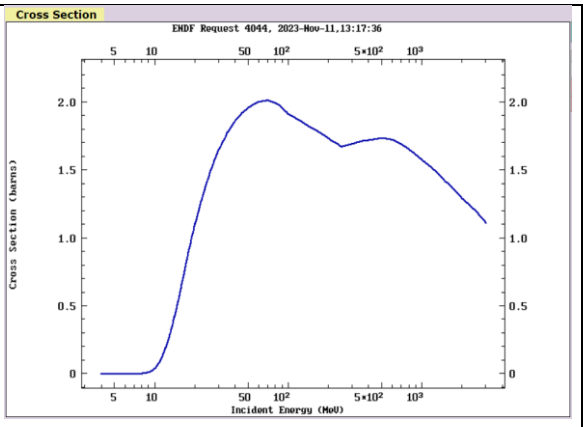

Fig.6.21. Cross section of ^{239}Pu given in EXFOR database.

The energy range in Fig.6.21 is from 10 to 1000 MeV, and cross section values is barn unit. As a results, obtained simulation value is similar to data from EXFOR database. Total cross section values given by PHITS code for energy 660 MeV and $^{239}PuO_2$ target ≈ 1.2 barn. In case of cross section of pure ^{239}Pu, EXFOR database provides result ≈ 1.7 barn for energy 660 MeV.

T-Yields tally result of simulation

The T-Yields tally was used for obtaining information about production yield of residual nuclides (in PHITS). When the nucleus is specified, the isotope distribution is applied to the mass number distribution. In case of the study reaction, the T-Yields tally provides information about the production of specific nuclides as a result of p + $^{239}PuO_2$ interactions.

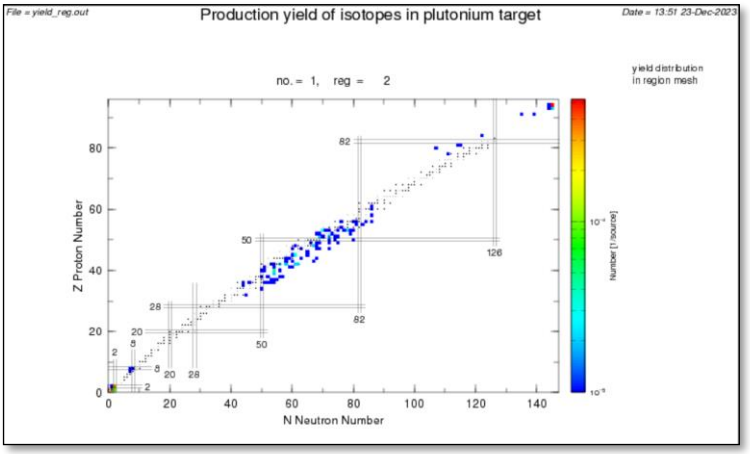

Fig.6.22. Production yield of residual nuclides of reaction.

In Fig.6.22 shown nuclear chart of proton numbers (Z) is plotted versus neutron number (N) of isotopes which obtained in proton-induced reactions on plutonium target. The

doble black lines are at the magic numbers.

The dchain-sp tally results of simulation

PHITS code, estimates nuclide yields produced in target materials (plutonium in this case) of protons (also with neutrons, and pions) with energies higher than 20 MeV by using NMTC/JAM - high-energy particle transport calculation code.

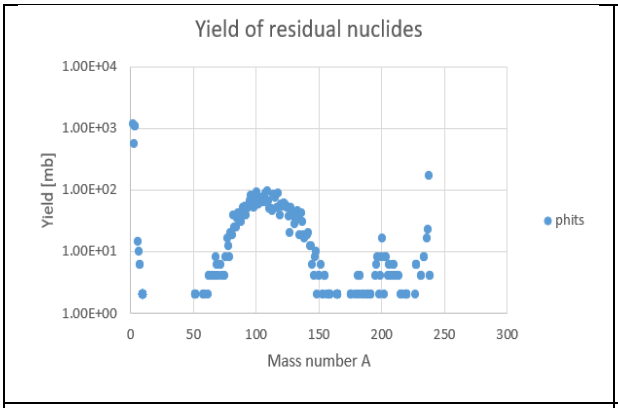

Fig.6.23. Production yield of residual nuclides per their mass number (A).

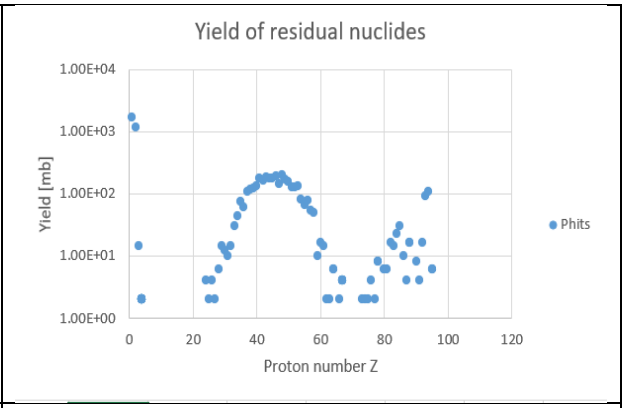

Fig.6.24. Production yield of residual nuclides per their proton number (Z).

The NMTC/JAM code integrates the Generalized Evaporation Model (GEM) into its nuclear reaction analysis, aiming to improve the accuracy of yields for light fragments like beryllium generated from proton-induced reactions. Additionally, the calculation approach has undergone a transformation from its original Monte Carlo sampling method to adopting experimental cross section data for the estimation of nuclide yields.

Fig.6.25 and Fig.6.26 below depict the distributions of proton and neutron flux in the study geometry. The color and shading in the distribution plot indicate the intensity of the proton flux, with brighter colors like red or yellow representing higher intensity regions. This distribution offers insights into the traversal and interaction patterns of protons within the study geometry.

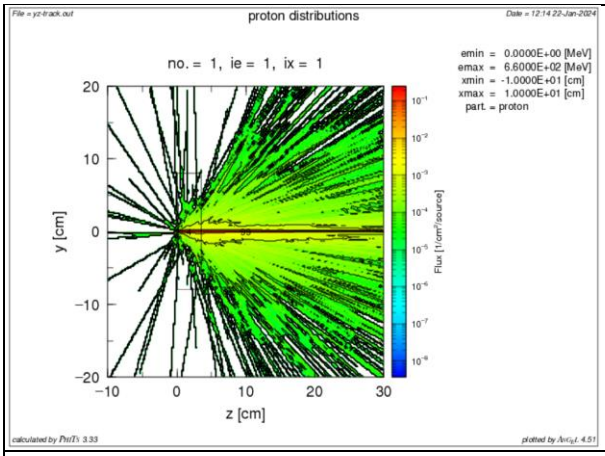

Fig.6.25. Proton flux distributions in the geometry.

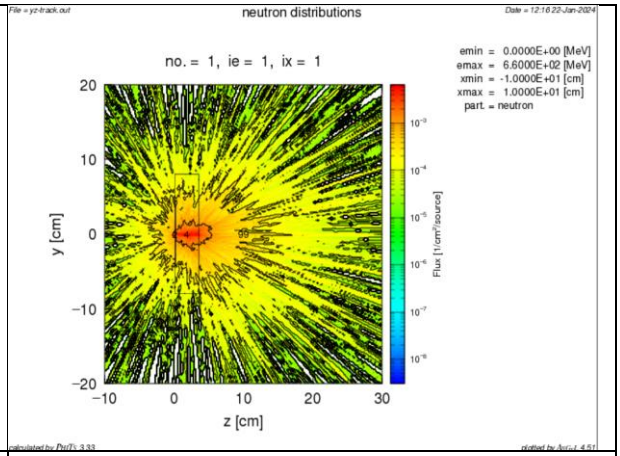

Fig.6.26. Neutron flux distributions in the geometry.

Similarly, to the distribution of proton flux, the neutron flux is depicted by the spatial

arrangement and energy spectrum of neutrons. The neutrons are generated as secondary particle in this experiment. The neutron flux intensity is visually represented in the distribution plot, with different colors or shades indicating varying levels of neutron presence. This distribution is a valuable source of information on neutron behavior, including penetration depths and potential interaction sites within the studied geometry.

The range example results

The Plot of generated particles in spallation reaction 660 MeV with plutonium target is shown in Fig. 6.27. Particles, except spallation products, were generated in spallation and fission reaction such as proton, neutron, pion+, muon-, deuterons, tritons, ^{3}He and ^{4}He.

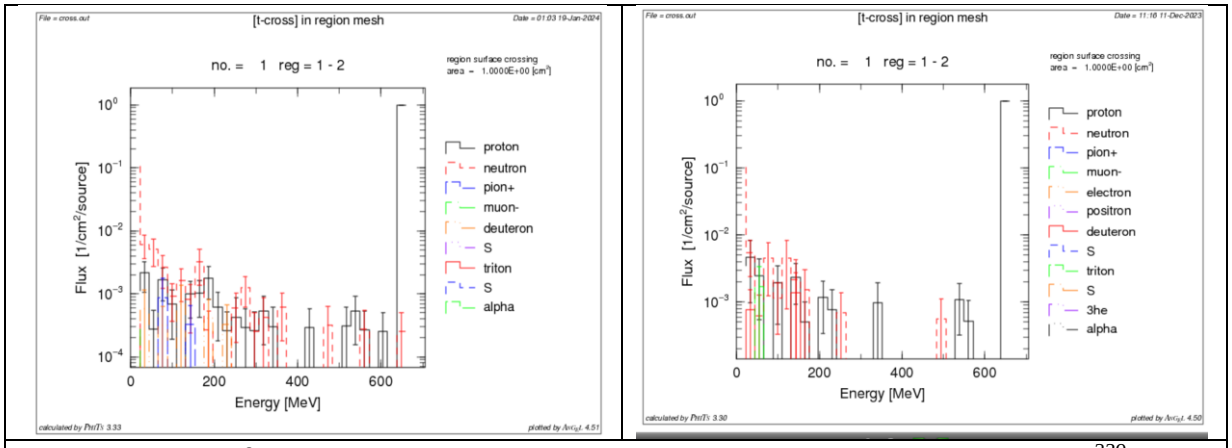

Fig.6.27. Type of particle which are generated in spallation reaction 660 MeV p + $^{239}PuO_2$.

The range tally in the PHITS code provides information about particle which generated with difference energy range in study target. The range tally is essential for understanding the spatial distribution of particle interactions within a target or material.

6.3 Discussion

Analysis of γ-spectra was carried out with the DEIMOS32 program. After obtaining output files from the DEIMOS32, were calculated efficiency of calibration for measurements detectors (Efektfit.exe) and fitting coefficients of efficiency (EfektFit.exe) for each measurements position. Next steps were calculated nonlinearity coefficients. After calculation and collection all necessary data and information, all details were put in AD4HEL code, which calculates the reaction rate of residual nuclides with decay curve and half-time of study nuclides. After obtaining the results, by using equations from Chapter 2, cross section for experimental data was calculated.

In many cases, measuring radioisotopes with a long half-life often generates low-energy γ-quanta, which makes it difficult to process a region below 200 keV. In case of measuring isotopes with short half-lives, difficulty is that they have rapid radioactive decay. One more complication, for determining exactly radionuclides, was that the measured spectra contained many γ-lines, which very often overlap. For this reason, data processing was not started until the last spectrum measurement was completed. The latter measurement usually

consists of products with shorter half-lives that are no longer visible in the latter spectra. Processing of the obtained spectra began with the last spectra and continued in stages towards the first measurement.

The calculation of experimental results of the residual nuclides for the cross sections generated in the $^{239}PuO_2$ target during the irradiation study with proton energy of 660 MeV is presented in Table 20 and 22. In this study, the reaction rates, and cross sections for a total of 65 nuclides from the byproducts of plutonium fission were determined. Table 26 specifically represents the isomers obtained in the target after the reactions.

Table 26. The isomers that obtained in plutonium target after reactions.

Detector	Isotope	E, keV	I_γ,%	$\sum\sigma$,barn	$\sum d\sigma$, barn	$T_{1/2fit}$, h	$T_{1/2tab}$, h
CANBERRA	^{98m}Nb	722	73.8	1.17E-04	9.19E-06	1.56	0.85
		787	93			0.8	0.85
		1169	17.8			1.26	0.85
	^{91m}Y	555	95	5.12E-05	4.65E-06	1.3	0.83
	^{90m}Y	479	90.7	2.52E-05	1.27E-06	3.49	3.19
	^{201m}Bi	846	5	9.87E-05	4.45E-06	1.33	0.98
	^{135m}Cs	846	95.9	3.58E-05		0.67	0.88
		786	100		2.68E-06	0.89	0.88
	^{118m}Sb	1229	100	8.87E-05		2.85	5
		1050	97		6.05E-06	5.19	5
	^{116m}SbD	843	11.2	3.05E-04		0.16	1
		1293	100		4.45E-05	0.94	1
	^{116m}In	1293	84.4	1.84E-04		0.93	0.9
		1097	56.2		9.66E-06	0.91	0.9
ORTEC	^{69m}Zn	438.71	94.8	1.74E-05	2.03E-06	14.58	13.76
	^{131m}Te	772.99	49.9	4.70E-04	7.11E-05	27.32	30
	^{120m}Sb	1171.2	100	8.21E-05		135.2	138.2
		1024.1	99.4		1.32E-05	62.37	138.4
	^{117m}Cd	1065.8	23.1	2.27E-05		2.5	2.49
		1997.6	26			2.78	2.49
		1432.9	13.4		4.65E-06	3.48	2.49

Additionally, as mentioned earlier, unstable isotopes may transform into more stable isotopes through radioactive decay. The original unstable isotope is referred to as the parent isotope, and the resulting stable isotope is termed the daughter isotope. In the study, daughter isotopes obtained as a result of decay are listed in Table 27. The parents were identified by tracing the radioactive decay patterns using the Table of Isotopes [167].

Table 27 presents the decay patterns for the parent isotopes. As evident from both Table 27 and Table 26, in the initial measurements using the CANBERRA detector, isomers predominate, whereas with the ORTEC detector, daughter isotopes are more prominent.

Table 27. The generation of daughter isotopes during proton-induced reactions with plutonium target.

Detector	Daughter Isotope	∑ σ,barn	Σdσ, barn	Decay pattern [167]
CANBERRA	^{88}RbD	1.03E-05	6.42E-07	^{88}Kr -> ^{88}Rb
	^{116m}SbD	3.05E-04	4.45E-05	^{116}Te -> ^{116m}Sb
ORTEC	^{97}NbD	1.68E-04	1.88E-05	^{97}Zn -> ^{97}Nb
	^{117}InD	2.11E-04	3.48E-05	^{117}Cd -> ^{117}InD
	^{116}SbD	1.51E-05	2.27E-06	^{116}Te -> ^{116}Sb
	^{112}AgD	6.30E-03	7.26E-04	^{112}Pb -> ^{112}Ag
	^{92}YD	9.35E-05	1.61E-05	^{92}Sr -> ^{92}Y
	^{132}ID	2.12E-04	4.03E-05	^{132}Te -> ^{132}I
	^{135}XeD	8.54E-05	9.82E-06	^{135}I -> ^{135}Xe

For instance, detailed decay modes for some of these isotopes are provided below, another see Appendix V [167]. (The common radioactive decay for plutonium, see Appendix VI).

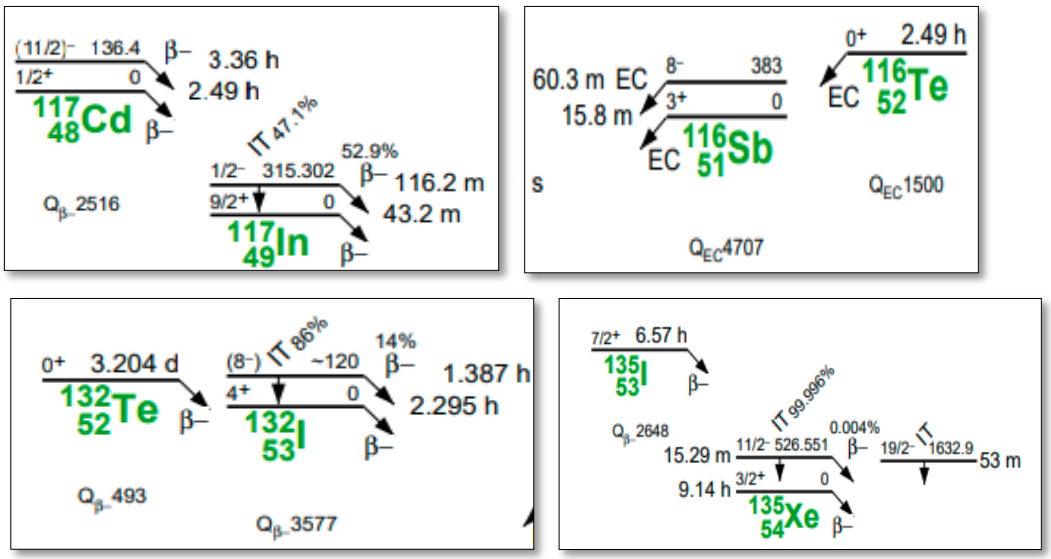

Fig.6.28 and Fig.6.29 distinctly distinguish two major reaction modes, namely fission and spallation. Residual products are observed in the region of the target mass of plutonium and approximately at half the target mass, with a clear gap between them. This gap ranges from mass number 150 to 182 and charge number from 64 to 76. Fission products manifest as a double peak in the mass distributions at the top, appearing higher than others. The radionuclides observed in the area of the study target are created by several reactions, including preequilibrium reactions, deep spallation, and spallation processes.

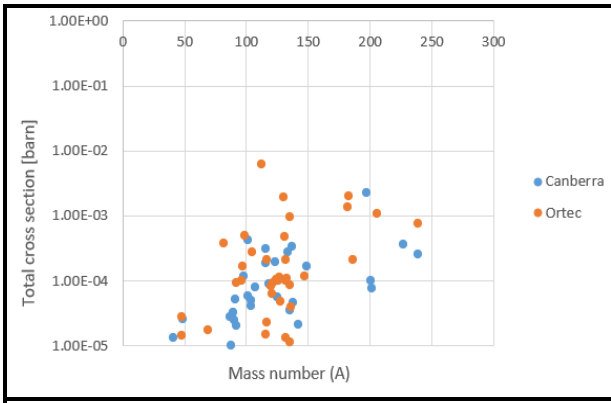

Fig.6.28. Cross sections correspond to the mass number (A) of radionuclides measured by detectors.

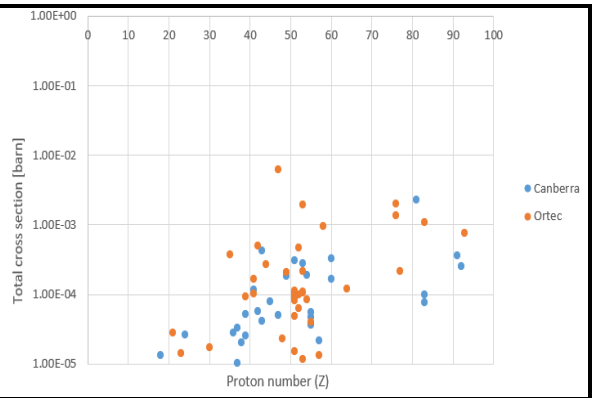

Fig.6.29. The relationship between cross section and proton number (Z) of radionuclides measured by detectors.

The selection of nuclides was based on the following criteria:

i. A candidate nuclide is determined by the presence of all significant photo peaks associated with a study nuclide in the gamma spectra.

ii. All visible energy peaks of one study nuclide should be present in the same measurement position.

iii. The photo peaks that are being analyzed must solely correspond to the nuclide of interest, with no other nuclides sharing the same gamma energy or should be present in difference position, with different parameters such as half-lives or reaction rate.

iv. The decay curve of the selected photo peak must align with the half-life of the nuclide of study. For analysis, only photo peaks with an experimental half-life that is within 10% of the reference value are selected [168].

v. The energy peaks were chosen which have high intensity.

That proved obtained experimental results is obligatory compare experimental data with theoretical simulation. The comparison experimental data with theoretical results are presented in Fig.6.30 and Fig.6.31. Figures below shown relationship between total cross section of residual nuclides and mass number (A) at the Fig.6.30, and relationship between total cross section of residual nuclides and proton number (Z) at the Fig.6.31.

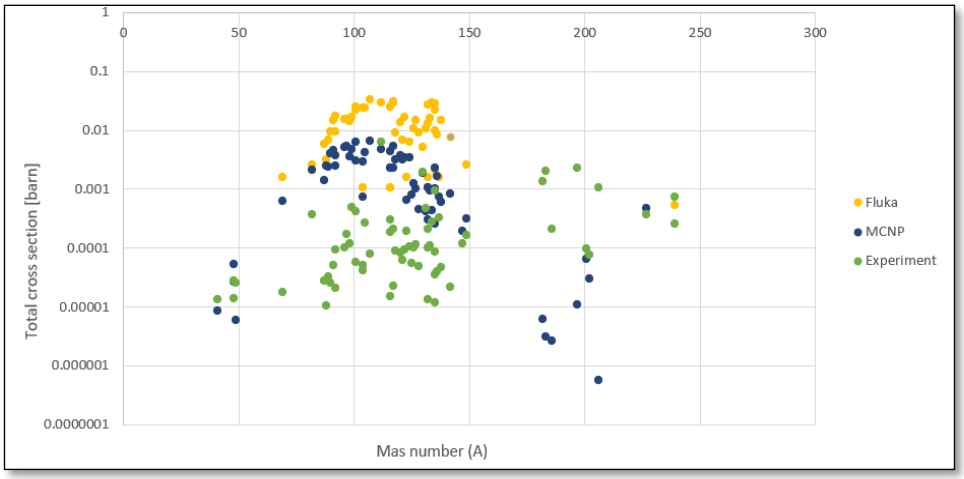

Fig.6.30. Cross sections of radionuclides which obtained after irradiation of $^{239}PuO_2$ by 660 MeV protons, experimental results compare with theoretical simulation.

In Fig.6.30, the cross sections of fission and spallation reactions for ^{239}Pu nuclei are presented, with dependence on the mass number A. The green points correspond to experimental data obtained during measurements for both detectors combined. The dark blue dots represent the results of theoretical calculations using MCNP v.6.1, while the yellow dots depict the results of simulations using the FLUKA code.

It's noteworthy that some radionuclides identified in the experimental data are not found in the FLUKA code simulation but are present in the MCNP v.6.1 simulation results. Conversely, only one radionuclide, ^{239}U, is not present in the MCNP v.6.1 simulation results. Additionally, in the FLUKA code, almost all radionuclides with high mass numbers and high proton numbers are not available.

This discrepancy underscores the differences and limitations between the simulation codes in accurately representing certain radionuclides in the given experimental conditions. This discrepancy may arise due to the fact that in present measurements were used two different detectors with different parameters, that makes normalization problem. That is applicable to Fig.6.30 and Fig.6.31.

Normalization is essential in experimental setups to account for variations in detector efficiency, energy response, and other factors that could affect the measured data. However, when two detectors with differing parameters are employed, achieving accurate normalization becomes challenging.

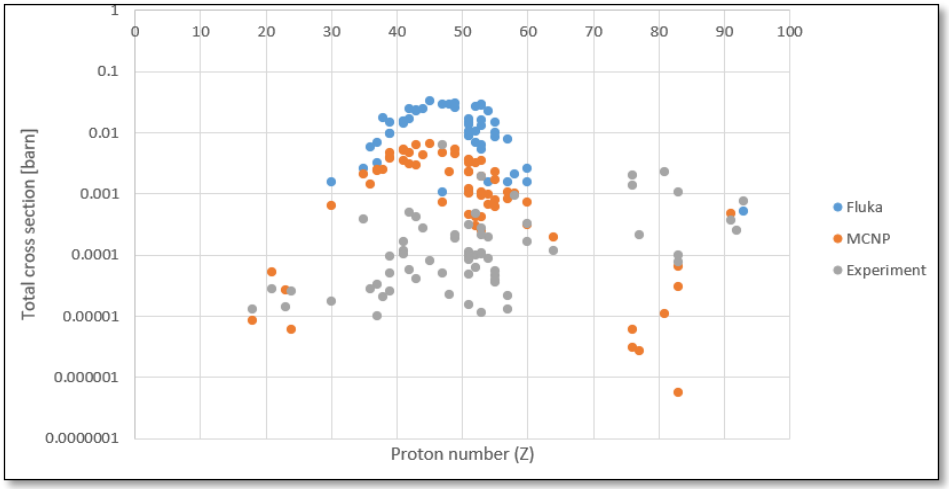

Fig.6.31. Cross sections of radionuclides which obtained after irradiation of $^{239}PuO_2$ target by 660 MeV protons, experimental results compare with theoretical simulation.

In Fig.6.31, the cross sections of fission and spallation reactions for $^{239}PuO_2$ nuclei are depicted based on the proton number Z. The grey points represent experimental data for every other residual nuclide, while the orange dots and blue dots indicate the results of theoretical calculations using MCNP v.6.1 and simulations by the FLUKA code, respectively. Similar to the previous case study with Fig.6.30, the overall shapes and accumulation regions of the data are consistent, but there is an observed difference in the total cross section values between the theoretical simulations and experimental results.

Several factors could contribute to this difference. Experimental setups may have inherent limitations such as measurement errors, instrument calibration issues, electrical noise, and systematic errors. The experimental data might not have considered corrections for background, beam, or coincidence during measurements, leading to potential discrepancies in the cross section values. On the other hand, theoretical simulations are based on models

created from experimental results. While some experiments provide a wealth of data covering various energy ranges and target materials, certain experiments may be challenging and costly to conduct. Therefore, it is crucial to conduct further investigations and experiments in the nuclear field to gather sufficient information, data, and materials for comprehensive comparisons and the development of accurate models. This ongoing research is essential for refining theoretical models and improving their alignment with experimental results.

Background correction: In this measurement, background correction was not performed. The purpose of background correction is to account signals or counts that do not directly relate to the study (measurement) sample. However, in certain situations, such as measurement of target materials (elements) with high intensity or elements that are strong gamma-ray's emitters, background correction became less practical or even it's not made any big influence on results. Additionally, in case of short irradiation times (like 5.25 min), the background signal may stay relatively stable and consistent throughout the measurement duration. In these situations, the impact of background on the overall signal may be minimal, and the benefits of background correction may be negligible.

For instance, Fig.6.32 depicts ^{239}Pu spectrum characteristics across various low-energy scenarios.

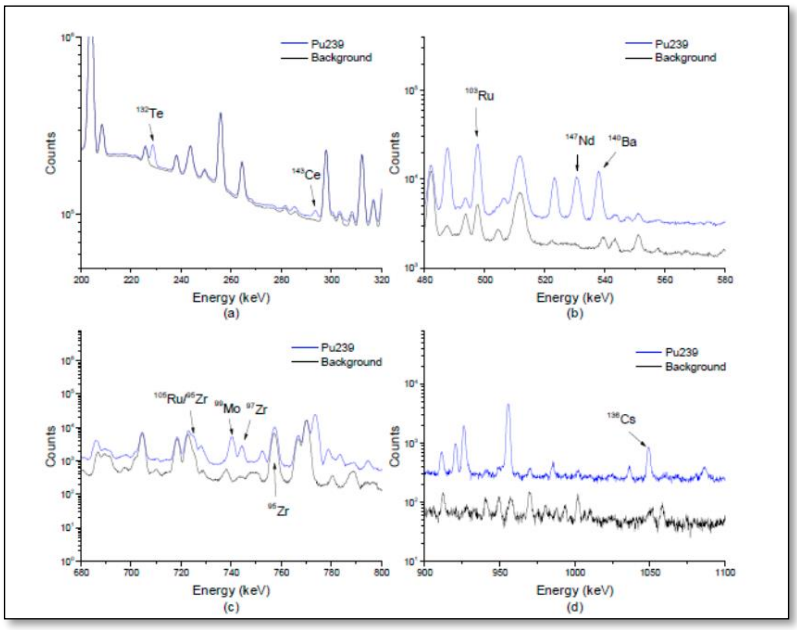

Fig.6.32. Examples of ^{239}Pu spectrum characteristics across various low-energy scenarios [169].

Beam correction: In many cases of measurements beam correction factor affect accuracy of measured results. However, in case if assume that the beam characteristics, such as intensity and energy, remain relatively uniform during the irradiation time, they might neglect the beam correction factor. In this study case, irradiation time was just 5.25 minutes, and proton beam was stable. All parameters of proton beam are described in Chapter 5. This assumption can simplify the analysis but may be valid only under certain conditions such in this study.

Correction for coincidence: In this study, distance between detector and target was not big, it's why this correction were not considered. Coincidence corrections are typically

used when during measurement is possible detecting two or more particles at the same time. It can happen due to the spread of particles, depending on their trajectories. This correction may be not to include if the experimental setup ensures a low probability of coincident events, for example, through the close distance between the detector and target. In this experiment, the distance between the detectors and plutonium target was small, that suggests that the probability of coincidence events is inherently low.

As a result of the comparison between experimental data and theoretical simulations, several conclusions can be drawn:

- In terms of mass number and proton number, the experimental results align closely with the theoretical calculations conducted by both MCNP v.6.1 and FLUKA codes.
- However, when examining the total cross section values for each specific radionuclide detected by the detectors (as shown in Figures 6.30 and 6.31), there is a noticeable difference. Experimental data tend to have smaller cross section values compared to the higher values obtained through theoretical simulations.
- Figure 6.30 further illustrates the alignment between theoretical and experimental calculations, indicating that radionuclides are distributed in regions resulting from fission, deep spallation, and spallation reactions.
- Overall, despite variations in absolute cross section values, the experimental results and theoretical simulation data exhibit similar trends. The accumulation of residual nuclides follows a consistent pattern in both experimental and theoretical calculations.

Fig.6.33 provides an illustrative example of the distribution of residual nuclei and the processes that occurred in a lead (Pb) target after irradiation with a proton beam energy of 1 GeV. This serves as a valuable reference for understanding the processes involved in the interaction of high-energy protons with heavy targets. It draws parallels with the study case involving protons with a 660 MeV energy proton beam and a plutonium ($^{239}PuO^{2}$) target.

From the Fig.6.33, it is evident that the production of residual nuclides occurs through various processes, including evaporation, fragmentation, fission, deep spallation, spallation, and quasi-elastic reactions. Each process contributes to the creation of specific nuclides, and the distribution provides insights into the complex dynamics and outcomes of proton-induced reactions with high target materials.

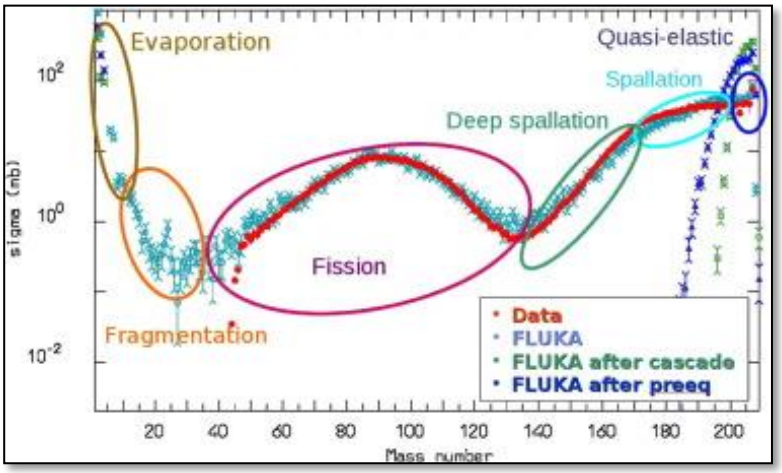

Fig.6.33. Production of residual nuclei from 1 GeV protons on Lead (Pb) [170].

The FLUKA evaporation model, which is based on the Weisskopf–Ewing approach, has undergone continuous updates over the years. These updates include enhancements such as sub-barrier emission, a full level density formula, and evaporation of nuclear fragments up to $A \leqslant 24$. Recent improvements in fission treatment and the incorporation of adopted level densities have proven highly effective in accurately describing the production of residual nuclei from heavy targets.

It's essential to note that no single model or code can provide perfect performance in all scenarios. Each code has its strengths and limitations, and there is no clear-cut result that designates one as universally superior, especially in specific regions of radioisotope distribution. Challenges may arise, particularly in dealing with heavy target elements, and issues related to the fission channel, especially in the context of elements like uranium or plutonium. The competition between spallation and fission in cases involving these target elements can present complexities that impact the accuracy of predictions [171].

Systematic errors in simulations can stem from various sources, and several of them are described below:

Physics Models: The physics models underlying simulation codes are not perfect, especially in nuclear physics. Deviations between theoretical models and the actual physical processes can introduce systematic errors.

Artifacts: Imperfections in algorithms, such as energy deposition in the middle of a step or missing corrections for cross section changes and energy loss over a step, can contribute to errors. This parameter can be improved by using thick targets or complex geometries.

Data Uncertainty: The accuracy of theoretical results is limited by the quality of experimental data available. Systematic errors can arise if experimental data have uncertainties or limitations, impacting the reliability of theoretical simulations.

Material Composition: The composition of materials used in simulations might not be well-known. Variations in the actual composition, such as the presence of more water, air, impurities, or undefined additional materials, can introduce uncertainties.

Geometry Reproduction: Exact reproduction of geometries used in experimental setups may be challenging. Sometimes, geometries cannot be reproduced exactly in theoretical simulations, leading to discrepancies in results.

Addressing systematic errors involves continuous improvement in physics models, algorithm refinement, reducing uncertainties in experimental data, enhancing knowledge of material compositions, and striving for better reproducibility of experimental setups in theoretical simulations. Ongoing research and advancements in simulation techniques contribute to minimizing these systematic errors and improving the accuracy of predictions.

Some examples, where experimental results are not exactly fit and depending on different simulation codes based on different physical models.

In the study [172], the investigation focused on isotope production, specifically the measurement of production rates of volatile elements, using a proton beam irradiated LBE target. Experimental results were compared with theoretical simulations for various isotopes including He, Ar, Kr, Xe, I, Hg, and At. The Fig.6.34 illustrates the comparison of experimental results with calculations from FLUKA and MCNP v.6.1. The Figure serves to

highlight instances where there are discrepancies between experimental data and simulations based on different physical models employed by FLUKA and MCNPX.

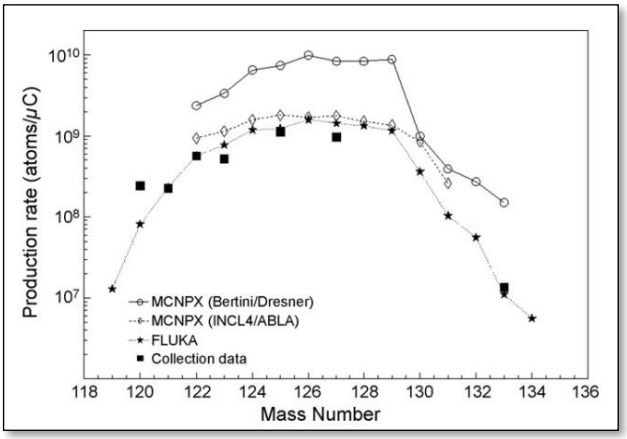

Fig.6.34. Comparison experimental results of production rates for Xe isotopes with MCNPX and FLUKA codes [172].

The black squares represent measured points, open circles - MCNPX (Bertini/Dresner model combination), diamonds show MCNPX (INCL4/ABLA), and stars represent FLUKA codes. There is a significant discrepancy between the measured values and those calculated with MCNPX with Bertini/Dresner. However, the other two calculated results are quite close to the measured points.

The next example [171] is a comprehensive study of residual nuclide production at intermediate energies. At the Fig.6.35 and Fig.6.36 are shown experimental results of reactions proton (500 MeV and 1 GeV) with ^{208}Pb and comparison these results with 15 different similar studies. Cross section is given in [mb]. It can be observed in the picture below that the mass and charge distribution are influenced by the proton energy.

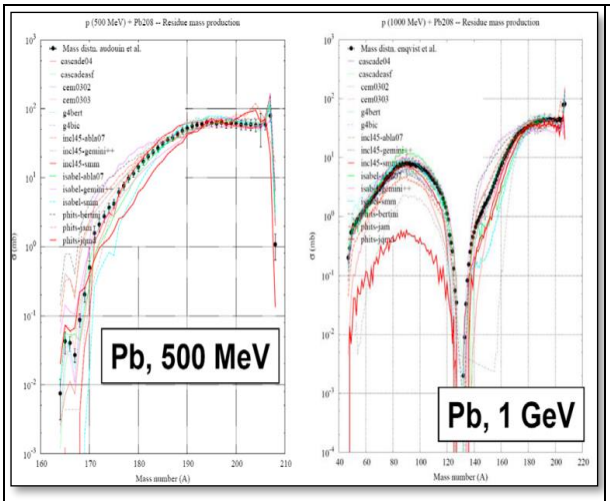

Fig.6.35. Mass and cross section distributions for lead at 500 GeV and 1 GeV compared with another calculated data [171].

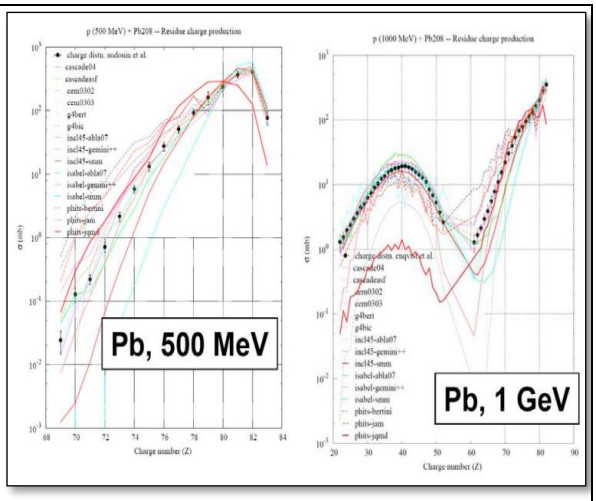

Fig.6.36. Charge and cross section distributions for lead at 500 GeV and 1 GeV compared with another calculated data [171].

Furthermore, Fig.6.37 presents the results of interactions between a proton beam with

an energy of 1000 MeV and a ^{238}U target. The figure displays the mass and charge distribution versus cross section (mb). Similar to previous cases, experimental results are compared with other calculated data. The figures reveal fluctuations in results across different experiments. While some data points have similar values, several results differ from each other. This variability emphasizes the influence of experimental conditions and the inherent uncertainties in the interactions between protons and the ^{239}U target.

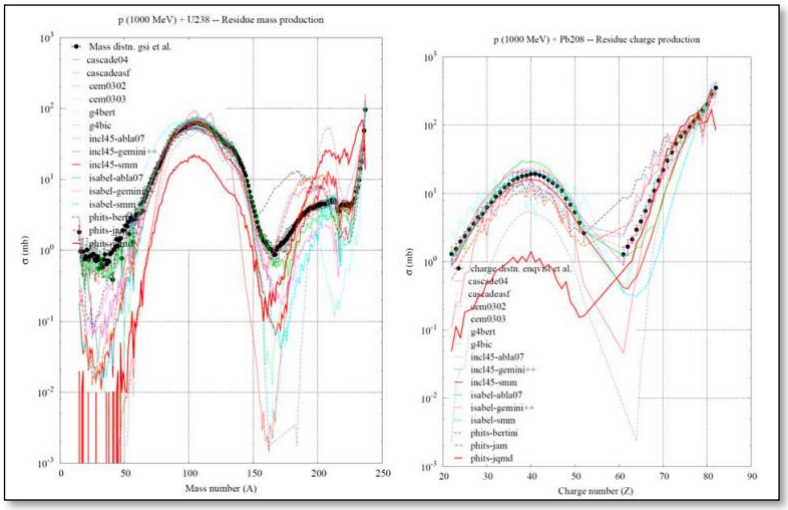

Fig.6.37. Mass and charge distributions measured by inverse kinematics for U-238 at 1 A GeV compared with calculated data [171].

In another experiment detailed in [173], natural uranium was subjected to various proton energies. Fig.6.38 illustrates the experimental cross sections plotted against product masses. The fission channel becomes evident, initiating at approximately 200 MeV. The graph distinctly showcases two major reaction modes: fission and spallation.

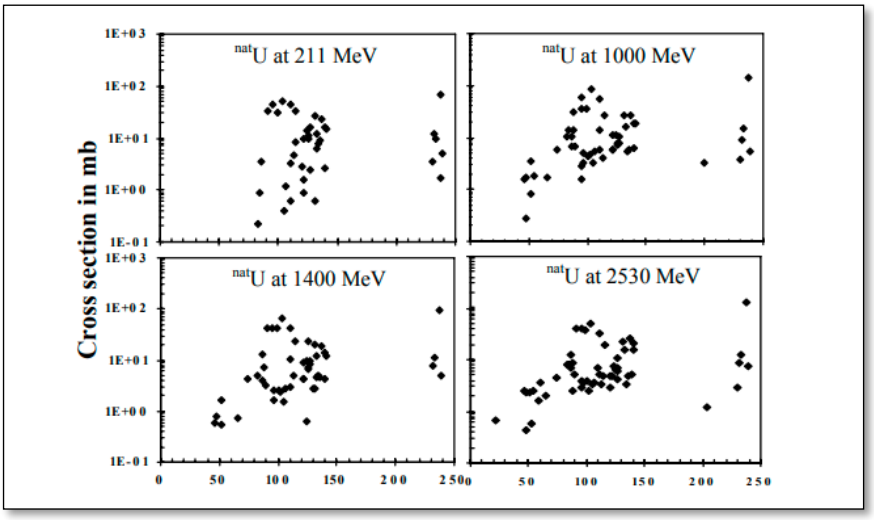

Fig.6.38. Cross sections for the production of residual nuclides from uranium as function of the product mass numbers [173].

Another experiment [150] describes cross sections of nuclei formation during irradiation of thorium foils with protons with an energy of 800 MeV. The cross sections of isotopes can be summed if cumulative cross sections for isotopes of the same mass number are measured on both sides of the valley of stability.

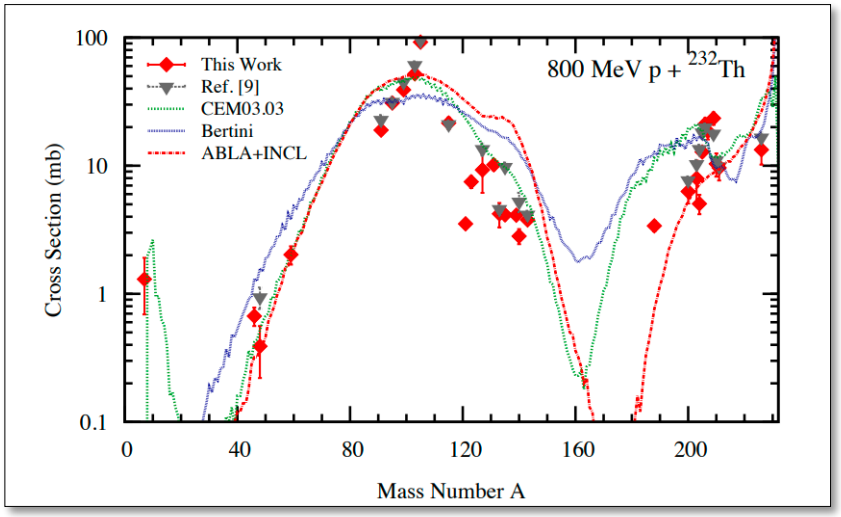

Fig.6.39. The comparison between predicted product yield mass distributions from 800 MeV p + ^{232}Th by CEM03.03, Bertini, and INCL+ABLA with cumulative cross sections measured in this study [150] and previously by Titarenko et al. [148].

Authors [150] suggest that discrepancies in cross sections value may be cased from factors such as small counting statistics or difficulties in accurately fitting peaks. The comparisons clearly demonstrate that models that were tested in this experiment should be improved to accurately predict isotope yields in arbitrary reactions. Furthermore, it is noted that the models discussed provide aggregated data for isomeric states of isotopes, potentially resulting in calculated estimates that exceed independently measured cross sections for individual isomeric states.

In this part, the comparison between experimental and simulated cross sections of radionuclides generated from the 660 MeV p + ^{239}Pu reaction was discussed. Additionally, examples of different similar experiments in high-energy protons on spallation targets are provided. The section demonstrates and describes possible reasons for the observed discrepancies between experimental cross section values and theoretical predictions.

6.3.1 Difference between experimental and calculation data

Experimentally obtained values should be compared with theoretical calculations, moreover, also with another similar experiments or database (if data is available). Comparison is performed by using < F > - factor and its deviation σ ($< F >$). The ratio shows average deviation of experimental data to calculation. The results will be more appropriate if this value is approximately equal to 1 or close to 1.

The < F > - factor is often used for estimation of different models and is given by formula [160]:

$$< F >= 10^{\sqrt{\langle\left(log\left[\frac{\sigma_{cal}}{\sigma_{exp}}\right]\right)^2\rangle}}; \quad (6.4)$$

The deviation $\sigma\ (< F >)$ is calculated by formula (6.5), below:

$$\sigma\ (< F >) = 10\sqrt{\langle\left\{\left|log\left[\frac{\sigma_{cal}}{\sigma_{exp}}\right]\right| - log(\langle F\rangle)\right\}^2\rangle} \tag{6.5}$$

Comparison by < F > - factor of all results is shown in the Fig.6.39 below. For comparison, radioisotopes which experimental and calculated cross section have difference less than 30 % were used. Results of calculations < F > - factor and its deviation $\sigma\ (< F >)$ are given in Appendix VII.

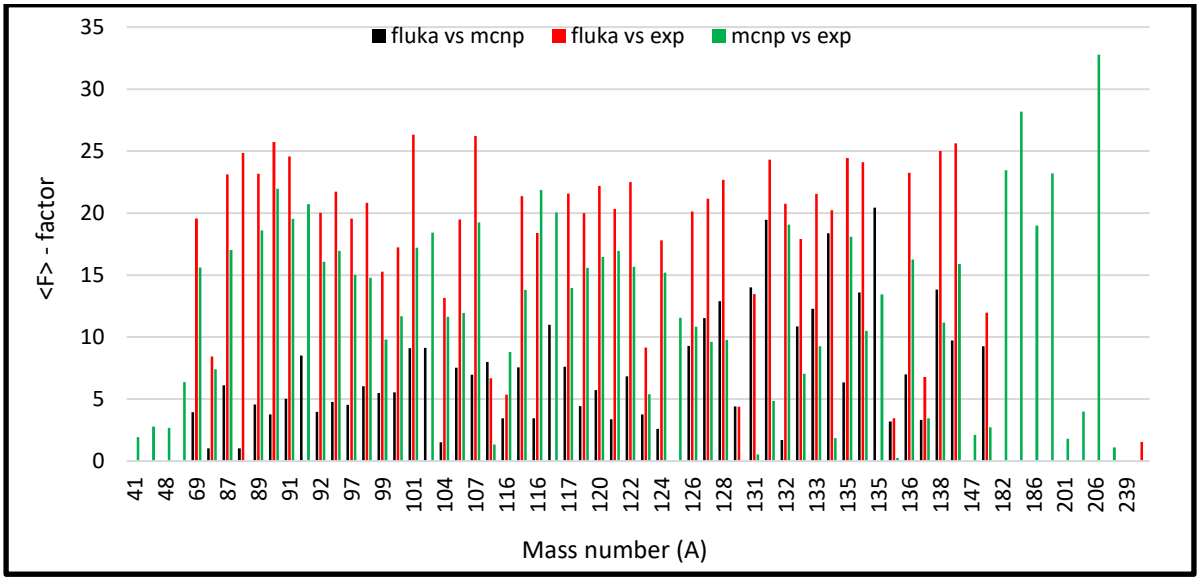

Fig.6.40. Value of <F> - factor for all residual nuclides in respect to FLUKA, MCNP and experimental results to mass number.

To compare experimental results with theoretical models, the C/E ratio (calculation results vs experimental results) was calculated, was also calculated. In Fig.6.40, the comparison of cross section data between FLUKA, MCNP v.6.1 and experiment results are shown as blue, and orange dots, respectively.

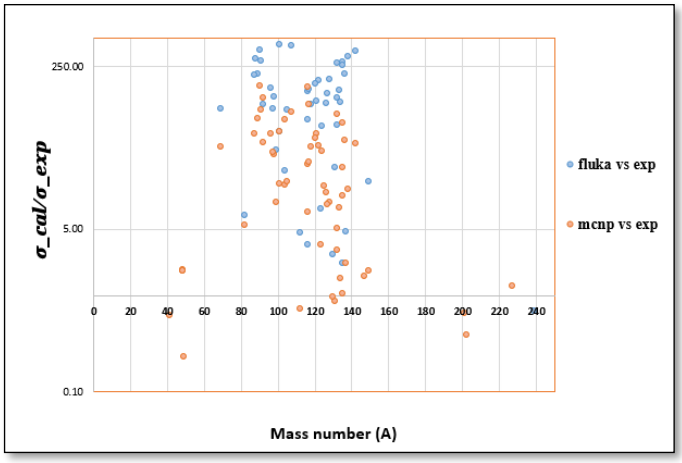

Fig.6.41. Comparison of experimental cross section results with FLUKA and MCNP v.6.1 data.

The detailed processing of the measurement results and especially their comparison with theoretical simulations brought significant information. Fig.6.40 shows that the results of the experiment have similar trend, but cross section values have certain deviations. Reasons for these differences can be found in the start of section 6.3 where the possible errors have been explained in detail.

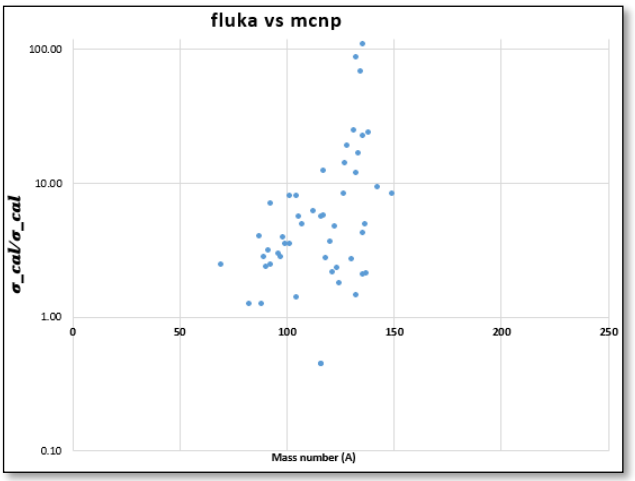

Fig.6.42. Comparison of cross section data between FLUKA and MCNP v.6.1 codes.

In Fig.6.41, a comparison is shown between the results of cross section calculations using the FLUKA and MCNP v.6.1 codes. The differences observed between these two codes can be attributed to their specific nuclear models and different databases that they use for modeling specific interactions or reactions. Additionally, an important point to note is that the FLUKA code provides more detailed input files regarding geometry, proton beams, and nuclear models compared to simulation conducted with MCNP v.6.1.

The simulations results are more comprehensive than the limited number of residual nuclides which are used in theoretical calculations and subsequently presented in figures given before. In the Fig.6.42 all data which were obtained during simulations and experimental measurements is present.

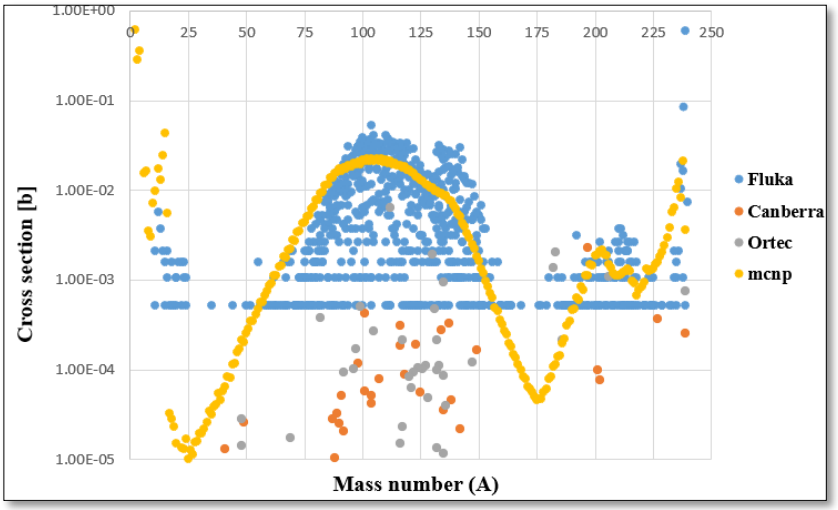

Fig.6.43. Mass and cross section distributions for plutonium at 660 MeV.

In Fig.6.42, the MCNP v.6.1 results represent a summary of all nuclides with the same

mass number, along with their corresponding cross section data. It is clear from the above figure that all experimental data have similar trend of distribution radionuclides after reactions in plutonium target, however, cross section value are smaller in comparison with simulation results. This demonstrates that a 660 MeV proton energy is sufficient for inducing fission and spallation reactions in a plutonium target, suggesting that this method can be utilized to transmute plutonium into short-lived radionuclides.

Therefore, this dissertation thesis delved into the challenges faced during measurements and processing spectra, searching good methodology for obtained correct results, etc. Results include the identification of numerous parameters, such as efficiency of detectors, different correction, determination of radionuclides, their half-life, reaction rate and cross section data. Additionally, creation of simulation by using computer codes.

The dissertation aims to enhance the understanding of nuclear reactions, particularly spallation and fission reactions, by comparing experimental data with theoretical simulations using the MCNP v.6.1 and FLUKA codes. This comparison sheds light on the general trends in the accumulation and creation of radionuclides. The overarching goal is to contribute valuable insights to the field, potentially providing new information about accelerator driven systems that can aid in the reduction of nuclear waste. Throughout this research, attention is given to acknowledging potential systematic errors and identifying sources of discrepancies in the comparison between experimental and theoretical results.

CONCLUSION

This dissertation thesis can be divided in two parts: the first part is theoretical, where are all details related to Accelerator driven system, transmutation, spallation and fission process, methodology of processing of gamma-spectra, computer codes and description of calculation of reaction rate, cross section and correction is described. Second part is focuses exactly on experiment with plutonium ($^{239}PuO_2$) target, experimental results, and comparison with simulations.

In this experiment, the reactions of spallation and fission of the ^{239}Pu nucleus at an energy of 660 MeV were investigated. The experiment focused on determining short-lived radionuclides which occurred in target as a result of above-mentioned reactions. The sample was irradiated with a direct proton beam; γ - spectrometry and direct kinematics were employed for analysis. The direct kinematics method was used to accurately determine the effective cross sections of nuclear reactions at high energies. The residual products produced in the target were detected by γ-spectroscopy and mass spectrometry.

Analysis and process of γ-spectra was carried out by using several programs, the DEIMOS32 program – processing spectra, Efektfit.exe - calculation efficiency, EfektFit.exe for fitting coefficients of efficiency, AD4HEL code – to calculate reaction rate of residual nuclides and half-time of residual nuclides. Total cross section of experimentally identified radionuclides was calculated. Additionally, experimental results of total cross section were compared with theoretical data from MCNP v.6.1 and FLUKA codes.

Out of the copious number of plutonium spallation, multifragmentation, evaporation, fission, and other non-elastic reaction products is presented, namely for ^{99}Mo, ^{97}Nb, ^{91m}Y, ^{82}Br, ^{48}Sc, ^{134}I, ^{123}Xe, ^{131m}Te, ^{121}Te, ^{117}Cd, ^{69m}Zn, ^{137}Nb, ^{135m}Cs, ^{133}I, ^{132}Te, ^{130}I, ^{128}Sb, ^{124}I, ^{138}Cs, ^{105}Ru and another (see Table 20, and Table 22), quantitative data were determined. Was determined a total about 66 total cross sections for residual nuclides which were measured in all positions. From Fig.6.30 and Fig.6.31 clearly are distinguishing two major reaction modes, such as fission and spallation.

As expected, the results are dominated by radionuclides with short half-lives. In the irradiated plutonium ($^{239}PuO_2$) target, 130 γ - lines were detected, which belong to 66 radionuclides. Radionuclides with half-life ranging from 18.3 minutes to 17.68 days were identified. Residual products are observed in the region of the target mass of plutonium and approximately at half the target mass, with a clear gap between them. This gap ranges from mass number 150 to 182.

The comparison between experimental data and theoretical simulations using MCNP v.6.1 and FLUKA codes highlights the accumulation and creation of radionuclides, following general trends, while also acknowledging potential systematic errors and sources of discrepancies which were described in Chapter 6 (6.3 Discussions). The overarching aim of this dissertation was to contribute to a better understanding of nuclear reactions, such as spallation and fission reactions, potentially adding new information about transmutation process which is related to Accelerator Driven Systems that will aid in nuclear waste reduction efforts.

The results of research or innovation to optimize the process of transmutation and geological storage for spent fuel can have an economic effect and are useful for the scientific community. In particular, minimal impact of radioactivity of spent nuclear fuel on the environment and humans is very important. According to the approaches proposed in this

thesis, the determination of radiation properties, such as reaction rate, cross section, etc., will be performed and narrowed to increase the accuracy of further goals in the current field of research. The work describes the conditions of the experiment and gives certain conclusions that can be very valuable for the needs of testing models of the fragmentation, fission, and spallation reactions, and they can be a supplement to the nuclear database.

The database is valuable for upcoming applications of accelerator driven nuclear waste transmutation and energy amplification, such as subcritical reactors. The results suggest that a subcritical system can effectively transmute plutonium, with a notably high plutonium fission rate.

In conclusion, the dominance of short-lived nuclides among the reaction products indicates the effectiveness of the transmutation process of ^{239}Pu which considered as a longer-lived isotope ($T_{1/2} = 24.110$ years). This finding has broader implications for nuclear waste management strategies and the development of technologies aimed at mitigating the long-term impact of nuclear waste on the environment and human health. Additionally, reducing the quantity of plutonium present in spent nuclear fuel, plays a significant role in non-proliferation risk. This comprehensive approach aims to positively impact resource utilization and public perception of nuclear energy.

Research in nuclear physics and accelerator driven system offers fascinating horizons for the future investigations. One possible avenue for further exploration is the use of alternative actinides (thorium, or synthetically produced plutonium), as a source of nuclear energy. The investigation of their properties (such as cross section of radionuclides after fission and spallation reaction), energy production and reactivity may help to understand how to use them more efficiently in nuclear reactors, moreover, find solution for safely utilizing spent nuclear fuel. Additionally, future research may enhance the possibilities of using protons, neutrons, electrons, etc., in advance technology. In short, the future of nuclear physics and accelerator driven system is full of challenges and opportunities, that's why investigation of fission and spallation reaction of actinides can help overcome the energy and environmental challenges of the 21st century.

REFERENCES

[1] World Nuclear Association. Nuclear Power in the World Today. November 2023. Online source. Available from: https://world-nuclear.org/information-library/current-and-future-generation/nuclear-power-in-the-world-today.aspx

[2] TRINH Le. Spent Nuclear Fuel Storage and Disposal. STIMSON. June 17, 2020. Online source. Available from: https://www.stimson.org/2020/spent-nuclear-fuel-storage-and-disposal/

[3] CARMINATI; KLAPISCH, R.; REVOL, J.P.; ROCHE, Ch.; RUBIO, J.A.; RUBBIA, C. CERN Report CERN/AT/93-47(ET), 1993; RUBBIA, C.; RUBIO, J.A.; BUONO, S.; CARMINATI, F.; FIE´ TIER, N.; GALVEZ, J.; GELE` S, C.; et al. CERN Report CERN/AT/95-44(ET), 1995.

[4] BOWMAN, D. Nuclear Transmutation of Long-Lived Nuclear Power Radiowastes. Workshop. Obninsk, Russia, 1—5 July 1991, p. 127; C.D. Bowman, in: E.D. Arthur, A. Rodriguez, S.O. Schriber (Eds.). Accelerator-Driven Transmutation Technologies and Applications. Conference. Las Vegas, NV 25—19 July 1994, AIP Conf. Proc. 346, 1994. p. 22.

[5] TAKIZUKA, T.; TAKADA, H.; KANNO, I. in: Proc. Workshop on Nuclear Transmutation of Long-Lived Nuclear Power Radiowastes, Obninsk, Russia, 1—5 July 1991, p. 79; T. Takizuka, T. Nishida, T. Sasa, H. Takada, S. Meigo, M. Mizumoto, K. Hasegawa, in: Proc. Int. Conf. on Evaluation of Emerging Nucl. Fuel Cycle Systems, GLOBAL ’95, Versailles, France, 11—14 September 1995, p. 489.

[6] KAZARITSKY, V. D. Accelerator-Driven Transmutation Technologies and Applications. International Conference. Kalmar, Sweden, 3—7 June 1996, Uppsala University Press, 1997, vol. 1, p. 77.

[7] TITARENKO, Yu. E.; SHVEDOV, O. V.; IGUMNOV, M. M.; MASHNIK, S. G.; KARPIKHIN, E. I.; KAZARITSKY, V. D.; BATYAEV, V. F.; KOLDOBSKY, A. B.; ZHIVUN, V. M. Experimental and computer simulation study of the radionuclides produced in thin ^{209}Bi targets by 130 MeV and 1.5 GeV proton induced reactions. Nuclear Instruments and Methods in Physics Research A 414 (1998) 73-99. 13 November 1997. P. 27.

[8] MOSS, W. and ECKHARDT, R. The Human Plutonium Injection Experiments. Los Alamos Science. Number 23. 1995.

[9] BÁTĚK, D. Nuclear reactor fuels and the fuel cycle. Brno: Vysoké Učení Technické v Brně; 2010.

[10] CABIN, E. Accelerator-controlled subcritical reactor. [Electronic source] - Available from: http://nuclphys.sinp.msu.ru/ne/ne7.htm (in Russian).

[11] VAN ATTA, C.M., A brief History of the MTA Project, ERDA Information, Meeting on Accelerator Breeding, January 19–29 (1977).

[12] A Roadmap for developing Accelerator Transmutation of Waster (ATW) Technology, Report to Congress, DOE-RW-0519, October 1999.

[13] MYRRHA Accelerator. [Electronic resource]. Available from: https://myrrha.be/myrrha-project/myrrha-accelerator/

[14] FOKA, A. Accelerator-Driven Systems: Source Efficiency and Reactivity Determination, Licentiate Thesis Stockholm, Sweden 2010. ISBN 978-91-7415-577-8.

[15] PICOT, Wolfgang; VARGAS, Adriana; CHARISOPOULOS, Sotirios. What Are Particle Accelerators? IAEA. September 2023. Available from: https://www.iaea.org/newscenter/news/what-are-particle-accelerators

[16] RUBENS, J. M. Accelerator Driven System (ADS): an Innovative Reactor to be used as Dedicated Waste Burner and a Multipurpose Neutron Source. 005 International Nuclear Atlantic Conference - INAC 2005 Santos, SP, Brazil, August 28 to September 2, 2005. ISBN: 85-99141-01-5.

[17] YAN, X.; YANG, Lei; ZHANG, X.; ZHAN, W. Concept of an accelerator-driven advanced. Nuclear Energy system. Energies 2017, 10(7), 944. Available from: https://doi.org/10.3390/en10070944

[18] IAEA-TECDOC-1766. Status of accelerator driven systems research and technology development. — Vienna: International Atomic Energy Agency, June 2015, ISSN 1011–4289.

[19] SHVETSOV, V. Transmutation of spent nuclear fuel and radioactive waste is one of the options for the strategic development of the nuclear industry. N6 (2003) [Electronic source] - Available from: http://nuclphys.sinp.msu.ru/ecology/trans.htm (in Ukrainian)

[20] DURST, P. C; THERIOS, I.; BEAN, R.; DOUGAN, A; BOYER, B.; WALLACE, R. L.; EHINGER, M. H.; KOVACIC, D. N.; TOLK, K. Advanced Safeguards Approaches for New Fast Reactors. Technical Report: Advanced Safeguards Approaches for New Fast Reactors. 2007. https://doi.org/10.2172/949148.

[21] HOLZMAN, Simon. Accelerators for Society. [Electronic source] - Available from: http://www.accelerators-for-society.org/prospects/index.php?id=10

[22] INTERNATIONAL ATOMIC ENERGY AGENCY, Status of Accelerator Driven Systems Research and Technology Development, IAEA-TECDOC-1766, IAEA, Vienna, 2015.

[23] INTERNATIONAL ATOMIC ENERGY AGENCY, Status of Accelerator Driven Systems Research and Technology Development, IAEA-TECDOC-1766, IAEA, Vienna, 2015.

[24] NEMA, P. K. Application of Accelerators for Nuclear Systems: Accelerator Driven System (ADS). MD&PD Division, BARC, Trombay, Mumbai 400 085, INDIA.

[25] WORLD NUCLEAR ASSOCIATION [Electronic source]. - Available from: https://www.world-nuclear.org/information-library/current-and-future-generation/accelerator-driven-nuclear-energy.aspx

[26] DEGWEKER, S.B.; BHAGWAT, P.V.; KRISHNAGOPAL, S.; SINHA, Amar. Physics and technology for development of accelerator driven systems in India. Bhabha Atomic Research Centre, Trombay, Mumbai 400085 India. Progress in Nuclear Energy 101 (2017) 53-81.

[27] CHALMERS, M. High-power linac shows promise for accelerator-driven reactors. April 2021 [Electronic source] - Available from: https://cerncourier.com/a/high-power-linac-shows-promise-for-accelerator-driven-reactors/

[28] THE OECD NUCLEAR ENERGY AGENCY. Independent evaluation of the MYRRHA project. Report by an international team of experts. 2009. ISBN 978-92-64-99114-9.

[29] GAROBY, R.; VERGARA, A.; and others. The European Spallation Source Design, Physical Scripta, 2018, 93(1), 1-121. Available from: https://doi.org/10.1088/1402-4896/aa9bff

[30] JOINT INSTITUTE FOR NUCLEAR RESEARCH. [Electronic resource] - Available from: https://www.jinr.ru/main-en/

[31] KUKHOTSKYI, O. V.; BILODID, I.I.; SHEPITCHAK, A. V.; NEMTSOVA, S. A. About the issue of a separate permit NSC KIPT. Nuclear and radiation safety 4(84). 12 April 2019. ISSN 2073-6231 (in Ukrainian).

[32] GOHAR, Y.; Bolshinsky, I.; Karnaukhov, I. KIPT ADS Facility. EuCARD - Status of Accelerator Driven Systems Research and Technology Development CERN, February 7-9, 2016, p. 4.

[33] SAITO, S.; OBAYASHI, H. and others. Design of LBE Spallation Target for ADS Target Test facility (TEF-T) In J-PARC. AccApp '17, Quebec, Canada, July 31-August 4, 2017. pp. 448-457. (J-PARC Transmutation Experimental Facility Program. Fujio MAEKAWA and Transmutation Experimental Facility Design Team J-PARC Center, Japan Atomic Energy Agency, Tokai-mura, Ibaraki 319-1195, Japan. Volume 13, 2505045 (2018). DOI: 10.1585/pfr.13.2505045)

[34] WORLD NUCLEAR NEWS. Chinese lead-bismuth test reactor starts up. 16 October 2019. [Electronic source] - Available from: https://www.world-nuclear-news.org/Articles/Chinese-lead-bismuth-test-reactor-starts-up.

[35] NUCLEAR FUTURES AT BANGOR UNIVERSITY. Thermal Hydraulics Open-access Research (THOR) Facility. [Electronic source] - Available from: https://nubu.nu/reactor-design/thor/

[36] OIKAWA, H. Transmutation of Long-Lived Nuclear Wastes. Japan Atomic Energy Agency. June 1-6, 2014. Presentence [Electronic source] - Available from: https://slideplayer.com/slide/5277033/

[37] ERIKSSON, M. Accelerator-driven Systems: Safety and Kinetics, Doctoral thesis, Royal Institute of Technology Stockholm 2005. Accelerator-driven Systems: Safety and Kinetics, p. 20-32.

[38] WORLD NUCLEAR ASSOCIATION WEBSITE. What is nuclear waste, and what do we do with it? Available from: https://world-nuclear.org/nuclear-essentials/what-is-nuclear-waste-and-what-do-we-do-with-it.aspx

[39] KIM, K. K. Lecture 4: Nuclear Reactors and Nuclear Power. PWR Spent Nuclear Fuel. March 14, 2023. P. 60.

[40] Fission Fragments. Source Website. Available from: https://www.nuclear-power.com/nuclear-power/fission/fission-fragments/

[41] BOWMAN, C. D. et al. Nuclear energy generation and waste transmutation using an accelerator-driven intense thermal neutron source. Nuclear Instruments and Methods in Physics Research. A 320 (1992) 336-367.

[42] LOCH, P. Calorimetry in High Energy and High Intensity Particle Physics Applications. Department of Physics University of Arizona Tucson, Arizona, USA.

December 1, 2017. Available from: https://indico.cern.ch/event/697598/contributions/2871229/attachments/1594649/2525097/CalorimetersUniGoettingen.12.01.2017.pdf

[43] MASON, T.E.; ABERNATHY, D.; ANDERSON, I.; ANKNER, J.; EGAMI, T.; EHLERS, G. and other. The Spallation Neutron Source in Oak Ridge: A powerful tool for materials research. USA. 2008.

[44] SYED, N. A. Properties, and sources of radiation in Physics and Engineering of Radiation Detection (Second Edition), p. 49, 2015.

[45] KAREN, C. K. Gadolinium-148 and Other. Spallation Production Cross Section Measurements for Accelerator Target Facilities. January 2004.

[46] CUGNON, J. Cascade models and particle production: A comparison, Particle Production in Highly Excited Matter, NATO Science Series B 303 (1993) 271-293. ISBN 0-306-44413-5.

[47] The strange version of INCL. 2020. [Electronic resource] - Available from: http://irfu.cea.fr/dap/en/Phocea/Vie_des_labos/Ast/ast.php?t=fait_marquant&id_ast=4760

[48] KRÁSA, A. Neutron Emission in Spallation Reactions of 0.7 – 2.0 GeV Protons on Thick, Lead Target Surrounded by Uranium Blanket. Dissertation Thesis. Prague, 2008.

[49] BAUER, G.S. Overview on spallation target design concepts and related materials issues. Forschungszentrum Jülich, D-52425 Jülich, German. Journal of Nuclear Materials 398 (2010) 19–27.

[50] SYED, N. A. Physics and Engineering of Radiation Detection. Elsevier; 2nd edition. December 10, 2014. P.784. SBN-10. 012801363X.

[51] FEGHHI, S. A. H.; GHOLAMZADEH, Z; TENREIRO, C. Investigation of the optimal material type and dimension for spallation targets using simulation methods. Journal of Theoretical and Applied Physics 8(1). December 2013. DOI: 10.1186/2251-7235-8-1.

[52] ANDERSSON, M. and ZANINI, L. Measurement of gas and volatile elements production rates in molten lead bismuth target. Diploma Work in Nuclear Physics. Paul Scherrer Institute, Villigen Switzerland. January 2004.

[53] KRASA, A. Manuscript from the lecture “Neutron Sources for ADS" Řež, May 2010.

[54] INSTITUTE OF RESEARCH INTO THE FUNDAMENTAL LAWS OF THE UNIVERSE. Nuclear Physics Division. [Electronic source] - Available from: http://irfu.cea.fr/dphn/en/Phocea/Vie_des_labos/Ast/ast.php?t=fait_marquant&id_ast=4515

[55] TITARENKO, Yu. E. et al. Experimental and computer simulation study of the radionuclides produced in thin ^{209}Bi targets by 130 MeV and 1.5 GeV proton-induced reactions. Nuclear Instruments and Methods in Physics Research A 414 (1998) 73-99.

[56] MICHEL, R. et al. Cross sections for the production of residual nuclides by low- and medium-energy protons from the target elements C, N, O, Mg, Al, Si, Ca, Ti, V, Mn, Fe, Co, Ni, Cu, Sr, Y, Zr, Nb, Ba and Au, Nuclear Instruments and Methods in Physics Research B 129 (1997) 153-193.

[57] ENQVIST, T. et al. Isotopic yields and kinetic energies of primary residues in

1 A GeV ^{208}Pb+p reactions, Nuclear Physics A 686 (2001) 481-524.

[58] BOYKO, V. I. and SILAEVA, M. E. Methods and devices for measuring nuclear and other radioactive materials. p. 356. (in Ukrainian)

[59] GIGAHERTZ. Calibration of Detectors. [Electronic source] - Available from: https://www.gigahertz-optik.com/en-us/service-and-support/knowledge-base/basics-light-measurement/detector-calib/

[60] CHANDRAMOULEESWARAN, S. and JAYSHREE, R. Mass Spectrometry: A Boon to Nuclear Industry. J Anal Bioanal Techniques S6:005. 2014. DOI: 10.4172/2155-9872.S6-005

[61] BENYON, JH. and MORGAN, RP. The development of mass spectroscopy: An historical account. Int J Mass Spectrom Ion Physics 27. 1978. P. 1-30.

[62] KOCH, L.; COTTONE, G. and GEERLINGS, MW. ^{148}Nd Analyse zur Abbrandbestimmung von Kernbrennstoffen. Radiochimica Acta. December 1, 1968. Available from: https://doi.org/10.1524/ract.1968.10.34.122 (in German)

[63] GUILLAUMONT, R. Éléments chimiques à considérer dans l'aval du cycle nucléaire. Volume 7, Issue 12, December 2004, Pages 1129-1134. Available from: https://doi.org/10.1016/j.crci.2003.09.014 (in French)

[64] LEE, CH; SUH, MY; CHOI, KS; KIM. JS; SONG, BC, et al. Separation of fission products from spent pressurized water reactor fuels by anion exchange and extraction chromatography for inductively coupled plasma atomic emission spectrometric analysis. Analytica Chimica Acta. Volume 428, Issue 1, 1 February 2001, Pages 133-142. Available from: https://doi.org/10.1016/S0003-2670(00)01120-X

[65] WOLF, SF; BOWERS, DL; CUNNANE, JC. Analysis of high burnup spent nuclear fuel by ICP-MS. 2005. J Radioanal Nucl Chem 263: 581-586.

[66] WOLF, SF and TSAI, Y. Application of ICP-MS and HR-ICP-MS for the characterization of solutions generated from corrosion testing of spent nuclear fuel. Volume 263, pages 575–579, (2005). DOI: https://doi.org/10.1007/s10967-005-0626-8

[67] BECKER, JS; KERL, W., and DIETZE, H. Nuclide analysis of an irradiated tantalum target of a spallation neutron source using high performance ion chromatography and inductively coupled plasma mass spectrometry. Volume 387, Issue 2, 22 April 1999, pages 145-154. Available from: https://doi.org/10.1016/S0003-2670(99)00093-8.

[68] GLAGOLENKO, I., HILTON, B., GIGLIO, J. et al. Fission yield measurements by inductively coupled plasma mass-spectrometry. J Radioanal Nucl Chem 282, 651–655 (2009). Available from: https://doi.org/10.1007/s10967-009-0209-1.

[69] MORENO, JMB; BETTI, M; NICOLAOU, G. Determination of cesium and its isotopic composition in nuclear samples using isotope dilution-ion chromatography-inductively coupled plasma mass spectrometry. Journal of Analytical Atomic Spectrometry. Issue 5,1999. Available from: https://doi.org/10.1039/A806467I

[70] ALONSO, JIG; SENA, F.; ARBORE, P.; BETTI, M.; KOCH, L. Determination of fission products and actinides in spent nuclear fuels by isotope dilution ion chromatography inductively coupled plasma mass spectrometry. Journal of Analytical Atomic Spectrometry. 1995, 10, p. 381-393. Available from:

https://doi.org/10.1039/JA9951000381

[71] BETTI, M. Use of ion chromatography for the determination of fission products and actinides in nuclear applications. 1997. Available from: https://doi.org/10.1016/S0021-9673(97)00784-X.

[72] GUTKO, V.I. Activation analysis. Sakharov Moscow State Geological University, 2008. P.74. ISBN 978-985-6823-57-5. (In Russian)

[73] TALIP, Z.; DRESSLER, R.; SCHACHERL, B.; JEAN-CHRISTOPHE, D.; VOCKENHUBER, C. and SCHUMANN, D. Radiochemical Determination of Long-Lived Radionuclides in Proton-Irradiated Heavy Metal Targets: Part II Tungsten. Analytical Chemistry 2021 93 (31), 10798-10806.

[74] TÖLGYESSY, J. and HARANGOZÓ, M. Radiochemical methods. Food and Environmental Applications. Encyclopedia of Analytical Science (Second Edition), 2005.

[75] INTERNATIONAL ATOMIC ENERGY AGENCY. Neutron capture gamma-ray spectroscopy. Vienna, 1969.

[76] Germanium Detectors User's Manual. Copyright 2003, CANBERRA Industries.

[77] Development of a PET Cyclotron Based Irradiation setup for Proton Radiobiology. September 2014. Thesis for: PhD in Physics Engineering. Sharif Ghithan.

[78] HURTADO, S.; GARCI´-LEON, M.; GARCIA-TENORIO, R. A revision of energy and resolution calibration method of Ge detectors. March 2006. Nuclear Instruments and Methods in Physics Research A 564 (2006) 295–299.

[79] WHITE PAPER. Why High-Purity Germanium (HPGe) Radiation Detection Technology is Superior to Other Detector Technologies for Isotope Identification.

[80] NUCLEAR POWER. Advantages and Disadvantages of HPGe Detectors. [Electronic source] - Available from: https://www.nuclear-power.com/nuclear-engineering/radiation-detection/semiconductor-detectors/high-purity-germanium-detectors-hpge/advantages-and-disadvantages-of-hpge-detectors/

[81] LAURA VAN DER SCHAA. Calibration of a Germanium Detector. Bachelor thesis. August 23, 2012.

[82] Germanium Detectors User's Manual. Copyright 2003, CANBERRA Industries.

[83] KAREN, C. K. Gadolinium - 148 et al. Spallation Production Cross Section Measurements for Accelerator Target Facilities. Nuclear and Radiological Engineering Georgia Institute of Technology. January 2004.

[84] SÚRO. Energy calibration. Appendix V. Detection system settings. Energy calibration. P.15. (Příloha V. Nastavení detekčních systému. Energetická kalibrace.) Available from: https://www.suro.cz/files/2021-03/Priloha%20V_Nastaveni%20detekcnich%20systemu.pdf (in Czech)

[85] FRÁNA, J.: Program DEIMOS32 for gamma-ray spectra evaluation. Journal of Radioanalytical and Nuclear Chemistry, ročník 257, č. 3, 2003: s. 583–587, ISSN 1588-2780, doi:10.1023/A:1025448800782.

[86] TITARENKO, Y. E.; BATYAEV, V. F.; KARPIKHIN, E. I.; MULAMBETOV, R. D.; KOLDOBSKY, A. B. et al. Final Project Technical Report of ISTC 83B-99,

International Nuclear Data Committee of the International Atomic Energy Agency Report INDC(CCP)-434, Vienna, February 2003.

[87] Oncology Medical Physics. Detection Efficiency and Dead Time. Online source. Available from: https://oncologymedicalphysics.com/detection-efficiency-and-dead-time/

[88] SÚRO. Appendix V. Detection system settings. Energy calibration. P.16. (in Czech)

[89] MOLNAR, G.L.; REVAY, Zs. and BELGYA, T. Wide energy range efficiency calibration method for Ge detectors. Institute of Isotope and Surface Chemistry, Chemical Research Centre, H-1525 Budapest, Hungary. Received 19 October 2001; received in revised form 12 March 2002; accepted 17 March 2002.

[90] HARB, S; SALAHEL DIN, K. and ABBADY, A. Study of Efficiency Calibrations of HPGe Detectors for Radioactivity Measurements of Environmental Samples. Physics department, Faculty of Science, South Valley University, 83523 Qena, Egypt. Proceedings of the 3rd Environmental Physics Conference, 19-23 Feb. 2008, Aswan, Egypt.

[91] AMETEK ADVANCE MEASUREMENT TECHNOLOGY. Website. Overview of Semiconductor Photon Detectors. ORTEC. Available from: https://www.ortec-online.com/-/media/ametekortec/other/overview-of-semiconductor-photon-detectors

[92] MOHSEN, B. Challan. Gamma-ray efficiency of a HPGe detector as a function of energy and geometry.

[93] PcRadonTMR gamma probe probing instructions, manual, 2015. (Návod na přibondování/ odbondování gama sond programem PcRadonTMR, manuál, 2015.) (in Czech)

[94] CANBERRA Industries, Inc.: Genie 2000™ Customization Tools Manual, Version 3.3, 2013.

[95] BECKMAN, I.N. Nuclear physics [Electronic source] - Available from: http://profbeckman.narod.ru/RR0.files/L2_4.pdf (in Russian).

[96] FEGHHI, S. A. H.; GHOLAMZADEH, Z.; TENREIRO, C. Investigation of the optimal material type and dimension for spallation targets using simulation methods. Journal of Theoretical and Applied Physics 8(1). December 2013. DOI: 10.1186/2251-7235-8-1

[97] TITARENKO, Yu. E.; BATYAEV, V. F.; TITARENKO, A. Yu.; BUTKO, M. A.; PAVLOV, K. V. at al. Cross-sections for nuclide production in ^{56}Fe target irradiated by 300, 500,750, 1000, 1500, and 2600 MeV protons compared with data on hydrogen target irradiation by 300, 500, 750, 1000, and 1500 MeV/nucleon ^{56}Fe ions.

[98] ZEMAN, M.; ADAM, J.; BALDIN, A. A.; CHILAP, V.V.; FURMAN, W.I.; KATOVSKY, K.; KISH, YU.; KHUSHVATKOV, J.; SOLNYSHKIN, A. A. at al. Reaction rates of residual nuclei produced of ^{59}Co at the target QUINTA. XXII International Baldin Seminar of High Energy Physics Problem, 16 September 2014.

[99] VESPALEC, R. YASNAPP-2 program package for data analysis 1.4 (YAPP.1.4) user's manual. October 10, 2016. P.14.

[100] KARAPETYAN, G. S. Fission and spallation data evaluation using induced-activity method. Online. The European Physical Journal Plus. 2015, roč. 130, č. 9. p.180. ISSN 2190-5444. Available from: https://doi.org/10.1140/epjp/i2015-15180-7.

[101] BALABEKYAN, A.; KARAPETYAN, G.; DEMEKHINA, N.; at al. Symmetric and asymmetric fission modes in proton-induced fission at 660 MeV of ^{238}U. Phys. At. Nucl. 2010. 73(11). pp. 1814-1819. ISSN 1562-692X. Available from: https://doi.org/10.1134/S1063778810110025

[102] TITARENKO, Yu. E.; BATYAEV, E.I.; KARPIKHIN, R.D.; MULAMBETOV, A.B.; KOLDOBSKY, V.M.; at al. Experimental and Theoretical Study of the Yields of Residual Product Nuclei Produced in Thin Targets Irradiated by 100-2600 MeV Protons. Institute for Theoretical and Experimental Physics (ITEP). February 2003.

[103] MIYAHARAA, S.; ODAIRAA, N.; ARITAA, Y.; MAEKAWAB, F.; MATSUDAB, H.; SASAB, T.; MEIGOB, S. The analytical study of inventories and physicochemical configuration of spallation products produced in Lead-Bismuth Eutectic of Accelerator Driven System. Research Institute of Nuclear Engineering, University of Fukui, 1-3-33 Kanawa-cho, Tsuruga, Fukui-Pref. 914-0055, Japan b J-PARC Center, Japan Atomic Energy Agency, 2-4 Shirakata, Tokai, Ibaraki-Pref. 319-1195, Japan.

[104] ADAM, I.; PRONSKIKH, V.S.; BALABEKYAN, A.R.; KALINNIKOV, V.G.; MRAZEK, J.; PRIEMYSHEV, A.N.; FRANA, J. Program System and Additions to the Method of Activation Analysis for Determination of Nuclear Reaction Cross Sections. (in Russian)

[105] PLOMPEN, A. Cross section measurements and uncertainties of cross section data. Volume 26. 2008. ISBN 978-92-64-99053-1.

[106] ZEMAN, M. Experimental investigation of the neutron field in an accelerator driven subcritical reactor. Doctoral thesis. Brno, 2022. P. 72-73.

[107] DEBERTIN, K.; HELMER, R. G.: Gamma- and X-ray spectrometry with semiconductor detectors. Nizozemsko: Severní Holandsko, 1988, ISBN 978-0444871077.

[108] DEBERTIN, K. and HELMER, R.G. Gamma- and X-ray spectrometry with semiconductor detectors, Elsevier, Amsterdam, (1988).

[109] ZEMAN, M. Experimental investigation of the neutron field in an accelerator driven subcritical reactor. Doctoral thesis. Brno, 2022. P. 68-71.

[110] BHATIA, Ch. A Study of the Role of (n,xn) Reactions in Accelerator Driven Sub-Critical System. PhD thesis, University of Rajasthan, 2010.

[111] VESPALEC, R. YASNAPP-2 program package for data analysis 1.4 (YAPP.1.4) user's manual. October 10, 2016. P.11.

[112] ZÁVORKA, L. Transmutation of Actinides Using Spallation Reactions. Minor Thesis. Dubna – Praha, 2013. P. 19.

[113] FRÁNA, J. Program DEIMOS32 for gamma-ray spectra evaluation. Journal of Radioanalytical and Nuclear Chemistry, 257, 2003: p. 583–587, ISSN 1588-2780, doi:10.1023/A:1025448800782.

[114] ADAM, J. B.; ADAM J. J.; HONUSEK, M.; KALINNIKOV, V.G. and PRONSKICH, V. S. Analysis of complex spectra of gamma radiation. In Proceeding of the International Conference on Nuclear Physics, page 318, 1998.

[115] FEGHHI, S. A. H.; GHOLAMZADEH, Z.; TENREIRO, C. and ALIPOOR, Z. Comparison of different INC physical models of MCNPX to compute spallation

neutronics of LBE target. Journal of Physics Conference Series. April 2015. doi:10.1088/1742-6596/590/1/012043.

[116] ADAM, I.; PRONSKICH, V. at al. Program Package and Supplements to Activation Analysis for Calculations of Nuclear Reaction Cross-Section. Dubna, Measuring technique, 2000 (in Russian).

[117] AD4HEL - Activation detectors for high energy lasers: využití kvasi-offline metod pro detekci laserem generovaných neutronů, 2019-2021.

[118] WERNER, C.J. (editor), "MCNP User's Manual - Code Version 6.2", LA-UR-17-29981, 2017.

[119] KWIATKOWSKI, R**.** Monte Carlo Simulation — a practical guide. Jan 31, 2022. Available from: https://towardsdatascience.com/monte-carlo-simulation-a-practical-guide-85da45597f0e

[120] FAGHIH, S. A. H.; GHOLAMZADEH, Z. and TENREIRO, C. A MCNP simulation study of neutronic calculations of spallation targets. DOI: 10.2298/NTRP1302128F

[121] PELOWITZ, B.; GOORLEY, J. T.; JAMES, M. R.; BOOTH, T. E.; BROWN, F. B.; BULL, J. S.; COX, L. J.; DURKEE J. W. at al. MCNP6 User's Manual. Los Alamos National Laboratory Tech. Rep. LA-CP-13-00634. Los Alamos, NM, USA. May 2013. This document is provided in the MCNP6 release package available from RSICC and is not accessible from the MCNP website. Code Version 6.1.

[122] JAMES, M. R.; PELOWITZ, D. B.; FALLGREN, A. J.; MCMATH, G. E.; BOOTH, T. E.; BROWN, F. B.; BULL, J. S.; COX, L. J.; ELSON, J. S. at al. MCNP6™ User's Manual Code Version 6.1.1 Beta. Los Alamos National Laboratory Tech. Rep. LA-CP-14-00745. Los Alamos, NM, USA. June 2014.

[123] LOS ALAMOS NATIONAL LABORATORY. The MCNP code. August 29, 2023**.** Internet source. Available from: https://mcnp.lanl.gov/index.html

[124] FEGHHI, S. A. H.; GHOLAMZADEH, Z.; TENREIRO, C. and ALIPOOR, Z. Comparison of different INC physical models of MCNPX to compute spallation neutronics of LBE target. Journal of Physics Conference Series, April 2015. doi:10.1088/1742-6596/590/1/012043.

[125] FLUKA main page. FLUKA Team 2000–2024. [Electronic source] - Available from: www.fluka.org

[126] FASSÒ, A.; FERRARI, A. and SALA, P.R.: "Designing Electron Accelerator Shielding with FLUKA," Proc. ICRS8, Arlington, Texas, Apr. 24–28 (1994), p. 643–649.

[127] BATTISTONI, G.; BÖHLEN, TT.; CERUTTI, F.; CHIN, PW.; ESPOSITO, LS.; FASSÒ, A. et al. Overview of the FLUKA code. Ann Nucl Energy (2015) **82**:10. doi: 10.1016/j.anucene.2014.11.007

[128] FERRARI, A.; SALA, PR.; FASSÒ, A.; RANFT, J. FLUKA: A Multi-Particle Transport Code. Technical report CERN-2005-10, INFN/TC_05/11, SLAC-R-773, CERN, INFN, SLAC. Geneva: CERN (2005).

[129] FLUKA Code: Total Cross Section Calculation. Physics forums. Nov 3, 2015. Available from: https://www.physicsforums.com/threads/fluka-code-total-cross-section-calculation.841073/

[130] FLUKA Scoring. FLUKA Advanced Course. Presentation. Available from: https://agenda.infn.it/event/20624/contributions/105895/attachments/68619/85014/AdvancedScoring2019.pdf

[131] FLUKA Advanced Interface. [Electronic source] - Available from: https://www.fluka.org/flair/

[132] FERRARI, A.; SALA, P. R.; FASS`O, A.; RANFT, Johannes. FLUKA manual. CERN–2005–00X. FLUKA: a multi-particle transport code. INFN TC 05/11. SLAC–R–773 31. August 2005.

[133] FLUKA website. Estimators and Scorings. [Electronic source] - Available from: https://indico.cern.ch/event/753612/contributions/3121542/attachments/1974589/3285974/Scoring_2019.pdf

[134] JAPAN ATOMIC ENERGY AGENCY. PHITS Ver. 3.25 user's guide. P. 339.

[135] Estimators and Scorings. 21st FLUKA Beginner's Course ALBA – Barcelona, Spain 08 – 12 April 2019. Available from: https://www.sciencedirect.com/science/article/pii/S0306454914004083

[136] QUANZHI, Yu. Energy deposition calculated by PHITS code in Pb spallation target. Volume 367, 15 January 2016, Pages 8-13. Available from: https://doi.org/10.1016/j.nimb.2015.11.014

[137] Live Chart of Nuclides. [Electronic source] - Available from: https://www-nds.iaea.org/relnsd/vcharthtml/VChartHTML.html

[138] SUN, Xiang-yang; LAN, Haoyang; HAN, Liang-hu; LIU, Lie. Improvement of LLFPs transmutation efficiency by moderator loading in lead-based fast neutron reactor. Annals of Nuclear Energy. 196 (2024) 110227.

[139] KOOYMAN, T. Current state of partitioning and transmutation studies for advanced nuclear fuel cycles. Annals of Nuclear Energy. 157 (2021) 108239.

[140] ALEXANDROV, Yu. V.; EISMONT, V.P.; IVANOV, R.B.; MIKHAILOVA, M.A.; PRIKHODTSEVA, V.P.; SAULSKY, A.V.; VASILJEV, S.K.; KHLOPIN, V.G. Radiation institute St. Petersburg. New data to produce radionuclides in thin lead target by 660 MeV protons.

[141] LAPTEV, A. Fission Cross Section Measurements at Intermediate Energies. Japan Nuclear Cycle Development Institute. JAERI-Conf 2005-003.

[142] EVENSEN, A.H.M.; CATHERALL, R.; DRUMM, P.; VAN DUPPEN, P.; JONSSON, O.C.; KUGLER, E.; LETTRY, J.; TENGBLAD, 0.; TIKHONOV, V.; RAVN, H.L. ISOLDE Collaboration, "Release and yields from thorium and uranium targets irradiated with a pulsed proton beam," Nuclear Instruments and Methods in Physics Research B 126, 65, 1997.

[143] SERER, B.; KORKMAZ, M. E.; GUNEY, M.; AYDIN, A. Monte Carlo studies in accelerator-driven systems for transmutation of high-level nuclear waste. March 2008.

[144] WANL, l-S.; LANGROCK, E.; WESTMEIER, W.; VATER, P.; BRANDT, R.; ADAM, J.; BALABEKIAN, A.; BAMBLEVSKI, V.P. at al. First radiochemical studies on the transmutation of ^{239}Pu with spallation neutrons.

[145] KATOVSKY, K.; ADAM, J.; BALABEKYAN, A.; PRONSKIKH, V.S.; Solnyshkin, A.A.; STEGAILOV, V.I. and TSOUPKO-SITNIKOV, V.M. Experimental

determination of residual nuclei formation cross sections in 660 MeV proton reactions with ^{239}Pu and ^{nat}U.

[146] ADAM, J.; ADLOFF, J. C.; BALABEKYAN, A.; BAMBLEVSKI, V. P.; BARABANOV, M. Y.; BRANDT, R.; BRADNOVA, V.; CHALOUN, P. at al. Transmutation of ^{239}Pu and other nuclides using spallation neutrons produced by relativistic protons reacting with massive U- and Pb-targets. Received February 5, 2001.

[147] TITARENKO, Yu. E.; BATYAEV, V.F.; KARPIKHIN, E.I.; MULAMBETOV, R.D.; KOLDOBSKY, A.B.; ZHIVUN, V.M.; MULAMBETOVA, S.V.; LIPATOV, K.A. at al. Experimental and Theoretical Study of the Yields of Residual Product Nuclei Produced in Thin Targets Irradiated by 100-2600 MeV Protons. February 2003. IAEA Nuclear data section, Wagramer Strasse 5, A-1400 Vienna.

[148] TITARENKO, Yu. E.; BATYAEV, V.F.; KARPIKHIN, E.I.; MULAMBETOV, R.D.; KOLDOBSKY, A.B.; ZHIVUN, V.M.; MULAMBETOVA, S.V.; LIPATOV, K.A. at al. Final Project Technical Report of ISTC 83B-99, International Nuclear Data Committee of the International Atomic Energy Agency Report INDC(CCP)-434, Vienna, February 2003.

[149] TITARENKO, Yu. E.; BATYAEV, V.F.; TITARENKO, A. Yu.; BUTKO, M. A.; PAVLOV, K. V.; FLORYA, S. N.; TIKHONOV, R. S. at al. Cross-sections for nuclide production in ^{56}Fe target irradiated by 300, 500,750, 1000, 1500, and 2600 MeV protons compared with data on hydrogen target irradiation by 300, 500, 750, 1000, and 1500 MeV/nucleon ^{56}Fe ions.

[150] ENGLE, J.W.; MASHNIK, S. G.; WEIDNER, J. W.; WOLFSBERG, L. E.; FASSBENDER, M. E.; JACKMAN, K.; COUTURE, A.; BITTEKER, L. J. at al. Cross sections from proton irradiation of thorium at 800 MeV. Los Alamos National Laboratory, Los Alamos P.O. Box 1663, 87545, June 2013. DOI: 10.1103/PhysRevC.88.014604

[151] ZHADAN, A.A.; SOTNIKOV, V.V.; VORONKO, V.A.; BALDIN, A.A.; TYUTYUNNIKOV, S.I.; BUKHAL, O.V. at al. Experimental studies of the nuclear-physical characteristics of the extended uranium target irradiated by relativistic protons, deuterons and ^{12}C nuclei. ВАНТ, №3 pp.127, 2020.

[152] HOLOMB, R.R.; TARI, S.A.; KATOVSKY, K.; HAYSAK, I.; ADAM, J. Cross sections of nuclear isomers from the interaction of protons with the thin thorium target. EPJ Web of Conferences p. 204, 2019.

[153] ADAM, J.; ADLOFF, J. C.; BALABEKYAN, A.; BAMBLEVSKI, V. P.; BARABANOV, M. Y.; BRANDT, R.; BRADNOVA, V. Transmutation of ^{239}Pu and other nuclides using spallation neutrons produced by relativistic protons reacting with massive U- and Pb-targets. Article in Radiochemical Acta, München, August 2002.

[154] ZAVORKA, L.; ADAM, J.; FURMAN, WALTER, I.; KATOVSKÝ, K.; KHUSHVAKTOV, J.; SOLNYSHKIN, A. A.; STOYANOVA, M.; SUCHOPÁRE, M. at al. Transmutation efficiency of the spallation neutron target measured with the actinide sandwiches. Vol. 988, February 2021.

[155] BALABELYAN, A. R. et al. Investigation of fission reactions with ^{120}Sn and reactions (d,xn), (d,pxn), (p,xn), and (p,pxn) with enriched tin isotopes. Sov. Nucl. Phys. 2005. V. 68, No. 2. P.192-200. (these proceedings).

[156] HENZL, V. et al. International Conference on Nuclear Data for Science and Technology. Proceedings of the ND'2001 Conference, Suppl. 2, JAERI (2002). p. 1248.

[157] ADAM, J. et al. International Conference on Nuclear Data for Science and Technology. Proceedings of the ND'2001 Conference, Suppl. 2, JAERI (2002), p. 272.

[158] KATOVSKY, K. ADAM, J., and et al. Experimental determination of residual nuclei formation cross sections in 660 MeV proton reactions with ^{239}Pu and ^{nat}U. 2007. DOI: 10.1051/ndata:07627.

[159] KATOVSKY, K. Studium sekundárních neutronů a jader vznikajících při reakcích protonů a neutronů v terčích z uranu a plutonia. Disertační práce. České vysoké učení technické v Praze. 2001-2008.

[160] IAEA database. August 2017. [Electronic resource] - Available from: https://www-nds.iaea.org/medical/alp24na0.html

[161] KARAPETYAN, G. Fission and spallation data evaluation using induced-activity method. European Physical Journal Plus, September 2015 130, p. 180. DOI: 10.1140/epjp/i2015-15180-7.

[162] TITARENKO, Y. E. Experimental and Theoretical Study of the Yields of Residual Product Nuclei Produced in Thin Targets Irradiated by 100-2600 MeV Protons. Institute for Theoretical and Experimental Physics (ITEP). February 2003. P. 46.

[163] SZELECSÉNYIA, F.; STEYN, G. F.; NORTIER, F. M. and Kovács, Z. New cross sections for the ^{27}Al(p,x)^{7}Be nuclear process: Monitoring proton beam energy via the ^{22}Na/^{7}Be cross-section ratio between 45 and 200 MeV. EPJ Web of Conferences 146, 08011 (2017).

[164] KATOVSKY, K.; ADAM, J.; BALABEKYAN, A.; PRONSKIKH, V.S.; SOLNYSHKIN, A.A.; STEGAILOV, V.I. and TSOUPKO-SITNIKOV, V.M. Experimental determination of residual nuclei formation cross sections in 660 MeV proton reactions with ^{239}Pu and ^{nat}U. Available from: https://www.researchgate.net/publication/43965187_Experimental_determination_of_residual_nuclei_formation_cross_sections_in_660_MeV_proton_reactions_with_239Pu_and_natU

[165] CHIRKOV, A. Fazotron. Dubna: JINR. 16 July 2007. [Electronic resource] - Available from: http://phasotron.jinr.ru/ (in Russian).

[166] RICHARD, B.; FIRESTONE, Virginia S.; SHIRLEY, S.Y. Editor FRANK CHU, CD-ROM. Editor Coral M. Baglin and Jean Zipkin Assistant Editors. Table of Isotopes. CD ROM Edition. Version 1.0. March 1996.

[167] KOTOV, A.A.; VAISHNENE, L.A.; Vovchenko, V.G.; GAVRIKOV, Yu.A.; POLIAKOV, V.V.; TVERSKOY, M.G.; FEDOROV, O.Y. at al. Energy dependence of proton induced fission cross sections for heavy nuclei in the energy range 200-1000 MeV. Available from: https://journals.aps.org/prc/abstract/10.1103/PhysRevC.74.034605

[168] TORNOW, W. Energy Dependence of Fission – Product Yields from ^{235}U, ^{238}U and ^{239}Pu for Incident Energies between 0.5 and 15 MeV. Duke University & TUNL.

[169] BATTISTONI, G.; BOEHLEN, T.; CERUTTI, F.; CHIN, P. W.; ESPOSITO, L. S.; FASSÒ, A.; FERRARI, A.; at al. Overview of the FLUKA code. Annals of Nuclear Energy Volume 82, August 2015, Pages 10-18. Available from: https://www.sciencedirect.com/science/article/pii/S0306454914005878

[170] MICHEL, R. Benchmark of Spallation Models 2009: Production of Residual Nuclides. Available from: https://www-nds.iaea.org/spallations/2010ws/michel-report.pdf

[171] FAZIO, F.; GROSCHEL, W.; WAGNER, K.; THOMSEN, B.L.; SMITH, R.; STIEGLITZ, L.; ZANINI, A.; GUERTIN, A.; CADIOU, J.; HENRY, P. at al. The MEGAPIE-TEST project: Supporting research and lessons learned in first-of-a-kind spallation target technology. 2007.

[172] SHAMS, A.M.; ISSA, M.A.M.; UOSIF, R.; MICHELA, J.-L.; FLAMENT, J.-C.; DAVI, S. Leray. Cross Sections for the Production of Residual Nuclides by Proton-Induced Reactions with Uranium at Medium Energies. IX Radiation Physics & Protection Conference, 15-19 November 2008, Nasr City - Cairo, Egypt.

Appendix I

Efficiency values of CANBERRA detector

Position 2

Polynomial degree: 7(8 parameters)
Number of exp. points: 30

Energy [keV]	EffExp [-]	UncEffExp [-]	EffCalc [-]	Difference [-]
121.782	0.0006610905	0.0000117662	0.0006610550	-0.0000000355
238.632	0.0015426023	0.0000214772	0.0015607652	0.0000181629
240.986	0.0015271940	0.0000269850	0.0015498584	0.0000226644
241.997	0.0016844726	0.0000519564	0.0015455485	-0.0001389241
277.371	0.0015498758	0.0000759099	0.0014901990	-0.0000596768
295.224	0.0014712342	0.0000445551	0.0014984504	0.0000272162
300.087	0.0015642852	0.0000275704	0.0015018980	-0.0000623872
351.932	0.0012502064	0.0000378628	0.0015185478	0.0002683414
510.770	0.0012977078	0.0000199289	0.0011637079	-0.0001339999
583.187	0.0009339016	0.0000106352	0.0009885498	0.0000546482
609.312	0.0009024938	0.0000273337	0.0009381127	0.0000356189
665.453	0.0008675086	0.0000431861	0.0008514662	-0.0000160424
727.330	0.0007909025	0.0000151172	0.0007839028	-0.0000069997
768.356	0.0007674439	0.0000277215	0.0007507658	-0.0000166781
785.370	0.0007323993	0.0000170635	0.0007390146	0.0000066153
785.960	0.0007572707	0.0000650989	0.0007386246	-0.0000186461
806.174	0.0008358952	0.0000359021	0.0007258909	-0.0001100043
860.557	0.0007095465	0.0000128209	0.0006962767	-0.0000132698
934.061	0.0006663485	0.0000270695	0.0006618188	-0.0000045297
1120.287	0.0005630113	0.0000178257	0.0005750258	0.0000120145
1155.190	0.0005348078	0.0000222552	0.0005584255	0.0000236177
1173.228	0.0005447099	0.0000069776	0.0005500177	0.0000053078
1238.110	0.0005314842	0.0000197589	0.0005217363	-0.0000097479

1280.960	0.0004857041	0.0000216975	0.0005057497	0.0000200456
1332.492	0.0004918330	0.0000062985	0.0004908114	-0.0000010216
1377.669	0.0004755798	0.0000185942	0.0004828200	0.0000072402
1401.500	0.0004732804	0.0000223847	0.0004809807	0.0000077003
1407.980	0.0005177297	0.0000232896	0.0004808027	-0.0000369270
1408.006	0.0004913766	0.0000084839	0.0004808023	-0.0000105743
1509.228	0.0004439940	0.0000224442	0.0005006446	0.0000566506

Chi squared: 163.64734
Reduced Chi squared: 7.43852

Position 3

Polynomial degree: 7(8 parameters)
Number of exp. points: 37

Energy [keV]	EffExp [-]	UncEffExp [-]	EffCalc [-]	Difference [-]
240.986	0.0024647212	0.0000435429	0.0024757546	0.0000110334
241.997	0.0024607612	0.0000758982	0.0024700036	0.0000092424
276.399	0.0023215465	0.0000344692	0.0022693003	-0.0000522462
295.224	0.0021492345	0.0000650872	0.0021675891	0.0000183546
300.087	0.0021745654	0.0000383266	0.0021428755	-0.0000316899
302.851	0.0020639110	0.0000270627	0.0021291235	0.0000652125
344.279	0.0020054330	0.0000259449	0.0019471700	-0.0000582630
356.013	0.0018715933	0.0000201542	0.0019029231	0.0000313298
383.849	0.0018116717	0.0000306403	0.0018081149	-0.0000035568
510.770	0.0015209240	0.0000233483	0.0014883137	-0.0000326103
583.187	0.0013364086	0.0000152177	0.0013527606	0.0000163520
609.312	0.0013186347	0.0000399368	0.0013093736	-0.0000092611
665.453	0.0012665675	0.0000630519	0.0012244770	-0.0000420905
727.330	0.0011321155	0.0000216343	0.0011424849	0.0000103694
768.356	0.0011213291	0.0000404983	0.0010939586	-0.0000273705
785.370	0.0010473598	0.0000244015	0.0010750653	0.0000277055
860.557	0.0010157289	0.0000183444	0.0009992719	-0.0000164570

934.061	0.0009728997	0.0000395227	0.0009356416	-0.0000372581
1120.287	0.0008228893	0.0000260510	0.0008084243	-0.0000144650
1155.190	0.0007817044	0.0000325142	0.0007886382	0.0000069338
1173.228	0.0007724911	0.0000090118	0.0007788053	0.0000063142
1173.228	0.0007789293	0.0000099779	0.0007788053	-0.0000001240
1238.110	0.0007768948	0.0000288751	0.0007454113	-0.0000314835
1280.960	0.0007091254	0.0000316782	0.0007248605	0.0000157351
1332.492	0.0007033161	0.0000090069	0.0007015118	-0.0000018043
1332.492	0.0006981624	0.0000081420	0.0007015118	0.0000033494
1377.669	0.0006953154	0.0000271752	0.0006821268	-0.0000131886
1401.500	0.0006910276	0.0000326835	0.0006722695	-0.0000187581
1509.228	0.0006482587	0.0000327700	0.0006304824	-0.0000177763
1620.500	0.0005908675	0.0000193400	0.0005913822	0.0000005147
1661.280	0.0005875993	0.0000307384	0.0005779465	-0.0000096528
1729.595	0.0005449129	0.0000210354	0.0005564198	0.0000115069
1764.494	0.0005365841	0.0000171671	0.0005458766	0.0000092925
1847.420	0.0005379745	0.0000272987	0.0005220046	-0.0000159699
2118.550	0.0004657094	0.0000316460	0.0004551108	-0.0000105986
2447.860	0.0003973955	0.0000234059	0.0003968939	-0.0000005016
2614.511	0.0003774141	0.0000046254	0.0003774945	0.0000000804

Chi squared: 28.18872
Reduced Chi squared: 0.97202

Position 4

Polynomial degree: 7(8 parameters)
Number of exp. points: 34

Energy [keV]	EffExp [-]	UncEffExp [-]	EffCalc [-]	Difference [-]
241.997	0.0063760272	0.0002018485	0.0063800529	0.0000040257
277.371	0.0060462191	0.0003139293	0.0059590201	-0.0000871990
295.224	0.0056737777	0.0001748886	0.0057556485	0.0000818708

300.087	**0.0057389598**	**0.0001346686**	**0.0057012567**	**-0.0000377031**
351.932	**0.0051261123**	**0.0001560021**	**0.0051542662**	**0.0000281539**
510.770	**0.0039695897**	**0.0000736451**	**0.0039209988**	**-0.0000485909**
583.187	**0.0035133960**	**0.0000448026**	**0.0035413867**	**0.0000279907**
609.312	**0.0034257009**	**0.0001048770**	**0.0034240464**	**-0.0000016545**
727.330	**0.0030099519**	**0.0000742407**	**0.0029886294**	**-0.0000213225**
768.356	**0.0029178571**	**0.0001125965**	**0.0028653047**	**-0.0000525524**
785.370	**0.0027855376**	**0.0001335258**	**0.0028174951**	**0.0000319575**
806.174	**0.0027401336**	**0.0001400620**	**0.0027614451**	**0.0000213115**
860.557	**0.0026293593**	**0.0000700830**	**0.0026261800**	**-0.0000031793**
934.061	**0.0024679696**	**0.0001147878**	**0.0024653718**	**-0.0000025978**
1112.074	**0.0021677900**	**0.0000375913**	**0.0021542285**	**-0.0000135615**
1120.287	**0.0021174950**	**0.0000692995**	**0.0021419915**	**0.0000244965**
1155.190	**0.0020569603**	**0.0000981747**	**0.0020917183**	**0.0000347580**
1173.228	**0.0020780215**	**0.0000232414**	**0.0020667844**	**-0.0000112371**
1212.948	**0.0019865912**	**0.0001538264**	**0.0020142237**	**0.0000276325**
1238.110	**0.0019159307**	**0.0000760586**	**0.0019824948**	**0.0000665641**
1280.960	**0.0018407879**	**0.0000927656**	**0.0019310440**	**0.0000902561**
1299.140	**0.0018454991**	**0.0000915224**	**0.0019101374**	**0.0000646383**
1332.492	**0.0018604770**	**0.0000208008**	**0.0018731160**	**0.0000126390**
1377.669	**0.0018260048**	**0.0000786610**	**0.0018255318**	**-0.0000004730**
1401.500	**0.0017733888**	**0.0000998939**	**0.0018015324**	**0.0000281436**
1408.006	**0.0018282905**	**0.0000300948**	**0.0017951053**	**-0.0000331852**
1509.228	**0.0016508803**	**0.0001026755**	**0.0017013726**	**0.0000504923**
1620.500	**0.0016406222**	**0.0000808971**	**0.0016098284**	**-0.0000307938**
1661.280	**0.0015822202**	**0.0001152040**	**0.0015787282**	**-0.0000034920**
1729.595	**0.0015681474**	**0.0000658837**	**0.0015290559**	**-0.0000390915**
1764.494	**0.0015145444**	**0.0000501905**	**0.0015047061**	**-0.0000098383**
1847.420	**0.0013884033**	**0.0000643602**	**0.0014491554**	**0.0000607521**
2447.860	**0.0010803954**	**0.0000719255**	**0.0010878562**	**0.0000074608**
2614.511	**0.0009876218**	**0.0000154668**	**0.0009872541**	**-0.0000003677**

Chi squared: 7.81973
Reduced Chi squared: 0.30076

Position 5

Polynomial degree: 7(8 parameters)
Number of exp. points: 41

Energy [keV]	EffExp [-]	UncEffExp [-]	EffCalc [-]	Difference [-]
122.061	0.0047135012	0.0000558139	0.0047181025	0.0000046013
136.474	0.0067739398	0.0001127529	0.0067507699	-0.0000231699
244.698	0.0109580524	0.0001848721	0.0111028281	0.0001447757
276.399	0.0107986416	0.0001670995	0.0106755978	-0.0001230438
302.851	0.0100963312	0.0001323864	0.0102155891	0.0001192579
344.279	0.0097358011	0.0001149387	0.0094557535	-0.0002800476
351.932	0.0090954076	0.0002754470	0.0093177589	0.0002223513
356.013	0.0092247817	0.0000962920	0.0092448675	0.0000200858
383.849	0.0085756933	0.0001185309	0.0087635370	0.0001878437
411.116	0.0085611341	0.0002354349	0.0083232510	-0.0002378831
443.965	0.0076875981	0.0001999210	0.0078370711	0.0001494730
609.312	0.0059160230	0.0001800490	0.0060345965	0.0001185735
665.453	0.0056173614	0.0002796418	0.0056080136	-0.0000093478
768.356	0.0050074111	0.0001830631	0.0049858745	-0.0000215366
778.904	0.0049535266	0.0000859673	0.0049314400	-0.0000220866
806.174	0.0047090273	0.0002141828	0.0047973959	0.0000883686
867.373	0.0045336868	0.0001406969	0.0045276308	-0.0000060560
934.061	0.0042866356	0.0001793369	0.0042741558	-0.0000124798
964.079	0.0042190666	0.0000697202	0.0041714298	-0.0000476368
1085.869	0.0038738289	0.0000676101	0.0038110234	-0.0000628055
1112.074	0.0037513673	0.0000620626	0.0037431571	-0.0000082102
1120.287	0.0036490526	0.0001155005	0.0037224785	0.0000734259
1155.190	0.0034561293	0.0001458309	0.0036375273	0.0001813980
1173.228	0.0035936369	0.0000401927	0.0035953670	0.0000017301
1212.948	0.0035347556	0.0002577409	0.0035063366	-0.0000284190

1238.110	**0.0033466938**	**0.0001275413**	**0.0034524303**	**0.0001057365**
1280.960	**0.0032382596**	**0.0001861537**	**0.0033646343**	**0.0001263747**
1299.140	**0.0031986055**	**0.0001405710**	**0.0033287889**	**0.0001301834**
1332.492	**0.0032176915**	**0.0000359750**	**0.0032650199**	**0.0000473284**
1377.669	**0.0031745868**	**0.0001256512**	**0.0031824104**	**0.0000078236**
1401.500	**0.0032742615**	**0.0001548625**	**0.0031404308**	**-0.0001338307**
1407.980	**0.0031335798**	**0.0001442174**	**0.0031291947**	**-0.0000043851**
1408.006	**0.0032171531**	**0.0000504519**	**0.0031291498**	**-0.0000880033**
1509.228	**0.0029348706**	**0.0001526641**	**0.0029625790**	**0.0000277084**
1661.280	**0.0027366704**	**0.0001524089**	**0.0027385749**	**0.0000019045**
1729.595	**0.0026935438**	**0.0001148345**	**0.0026462381**	**-0.0000473057**
1764.494	**0.0025916782**	**0.0000838073**	**0.0026007900**	**0.0000091118**
1847.420	**0.0024935193**	**0.0001042615**	**0.0024970870**	**0.0000035677**
2118.550	**0.0022814918**	**0.0001459534**	**0.0021948232**	**-0.0000866686**
2204.210	**0.0020620781**	**0.0000808692**	**0.0021097467**	**0.0000476686**
2447.860	**0.0019067681**	**0.0001060445**	**0.0018923441**	**-0.0000144240**

Chi squared: 25.20850
Reduced Chi squared: 0.76389

Appendix II

Efficiency values of ORTEC detector

Position 6

Polynomial degree: 7(8 parameters)
Number of exp. points: 50

Energy [keV]	EffExp [-]	UncEffExp [-]	EffCalc [-]	Difference [-]
88.034	0.0002717521	0.0002717521	0.0002729353	0.0000011832
121.782	0.0022408326	0.0022408326	0.0022603688	0.0000195362
122.061	0.0023125207	0.0023125207	0.0022801324	-0.0000323883
136.474	0.0031710453	0.0031710453	0.0032412470	0.0000702017
238.632	0.0052747703	0.0052747703	0.0052077938	-0.0000669765
240.986	0.0051735615	0.0051735615	0.0051967703	0.0000232088
241.997	0.0050271610	0.0050271610	0.0051917615	0.0001646005
244.698	0.0050953938	0.0050953938	0.0051776186	0.0000822248
276.399	0.0050769836	0.0050769836	0.0049530655	-0.0001239181
295.224	0.0047597841	0.0047597841	0.0047918628	0.0000320787
300.087	0.0047903588	0.0047903588	0.0047488839	-0.0000414749
302.851	0.0046726499	0.0046726499	0.0047243313	0.0000516814
344.279	0.0043579535	0.0043579535	0.0043580173	0.0000000638
351.932	0.0041757953	0.0041757953	0.0042925469	0.0001167516
356.013	0.0043258154	0.0043258154	0.0042580740	-0.0000677414
383.849	0.0039864059	0.0039864059	0.0040321811	0.0000457752
411.116	0.0035830857	0.0035830857	0.0038279354	0.0002448497
443.965	0.0034782219	0.0034782219	0.0036047248	0.0001265029
510.770	0.0033042178	0.0033042178	0.0032214572	-0.0000827606
583.187	0.0028825403	0.0028825403	0.0028941362	0.0000115959
727.330	0.0025389017	0.0025389017	0.0024300738	-0.0001088279
768.356	0.0022858284	0.0022858284	0.0023296773	0.0000438489
778.904	0.0023268486	0.0023268486	0.0023055752	-0.0000212734

785.370	**0.0023108499**	**0.0023108499**	**0.0022911199**	**-0.0000197300**
806.174	**0.0023207455**	**0.0023207455**	**0.0022461784**	**-0.0000745671**
860.557	**0.0021475160**	**0.0021475160**	**0.0021388602**	**-0.0000086558**
867.373	**0.0021092587**	**0.0021092587**	**0.0021263411**	**0.0000170824**
934.061	**0.0019691728**	**0.0019691728**	**0.0020131615**	**0.0000439887**
964.079	**0.0020027133**	**0.0020027133**	**0.0019670683**	**-0.0000356450**
1085.869	**0.0017842947**	**0.0017842947**	**0.0018039383**	**0.0000196436**
1089.737	**0.0017573697**	**0.0017573697**	**0.0017992814**	**0.0000419117**
1112.074	**0.0016892232**	**0.0016892232**	**0.0017729215**	**0.0000836983**
1120.287	**0.0017218619**	**0.0017218619**	**0.0017634493**	**0.0000415874**
1155.190	**0.0017374515**	**0.0017374515**	**0.0017244267**	**-0.0000130248**
1173.228	**0.0017194056**	**0.0017194056**	**0.0017049928**	**-0.0000144128**
1212.948	**0.0016540222**	**0.0016540222**	**0.0016638021**	**0.0000097799**
1238.110	**0.0016225871**	**0.0016225871**	**0.0016387596**	**0.0000161725**
1280.960	**0.0015118965**	**0.0015118965**	**0.0015978058**	**0.0000859093**
1299.140	**0.0015227882**	**0.0015227882**	**0.0015810256**	**0.0000582374**
1332.492	**0.0015568998**	**0.0015568998**	**0.0015510892**	**-0.0000058106**
1401.500	**0.0014884707**	**0.0014884707**	**0.0014923007**	**0.0000038300**
1408.006	**0.0015358381**	**0.0015358381**	**0.0014869590**	**-0.0000488791**
1509.228	**0.0013765519**	**0.0013765519**	**0.0014077683**	**0.0000312164**
1620.500	**0.0013909718**	**0.0013909718**	**0.0013281061**	**-0.0000628657**
1661.280	**0.0012444709**	**0.0012444709**	**0.0013005892**	**0.0000561183**
1764.494	**0.0011950754**	**0.0011950754**	**0.0012345241**	**0.0000394487**
1847.420	**0.0011815386**	**0.0011815386**	**0.0011848687**	**0.0000033301**
2118.550	**0.0010480046**	**0.0010480046**	**0.0010414074**	**-0.0000065972**
2447.860	**0.0009258088**	**0.0009258088**	**0.0009019255**	**-0.0000238833**
2614.511	**0.0008434891**	**0.0008434891**	**0.0008446289**	**0.0000011398**

Chi squared: 38.18095
Reduced Chi squared: 0.90907

Position 7

Polynomial degree: 7(8 parameters)
Number of exp. points: 46

Energy [keV]	EffExp [-]	UncEffExp [-]	EffCalc [-]	Difference [-]
88.034	0.0005121326	0.0000161356	0.0005168950	0.0000047624
121.782	0.0043810649	0.0000650963	0.0043816968	0.0000006319
122.061	0.0044897580	0.0000555743	0.0044212826	-0.0000684754
136.474	0.0061629907	0.0001067566	0.0063668985	0.0002039078
241.997	0.0100495760	0.0003123859	0.0102121574	0.0001625814
244.698	0.0099154898	0.0001672831	0.0101758975	0.0002604077
276.399	0.0099994743	0.0001484673	0.0096410745	-0.0003583998
295.224	0.0094905142	0.0002905236	0.0092781582	-0.0002123560
300.087	0.0094179719	0.0002770930	0.0091831822	-0.0002347897
302.851	0.0091901117	0.0001205038	0.0091292168	-0.0000608949
344.279	0.0086546499	0.0001068342	0.0083454051	-0.0003092448
351.932	0.0077515403	0.0002347504	0.0082090037	0.0004574634
356.013	0.0078743449	0.0000847948	0.0081375864	0.0002632415
383.849	0.0076497340	0.0001293778	0.0076761291	0.0000263951
411.116	0.0069783278	0.0001681001	0.0072679704	0.0002896426
443.965	0.0067482506	0.0001480459	0.0068308696	0.0000826190
510.770	0.0063014518	0.0001299328	0.0060994281	-0.0002020237
583.187	0.0054677959	0.0000762901	0.0054899809	0.0000221850
727.330	0.0047394454	0.0001276390	0.0046379799	-0.0001014655
768.356	0.0045484764	0.0001684650	0.0044532964	-0.0000951800
778.904	0.0043569734	0.0000791709	0.0044088332	0.0000518598
785.370	0.0045309223	0.0001998646	0.0043821373	-0.0001487850
806.174	0.0043574696	0.0002227321	0.0042989827	-0.0000584869
860.557	0.0041639255	0.0001332123	0.0040992375	-0.0000646880
867.373	0.0040915670	0.0000970907	0.0040758083	-0.0000157587
934.061	0.0037672833	0.0001599776	0.0038625111	0.0000952278
964.079	0.0037379344	0.0000647523	0.0037747820	0.0000368476

1085.869	0.0036294605	0.0000662919	0.0034596364	-0.0001698241
1089.737	0.0034231558	0.0002153053	0.0034505280	0.0000273722
1112.074	0.0034529123	0.0000571250	0.0033988538	-0.0000540585
1120.287	0.0033157981	0.0001060483	0.0033802370	0.0000644389
1155.190	0.0032523930	0.0001393425	0.0033032788	0.0000508858
1173.228	0.0032051078	0.0000373901	0.0032648001	0.0000596923
1212.948	0.0032319329	0.0002417643	0.0031829299	-0.0000490030
1238.110	0.0030281771	0.0001153854	0.0031329635	0.0001047864
1280.960	0.0029647768	0.0001364960	0.0030509780	0.0000862012
1332.492	0.0029435375	0.0000343273	0.0029571230	0.0000135855
1401.500	0.0029226649	0.0001423731	0.0028386992	-0.0000839657
1407.980	0.0029179954	0.0001359245	0.0028279733	-0.0000900221
1509.228	0.0027607603	0.0001456440	0.0026683632	-0.0000923971
1620.500	0.0025202512	0.0001542171	0.0025085824	-0.0000116688
1661.280	0.0024639666	0.0001554747	0.0024537206	-0.0000102460
1847.420	0.0022739615	0.0001186985	0.0022259117	-0.0000480498
2118.550	0.0020013186	0.0001408980	0.0019529212	-0.0000483974
2447.860	0.0017369908	0.0001023058	0.0017020921	-0.0000348987
2614.511	0.0016001310	0.0000302466	0.0016049480	0.0000048170

Chi squared: 59.43380
Reduced Chi squared: 1.56405

Position 8

Polynomial degree: 7(8 parameters)
Number of exp. points: 50

Energy [keV]	EffExp [-]	UncEffExp [-]	EffCalc [-]	Difference [-]
80.895	0.0002691593	0.0000211169	0.0002901637	0.0000210044
88.034	0.0008777486	0.0000290675	0.0008599223	-0.0000178263
121.782	0.0079003187	0.0001073910	0.0081504500	0.0002501313
122.061	0.0083616757	0.0000916798	0.0082212796	-0.0001403961

136.474	0.0117038201	0.0001736189	0.0116098281	-0.0000939920
238.632	0.0185965696	0.0002693708	0.0184997752	-0.0000967944
240.986	0.0182714496	0.0003973805	0.0184668115	0.0001953619
241.997	0.0179636001	0.0005810494	0.0184516215	0.0004880214
244.698	0.0179606062	0.0002762823	0.0184081493	0.0004475431
276.399	0.0178934467	0.0002768854	0.0176642323	-0.0002292144
295.224	0.0168961427	0.0005172222	0.0170993354	0.0002031927
300.087	0.0175093323	0.0004544466	0.0169459935	-0.0005633388
302.851	0.0167802211	0.0002372685	0.0168579552	0.0000777341
344.279	0.0153286593	0.0001809662	0.0155151551	0.0001864958
351.932	0.0153020056	0.0004656791	0.0152708257	-0.0000311799
356.013	0.0155971137	0.0001679573	0.0151418068	-0.0004553069
383.849	0.0143634535	0.0002145114	0.0142918032	-0.0000716503
411.116	0.0131452919	0.0003166553	0.0135200251	0.0003747332
443.965	0.0124942636	0.0002838959	0.0126785346	0.0001842710
510.770	0.0112486117	0.0002848607	0.0112548975	0.0000062858
583.187	0.0097892388	0.0001365756	0.0100784486	0.0002892098
609.312	0.0094123984	0.0002881539	0.0097283490	0.0003159506
665.453	0.0090703627	0.0005038926	0.0090800550	0.0000096923
727.330	0.0088369005	0.0002379513	0.0084947491	-0.0003421514
768.356	0.0081268410	0.0003092160	0.0081630165	0.0000361755
778.904	0.0080500727	0.0001270760	0.0080836099	0.0000335372
785.370	0.0081560165	0.0003675460	0.0080360005	-0.0001200160
806.174	0.0076635410	0.0003804657	0.0078879530	0.0002244120
860.557	0.0077162775	0.0002398218	0.0075327967	-0.0001834808
867.373	0.0074310109	0.0001963374	0.0074910634	0.0000600525
934.061	0.0069893875	0.0003201624	0.0071083503	0.0001189628
964.079	0.0070049763	0.0001103279	0.0069485361	-0.0000564402
1085.869	0.0064013036	0.0001017402	0.0063530852	-0.0000482184
1089.737	0.0063863460	0.0003823281	0.0063352229	-0.0000511231
1112.074	0.0063329891	0.0000951433	0.0062330506	-0.0000999385

1120.287	0.0059960704	0.0001962157	0.0061958830	0.0001998126
1155.190	0.0059889021	0.0002813722	0.0060401292	0.0000512271
1173.228	0.0062802932	0.0000702413	0.0059609341	-0.0003193591
1212.948	0.0058160077	0.0004034804	0.0057893992	-0.0000266085
1238.110	0.0053539888	0.0002124736	0.0056826496	0.0003286608
1299.140	0.0052217172	0.0002101305	0.0054295926	0.0002078754
1332.492	0.0049884117	0.0000557723	0.0052947646	0.0003063529
1401.500	0.0047890859	0.0002584332	0.0050237744	0.0002346885
1620.500	0.0046779603	0.0002818974	0.0042448212	-0.0004331391
1661.280	0.0041916095	0.0003158074	0.0041153618	-0.0000762477
1729.595	0.0040742403	0.0001711292	0.0039107336	-0.0001635067
1764.494	0.0039965869	0.0001324239	0.0038123296	-0.0001842573
2118.550	0.0034601032	0.0002133378	0.0030642033	-0.0003958999
2447.860	0.0029890973	0.0002042235	0.0027989254	-0.0001901719
2614.511	0.0028160225	0.0000508455	0.0028407079	0.0000246854

Chi squared: 102.60727
Reduced Chi squared: 2.44303

Position 9

Polynomial degree: 7(8 parameters)
Number of exp. points: 53

Energy [keV]	EffExp [-]	UncEffExp [-]	EffCalc [-]	Difference [-]
80.895	0.0003262707	0.0000349311	0.0004193751	0.0000931044
88.034	0.0013186786	0.0000425398	0.0012680509	-0.0000506277
121.782	0.0128668470	0.0001827711	0.0135942679	0.0007274209
122.061	0.0140662124	0.0001542259	0.0137230194	-0.0003431930
136.474	0.0203159748	0.0002909222	0.0200323840	-0.0002835908
238.632	0.0340233652	0.0004821355	0.0333159163	-0.0007074489
241.997	0.0321237273	0.0010169674	0.0332108736	0.0010871463
244.698	0.0313116721	0.0004816575	0.0331173978	0.0018057257
276.399	0.0323412508	0.0004801869	0.0315887775	-0.0007524733

295.224	0.0299157331	0.0009103817	0.0304661554	0.0005504223
300.087	0.0312276870	0.0006358789	0.0301647235	-0.0010629635
302.851	0.0299145900	0.0004068089	0.0299921968	0.0000776068
344.279	0.0266593337	0.0003147325	0.0273986378	0.0007393041
351.932	0.0263850789	0.0007990519	0.0269327875	0.0005477086
356.013	0.0275600517	0.0002967801	0.0266873927	-0.0008726590
383.849	0.0257182028	0.0003691616	0.0250795929	-0.0006386099
411.116	0.0224749726	0.0005601970	0.0236305034	0.0011555308
443.965	0.0215616805	0.0005071781	0.0220587017	0.0004970212
510.770	0.0192483001	0.0003964202	0.0194108420	0.0001625419
583.187	0.0168127067	0.0002056524	0.0172283992	0.0004156925
609.312	0.0160907268	0.0004897043	0.0165802662	0.0004895394
665.453	0.0152709285	0.0007922092	0.0153843856	0.0001134571
727.330	0.0144367003	0.0003256699	0.0143151106	-0.0001215897
768.356	0.0135881081	0.0005032390	0.0137175706	0.0001294625
778.904	0.0139033543	0.0002194741	0.0135758645	-0.0003274898
785.370	0.0132518152	0.0004479820	0.0134911917	0.0002393765
806.174	0.0133139502	0.0006144276	0.0132294133	-0.0000845369
860.557	0.0130097933	0.0003030419	0.0126126168	-0.0003971765
867.373	0.0128684857	0.0003400028	0.0125413457	-0.0003271400
934.061	0.0121019436	0.0005139088	0.0119018465	-0.0002000971
964.079	0.0118947116	0.0001873382	0.0116430508	-0.0002516608
1085.869	0.0108259706	0.0001720644	0.0107246601	-0.0001013105
1089.737	0.0105065110	0.0006241430	0.0106981926	0.0001916816
1112.074	0.0105774070	0.0001589091	0.0105479071	-0.0000294999
1120.287	0.0105820185	0.0003384259	0.0104936903	-0.0000883282
1155.190	0.0100359099	0.0004233972	0.0102689434	0.0002330335
1173.228	0.0099875709	0.0001117050	0.0101560756	0.0001685047
1212.948	0.0099894685	0.0007537098	0.0099144420	-0.0000750265
1238.110	0.0096215716	0.0003715317	0.0097657544	0.0001441828
1280.960	0.0093209872	0.0005667136	0.0095193493	0.0001983621

1299.140	**0.0093359182**	**0.0004277633**	**0.0094171419**	**0.0000812237**
1332.492	**0.0090804762**	**0.0001015231**	**0.0092328988**	**0.0001524226**
1401.500	**0.0090133914**	**0.0004390734**	**0.0088636817**	**-0.0001497097**
1408.006	**0.0089133933**	**0.0001266561**	**0.0088296378**	**-0.0000837555**
1509.228	**0.0084740335**	**0.0004469010**	**0.0083154031**	**-0.0001586304**
1620.500	**0.0081235185**	**0.0003577447**	**0.0077818131**	**-0.0003417054**
1661.280	**0.0078515917**	**0.0005521031**	**0.0075944952**	**-0.0002570965**
1729.595	**0.0074772233**	**0.0002923640**	**0.0072908998**	**-0.0001863235**
1764.494	**0.0071807851**	**0.0002322143**	**0.0071408836**	**-0.0000399015**
1847.420	**0.0069118377**	**0.0003450497**	**0.0067987735**	**-0.0001130642**
2118.550	**0.0058683669**	**0.0003800202**	**0.0058328312**	**-0.0000355357**
2447.860	**0.0050688833**	**0.0002860219**	**0.0050025741**	**-0.0000663092**
2614.511	**0.0047228155**	**0.0000703384**	**0.0047324291**	**0.0000096136**

Chi squared: 96.84489
Reduced Chi squared: 2.15211

Appendix IV

Fitting coefficients of efficiency

Position 3

P3C 7 0.97		
P3BF	6.78644361	0.01052074
P3BF	-0.80325355	0.03440297
P3BF	-0.00211373	0.12881751
P3BF	-0.03486588	0.15825312
P3BF	-0.24054501	0.37741600
P3BF	-0.05725847	0.15604118
P3BF	0.17605281	0.28310791
P3BF	0.08640609	0.13563547

Position 2

P2C 7 0.89		
P2BF	6.43385927	0.00961783
P2BF	-0.79237481	0.03603015
P2BF	-0.10902665	0.08673917
P2BF	-0.09946121	0.17102235
P2BF	-0.05334652	0.21375480
P2BF	0.04652788	0.11383181
P2BF	0.08837317	0.17161192
P2BF	0.03695582	0.04877597

Position 4

P4C 7 1.65		
P4BF	7.75324996	0.01380525
P4BF	-0.74570657	0.04699703
P4BF	0.04469751	0.18241443
P4BF	-0.18971194	0.27128817
P4BF	0.10560309	0.62850526
P4BF	0.19626206	0.32185188
P4BF	-0.20259523	0.49737647
P4BF	-0.13974123	0.25904742

Position 5

P5C 7 0.86		
P5BF	8.31007742	0.00614593
P5BF	-0.75152246	0.03158568
P5BF	0.06302970	0.06216891
P5BF	-0.17247982	0.14330474
P5BF	-0.17741038	0.08780181
P5BF	0.07030002	0.14860185
P5BF	0.09287181	0.10966107
P5BF	0.02740169	0.02374720

Position 6

P6C 7 2.31		
P6BF	7.56605135	0.00984894
P6BF	-0.85259915	0.06198319
P6BF	-0.08723138	0.15946860
P6BF	0.79805388	0.57133064
P6BF	2.06060659	1.32683024
P6BF	1.89006036	1.19850168
P6BF	0.74244258	0.47164361
P6BF	0.11319407	0.06781391

Position 7

P7C 7 14.0		
P7BF	8.22297064	0.00696722
P7BF	-0.96099704	0.04816788
P7BF	0.07205845	0.12502315
P7BF	1.18701200	0.47601769
P7BF	1.58634212	1.05838433
P7BF	0.82986546	0.94671472
P7BF	0.17633813	0.37175652
P7BF	0.01800387	0.05344142

Position 8

P8C 7 2.29		
P8BF	8.84074138	0.00826869
P8BF	-0.62836417	0.05195839
P8BF	-0.67798237	0.12966288
P8BF	-2.62686431	0.48916476
P8BF	-2.97937564	1.04237251
P8BF	-1.46046022	0.90574492
P8BF	-0.30866885	0.34832482
P8BF	-0.01276252	0.04927469

Position 9

P9C 7 4.27		
P9BF	9.38269594	0.00807171
P9BF	-0.77382820	0.04659224
P9BF	-0.66016382	0.16352254
P9BF	-0.49300090	0.22416381
P9BF	1.61500959	0.58637863
P9BF	2.36469676	0.60269901
P9BF	1.10067737	0.25310246
P9BF	0.17960555	0.03779067

Appendix V

Scheme of radioactive decay [167]

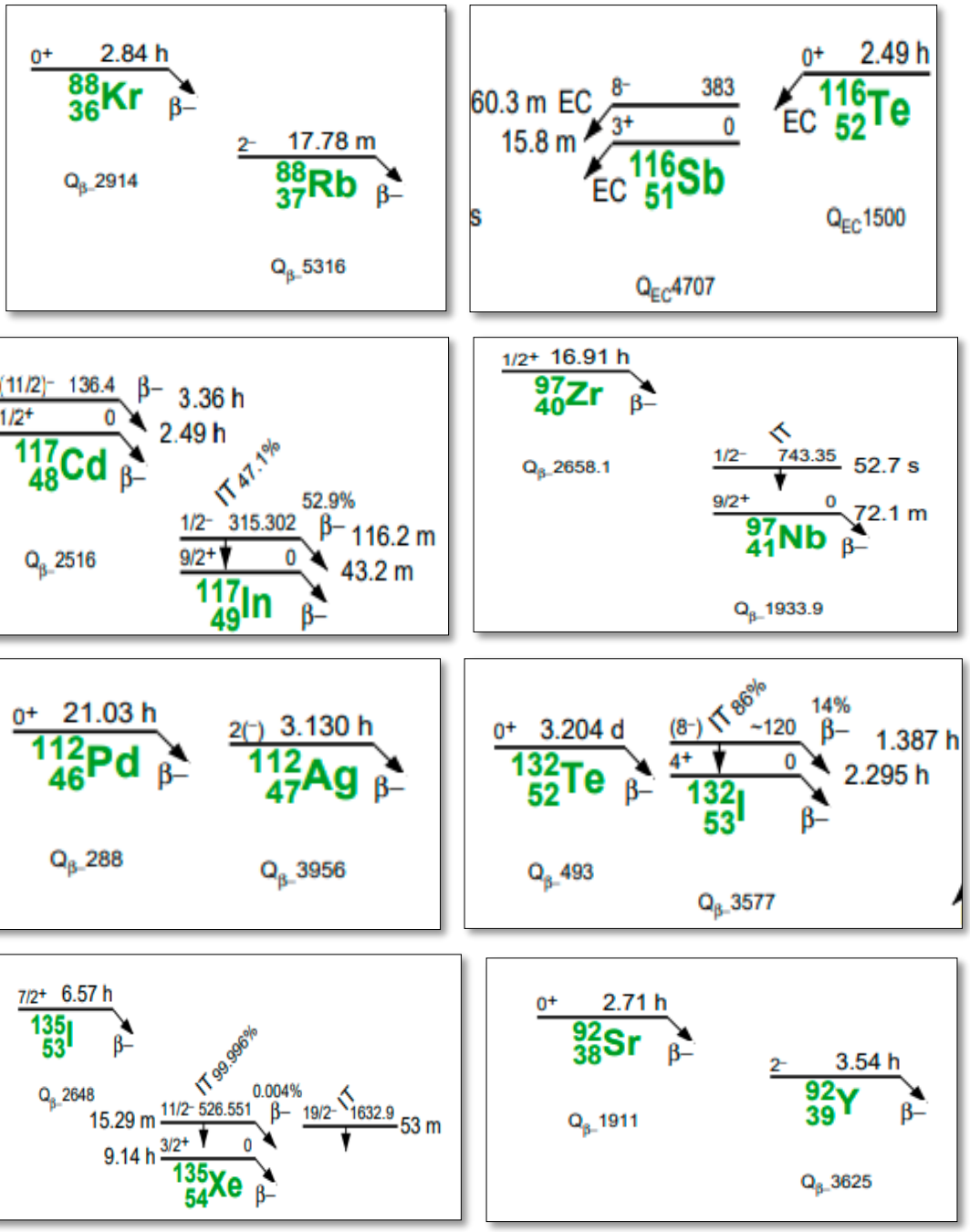

Appendix VI

Plutonium radioactive decay

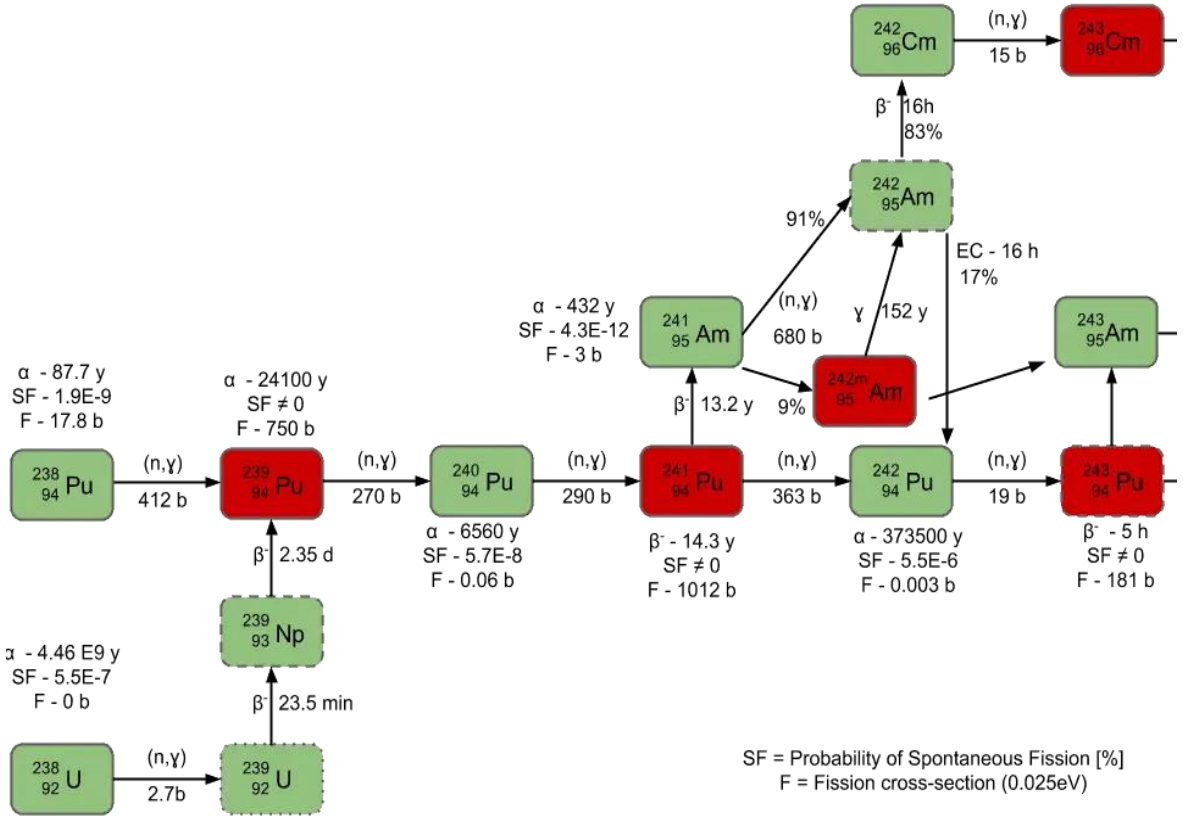

Source of data: JANIS (Java-based Nuclear Data Information Software); The JEFF-3.1.1 Nuclear Data Library

Appendix VII

The difference between experimental and simulation cross section data

Table 28. Results of calculation Cal/Exp, Cal/Cal, < F > - factor and σ (< F >).

Isotope	C/E	C/E	C/C	< F > - faktor	< F > - faktor	< F > - faktor	σ (< F >)	σ (< F >)	σ (< F >)
	FLUKA/exp.	MCNP/exp.	FLUKA/MCNP	FLUKA/exp.	MCNP/exp.	FLUKA/MCNP	FLUKA/exp.	MCNP/exp.	FLUKA/MCNP
^{98m}Nb	120.59	30.14	4.00	20.81	14.79	6.02	7.63	3.09	26.33
^{92}Sr		118.39	7.10		20.73	8.51		7.57	26.93
^{91m}Y	285.95	89.61	3.19	24.56	19.52	5.04	10.66	6.62	25.38
^{90m}Y	374.27	157.08	2.38	25.73	21.96	3.77	11.63	8.54	26.04
^{89}Rb	207.66	72.69	2.86	23.17	18.61	4.56	9.52	5.92	28.28
^{88}RbD	305.96		1.27	24.86		1.03	10.90		25.18
^{87}Kr	205.29	50.37	4.08	23.12	17.02	6.10	9.48	4.71	30.28
^{49}Cr		0.23			6.37			14.40	
^{41}Ar		0.64			1.94			4.82	
^{227}Pa		1.29			1.10			0.68	
^{202}Bi		0.40			4.01			10.03	
^{118m}Sb	100.24	36.11	2.78	20.01	15.58	4.43	7.00	3.65	27.02
^{201m}Bi		0.66			1.81			4.39	
^{197}Tl		0.00			23.20			36.86	
^{149}Nd	15.77	1.87	8.43	11.98	2.72	9.26	1.19	1.62	35.77
^{142}La	364.29	38.85	9.38	25.61	15.89	9.72	11.53	3.88	30.94
^{138}Cs	316.90	13.12	24.15	25.01	11.18	13.83	11.03	0.70	29.76
^{137}Nd	4.76	2.21	2.15	6.77	3.45	3.32	1.53	1.93	34.28
^{135m}Cs	278.02	64.50	4.31	24.44	18.10	6.35	10.56	5.52	28.07
^{134}I	105.26	1.53	68.67	20.22	1.85	18.37	7.16	0.83	28.01
^{125}Cs		14.35			11.57			0.94	
^{123}Xe	8.21	3.46	2.37	9.14	5.39	3.76	0.47	1.93	34.35
^{116m}SbD	3.43	7.58	0.45	5.35	8.79	3.44	1.93	0.65	36.67
^{116m}In	136.71	23.99	5.70	21.36	13.80	7.56	8.06	2.40	24.82
^{107}Rh	419.51	84.30	4.98	26.23	19.26	6.97	12.04	6.41	23.26
^{104}Tc		69.45	8.17		18.42	9.12		5.76	25.89
^{104}Ag	20.69	14.60	1.42	13.16	11.64	1.51	1.97	0.98	31.82
^{101}Mo	52.90	14.76	3.58	17.23	11.69	5.54	4.87	1.01	24.00
^{101}Tc	428.26	52.57	8.15	26.32	17.21	9.11	12.11	4.85	25.70
^{99}Mo	33.77	9.57	3.53	15.29	9.81	5.48	3.44	0.11	25.28

^{97}NbD	90.31	31.69	2.85	19.56	15.01	4.55	6.64	3.25	24.82
^{96}Nb	148.75	49.68	2.99	21.72	16.96	4.76	8.35	4.67	25.00
^{92}YD	100.72	40.40	2.49	20.03	16.06	3.97	7.01	4.00	26.29
^{82}Br	6.96	5.50	1.26	8.42	7.41	1.02	0.83	1.29	26.58
^{69m}Zn	90.20	36.45	2.47	19.55	15.62	3.93	6.64	3.68	34.04
^{48}V		1.90			2.78			1.66	
^{48}Sc		1.85			2.67			1.60	
^{239}Np	0.70	0.00		1.54			3.42		
^{206}Bi		0.00			32.79			47.94	
^{186}Ir		0.01			18.99			31.77	
^{183}Os		0.00			28.18			42.68	
^{182}Os		0.00			23.45			37.16	
^{147}Gd		1.63			2.12			1.14	
^{136}Cs	211.39	42.21	5.01	23.25	16.25	7.00	9.59	4.14	29.24
^{135}XeD	257.30	11.25	22.88	24.10	10.51	13.59	10.28	0.29	27.93
^{135}I		22.06	110.39		13.44	20.43		2.15	28.59
^{135}Ce	2.21	1.06	2.09	3.44	0.24	3.20	1.93	6.41	34.46
^{133}I	142.69	8.42	16.94	21.54	9.25	12.29	8.21	0.41	28.97
^{132}Te	269.24	3.06	88.00	24.30	4.86	19.44	10.45	2.01	28.64
^{132}La	118.90	80.56	1.48	20.75	19.06	1.69	7.58	6.26	30.36
^{132}ID	61.70	5.07	12.17	17.90	7.05	10.85	5.37	1.43	29.26
^{131m}Te	22.26	0.88	25.19	13.48	0.54	14.01	2.18	2.17	31.47
^{130}I	2.74	0.99	2.76	4.38	0.04	4.42	2.03	13.96	31.24
^{128}Sb	185.29	9.52	19.47	22.68	9.79	12.89	9.12	0.12	31.64
^{127}Sb	130.79	9.17	14.27	21.17	9.62	11.54	7.91	0.21	29.00
^{126}Sb	102.76	12.09	8.50	20.12	10.82	9.30	7.08	0.48	29.53
^{124}I	60.37	33.13	1.82	17.81	15.20	2.61	5.30	3.38	26.25
^{122}Sb	177.73	36.88	4.82	22.50	15.67	6.83	8.98	3.72	26.13
^{121}Te	107.79	49.68	2.17	20.33	16.96	3.36	7.25	4.67	26.98
^{120m}Sb	165.68	44.40	3.73	22.19	16.47	5.72	8.73	4.31	26.26
^{117m}Cd		101.19	12.53		20.05	10.98		7.03	25.82
^{117}InD	143.81	24.95	5.76	21.58	13.97	7.61	8.24	2.52	24.02
^{116}SbD	69.30	153.18	0.45	18.41	21.85	3.44	5.76	8.46	35.24
^{112}AgD	4.65	0.74	6.31	6.67	1.32	8.00	1.57	2.54	25.41
^{105}Ru	88.81	15.66	5.67	19.48	11.95	7.54	6.59	1.17	25.01